

**Transcriptional and epigenetic
regulation of neuronal migration and
circuitry development in the murine
hindbrain**

Inauguraldissertation

Zur Erlangung der Würde eines Doktors der Philosophie
vorgelegt der Philosophisch-Naturwissenschaftlichen
Fakultät der Universität Basel

von

Claudius Frank Kratochwil
aus Freiburg/Deutschland
Basel, April 2013

Genehmigt von der Philosophisch-Naturwissenschaftlichen Fakultät auf Antrag von:

Prof. Dr. Filippo Rijli

(Dissertationsleiter)

Prof. Dr. Alain Chédotal

(Korreferent)

Basel, den 23. April 2013

Prof. Dr. Jörg Schibler

(Dekan)

Table of Contents

Summary	3
Abbreviations	5
1 Introduction	7
1.1 Development of the mammalian nervous system	7
1.1.1 <i>From early patterning to cell-type specification</i>	7
1.1.2 <i>Neuronal migration</i>	11
1.1.3 <i>Development of neuronal circuitry</i>	13
1.1.4 <i>Classical examples of guidance factors: Netrins and Robos</i>	17
1.2 Mechanisms of transcriptional regulation in nervous system development	18
1.3 Epigenetic regulation of developmental processes	18
1.3.1 <i>The Polycomb complex</i>	18
1.4 The precerebellar system.....	20
1.4.1 <i>Function</i>	20
1.4.2 <i>Development</i>	24
1.5 The trigeminal system	27
1.6 Aim of this thesis	29
2 Materials and Methods	31
2.1 Molecular Biology	31
2.2 Generation of transgenic mice	33
2.3 Mouse lines	35
2.4 Plasmids	37
2.5 <i>In utero</i> electroporation.....	38
2.6 Neuronal tracing.....	38
2.7 3D-reconstructions	38

2.8	Immunostaining and <i>in situ</i> hybridization.....	39
2.9	Imaging and Picture Processing	39
2.10	Gene expression array and qPCR.....	39
2.11	Tissue dissection and Micro Chromatin Immunoprecipitation (microchip).....	40
2.12	Retinoic acid and tamoxifen treatment.	41
3	Results.....	42
3.1	Publications and Manuscripts	42
3.1.1	<i>“Ezh2 orchestrates topographic tangential migration and connectivity of precerebellar neurons” (accepted publication; Science 2013)</i>	<i>42</i>
3.1.2	<i>“Ezh2 orchestrates topographic tangential migration and connectivity of precerebellar neurons” (unpublished parts)</i>	<i>73</i>
3.1.3	<i>“Partial ipsilateral wiring of subcortical sensory inputs duplicates the facial map” (manuscript, in preparation)</i>	<i>90</i>
3.1.4	<i>“Mouse Hoxa2 genetic analysis provides a model for human microtia and auricle duplication” (submitted manuscript)</i>	<i>133</i>
3.1.5	<i>“The Cre/Lox system to assess the development of the mouse brain” (Book chapter, submitted manuscript, Methods in Brain Development).....</i>	<i>181</i>
3.2	Unpublished Results.....	206
3.2.1	<i>Further description of generated and analyzed transgenic lines</i>	<i>206</i>
3.2.2	<i>Combination of in utero electroporation and genetic tools to assess pontine nuclei connectivity</i>	<i>221</i>
3.2.3	<i>Combination of in utero electroporation and rabies virus tracing to assess cortico-ponto-cerebellar connectivity.....</i>	<i>228</i>
4	Discussion.....	234
5	References	243
	Acknowledgements	256
	Curriculum Vitae.....	258

Summary

Polycomb group proteins, including *Ezh2*, regulate many target genes, which control early cell fate decisions. We addressed whether *Ezh2*-dependent epigenetic regulation of transcriptional programs also orchestrates complex processes such as long-distance tangential neuronal migration in the developing nervous system.

We focused on the migratory behavior of the anterior extramural stream (AES) that contributes to the brainstem pontine nuclei (PN), the main relay between cortex and cerebellum.

We found that the PN neuron migratory behavior is largely pre-mapped at the progenitor stage. The AES stereotypic migratory pattern emerges through an inter-dependent interaction between: i) an intrinsic *Ezh2*-dependent transcriptional program established in PN progenitors, which is maintained in migrating neurons and enables appropriate response to environmental cues; and, ii) an *Ezh2*-dependent silencing program that regulates the spatial distribution of extrinsic signals in the migratory environment, such as *Ntn1*, also pre-mapped in ventricular progenitors.

Specifically, by restricting *Netrin1* expression to ventral hindbrain, *Ezh2* allows normal PN migration in a non-cell-autonomous manner. In conditional *Ezh2* mutants, ectopic *Netrin1* de-repression leads to abnormal migration and supernumerary nuclei that integrate the cortico-ponto-cerebellar circuitry. Importantly, we revealed for the first time an intrinsic topographic organization of the PN migratory stream, according to rostrocaudal progenitor origin. Neuronal position is maintained throughout migration and settling in the PN and correlates with patterned cortical input. By counteracting retinoid signaling, *Ezh2* sets graded *Hox* expression in migrating neurons which in turn maintain graded activity of repulsive receptors *Unc5b/Unc5c*, generating subsets with distinct responsiveness to *Netrin1*.

These findings point to a migratory protomap established in progenitors, whereby Polycomb-mediated epigenetic silencing is fundamental to establish these intrinsic and extrinsic programs. On the one hand, *Ezh2* sets the levels of environmental attractive/repulsive signals through dorsoventrally-restricted silencing of *Ntn1*. On the other hand, *Ezh2*-mediated repression contributes to set a heterogeneous *Hox*

transcriptional program in the AES that, in turn, provides neuronal subsets with distinct *Unc5b*-mediated repulsion to environmental *Ntn1*.

Our results extend the involvement of *Ezh2* beyond fate and subtype identity specification to a novel role in orchestrating epigenetic regulation of topographic neuronal guidance in the mammalian brain.

Lastly, the pontine gray nucleus is a fundamental relay station for the transformation of orderly motor and sensory maps in the cerebral cortex into ‘patchy’ representations of input in the granular layer of the cerebellar cortex. Little is known about the molecular and cellular mechanisms assembling these complex input-output wiring patterns in PN. Our results strongly suggest that the intrinsic pre-mapping of PN from progenitors of distinct rostrocaudal origin contributes to organize broad topographic input from distinct cortical areas.

To further investigate this, we established means to analyze cortico-ponto-cerebellar connectivity by using a) transgenic animals b) viral tracing and c) *in utero* electroporation. These methods will serve further in-depth analysis of the pontine nuclei circuitry and allow functional experiments.

This thesis encompasses the accepted publication “*Ezh2* orchestrates topographic tangential migration and connectivity of precerebellar neurons” (Di Meglio et al., 2013), two manuscripts that resulted from collaborations about “Partial ipsilateral wiring of subcortical sensory inputs duplicates the facial map” and “Mouse *Hoxa2* genetic analysis provides a model for human microtia and auricle duplication”, a manuscript for a book chapter about “The Cre/Lox system to assess the development of the mouse brain” as well as unpublished results that were part of previous versions of the Science publication (Di Meglio et al., 2013) and results from further investigations of cortico-ponto-cerebellar connectivity as well as in-depth analysis of generated and examined transgenic mouse lines.

Abbreviations

A-P	Anterior-Posterior
AES	Anterior Extramural Stream
ANR	Anterior Neural Ridge
C	Cranial spinal cord (used in Introduction)
C	Cingulate cortex (used in Results)
C1	CrusI
C2	CrusII
Cb	Cerebellum
ChAT	Choline Acetyl Transferase
Chr	Chordin
CN	Cochlear Nucleus
CO	Cytochrome Oxidase
COP	Copula Pyramidis
CP	Cerebellar Peduncle
CST	Corticospinal Tract
Ctx	Cortex
Di	Diencephalon
DLPN	Dorso Lateral Pontine Nucleus
DNA	Deoxyribonucleic acid
DRG	Dorsal Root Ganglia
E	Embryonal day
ECN	External Cuneate Nucleus
Ect	Ectorhinal cortex
EZH	Enhancer of Zeste Homolog
FGF	Fibroblast Growth Factor
Fl	Flocculus
FLEX	Flip-Excision (cassette)
FLOX	Flanked by LOX sites
FN	Facial Nucleus
FrA	Frontal Association cortex
GFP	Green Fluorescent Protein
H3K27me3	Trimethylated Lysine 27 of histone H3
Hb	Hindbrain
Hc	Hippocampus
I	Insular cortex
IHC	Immunohistochemistry
INT	Intergenic Region
ION	Inferior Olivary Nuclei
IRES	Internal Ribosomal Entry Site
ISH	<i>In Situ</i> Hybridization
IsO	Isthmic Organizer

L	Lumbar spinal cord
IRL	lower Rhombic Lip
LRN	Lateral Reticular Nucleus
LS	Lobus Simplex
M1	Primary Motor Cortex
M2	Secondary Motor Cortex
Md	Mandibular
Mes	Mesencephalon/ Midbrain
mGFP	membrane-tagged Green Fluorescent Protein
Mx	Maxillary
NLS	Nuclear Localization Signal
Oph	Ophthalmic
OT	Otic capsule
PES	Posterior Extramural Stream
PF1	Paraflocculus
PG	Paralog Group
PML	Paramedian Lobe
PN	Pontine Nuclei
Pr5	Principal trigeminal nucleus
PRC	Polycomb Repressive Complex
PRh	Perirhinal cortex
PRE	Polycomb Responsive Element
r	Rhombomere
R26R	ROSA26 reporter
RabiesG	Rabies-Glycoprotein
S1	Primary Somatosensory Cortex
S2	Secondary Somatosensory Cortex
Sc	Spinal cord
Shh	Sonic hedgehog
Sp5	Spinal trigeminal nucleus
T	thoracic spinal cord
Tel	Telencephalon
TGFβ	Transforming Growth Factor β
V1	Primary Visual Cortex
V2	Secondary Visual Cortex
WISH	Whole-mount <i>In Situ</i> Hybridization
ZLI	Zona Limitans Intrathalamica

1 Introduction

1.1 Development of the mammalian nervous system

1.1.1 From early patterning to cell-type specification

The nervous system differentiates from the ectodermal germ cell layer. Its first sign is the appearance of the neural groove, a fold of a part of the ectodermal layer called the neural plate. The groove closes at the top and detaches from the ectoderm, which itself develops into epidermis. The tubular structure evolving out of the neural groove, is now called neural tube, the presumptive central nervous system. All parts of the brain as well as the spinal cord develop from this structure.

One of the main mechanisms defining identity of brain and spinal cord regions as well as of cells types was conceptionally proposed by Lewis Wolpert's "French-Flag Model" (**Figure 1**, Wolpert, 1969). He postulated that a tissue could be patterned by the graded presence or activity of a single factor (a morphogen). Due to the differential responsiveness to higher or lower concentrations of this factor, expression of different genes can be triggered, resulting in different cell fates (Rogers and Schier, 2011).

The existence of these factors was first demonstrated in *Drosophila*. In the early *Drosophila* larvae the anterior-posterior (A-P) axis is patterned by a localized expression and a thereby resulting diffusion gradient of the transcription factor Bicoid (Driever and Nüsslein-Volhard, 1988a; Driever and Nüsslein-Volhard, 1988b). Many target factors downstream of morphogens are other transcription factors, further defining the identity of segments, structures, tissues or cell types.

Since then, many proteins have been found to be involved in a morphogene like fashion in the patterning process of many organisms and tissues (Tabata, 2001) including the nervous system (Gómez-Skarmeta et al., 2003).

The differentiation of the dorso-ventral axis (**Figure 2**, Lupo et al., 2006), which has been extensively studied in the spinal cord, is triggered by the graded action of dorsalizing factors as BMPs (Bone Morphogenetic Proteins) and other members of

the TGF β family (Transforming Growth Factor) released from dorsal neural tube (roof plate) and the adjacent non-neural ectoderm. Ventral domains of the neural tube are under the influence of Shh (Sonic hedgehog), released by cells of the notochord (a mesodermal structure ventral to the neural tube) and the ventral neural tube (floor plate). By the interplay of dorsalizing and ventralizing signals different classes of progenitors are specified giving rise to a diversity of gliogenic and neuronal cell types (Figure 2).

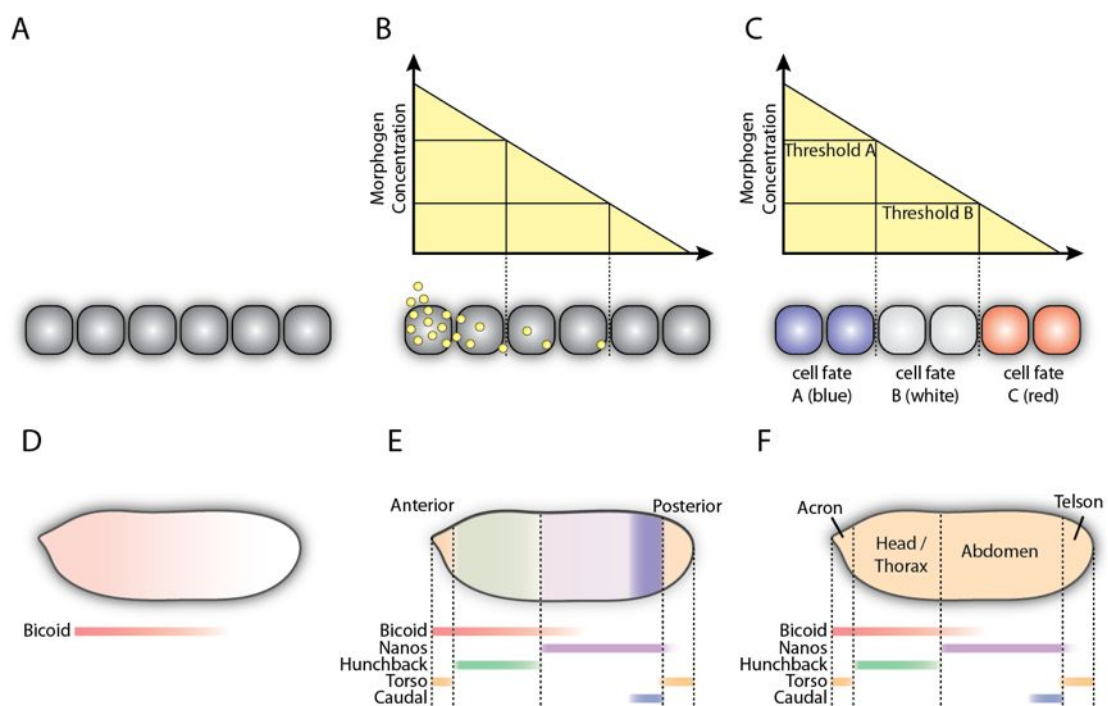


Figure 1 | The French-flag-model by Lewis Wolpert and the concept of morphogens in the *Drosophila* larvae. (A) At the beginning all cells (grey boxes) have the same phenotype. (B) A localized source of a morphogen generates a concentration gradient. (C) Depending on the concentration of the morphogen, cells acquire different fates: Blue at high morphogen concentrations, white at medium-scale concentrations and red at low concentrations. (D-F) The localized expression of the transcription factor *bicoid* (D) is the first sign of anterior-posterior polarity in the *Drosophila* larvae. Further transcription factors induced by different Bicoid concentrations start to be expressed at different axial levels (E) finally defining different body parts of the larvae (F). (Figure by C. Kratochwil based on Porcher and Dostatni, 2010; Rivera-Pomar and Jäckle, 1996; Rogers and Schier, 2011)

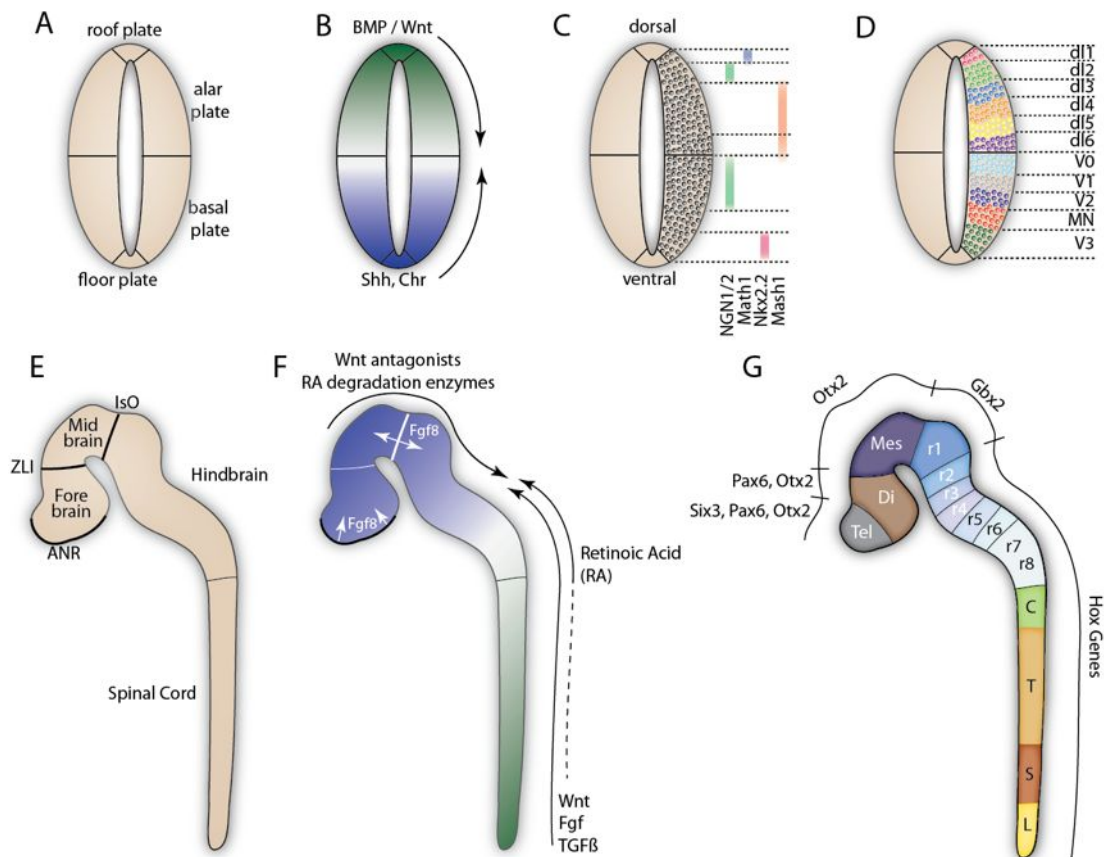


Figure 2 | Morphogen mediated patterning in the vertebrate nervous system. (A-D) In the vertebrate spinal cord the action of morphogens as BMP, Shh, Wnts and Chordin (Chr) (B) define the dorso-ventral axis and result in the nested expression of transcription factors (C) specifying the identity of different neuronal populations (D). **(E-G)** Along the anterior-posterior axis of the nervous system (E) the graded action of morphogens as retinoic acid (RA), Wnt, FGFs and TGF β from posterior and antagonists to Wnt and RA from anterior. Also signals from organizer centers as the anterior neural ridge (ANR), zona limitans intrathalamica (ZLI) and isthmus organizer (IsO) secrete factors as FGF8 locally and help to pattern their surroundings (F). Also here transcription factors are downstream guiding the differentiation of the distinct regions (G). Tel: Telencephalon; Di: Diencephalon; Mes: Mesencephalon/ Midbrain; r: rhombomere; C: cranial spinal cord; T: thoracic spinal cord; S: sacral spinal cord; L: lumbar spinal cord (Figure by C. Kratochwil based on Gómez-Skarmeta et al., 2003; Liu and Niswander, 2005)

Also the antero-posterior (A-P) axis of the embryo and of the nervous system itself is established with the help of morphogens. Besides signaling proteins as FGFs (Mason, 2007), Wnts (Ciani and Salinas, 2005) and TGF β s (Liu and Niswander, 2005) also retinoic acid (RA), a metabolic product of vitamin A plays a pivotal role in patterning the A-P axis (Maden, 2002).

On top of that signaling centers are developing e.g. in the diencephalon (zona limitans intrathalamica) and between mid- and hindbrain (isthmus organizer), further specifying and patterning the adjacent parts of the nervous system (Wilson and Houart, 2004; Wurst and Bally-Cuif, 2001, **Figure 2**).

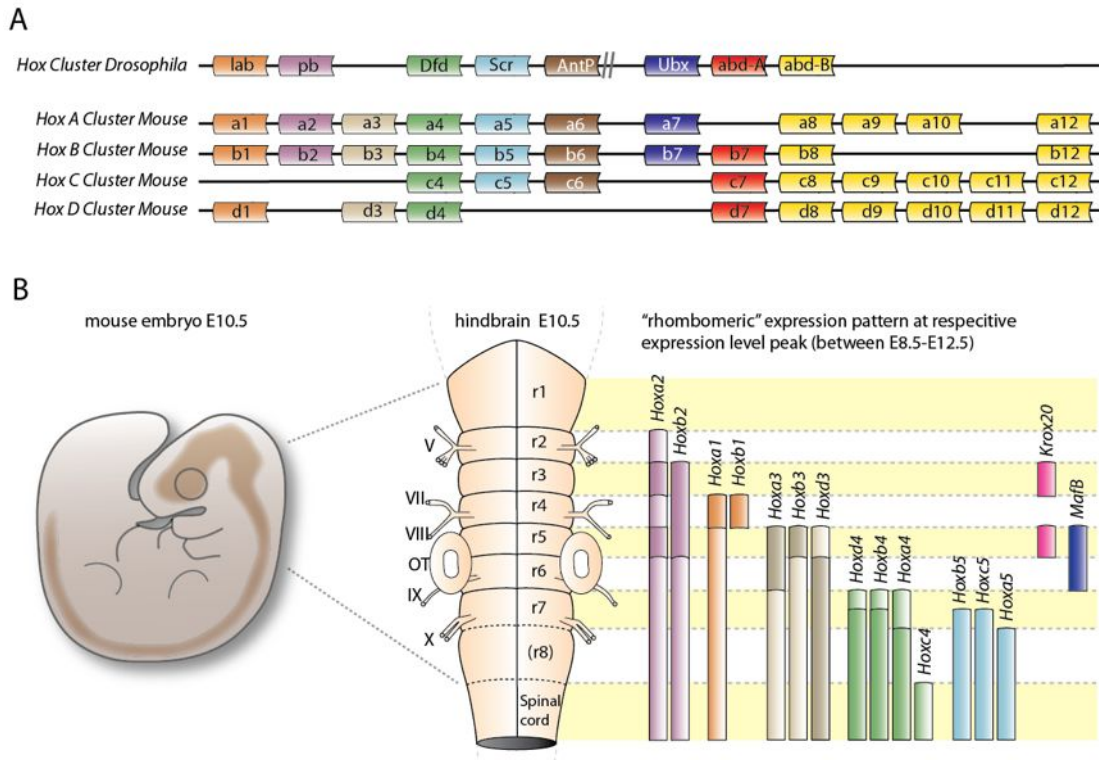


Figure 3 | *Hox* genes in evolution and hindbrain development. (A) It is suggested that the four *Hox* clusters in the mammalian genome derived from a single ancient *Hox* cluster, since many non-vertebrates just have one cluster. The homologies to the *Drosophila* cluster (A, top) are indicated by color. (B) The rhombomeres (r) of the hindbrain and their identity (e.g. which cranial nerve innervates (V, VIII, IX, X) or grows out (V, VII, IX, X) from the respective rhombomere) are defined by the expression of *Hox* genes and other transcription factors as e.g. *Krox20* and *MafB* (Kreislner). OT: Otic capsule (often used as reference for the position of r5/r6) (Figure by C. Kratochwil based on Guthrie, 2007; Nolte and Krumlauf, 2007; Pearson et al., 2005)

A very prominent class of factors, which provide cells with positional identity and define thereby their future fate are the *Hox* genes (Pearson et al., 2005). *Hox* genes have nested domains of expression with sharp anterior expression boundaries, providing a molecular spatial code. The 39 *Hox* genes in mammals are arranged in four different chromosomal complexes (*Hox* clusters *HoxA*, *HoxB*, *HoxC* and *HoxD*). Considering homologies between *Hox* genes of different clusters, they have been

furthermore classified as 13 paralog groups (PG) from PG1 (most anterior) to PG13 (most posterior). A distinguishing hallmark of *Hox* genes is that the chromosomal order inside the cluster recapitulates the order of (a) their expression along the A-P axis, as well as (b) the timing of their expression. This phenomenon has been described as colinearity (Lewis, 1978).

Hox genes are very conserved during bilateral animal evolution and 1-7 *Hox* clusters (although, in some clades the cluster(s) are more dispersed) can be found in all vertebrates and invertebrates (Lemons and McGinnis, 2006). It is thought, that the *Hox* genes are key factors during evolution, since they are able to orchestrate different morphological traits in different body segment. Therefore duplication of *Hox* genes and/or the modification of their downstream targets could be an initial step for higher morphological complexity (Lemons and McGinnis, 2006).

The characteristic feature of *Hox* genes is a conserved DNA motif of around 180 base pairs coding for the homeodomain. This domain binds to the major groove of specific DNA sequences and acts as an "on/off switch" for gene transcription. One structure, where the role of *Hox* genes has been intensively studied, is the vertebrate hindbrain (Narita and Rijli, 2009; Trainor and Krumlauf, 2000).

The mammalian hindbrain is segmented into anatomically visible metameric units called rhombomeres (r). Each rhombomere has a combination of *hox* genes (PG1-PG5) expressed in a tight spatio-temporal manner, giving each segment a unique molecular code. Loss-of-function studies with *hox* genes have demonstrated, that the morphological features of rhombomeres as well as their derivatives (that includes also neural crest cells) are strongly related to their "*Hox* code" (**Figure 3**, Alexander et al., 2009).

Another basic principle underlying the generation of diversity in the brain relies on the fact, that progenitors cannot only differ on an axis in space, but are also able to change their expression profile and thereby their identity in time. Therefore one progenitor can first generate cell-type A and a few cell divisions later cell-type B. This could rely on an internal clock of the cell or a changing environment. Both can lead to the expression of factors, which are changing the cellular fate (McConnell, 1995; Rakic, 1974).

1.1.2 Neuronal migration

The brain is not a uniform tissue, but consists of many distinct structures, which are patterned in different ways. Neural tissues like the cortex or the cerebellum consist of layers with different properties, cell types and functions. Other parts of the brain like thalamus or many parts of the hindbrain are arranged in a completely different fashion. Here assemblies of neurons called nuclei subservise particular functions. During the development of neural structures cells usually migrate from progenitor zones to their final location. There are two main types of neuronal migration, radial migration and tangential migration (**Figure 4**).

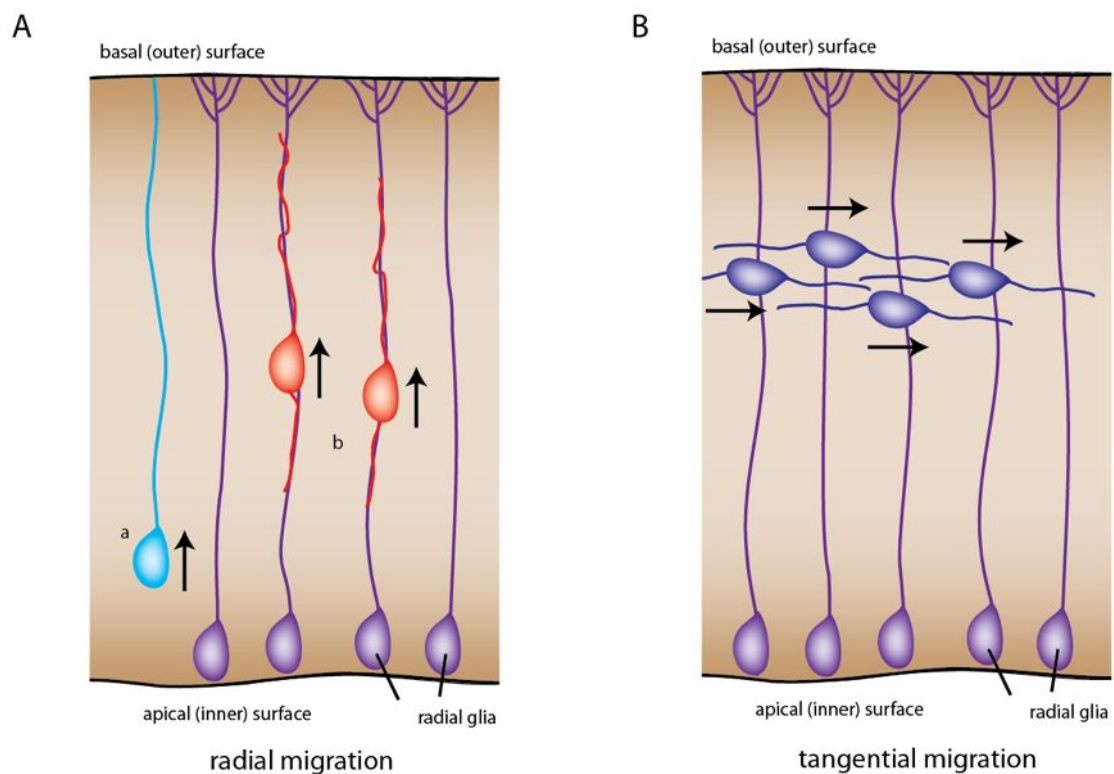


Figure 4 | The two canonical types of neuronal migration. (A) Radially migrating neurons either pull themselves in the direction of the basal surface (a) or use radial glia as a scaffold. (B) Tangentially migrating neurons migrate orthogonal to radial glia. (Figure by C. Kratochwil based on Ghashghaei et al., 2007)

For radial migration (e.g. cortical projection neurons migrate radially) radial glia are used as a scaffold for differentiating cells to migrate to the correct position. Radial glia extend from the basal side (the ventricular side) to the apical side (the outer side)

and therefore allow neurons to migrate “radially” and to position in different positions on the basal-apical axis. This kind of migration is the main mechanism to generate layered structures like the neocortex or the cerebellum. Herby, different cells (with different fates) migrate to different layers at different developmental stages.

A second way of migration is tangential migration. Hereby, neurons migrate tangentially to the surface of the brain. Well-studied examples are the telencephalic interneurons (Marín and Rubenstein, 2001) or the neurons of the precerebellar system (Altman and Bayer, 1987a; Altman and Bayer, 1987b). The development of precerebellar system will be discussed in detail in chapter 1.4.2. Tangential migration can be also followed by radial migration (Ono et al., 2004), which gives the neurons their final position on the basal-apical axis.

1.1.3 Development of neuronal circuitry

One of the major challenges for a developing brain is that its different parts and cells have to be connected in a way that all basal function that are needed for survival are given to a newborn animal, but that it maintains at the same time a high degree of plasticity to help the organism adapting to changing environments. For this the balance between fixed, “hardwired” connections and plastic connections that can be weakened or strengthened during learning processes has to be tightly regulated.

When the axonal process starts to grow out of a differentiated neuron, the tip of the axon forms a dynamic structure of multiple extensions called growth cone. This growth cone is guided to its target (the neurons, it will connect to) by extracting spatial information from the migratory environment. This process is called axon guidance. Spatial cues can either attract or repulse the growth cone or lead to a collapse of the growth cone resulting in growth arrest (**Figure 5**, Tessier-Lavigne and Goodman, 1996). These interactions can be mediated by a direct contact to other cells (contact-mediated repulsion/attraction) or by diffusible factors (long-range chemoattraction/ chemorepulsion) (Chen and Cheng, 2009). Usually, axon guidance is a multi-step process with intermediate targets (guideposts) and involves many signaling molecules. The guidance of an axon is very comparable to cell migration,

with the only difference that in cell migration also the cell body migrates. Therefore it is not surprising, that in neuronal migration similar strategies and guidance factors are used to lead the cell to its final position.

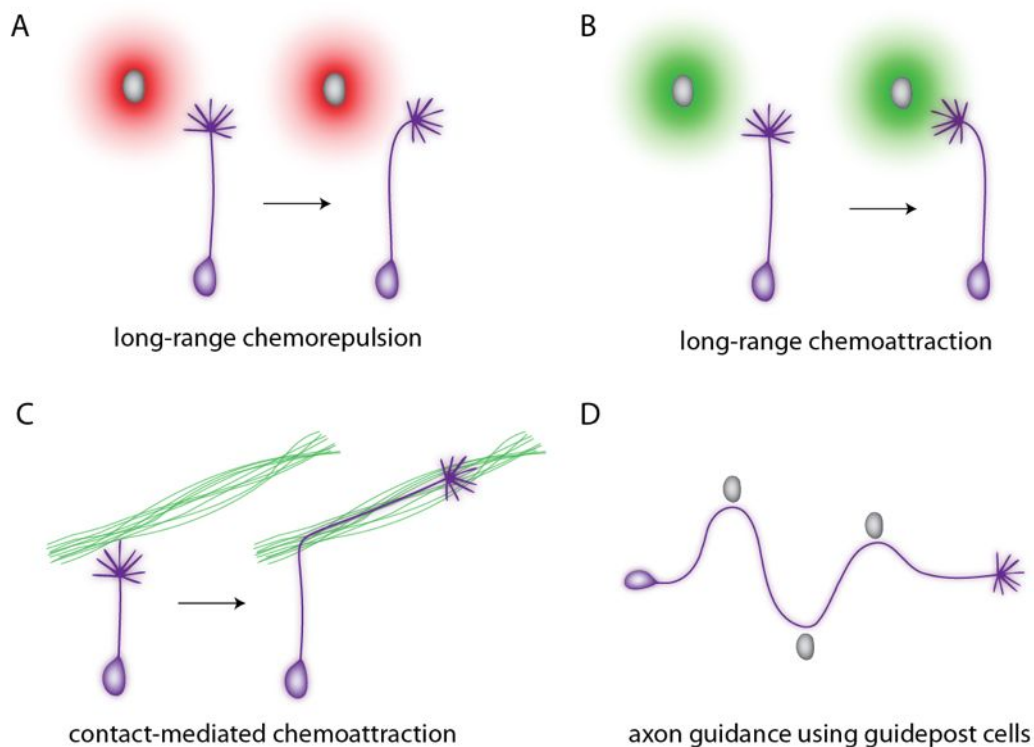


Figure 5 | Mechanisms of axon guidance. (A-C) If cells secrete diffusible molecules and corresponding receptors are expressed at the growth cone, the axon growth can be repelled from the source (A) or attracted to the source (B). Contact-mediated attraction or repulsion is realized by proteins expressed on the surface of a cell, cell extensions (e.g. axons) or the extracellular matrix. Herby the physical contact is necessary to mediate repulsion or attraction (C). (D) Complex axon pathways can be explained by the consecutive action of local guidance cues. Very often these cues are first attractive and become repulsive (due to a change of the responsiveness of the cell), when the growth cone reached the guidepost. (Figure by C. Kratochwil)

Long-range signaling molecules guiding cells or axons are usually secreted proteins that act as ligands and bind to receptors on the guided cell or axon. Receptor-Ligand complexes can trigger intercellular responses that can be local and influence e.g. the cytoskeleton (what can change the growth direction) or affect the whole cell (e.g. expression of new receptors). In general the cell-responses are concentration-dependent in a certain range.

In case of contact-mediated repulsion or attraction both receptor and ligand are connected to a membrane (or in case of the ligand at least anchored in the extracellular matrix; parts of the extracellular matrix can also serve themselves as “ligands”, like e.g. laminins (attraction) or tenascins (repulsion)). Contact-mediated attraction is also used to ease the guidance of later developing axonal projections that can simply follow a preexisting axonal scaffold (pioneer axons).

For the establishment of complex connectivity different mechanisms have been elucidated in the last two decades (**Figure 6**, Luo and Flanagan, 2007; Shen and Scheiffele, 2010). The simplest way to connect one cell to another is to make a point-to-point connectivity, by having a unique match between projecting cell(s) and target cell(s). This system is for example used in the olfactory system (Murthy, 2011; Wang et al., 1998). The connection can be enforced by mutual attraction or/and repulsion from other cells (**Figure 6**, B).

Many parts of the brain are organized in a topographic manner, maintaining the spatial order of the input-cells (or receptors) at higher orders of processing. These topographic neuronal maps can be found e.g. in the somatosensory system (somatotopy), the visual system (retinotopy) and in the auditory system (tonotopy). In these neuronal systems a more parsimonious mechanism sorts the axonal input. Similar as during cell-type specification (1.1.1) morphogenetic gradients are used as a way to sort axonal inputs on a spatial axis. By using inversed gradients of receptor and ligand on projecting cells and target cells, projections with high levels of a receptor mediating attraction stop already at low ligand concentrations, while projections with low levels are searching for higher ligand concentrations (**Figure 6**, F). By the combination of two different receptor-ligand systems a 2-dimensional topographic map can be generated.

Projections can also have a divergent (if e.g. a sensory feature is processed in different brain regions) or convergent character (e.g. the registration of movement in the visual system), which adds a further level of complexity (**Figure 6**, C-D).

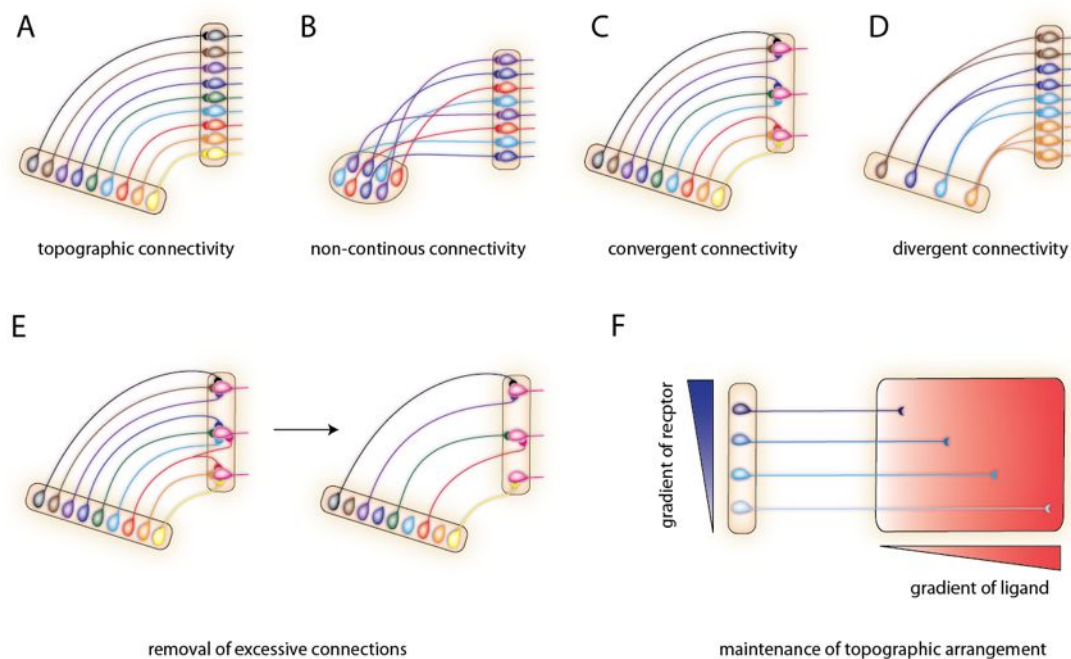


Figure 6 | Different types of neuronal network connectivity and involved mechanisms. (A) Many networks in the brain are organized in a topographic manner. The arrangement of cells processing same information is maintained at the next level. (B) Other projections are more complex, breaking up the continuity. (C-D) Projections from many cells can converge on a few cells (C) or diverge from one cell on many (D). (E) Most neuronal networks are redefined during development by removing unwanted input. (F) The current understanding of the development of topographic circuitry (A) is, that an interplay of receptors expressed in a graded manner in projecting cell and matches onto a tissue, where the ligand is presented in a graded fashion. Growth cones with many receptors stop already at low levels of ligand, while those with a few receptors can continue growing to higher ligand concentrations. (Figure by C. Kratochwil)

A general feature during nervous system development is that usually an excess of neurons is generated and that axonal innervation tends to be broader at the beginning. Later on, this overabundance of cells and projections is reduced sparing only cells and connections that are needed. This process of generating an excess of connectivity that is redefined later on obviously requires more resources (because more axons are generated than needed), but increases on the other hand the plasticity of the neuronal connectivity during development and evolution (because many different projections patterns are possible; **Figure 6, E**).

1.1.4 Classical examples of guidance factors: Netrins and Robos

1.1.4.1 *Netrin / DCC / Unc5*

Netrins are guidance cues that trigger attraction or repulsion in migrating cells (Alcántara et al., 2000; Yee et al., 1999) or during axon guidance (Kennedy et al., 1994). The bifunctional role as attractive and repulsive guidance cue can be explained by the existence of two receptors: DCC (just one homolog in vertebrates) and Unc5 (4 homologs: Unc5a-d in vertebrates). DCC and Unc5 are able to build homodimers or heterodimers. Solely homodimers of DCC mediate attraction (Huber et al., 2003; Round and Stein, 2007), while all other combinations mediate repulsion. *Netrin* is typically expressed at the midline (floor plate) of spinal cord and brain and attracts fibers from dorsal areas expressing DCC receptors.

1.1.4.2 *Robo / Slit*

Robo receptors and their Slit ligands are a further ligand-receptor pairing with crucial roles during nervous system development as well as in a variety of other developmental processes (Chédotal, 2007; Ypsilanti et al., 2010). Robos were discovered in *Drosophila*, while screening for molecules involved in axon guidance (Seeger et al., 1993). Slits were identified as ligands for Robo receptors and it could be shown that they have a conserved role for repulsion during axon guidance (Brose et al., 1999). Robo-1 and Robo-2 are strongly repelled by tissues expressing Slit-1 and/or Slit-2. Robo-3 (also called Rig-1) is itself not mediating repulsion, but negatively regulates Robo responsiveness to Slits (Sabatier et al., 2004). *Robo-1* and *Robo-2* are especially expressed in ipsilateral projecting neurons since they are repelled from the midline, a strong source of Slits. Contralaterally projecting neurons express *Robo3*, which negatively regulates Slit responsiveness. After the growth cone has crossed the midline, *Robo3* expression is shut down and Robo-1 and/or Robo-2 expels the axon out of the midline (Sabatier et al., 2004).

In combination with Netrin/DCC/Unc5 as well as other axon guidance molecules the behavior and positioning of axonal tracts and terminals can be tightly regulated.

1.2 Mechanisms of transcriptional regulation in nervous system development

Hindbrain and spinal cord are set up as an assortment of different neuronal pools and nuclei that share similar properties. The phenotype of cells is determined by guidance factors, which have been discussed in the last chapter, defining where the cells of a certain pool project, but also other factors, which define dendrite shape, input and other cell-architectural attributes. Still, these proteins that are finally realizing the cell fate, have to be orchestrated by transcriptional regulation as well as epigenetic regulation (see 1.3). The understanding of this process has been broadened extensively in the last decade by work (mainly on *Hox* transcription factors) in the hindbrain (Geisen et al., 2008; Narita and Rijli, 2009; Oury and Rijli, 2007) and spinal cord (Dasen et al., 2003; Dasen et al., 2005; di Sanguinetto et al., 2008; Jessell, 2000; Philippidou et al., 2012; Vrieseling and Arber, 2006).

1.3 Epigenetic regulation of developmental processes

In the last 10-15 years it has become more and more obvious, that there are more functionally relevant modifications of chromatin that are distinct from the pure nucleotide sequence. The expression of genes, the accessibility of the DNA, the structure of the whole chromatin can be modified by changing the state of the DNA itself, by methylation of nucleotides (adenine or cytosine) or by the modification of histones that help to pack the DNA in structures called nucleosomes. All modifications not based on changes in DNA sequence are referred to as epigenetics (Bird, 2007; Francis and Kingston, 2001).

1.3.1 The Polycomb complex

Polycomb is a complex of central importance for epigenetic regulations mediating repression. In vertebrates different complexes exist called Polycomb Repressive Complex 1 (PRC1), PRC2, PRC3 and PRC4. These complexes contain different protein components at different times. PRC1 and PRC2 were the first to be discovered and got the most attention in recent publications. Npcd, Cbx2/4/6/7/8, Phc1-3, Bmi1, Me118 and Ring1A/1B are considered as core components of the mammalian PRC1,

Ezh1/2, Eed, Suz12 and RbAp46/48 as core components of the mammalian PRC2 (Bantignies and Cavalli, 2006; Schwartz and Pirrotta, 2007, **Figure 7**).

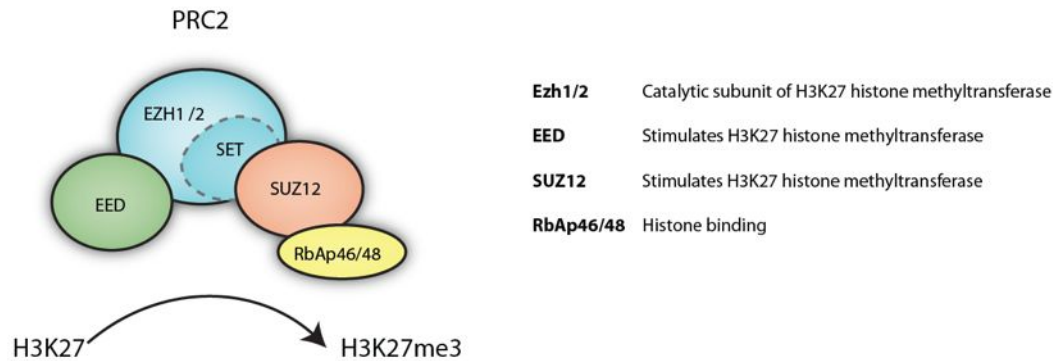


Figure 7 | The polycomb repressive complex 2 (PRC2). PRC2 is composed of four core units: Ezh1/2, EED, SUZ12 and RbAP46/48. Together they catalyze H3K27 trimethylation. (Figure by C. Kratochwil)

Polycomb trimethylates histone H3 on lysine 27 (H3K27me3) (**Figure 7**). Methylation at this residue is considered as a hallmark of transcriptionally silent chromatin (Schwartz and Pirrotta, 2007). Polycomb-mediated repression has been shown to be involved in the control of stem cell maintenance (Boyer et al., 2006; Chamberlain et al., 2008) and early events of lineage specification (Su et al., 2003; Terranova et al., 2008) as well as in tissue-specific stem cells in adults (Ezhkova et al., 2009) and cancer (Karanikolas et al., 2009; Leung et al., 2004; Suvà et al., 2009). Also the importance of polycomb members of PRC1 (Leung et al., 2004) and PRC2 (Hirabayashi et al., 2009; Pereira et al., 2010; Wang et al., 2010) for nervous system development has been shown recently.

The first targets of polycomb that have been described in *Drosophila* were *Hox* genes. Mutants for polycomb showed homeotic transformations suggesting that *Hox* genes become activated in body regions anteriorly of their normal expression domain (Jürgens, 1985; Moazed and O'Farrell, 1992; Struhl, 1981). Indeed it could be shown that two classes of proteins are acting to maintain and stabilize expression patterns of *Hox* genes on an epigenetic level: The polycomb group of proteins, repressing *Hox* genes anteriorly and the trithorax group of proteins keeping them stably activated in their expression domains (Simon and Tamkun, 2002).

While the actions of the trithorax proteins are not well understood in vertebrates, polycomb-mediated regulation seems to be more similar between invertebrates as *Drosophila* and vertebrates. This includes the tight control of *hox* gene expression (Soshnikova and Duboule, 2009a; Soshnikova and Duboule, 2009b), the control of A-P patterning (Sing et al., 2009; Wyngaarden et al., 2011) as well as their target elements, the Polycomb responsive elements (PREs) (Sing et al., 2009).

Especially *Ezh2* has been found to be pivotal for the functionality of PRC2 since it contains the domain (SET-domain) catalyzing the trimethylation of H3K27.

1.4 The precerebellar system

1.4.1 Function

The precerebellar system is located in the hindbrain and receives its major inputs from the cerebral cortex and the spinal cord. The neuron assemblies (nuclei) of the precerebellar system have therefore often been considered as a synaptic relay station between cortex/spinal cord and cerebellum. The precerebellar system constitutes of five bilaterally symmetric nuclei including basal pontine nuclei (PN), reticulotegmental nuclei (RTN), lateral reticular nuclei (LRN), external cuneate nuclei (ECN) and inferior olivary nuclei (ION). The RTN are located just dorsally of the PN and both share similarities in their development, connectivity and function (**Figure 8, B**).

The PN are hypothesized to adapt cortical signals for the use of the cerebellum (Schwarz and Thier, 1999) and serve as a first integrator of the information from different cortical regions including sensory cortices and motor cortex. The PN mainly receive projections from layer 5 of the cortex, which constitutes a major subcortical projection as a part of the cortico-fugal / cortico-spinal tract. The efferents of the PN project over the middle cerebellar peduncle to the ipsi- and contralateral side of the cerebellum. Ponto-cerebellar fibers terminate as mossy fibers in the granular cell layer (**Figure 8, A**).

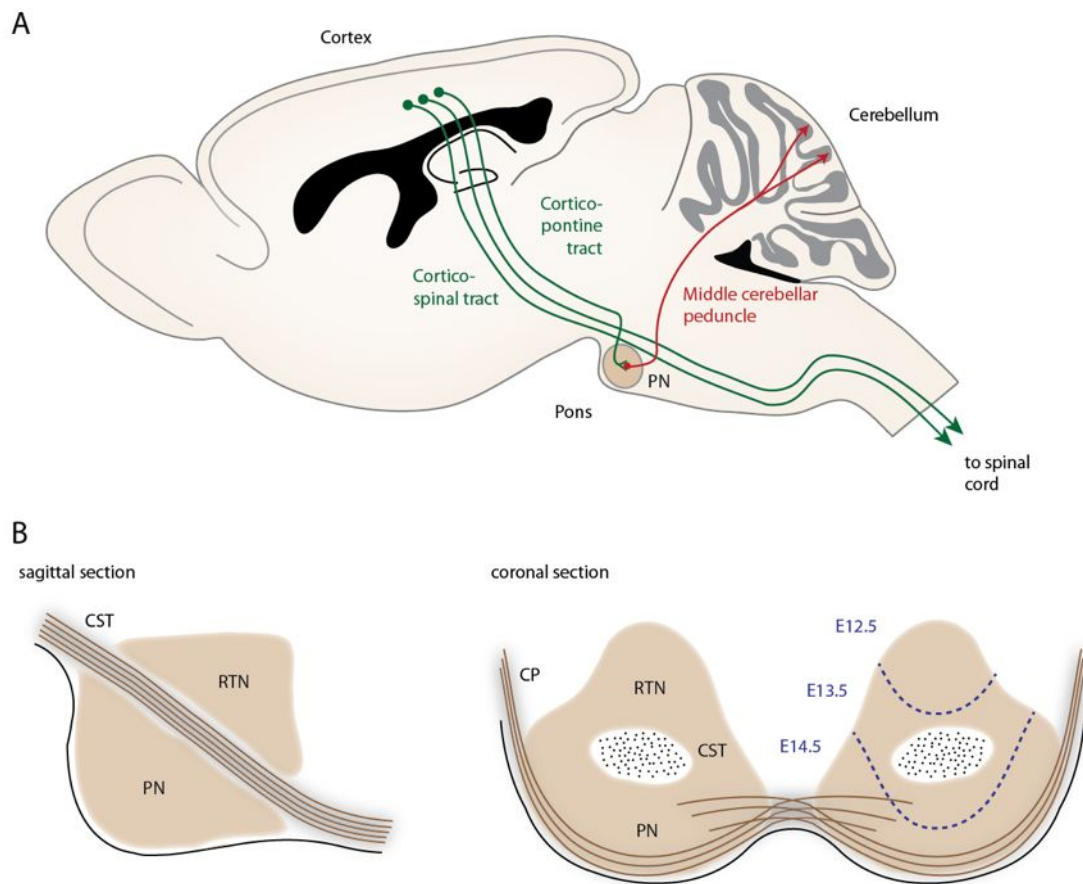


Figure 8 | Pontine Nuclei connectivity and anatomy. (A) The pontine nuclei are the main connection between neocortex and cerebellum. (B) The pontine nuclei can be divided in the basal pontine nuclei (PN) and reticulotegmental nucleus (RTN), both projecting to the cerebellum over the cerebellar peduncle (CP). Birthdays of PN and RTN cells are indicated on the coronal section scheme. (Figure by C. Kratochwil)

Simplified models of PN function suggest, that PN neurons receive a blind-copy of motor commands (a prediction of a movement) sent from cortex to spinal cord and processes this for the use of the cerebellum. Sensory feedback about the execution and degree of success are processed over spinal cord and inferior olive to the cerebellum. In the cerebellum motor plan and actual performance are compared and eventual arising discrepancies are fed back to the cortex to modify further motor plans (Grimaldi and Manto, 2011; Manto, 2009). This can also be understood as the basis of more complex motor behaviors, where sequences of muscle precise muscle contractions have to be executed as well as the basis for motor learning, because cerebellar circuits intrinsically have a very high degree of plasticity.

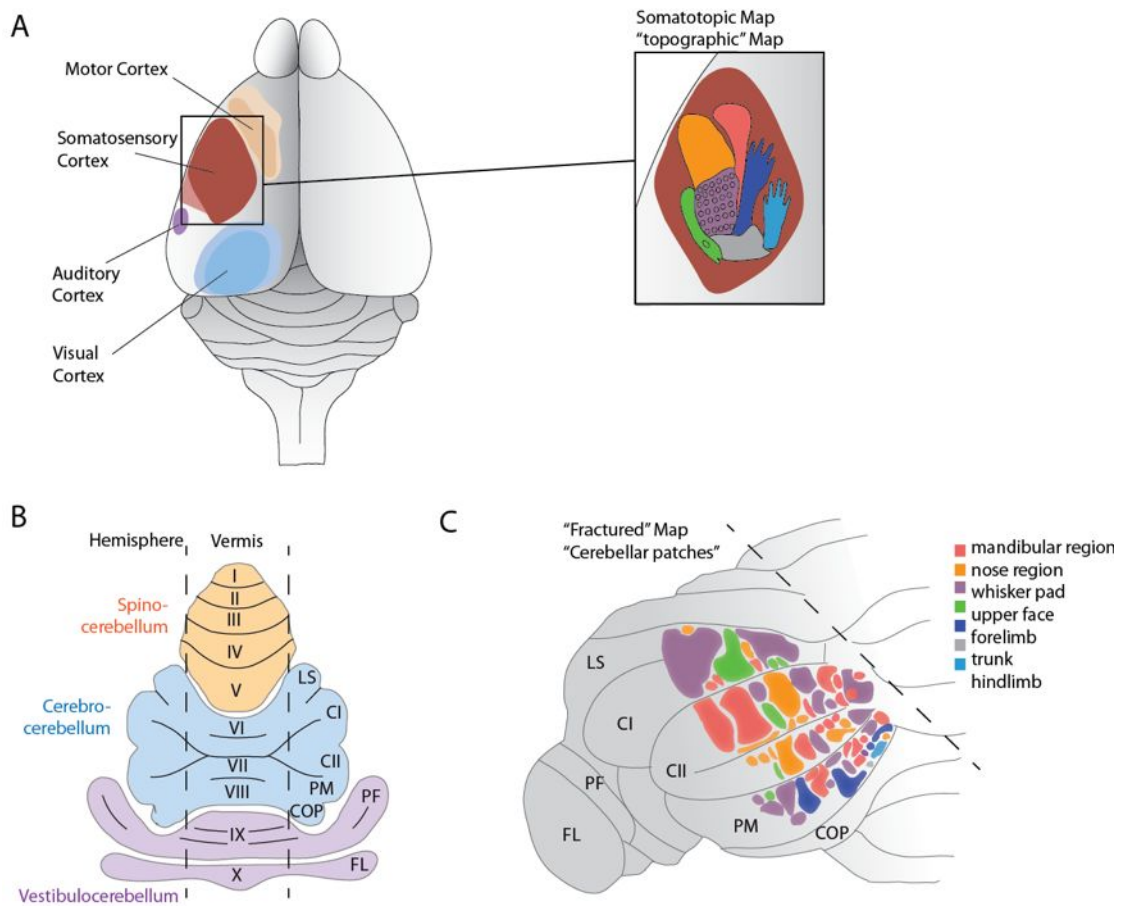


Figure 9 | Topographical representation in cortex and cerebellum. (A-C) Informations from different sensory modalities are processed differently in cortex (A) and cerebellum (B-C). While in the cortex information from vision, audition and somatosensation clearly possess separated processing areas, the cerebellum has a more "fractured" representation of different modalities (C). Still the cerebellum has been classically divided into spinocerebellum, cerebrocerebellum as well as vestibulocerebellum, since experiments suggest an enrichment of input in these regions (B). (Figure by C. Kratochwil)

Beside the functions raised in the model by Manto et al. PN and cerebellum have further equally complex functions in other behaviors. The PN have been shown to be involved in diverse other functions including e.g. saccadic eye movements or visually directed movements (Krauzlis, 2004; Strick et al., 2009; Tziridis et al., 2011).

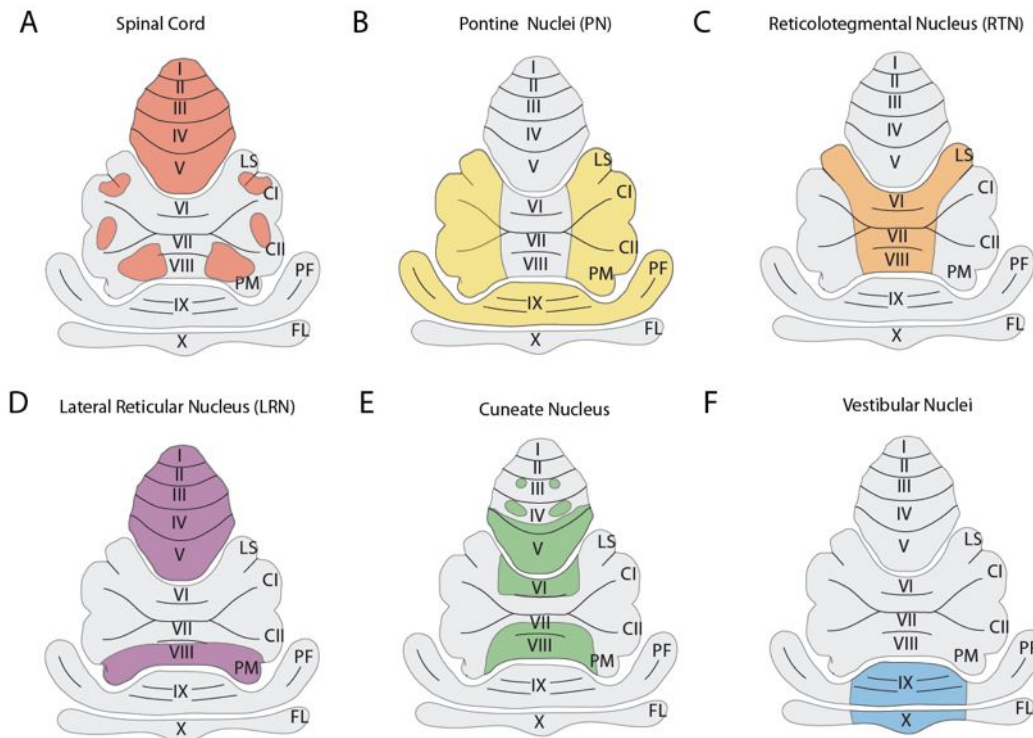


Figure 10 | Input topography in the cerebellum. (A-F) The main inputs to the cerebellum and their topographic arrangement. Spinal cord innervation and nuclei, which itself get mainly spinal cord inputs (Lateral Reticular Nucleus, Cuneate Nucleus) project mainly on the anterior vermis (A, D-E). PN fibers are the main input to the cerebellar hemispheres (B), while RTN has a bias to the vermis of lobes V-VIII. Lobes IX and X get mainly input from vestibular ganglion and nuclei (F). (Figure by C. Kratochwil after Altman and Bayer, 1997)

A somatotopic or at least partially topographic organization could be shown for the pathway from cerebral cortex to pons (Brodal, 1968; Mihailoff et al., 1982) and from pons to the cerebellum (Burne et al., 1978; Hoddevik, 1975). Although the projections are governed by a topographical pattern, convergent as well as divergent projections can be found (Mihailoff, 1983; Nikundiwe et al., 1994a). While the rough topography of corticospinal and corticopontine projections is mainly accepted and has been described in detail (Leergaard and Bjaalie, 2007; Leergaard et al., 2006), the description of connectivity to the cerebellum and its eventually topographic or more non-continuous and fractured character has been controversially discussed for the last 100 years (Apps and Hawkes, 2009). The different input nuclei to the cerebellum have partly overlapping termination zones with a strong bias of LRN and spinal cord

projections to the anterior lobes I-V and vestibular nuclei to lobes IX and X (**Figure 10** and Altman and Bayer, 1997)

1.4.2 Development

PN neurons originate from the rhombomere (r)6 to pseudorhombomere 8 (r8) derived lower rhombic lip, an embryonic proliferative neuroepithelium that lies in the dorsal rhombencephalon and surrounds the alar recess of the fourth ventricle (Altman and Bayer, 1987b). All precerebellar neurons except the inferior olive are derived from a defined dorso-ventral part of the rhombic lip specified by the expression of the transcription factor *Math1*. Inferior olive neurons derive from progenitors negative for *Math1*, but positive for *Ptf1a*, which are located ventrally of the *Math1*-domain. Precerebellar neurons are only generated from the lower rhombic lip. More anterior *Math1*-positive cells generate cells of the auditory system (r2/3-r5) or the granule cells of the cerebellum (r1) (Ray and Dymecki, 2009; Rodriguez and Dymecki, 2000; Wang et al., 2005; Wingate, 2005).

The specification of different nuclei from the same dorso-ventral and anterior-posterior domain is achieved by the generation of different nuclei at different times. ECN neurons are generated first, then LRN and RTN. PN neurons are the latest that are generated from the lower rhombic lip (Rodriguez and Dymecki, 2000, **Figure 11**). It can be postulated, that the migration and differentiation into different nuclei is due to a combination of extrinsic changes (inside the cells) and extrinsic changes (in the environment) of expression profiles of factors as e.g. guidance molecules.

From the rhombic lip, PN neurons undertake a long-distance tangential migration (via the anterior extramural stream (AES)) until they reach their final destination on the ventral surface of r3 and r4 (Geisen et al., 2008, **Figure 12**).

Many guidance molecules (Di Meglio et al., 2008; Geisen et al., 2008; Marillat et al., 2004; Qu et al., 2006; Yee et al., 1999; Zhu et al., 2009) as well as transcription factors (Engelkamp et al., 1999; Geisen et al., 2008; Kumbasar et al., 2009) have been shown to regulate the migration of pontine neurons and other precerebellar neurons (**Figure 13**).

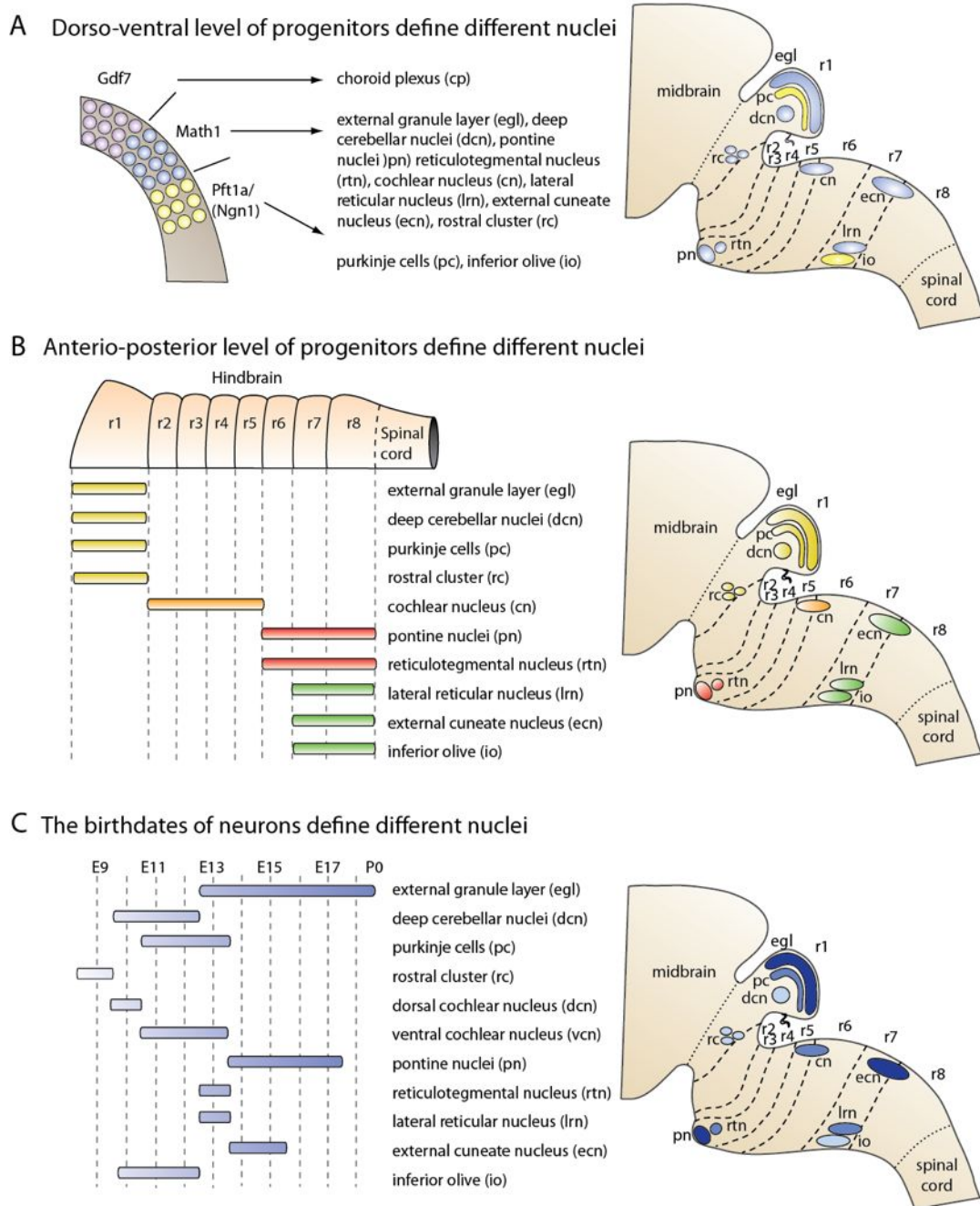


Figure 11 | The identity of hindbrain nuclei is defined on a 3-dimensional chrono-spatial axis. (A) The dorso-ventral axis is dorsally divided in 3 domains (Gdf7, Math1 and Pft1a) giving cells different specifications. **(B)** The hindbrain is patterned in rhombomeres, giving rise to different nuclei at different anterior-posterior levels. **(C)** At different time points, different nuclei are generated (even from the same spatial coordinates). (Figure by C. Kratochwil after Altman and Bayer, 1997; Wang et al., 2005; Wingate, 2005)

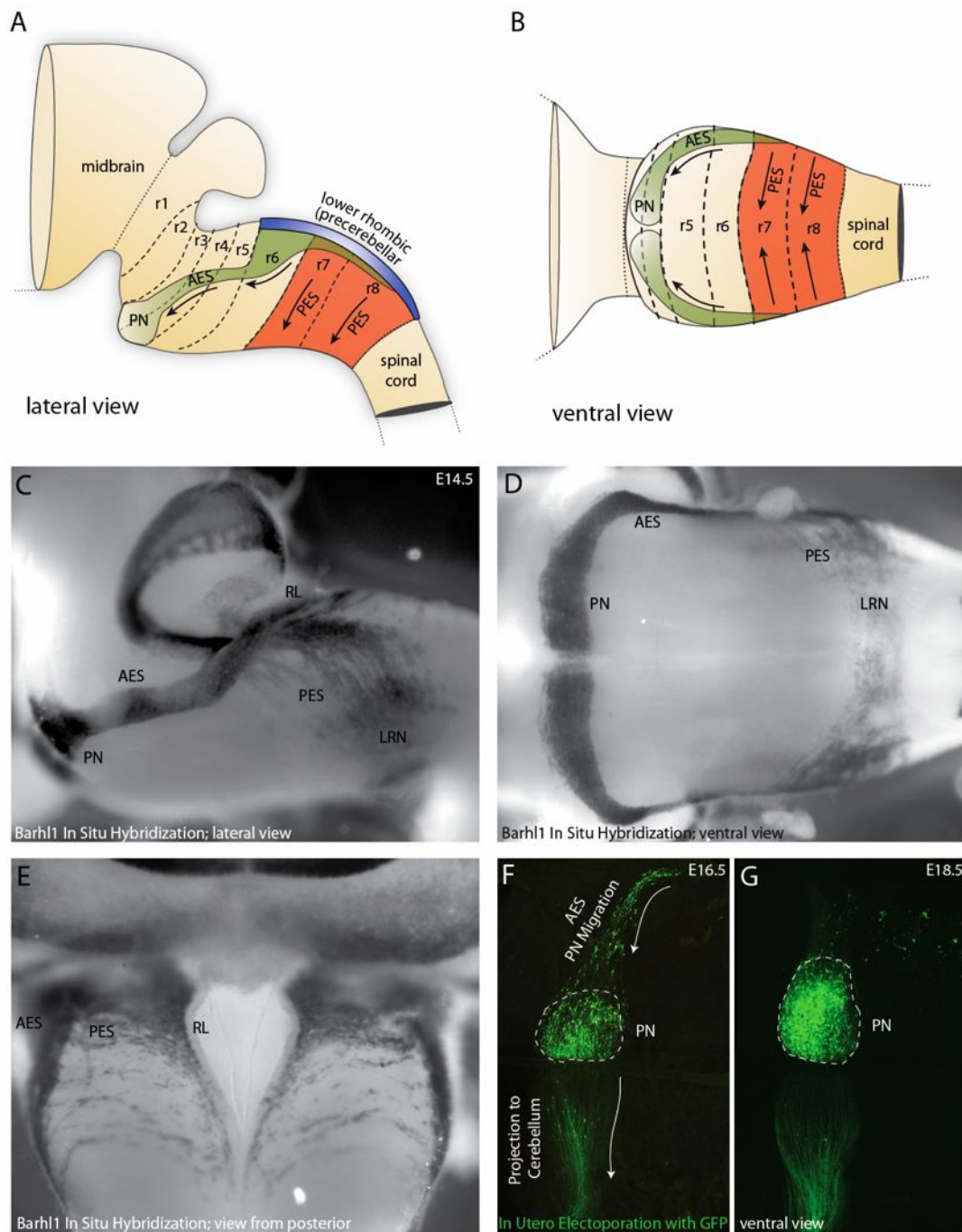


Figure 12 | Migration pathways of pontine (PN) and lateral reticular nucleus (LRN) neurons. (A-G) Migration is shown in schematic illustrations (A,B) and by *in situ* hybridizations (C-E) and *in utero* electroporation (F,G). Pontine neurons (from rhombomere 6 (r6) to r8) from the precerebellar rhombic lip (RL) take an anterior migratory pathway via the anterior extramural stream (AES), while LRN neurons from r7 to r8 take a more posterior migratory route, the posterior extramural stream (PES). (Illustrations and Data by C. Kratochwil (A-E) and T. di Meglio (F-G))

It has been shown that the PN, when they have arrived at r3/4 form regular concentric rings in an inside-out sequence around PN neurons, which have already settled down (Altman and Bayer, 1987b). Hereby neurons that have been generated first, build the inner core of the PN, while the neurons generated later build the outer shells (Altman and Bayer, 1987b). Interestingly, time point, order and origin of innervation by cortical afferents is correlated to the inside-out position inside the PN and therefore also to their time-point of generation, a phenomenon that has been denoted as chrono-architectonic hypothesis of the corticopontine projection (Leergaard et al., 1995).

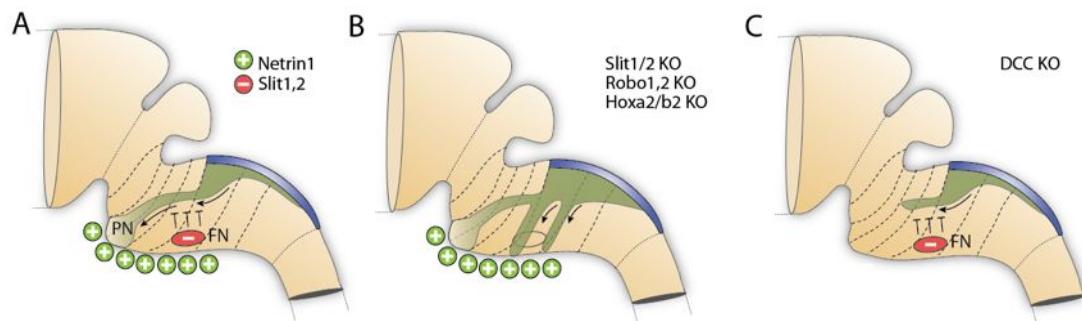


Figure 13 | Examples of mutation affecting pontine migration. (A-C) The main determinants of pontine migration are attractive signals (Netrin1/Dcc signaling) from the midline that guide neurons to the ventral surface of r3/r4. A premature attraction to the midline is inhibited by repressive signals (Slit/Robo signaling) coming from the facial nucleus (FN) in rhombomere 6 (A). Mutations affecting Robo/Slit signaling induce ectopic migration in more posterior positions (B), while knockout of the Netrin1-receptor dcc result in a dorsal migration arrest (C). (Figure by C. Kratochwil)

1.5 The trigeminal system

The trigeminal nerve is the fifth cranial nerve and has a sensory as well as a motor component. Sensory fibers relay sensory information from face, while motor fibers control the muscles of the jaw, essential for chewing, biting or swallowing. The trigeminal nerve is divided into 3 branches: the ophthalmic branch (covering forehead, upper nose, area around the eyes), the maxillary branch (covering the upper jaw, including the whiskers in mice) and the mandibular branch (covering lower jaw). All relay sensory information, while the mandibular branch contains also motor fibers. All sensory information is relayed by the trigeminal ganglion, which is

composed of pseudounipolar neurons innervating at the same time the face and project via the fifth cranial nerve into the hindbrain (Erzurumlu et al., 2010).

The main targets of the sensory part are neurons of the mesencephalic (Me5), principal (Pr5), spinal trigeminal nuclei interpolaris, oralis and caudalis (Sp5I, SP50, Sp5C) as well as the paratrigeminal nucleus (Pa5).

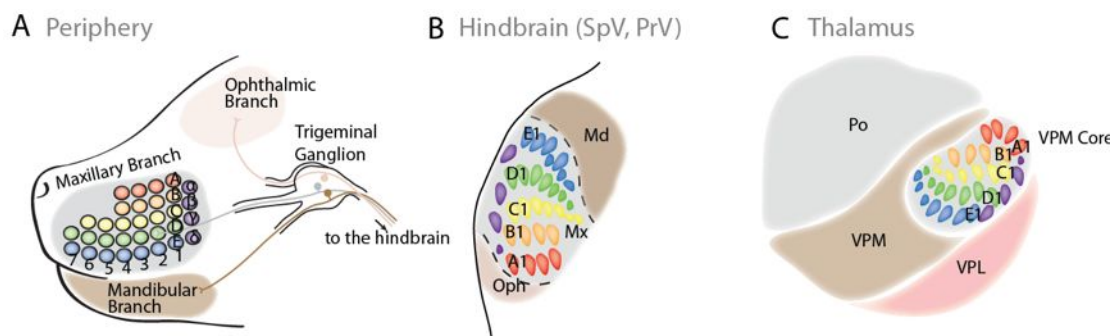


Figure 14 | The topography of the different stations of trigeminal sensory information processing. (A) The trigeminal ganglion gets input over three main branches, the ophthalmic branch (innervating the area around the eyes), the maxillary branch (innervating mainly the whisker pad) and the mandibular branch (innervating the lower jaw). (B) The axons project to the hindbrain innervating different sensory nuclei including the principal sensory trigeminal nucleus (PrV) and spinal sensory trigeminal nucleus. The topographic orientation of the different parts of the face as well as the whiskers itself is hereby maintained. (C) Also in the next stations of processing, thalamus (C) and cortex (not shown), this topographic representation is kept. (Figure by C. Kratochwil)

All neurons of the trigeminal system derive from a specific dorso-ventral domain of the basal plate that express the transcription factor *Drg11*. Neurons of the Pr5 are localized in rhombomere 2 (r2) and 3(r3), neurons of the Sp5 cover rhombomere 4 to pseudorhombomere 8 (Oury et al., 2006).

The trigeminal system as such, is from the organization of its connectivity highly topographic. This has been extensively studied for the sensory input from the whisker pad, for which the relative arrangement of neurons processing information from a certain whisker is maintained from the receptors at the skin to Pr5 and Sp5 in the hindbrain, to the ventral posteromedial nucleus (VPM) of the thalamus and to the barrel cortex in the somatosensory cortex. Due to the high concentration of dendrites and axonal terminals that contain many mitochondria, the areas corresponding to

certain whiskers (because of their 3-dimensional structure called “barrels” in the cortex, barreloids in the VPM and barrelettes in the hindbrain Pr5 (just r3) and Sp5i and Sp5c) can be visualized by cytochrome oxidase staining (CO), an enzymatic staining method labeling mitochondria (Erzurumlu et al., 2010).

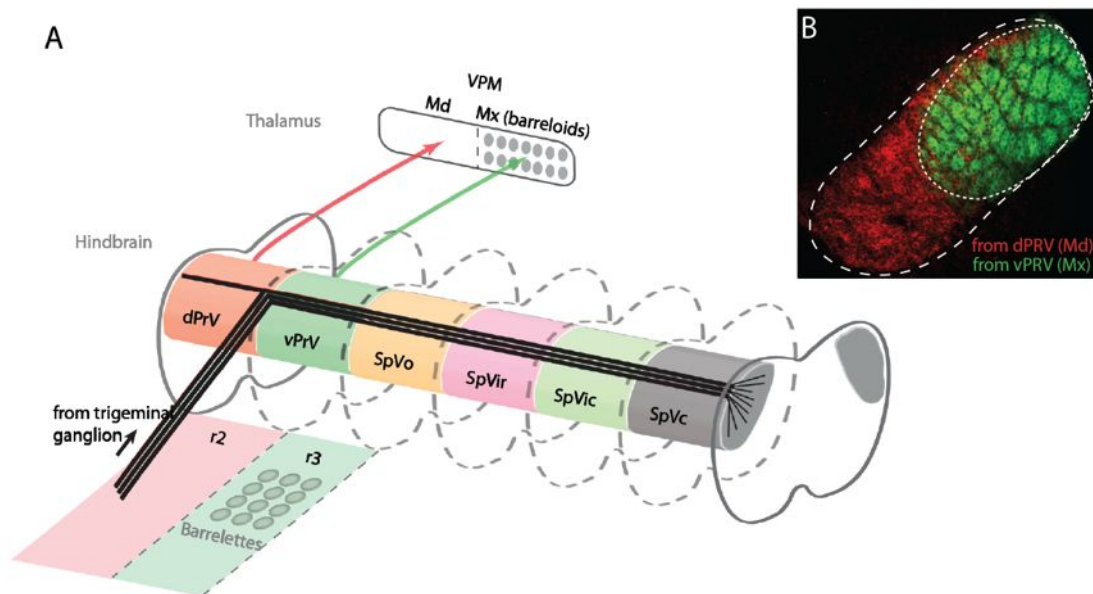


Figure 15 | The principal sensory trigeminal nucleus (PrV) and its thalamic projections. (A) The PrV can be subdivided into a dorsal PrV (dPrV, derived from rhombomere 2) and a ventral PrV (vPrV, derived from rhombomere 3). While the mandibular branch of the trigeminal ganglion only branches in dPrV, vPrV gets selective input from the maxillary branch and forms the so called barrelettes, reflecting the organization of the whisker pad. (B) The projections to the thalamus are segregated. The vPrV projections form barreloids. (Figure and Data by C. Kratochwil)

1.6 Aim of this thesis

The main object of this thesis was to understand how far the origin of cells along the rostro-caudal axis influences the cellular behavior during late processes of neural development and how epigenetic modifiers as Ezh2 regulate the expression of genetic determinants as transcription factors (as e.g. *Hox* genes) and guidance factors (as e.g. Netrin 1 or *Unc5b*) to regulate complex processes as migration and circuit formation. A major focus was hereby on the nuclei of the precerebellar system, especially the pontine nuclei (3.1.1, 3.1.2 and 3.2.1).

To achieve this goal it was important to generate genetic tools that map contributions of different rostral-caudal units, the rhombomeres to understand how rhombomeric subsets behave during neuronal migration and connectivity. Furthermore, tools were needed that allow the analysis of the neuronal connectivity of the pontine nuclei. By conditional knockout of *Ezh2* the focus was to gain a better understanding of cell- and non-cell-autonomous functions of an epigenetic regulator for the distinct steps of precerebellar system development. Our main hypothesis was hereby that progenitors exhibit an internal protomap of further developmental processes as migration and circuit formation (3.1.1).

Furthermore, we wanted to find out if the developmental organization of the PN along the anterior-posterior axis may correlate with patterned axonal input of layer 5 cortical neurons and/or with the projections to the cerebellum. The pontine nuclei are a relay station for the transformation of motor and sensory maps in the cerebral cortex into fractured representations of input in the cerebellar cortex. Little is known about the molecular and cellular mechanisms assembling these complex input-output wiring patterns in the PN. Results of 3.1.1, 3.1.2 and 3.2 suggest that intrinsic pre-mapping of PN from IRL progenitors of distinct rostrocaudal origin may also contribute to organize broad topographic input from distinct cortical areas and potentially also subsets of ponto-cerebellar projections. The cortico-ponto cerebellar connectivity possesses a high degree of divergence and convergence, redistributing permutations of information from cortical sensory and motor input to different areas of the cerebellum. Despite that, there seems to be a biased projection pattern of specific pontine nuclei pools that will be described in the “unpublished results” part (3.2).

Furthermore, knowledge and skills that have been acquired in this project were used for collaborations on the development of the external ear (3.1.4), a structure derived from hindbrain neural crest cells and the analysis of rhombomere specific mutants of the guidance cue *Robo3* in the trigeminal system (3.1.3).

2 Materials and Methods

2.1 Molecular Biology

Plasmid Preparation

Plasmids were prepared using Qiagen Mini-, Midi- or Maxikit. Cultures were incubated over night in 2xYT medium containing an antibiotic according to the plasmid resistance (Ampicillin 100 $\mu\text{g/ml}$; Kanamycin 30 $\mu\text{g/ml}$; Chloramphenicol 35 $\mu\text{g/ml}$). In case of minipreps maximal growth was achieved with 3 ml culture in 15ml falcon tubes. Preps were performed according to the standard protocol. For Mini-Preps of large constructs the Elution buffer was heated on 70 °C to increase yield.

Concentration measurement

Plasmid concentrations were measured using a ND-1000 Spectrophotometer. 2 μl were used to perform the measurement.

Transformation

Transformation was performed using chemical competent cells (Dh5 α (self-produced stock) or Top10 (Invitrogen)). After the plasmid was added to the bacteria, the mix was incubated for 5 minutes on ice, heatshocked in a 42 °C water bath for 45 seconds and then incubated on ice for one further minute. After adding 250 μl medium (Soc or 2xYT) cells were incubated in an incubator shaker for 45 to 90 minutes (500 RPM), depending on amplification characteristics of the plasmid.

BAC Storage:

For long-term storage BACs were maintained as glycerol stocks by adding 0.5 ml glycerol to 0.5 ml culture and storing at -80 °C.

Restriction digests

Restriction digests were performed using restriction enzymes and buffers from New England Biolabs (Beverly, MA, USA). Bovine serum albumin (BSA) end concentration was, if needed, 10 $\mu\text{g/ml}$. The amount of restriction enzyme was calculated according to unit concentration and amount of plasmid. To guarantee a

complete cutting of the plasmids the digestion time was prolonged to two hours and the 3-6 fold amount of enzyme was taken.

For isolation of single fragments, DNA was separated with gel electrophoresis. The band with the expected size was cut out with a scalpel and purified with Qiagen Qiaquick Gel extraction Kit.

Nucleic acid purification

Nucleic acids were purified using phenol-chloroform extraction. The nucleic acid solution is diluted and mixed 1:1 with phenol. After centrifugation the aqueous phase is mixed with a mixture of chloroform and isoamylalcohol. After a further centrifugation step the nucleic acids were precipitated by a 2-fold volume of 100 % Ethanol and 1/10 volume of 3 M NaOAc (pH 4.8). After 30 min at -20 °C and centrifugation the pellet is washed with 1 ml EtOH 70 % centrifuged again. After the pellet has dried it is diluted in an appropriate volume of water.

Alternatively, PCR Purification Kit (Quiagen) or Gel Extraction Kit (Quiagen) was used.

Gel electrophoresis

DNA was analysed by Gel electrophoresis (Agarose Matrix: 0.5-2 % Agarose, 1x TAE Buffer, 0.3 % ethidiumbromide in 1x TAE buffer, along with DNA size standards (2 µl; 1 kB or 100 KB (MBI Fermentas))).

Cloning

Ligation was performed over night at 25 °C in a volume of 10 µl using an insert-vector proportion of 7:1 and T4 DNA Ligase (MBI Fermentas) and the manufacturers buffer.

If vectors were cut with only one restriction enzyme, self ligation was prevented by dephosphorylation using CIAP (calf intestine alkaline phosphatase; MBI Fermentas) or preferentially SAP (Shrimp alkaline phosphatase; MBI Fermentas). In cloning procedures with a lack of compatible sites overhangs have been filled in using T4 polymerase (MBI Fermentas) in 1x T4 Polymerase buffer with 0.2 mM dNTP. Correct cloning was tested by restriction digest or sequencing. For the cloning of linkers or short synthetic DNA pieces oligos were mixed, heated for 10 minutes at 98

°C and slowly cooled down to room temperature. For ligation a vector-insert ratio of 1:7 was used.

Genotyping, Crossing schemes and mouse work

See 3.1.1 and 3.1.5.

2.2 Generation of transgenic mice

Transgenic mice were generated in which *Cre* or *mcherry* is driven by rhombomere-specific enhancers of *Hoxb3* (Yau et al., 2002; *r5-post::Cre*), *Hoxa3* (Manzanares et al., 1999; *r5-6::Cre*), or *Hoxb4* (Gould et al., 1997; *r7post::Cre* and *r7post::mcherry*).

The constructs were created by replacing the LacZ gene of the pKS- β -globin-LacZ vector (BGZ40) (Studer et al., 1996) with a *Cre* cassette (Clontech) or *mcherry* cassette (Clontech) using homologous recombination. Enhancers for *Hoxb3* (*r5-post::Cre*, 483 bp), *Hoxa3* (*r5-6::Cre*, 629 bp), *Hoxb4* (*r7-post::Cre*, 400 bp) as well as a truncated enhancer for *Hoxb3::Cre* (Yau et al., 2002) (*r6::Cre*, 427 bp), which was supposed to have a *r6*-restricted expression, were amplified by PCR from genomic DNA (**Table 1**)

The PCR bands were purified and inserted 5' of the β -globin promoter using restriction sites FsiI and XhoI (*r5-6::Cre*), BglII and PvuII (*r5-post::Cre*, *r7-post::Cre* and *r6::Cre*) and SacII and SpeI (*r7-post::mcherry*), thus generating constructs consisting of an enhancer, a β -globin minimal promoter and *Cre* recombinase /*mcherry* encoding sequence. The constructs were linearized, purified and microinjected into the pronuclei of blastocyst embryos. Founders were identified by PCR and screened at P0 after crossing with *R26RlacZ* animals. 130 animals were genotyped, 26 positively genotyped animals (founders) were screened by crossing to *R26RlacZ* animals (**Table 2**). 3/8 showed the expected recombination pattern at P0 for *r5post::Cre*; 2/8 for *r5-6::Cre*, 1/3 for *r7post::Cre*, 4/8 for *r7post::mcherry* and 0/6 for *r6::Cre*, while the other founders showed no, ubiquitous or ectopic patterns of recombination. See also 3.1.1 and 3.1.5.

<i>r5-post enhancer forward (f)</i>	5' ATATCCGCGG GATCGGAGAGGAGAGGGCAA
<i>r5-post enhancer reverse (r)</i>	5' CGCGACTAGT GATCTCCAAGGTCCCCTTTCA
<i>r56::Cre enhancer f</i>	5' ATATCCGCGG CAACTTGAAAGGGAAGAGCC
<i>r56::Cre enhancer r</i>	5' CGCGACTAGT GATATCAAATAGCAGCGAATCTTC
<i>r7-post::Cre enhancer f</i>	5' ATATCCGCGG TCCTTGGAAGGTATGAATAG
<i>r7-post::Cre enhancer r</i>	5' CGCGACTAGT TGTTACCTCTGAGCCTCTTG
<i>r6::Cre enhancer f</i>	5' ATATCCGCGG TGGTACAATGGGCTTATTGA
<i>r6::Cre enhancer r</i>	5' CGCGACTAGT ATAAATGATCTCCAAGGTCCC

Table 1 | Primers used for amplification of *Hox* enhancers.

Transgene	Injections	Offspring	Genotyping	Tested with Rosa-LacZ
<i>r6post::Cre</i> (AG)	1x	19	8 positives	7/8 confirmed positive (AG-3, AG-7, AG-18, AG-2, AG-8, AG-9, AG-12) 2 maintained (AG-3, AG-12)
<i>r7post::mCherry</i> (AI)	1x	31	8 positives	4/8 confirmed positive (AI-17, AI-8, AI-18, AI-6) 1 maintained (AI-17)
<i>r5-6::Cre</i> (AH)	2x	20+18	8 positives	3/6 confirmed positive (AH-14, AH-35, AH-38) 1 maintained (AH-35)
<i>r7post::Cre</i> (AK)	1x	27	3 positives	1/3 confirmed positive (AK-16) 2 maintained (AK16a, AK16b; two insertions)
„ <i>r6::Cre</i> “ (AJ)	1x	15	6 positives	4/6 confirmed positive (AJ4, AJ8, AJ10, AJ14)
	6x	130 pups	26 positives	19 positive; 6 maintained

Table 2 | Summary of animals screened for transgene insertion and expression.

2.3 Mouse lines

Mouse lines that were used in the thesis are summarized in **Table 3** including references. Most lines are also shown in P7 wholemounts crossed to the conditional R26R^{tdtomato} reporter (**Table 3; Figure 17**).

Mouse Line	Transgene / Knockin	Reference / generated by
<i>AG3::Cre</i>	Transgenic	C. Kratochwil, unpublished
<i>ChAT::Cre</i>	ChAT-IRES-Cre Knockin	(Lowell et al., 2006)
<i>Drg11::Cre</i>	BAC-Transgenic	S. Ducret, unpublished
<i>Emx1::Cre</i>	Emx1-IRES-Cre Knockin	(Gorski et al., 2002)
<i>Hoxa2::Cre</i>	Transgenic	(Di Meglio et al., 2013)
<i>Hoxa5::Cre</i>	BAC-Transgenic	(Di Meglio et al., 2013)
<i>Hoxb5::Cre</i>	BAC-Transgenic	S. Ducret, unpublished
<i>Krox20::Cre</i>	Transgenic	(Voiculescu et al., 2001)
<i>MafB::CreERT2</i>	BAC-Transgenic	(Di Meglio et al., 2013)
<i>Math1::Cre</i>	Transgenic	S. Ducret, unpublished
<i>Pcp2::Cre</i>	Transgenic	(Lewis et al., 2004)
<i>PN::Cre</i>	Transgenic	C. Kratochwil, unpublished
<i>r2::Cre</i>	Transgenic	(Ren et al., 2002)
<i>r4::Cre</i>	Transgenic	(Oury et al., 2006)
<i>r5-6::Cre</i>	Transgenic	(Di Meglio et al., 2013)
<i>r5post::Cre</i>	Transgenic	(Di Meglio et al., 2013)
<i>r7post::Cre</i>	Transgenic	(Di Meglio et al., 2013)
<i>r7post::mcherry</i>	Transgenic	C. Kratochwil, unpublished
<i>Wnt1::Cre</i>	Transgenic	(Danielian et al., 1998)
<i>R26R^{LacZ}</i>	Knockin with lox-stop-lox	(Soriano, 1999)
<i>R26R^{tdTomato}</i>	Knockin with lox-stop-lox	(Madisen et al., 2010)
<i>R26R^{ZsGreen}</i>	Knockin with lox-stop-lox	(Madisen et al., 2010)
<i>Ezh2^{fl/fl}</i>	Conditional knockout	(Puschendorf et al., 2008)
<i>Rig1/Robo3^{fl/fl}</i>	Conditional knockout	(Renier et al., 2010)

Table 3 | List of mouse lines.

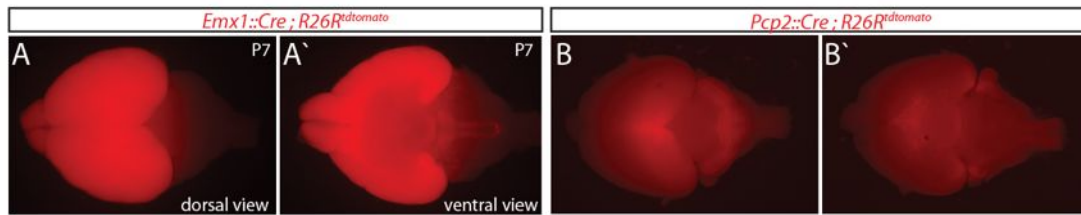
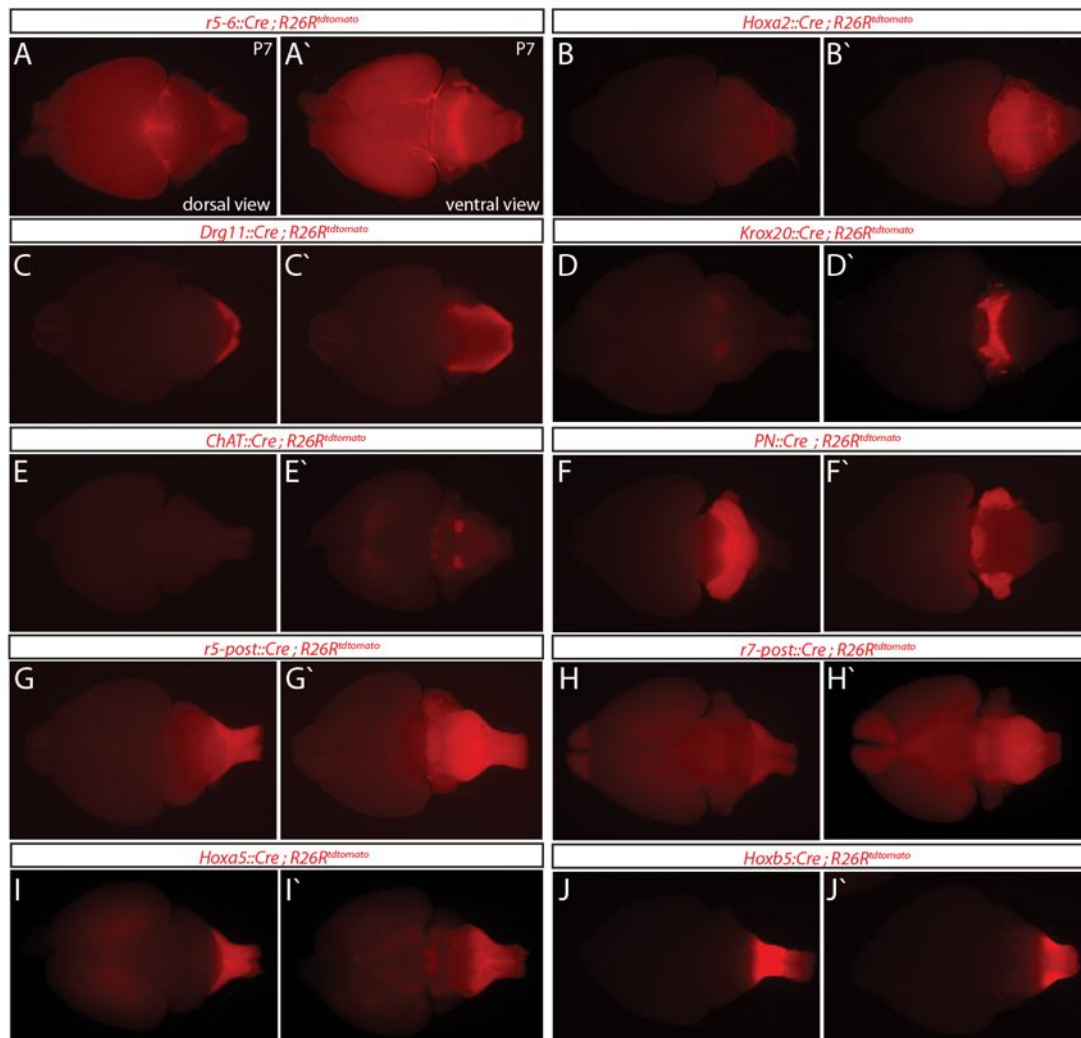


Figure 16 | Transgenic Lines to analyze cortical projections. (A-B') Wholemounts of the two transgenic lines were used to analyze projections to the pontine nuclei seen from dorsal (A, B) and ventral (A', B'): *Emx1::Cre* (A) and *Pcp2::Cre* (B). *Emx1::Cre* labels cortical progenitors and therefore the whole corticospinal tract including the projecting to the pontine. *Pcp2::Cre* is normally a marker for Purkinje cells but labels the medio-posterior part of the cortex.



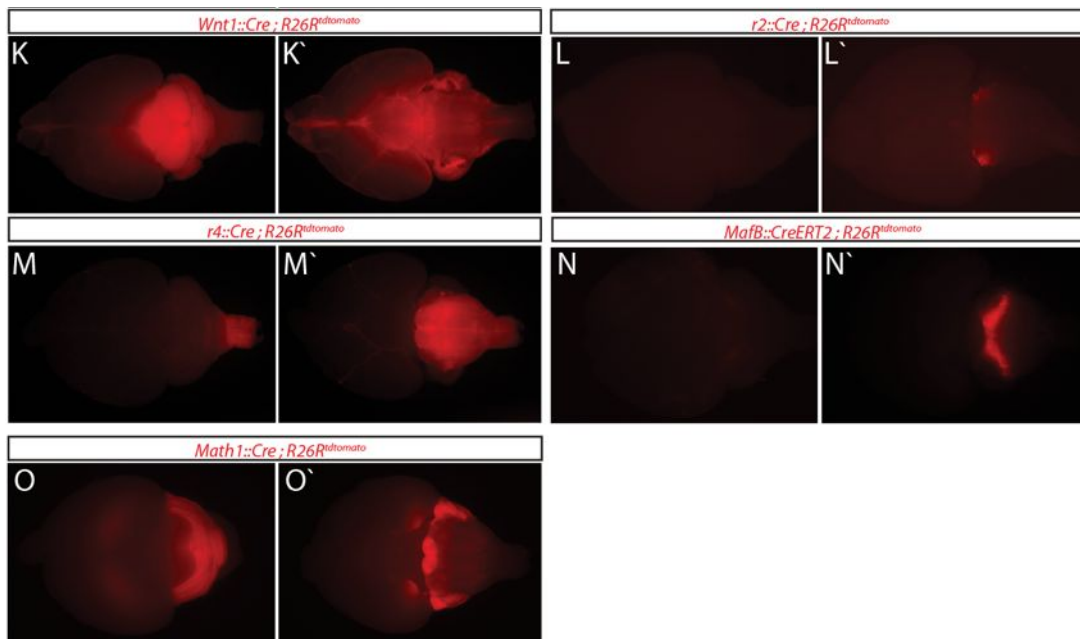


Figure 17 | Transgenic lines to analyze hindbrain connectivity. (A-O) Overview of transgenic lines used and/or tested for this thesis in dorsal (A-O) and ventral views (A'-O').

2.4 Plasmids

Constructs generated for this thesis are listed in **Table 4**.

Construct	Obtained / Generated by
<i>pCAG::GFP</i>	Addgene; (Okada et al., 2007)
<i>pCAG::mcherry</i>	C. Kratochwil, not published
<i>pCAG::Rabies-Glycoprotein</i>	C. Kratochwil, not published
<i>pCAG::flex-GFP</i>	C. Kratochwil, not published
<i>pCAG::flex-Rabies-Glycoprotein</i>	C. Kratochwil, not published
<i>pCAG::Synaptophysin-tdtomato</i>	C. Kratochwil, not published
<i>pCAG::NLS-tdtomato</i>	C. Kratochwil, not published
<i>pCAG::MARCKS-GFP</i>	C. Kratochwil, not published
<i>pCAG::MARCKS-GFP-2A-Cre</i>	C. Kratochwil, not published
<i>pCAG::MARCKS-GFP-2A-NLS-mcherry</i>	C. Kratochwil, not published

Table 4 | List of generated constructs.

2.5 *In utero* electroporation

In utero electroporation was performed on embryos at E13.5 or E14.5 as described in (Di Meglio et al., 2013).

2.6 Neuronal tracing

G-deleted rabies virus vectors encoding mCherry (*SADΔG-mCherry*) or eGFP (*SADΔG-eGFP*) were harvested from BHK-B19G cells (kind gift from E. Callaway) and centrifuged as described previously (Yonehara et al., 2011). Stereotaxic injections of viruses to different areas of neocortex or cerebellum were performed via pulled-glass pipettes using a microinjector (Narishige, IM-9B). Pups were anesthetized by hypothermia, injected at P2 and perfused at P7 (**Figure 18**, A-B). See also 3.1.1.

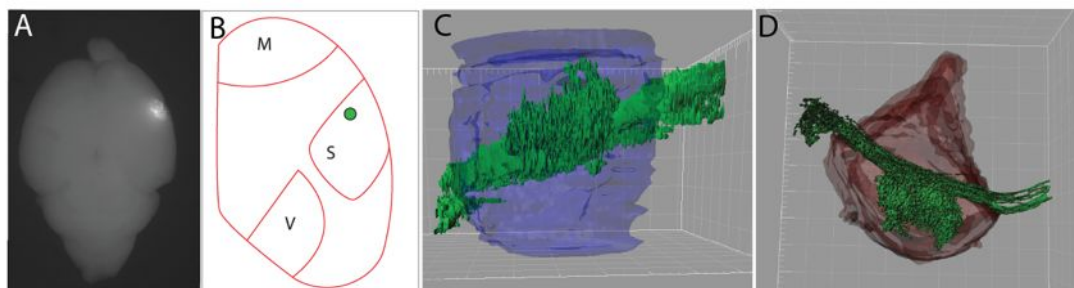


Figure 18 | Example of a Rabies- Δ G-GFP injection into the P7 cortex and reconstruction of the input at the level of the pontine nuclei. (A-C) Pups were injected into the cortex with Rabies- Δ G-GFP or Rabies- Δ G-mcherry; in this case into the somatosensory cortex. (C-D) The corticopontine projection (green) as well as the pontine nuclei itself (blue in C, brown in D) can be 3D-reconstructed from serial sagittal sections as seen here from ventral (C) and lateral (D).

2.7 3D-reconstructions

Pictures of consecutive vibratome sections ($40\ \mu\text{m}$) were taken with a LSM 700 confocal microscope. Sections were aligned using Bitplane AutoAligner 6.0.1 (Manual Alignment). If necessary important structures were artificially labeled in separated channels in Adobe Photoshop CS5.1. The artificially labeled structures as well as the fluorescence channels were transformed into surfaces in Bitplane Imaris 7.5.2 (Surface Area Detail level: $20\text{-}50\ \mu\text{m}$, Thresholding: Absolute Intensity). An example can be seen in (**Figure 18**, C-D).

2.8 Immunostaining and *in situ* hybridization

Immunohistochemistry, X-Gal revelation and *in situ* hybridization is described in detail in (Di Meglio et al., 2013).

2.9 Imaging and Picture Processing

Imaging of fluorescent signals was performed using an Axio imager Z2 upright microscope coupled to a LSM700 Zeiss laser scanning confocal 5x lens (NA 0.25), 10x lens (NA 0.45) or oil/glycerol/water immersion lens 25x (NA 0.8). Stitching of wholemounts (electroporated brains) was performed using Zen Software at postnatal stages, and using Xuvtools (<http://www.xuvtools.org>) at prenatal stages. Chromogenic staining was examined by classical wide-field or binocular microscopy (Nikon).

Whole-section pictures at later stages were performed by stitching a large number of tiles using Zen software.

The algorithm used to create 2-D projection neuron heatmaps of the cortex were created by Aaron Ponti (Imaging Facility Friedrich Miescher Institute) using Matlab (The Math Works).

2.10 Gene expression array and qPCR

To average possible variability between individuals, gene expression analysis was performed on a pool of four $r5-6::Cre;Ezh2^{fl/fl};R26R^{ZsGreen}$ and two control $r5-6::Cre;Ezh2^{fl/+};R26R^{ZsGreen}$ embryos from different litters. In brief, hand-dissected fluorescent tissue from E11.5 embryos were incubated in DMEM (Gibco) / 0.1% trypsin (Gibco) for 8 min at 37 °C. Tissue was then transferred to and rinsed 4 times in DMEM / 10% FBS before mechanical dissociation. Fluorescent r5-6 cells were collected by fluorescence-activated cell sorting. RNA was extracted using the PicoPure RNA Isolation Kit (Applied Biosystems, Calif., USA) and retro-transcribed. Each sample was hybridized to a microarray GeneChip Mouse Gene 1.0. (Affymetrix). Statistical analysis was performed using the R/Bioconductor package limma (the adjusted *P*-value was calculated using a Benjamini-Hochberg correction as implemented in the package). qPCR analysis of selected genes was performed

using the Fast SYBR Green PCR Master Mix (Applied Biosystem) and StepOne Plus real-time PCR.

2.11 Tissue dissection and Micro Chromatin

Immunoprecipitation (microchip)

r5-6-derived ZsGreen⁺ cells were obtained from E16.5 *r5-6::Cre;R26^{ZsGreen}* fetuses by fluorescence-activated cell sorter (FACS). r7-8-derived ZsGreen⁻ cells were collected with the same procedure. Specifically, the r7-8 domain was delimited rostrally by the r5-6 ZsGreen⁺ domain and caudally by the beginning of the spinal chord flexure. Cells were dissociated (trypsin 0.5%/EDTA at 37 °C for 10 minutes), rinsed (DMEM, 10% FBS), filtered and FACS-sorted. After sorting, microChIP was performed as described previously (Dahl and Collas, 2008) with some modifications. Briefly, 30,000 cells in PBS were cross-linked with 1% formaldehyde for 10 min at room temperature and quenched with 125 mM glycine (Merck). Cells were lysed with buffer containing 50 mM Tris-HCl pH 8.0, 10 mM EDTA, 1% SDS (Fluka), and protease inhibitors (Roche). The cell lysate was sonicated in a Diagenode Bioruptor to achieve a mean DNA fragment size of 400 bp. After clarification by centrifugation, the supernatants were diluted with RIPA buffer and incubated with anti-H3K4me3 (Millipore, 17-614) and anti-H3K27me3 (Millipore, 07-449) / protein G-magnetic bead complexes overnight at 4 °C. Ca. 9000 cells were used for each IP. The next day, the beads were washed four times with RIPA buffer and once with TE buffer and the bead-bound complexes incubated with complete elution buffer (20 mM Tris-HCl pH 7.5, 5 mM EDTA, 50 mM NaCl, 1% SDS, 50 mg/mL proteinase K) at 68 °C for DNA elution, cross-link reversal and protein digestion. Finally, DNA from the immunoprecipitates was recovered by phenol-chloroform extraction and ethanol precipitation and analyzed by quantitative real-time PCR. Primers for real-time PCR: *Hoxa2*: forward, 5` CGCCTGCAGTCATTAACAAA; reverse, 5` TCCCACTCTGCTCCTTTCTC; *Hoxa5*: forward, 5` cacccaaatattgggtacga; reverse, 5` cccattagtgcacgagttt. *Hoxb5*: forward, 5` cctccaaatcacccaaatg; reverse 5` agagctgccactgccataat; *Hoxa9*: forward, 5` GGAGGGAGGGGAGTAACAAA; reverse, 5` TCACCTCGCCTAGTTTCTGG; *Hoxc13*: forward, 5`

CCTCCAGGGCTAAGGAGTTC; reverse, 5` GAAAGAGCCCAGTGCTGGTA;
Int3: forward, 5` ATGCCCCTCAGCTATCACAC; reverse, 5`
GGACAGACATCTGCCAAGGT.

2.12 Retinoic acid and tamoxifen treatment

Trans retinoic acid (Sigma) was dissolved in DMSO and administered to pregnant mice by intraperitoneal injection (30 or 60 mg/kg). Tamoxifen was dissolved in corn oil (SIGMA: T-5648) and injected by gavage.

3 Results

3.1 Publications and Manuscripts

3.1.1 “*Ezh2* orchestrates topographic tangential migration and connectivity of precerebellar neurons” (accepted publication; Science 2013)¹

It is an outstanding question, how a seemingly homogenous population of progenitors in the rhombic lip of the murine hindbrain develops into neurons that position on different rostro-caudal and dorso-ventral levels, realizing different input-output patterns of connectivity and subserving different functions. During tangential migration migrating neurons have to respond correctly to environmental cues to reach their final destination. This publication reveals how the epigenetic silencer *Ezh2* controls the restricted expression of transcription factors, guidance cues and receptors to guide migrating precerebellar neurons to their correct position and to give them an intrinsic heterogeneity that can be used by the system to guide topographic map formation from cortex to pontine nuclei.

The study furthermore reveals an unknown role for the Netrin receptor *Unc5b* during neuronal migration, extending the understanding of how the expression of repulsion- and attraction-mediating guidance receptors is tightly regulated to allow stereotypic migratory behavior in tangentially migrating neurons.

¹ Statement of contribution: The publication “*Ezh2* orchestrates topographic tangential migration and connectivity of precerebellar neurons” is a shared co-first authorship with Thomas Di Meglio. I started the project on *Ezh2* and generated and screened most of the Cre-driver lines (except *Hoxa5::Cre* and *MafB::CreERT2*), I discovered the phenotype of the *r5-6::Cre; Ezh2^{fl/fl}* mice and performed all connectivity analysis. I performed all statistical analysis and generated all final figures. Lastly, I contributed to the design of the experiments, the writing of the paper as well as the analysis of migratory phenotypes and *in utero* electroporations.

Ezh2 Orchestrates Topographic Migration and Connectivity of Mouse Precerebellar Neurons

Thomas Di Meglio,^{1*} Claudius F. Kratochwil,^{1,2*} Nathalie Vilain,¹ Alberto Loche,^{1,2} Antonio Vitobello,^{1,2} Keisuke Yonehara,¹ Steven M. Hrycaj,³ Botond Roska,^{1,2} Antoine H. F. M. Peters,^{1,2} Anne Eichmann,^{3,4} Deneen Wellik,⁵ Sebastien Ducret,¹ Filippo M. Rijli^{1,2†}

We investigated the role of histone methyltransferase *Ezh2* in tangential migration of mouse precerebellar pontine nuclei, the main relay between neocortex and cerebellum. By counteracting the sonic hedgehog pathway, *Ezh2* represses *Netrin1* in dorsal hindbrain, which allows normal pontine neuron migration. In *Ezh2* mutants, ectopic *Netrin1* derepression results in abnormal migration and supernumerary nuclei integrating in brain circuitry. Moreover, intrinsic topographic organization of pontine nuclei according to rostrocaudal progenitor origin is maintained throughout migration and correlates with patterned cortical input. *Ezh2* maintains spatially restricted *Hox* expression, which, in turn, regulates differential expression of the repulsive receptor *Unc5b* in migrating neurons; together, they generate subsets with distinct responsiveness to environmental *Netrin1*. Thus, *Ezh2*-dependent epigenetic regulation of intrinsic and extrinsic transcriptional programs controls topographic neuronal guidance and connectivity in the cortico-ponto-cerebellar pathway.

In mammals, cortical motor and sensory information is mostly relayed to the cerebellum via the hindbrain precerebellar pontine nuclei (PNs), which include pontine gray and reticulotegmental nuclei. The developing hindbrain is rostrocaudally segregated into progenitor compartments, or rhombomeres (r1 to r8) (1), genetical-

ly defined by nested *Hox* gene expression (2). Mouse PN neurons are generated from r6 to r8 lower rhombic lip progenitors (3), undergo a long-distance caudorostral tangential migration via the anterior extramural stream (AES), and settle beside the ventral midline (Fig. 1, A and B) (4, 5). Intrinsic expression of transcription factors and

guidance receptors and extrinsic distribution of ligands are important for AES migration (6–8). However, little is known about the epigenetic regulation of these transcriptional programs. Here, we addressed the role of *Ezh2*, which is member of the Polycomb repressive complex 2 and trimethylates histone H3 at lysine 27 (H3K27me3) (9).

Ezh2 transcripts are maintained through late stages in lower rhombic lip progenitors, migratory stream, and PN neurons (fig. S1), whereas H3K27me3 is detected throughout the hindbrain (fig. S2). To conditionally inactivate *Ezh2*, we generated transgenic lines in which *Cre* is driven by rhombomere-specific enhancers in spatially restricted regions tiling the caudal hindbrain (10) (figs. S3 and S4). To assess cell-autonomous and/or region-specific non-cell autonomous *Ezh2* function in pontine neuron migration, we first crossed *Krox20::Cre* (10) to an *Ezh2*^{fl/fl} allele (10) (*Krox20::Cre;Ezh2*^{fl/fl}). Inactivation in r3

¹Friedrich Miescher Institute for Biomedical Research, Maulbeerstrasse 66, 4058 Basel, Switzerland. ²University of Basel, 4056 Basel, Switzerland. ³Yale Cardiovascular Research Center, Department of Internal Medicine, Yale University School of Medicine, New Haven, CT 06511-6664, USA. ⁴CIRB (Centre Interdisciplinaire de Recherche en Biologie), Inserm U1050, 11 Place Marcellin Berthelot 75005 Paris, France. ⁵Department of Cell and Developmental Biology, University of Michigan, Ann Arbor, MI 48109-2200, USA.

*These authors contributed equally to this work.

†To whom correspondence should be addressed. E-mail: filippo.rijli@fmi.ch

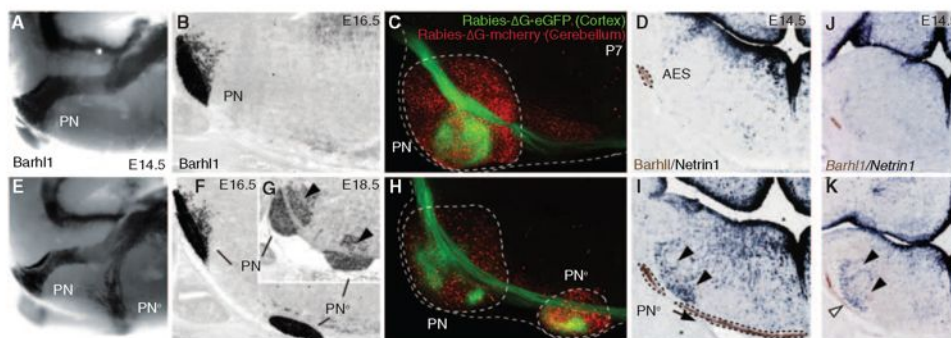


Fig. 1. *Ezh2* non-cell autonomous role in pontine neuron tangential migration. (A, B, E, F, and G) Migratory phenotypes in control (A) and (B) and *r5-6::Cre;Ezh2*^{fl/fl} mutants (E) to (G). *Barhl1* in situ hybridization in E14.5 whole-mount (A) and (E), E16.5 (B) and (F), and E18.5 (G) sagittal sections. Pontine gray and reticulotegmental [arrowheads (G)] nuclei (PNs) are duplicated (PN^s). (C and H) Tracings from P7 cortex (rabies-ΔG-eGFP) and cerebellum (rabies-ΔG-mCherry) in controls (C) and *r5-6::Cre;Ezh2*^{fl/fl} mutants (H). PNs and PN^s are connected to cortex and cerebellum. (D, I, J, and K) *Barhl1/Netrin1* expression in E14.5 control (D), *r5-6::Cre;Ezh2*^{fl/fl} (I), *r5post::Cre;Ezh2*^{fl/fl}; *Shh*^{fl/fl} (K), and *r5post::Cre;Ezh2*^{fl/fl}; *Shh*^{fl/fl} (J) coronal sections. Ectopic *Netrin1* [arrowheads: (I) and (K)] and PN^s ectopic migration [arrow and white arrowhead, respectively: (I) and (K)] are partially rescued (J).

and r5, which do not contribute to the pontine migratory stream (3), resulted in small ectopic PNs in posterior r5 (PN^s) (fig. S5), which supports an *Ezh2* non-cell autonomous role. Deletion in r5 and r6 (*r5-6::Cre;Ezh2^{fl/fl}*) resulted in a more prominent phenotype. A neuronal subset split from the migratory stream, turned ventrally, and generated an ectopic duplication of PNs (PN^s) (Fig. 1, E to G). PN^s neurons were nonrecombined *Ezh2^{+/+};H3K27me3⁺* located within the r5- and r6-derived territory mostly devoid of H3K27me3 (fig. S2), which confirmed *Ezh2*'s non-cell autonomous function.

To assess whether PN^s integrated cortico-cerebellar connectivity, we carried out cortex-to-PN and cerebellum-to-PN tracings. We injected viral constructs expressing green fluorescent protein (GFP) (rabies-ΔG-GFP) and/or mCherry (rabies-ΔG-mCherry) in postnatal day 2 (P2) wild type and *r5-6::Cre;Ezh2^{fl/fl}* and *Krox20::Cre;Ezh2^{fl/fl}* mutants. At P7, PNs and PN^s triggered collateralization of corticospinal axons and innervated the cerebellum (Fig. 1, C and H, and fig. S6).

To evaluate *Ezh2* cell-autonomous function, we used the *Wnt1::Cre* deleter (*10*). *Ezh2* transcripts and H3K27me3 were selectively deleted from lower rhombic lip and migratory stream in *Wnt1::Cre;Ezh2^{fl/fl}* mutants (figs. S2 and S7). Nonetheless, the mutation was not sufficient to induce ectopic posterior pontine neuron migration (Fig. 2, J and M, and figs. S5 and S7). The most severe phenotype was observed in *Hoxa2::Cre;Ezh2^{fl/fl}* mutants, where *Ezh2* was inactivated in both AES neurons and their migratory environment, i.e., throughout r3- to r6- and dorsal r7- to r8-derived structures including the lower rhombic lip (figs. S2 and S3). The whole AES did not migrate anterior to r6 and settled into a single posterior ectopic nu-

cleus (PN^e) (fig. S5). Thus, *Ezh2* has a non-cell autonomous role in AES migration, which is enhanced by a cell-autonomous function in progenitors and migrating neurons.

Netrin1 (Ntn1) and Slit1-3 are attractive or repulsive secreted cues that influence pontine neuron migration (6, 7). *Slit1-3* expression was not altered in embryonic day 14.5 (E14.5) *r5-6::Cre;Ezh2^{fl/fl}* mutants (fig. S8). In contrast, *Ntn1*, normally expressed in floor-plate and ventral ventricular progenitors (Fig. 1D and fig. S5) (11), was ectopically expressed in dorsal progenitors and the mantle layer medially to the AES in *r5-6::Cre;Ezh2^{fl/fl}*, *Krox20::Cre;Ezh2^{fl/fl}*, *Hoxa2::Cre;Ezh2^{fl/fl}*, and *r5post::Cre;Ezh2^{fl/fl}* mutants (Fig. 1I and fig. S5). Additional deletion of *Shh* was sufficient to prevent strong ectopic *Ntn1* activation in dorsal progenitors of E12.5 *r5post::Cre;Ezh2^{fl/fl};Shh^{fl/fl}* conditional mutants (fig. S5). At E14.5, ectopic *Ntn1* was almost undetectable and the *Ezh2* knockout was partially rescued (Fig. 1, J and K, and fig. S5). Therefore, *Ezh2* is required to restrict *Ntn1* expression to ventral progenitors by silencing *Ntn1* in the dorsal neural tube. However, *Ezh2* deletion is not sufficient to ectopically induce *Ntn1*, which additionally requires *Shh* signaling from the floor plate. Thus, in the dorsal neural tube, *Ezh2*-mediated epigenetic repression of *Ntn1* may normally counteract *Shh*-mediated activation.

Ectopic and/or increased environmental Ntn1 levels may trigger premature migration toward the midline. In E14.5 *r5-6::Cre;Ezh2^{fl/fl}* mutants, only a subset of pontine neurons split from the stream and entered the alternative ventral migratory pathway at the level of the ectopic *Ntn1* domain (Fig. 1I and fig. S5), which suggested that AES neurons may display intrinsic differential

responsiveness to Ntn1 signaling. To map the contributions of r6 (*r6RL^P*) or r7 and r8 (*r7-8RL^P*) lower rhombic lip-derived neuronal progenies into the pontine stream and nuclei (Fig. 2, B, C and H, and fig. S3), we crossed floxed reporter lines to *r5-6::Cre* or *r7post::Cre* (*Cre* is expressed up to the r6-r7 boundary) (fig. S3H) in which *Cre* is down-regulated before AES migration (fig. S4). *r6RL^P* mapping was confirmed by the tamoxifen-inducible *MafB::CreERT2* transgenic line, whose reporter expression pattern is restricted to r5 and r6, similar to that in *r5-6::Cre* (10) (fig. S3). To trace the whole precerebellar lower rhombic lip progeny (*r6-8RL^P*), we used *r5post::Cre* (figs. S3A and S4).

r6-8RL^P contributed to the whole PNs (fig. S3), whereas *r6RL^P* mapped to the most anterior (arrow in Fig. 2H and fig. S3), and *r7-8RL^P* filled the remaining posterior portions of PNs (fig. S3). This topographic organization of pontine neuronal subsets directly correlated with their relative position within the migratory stream. Namely, *r6RL^P* mapped to the dorsalmost AES, whereas *r7-8RL^P* contributed to the remaining portion ventrally to *r6RL^P* (Fig. 2, B and C). Thus, the precerebellar lower rhombic lip is rostrocaudally mapped onto the AES dorsoventral axis (Fig. 3E and fig. S1J) and, in turn, onto the PN rostrocaudal axis (fig. S1K), with neuronal subsets maintaining their relative position throughout migration and settling.

Next, we investigated molecular correlates of this intrinsic cellular regionalization and asked whether *Hox* paralog groups (PG) 2 to 5 maintain their spatially restricted progenitor expression patterns in pontine migratory stream and nuclei (Fig. 2). Indeed, *Hox* PG2 (*Hoxa2/Hoxb2*) and PG3 (*Hoxa3/Hoxb3*), expressed in the whole precerebellar rhombic lip, were correspondingly maintained throughout the pontine migratory stream and nuclei (6) (fig. S1). *Hoxb4* is normally expressed up to the r6-r7 boundary, whereas the *Hox* PG5 rostral expression limit is posterior to PG4 genes (2). In the AES and PNs, *Hoxb4⁺* neurons extended just ventrally and posteriorly, respectively, to *r6RL^P* (Fig. 2, C and D, and fig. S1L), whereas *Hoxa5* and *Hoxb5* transcripts and *Hoxa5* protein mapped to the ventralmost migratory stream and posteriormost PNs, respectively (Fig. 2, A, F, H and I, and figs. S1 and S2). Simultaneous detection of *Hoxa5* and *ZsGreen* in *r5-6::Cre;R26R^{ZsGreen}* specimens demonstrated rostrocaudal segregation of *r6RL^P* and *Hoxa5⁺* neurons within the PNs (Fig. 2H). To permanently label *Hoxa5*-expressing neurons, we generated a transgenic line in which *Cre* was inserted in-frame at the *Hoxa5* locus (*Hoxa5::Cre*) (10) (fig. S3). *Hoxa5::Cre*-expressing neurons segregated to the ventralmost AES and posteriormost PNs, faithfully overlapping endogenous *Hoxa5* distribution (Fig. 2, D, E, F and G, and figs. S1F, S3, and S4). Thus, pontine neuron subsets of distinct rostrocaudal origin maintain their relative topographic positions and *Hox* codes throughout migration and settling within the target nucleus (Fig. 4A and fig. S1).

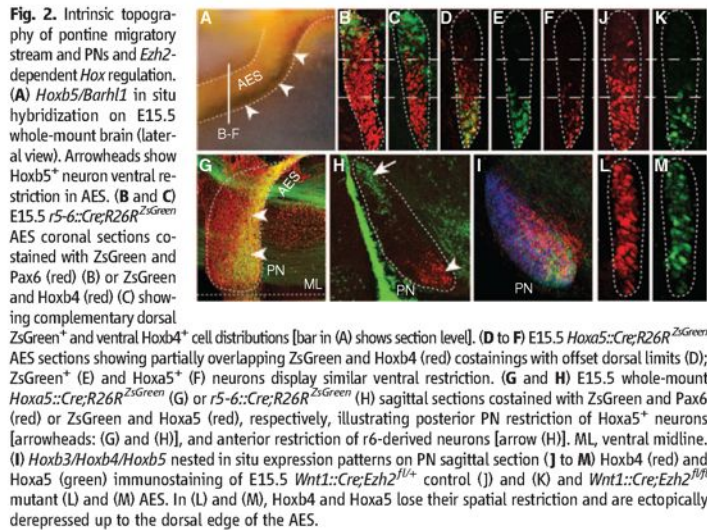


Fig. 2. Intrinsic topography of pontine migratory stream and PNs and *Ezh2*-dependent *Hox* regulation. (A) *Hoxb5/Barhl1* in situ hybridization on E15.5 whole-mount brain (lateral view). Arrowheads show *Hoxb5⁺* neuron ventral restriction in AES. (B and C) E15.5 *r5-6::Cre;R26R^{ZsGreen}* AES coronal sections costained with *ZsGreen* and *Pax6* (red) (B) or *ZsGreen* and *Hoxb4* (red) (C) showing complementary dorsal *ZsGreen⁺* and ventral *Hoxb4⁺* cell distributions [bar in (A) shows section level]. (D to F) E15.5 *Hoxa5::Cre;R26R^{ZsGreen}* AES sections showing partially overlapping *ZsGreen* and *Hoxb4* (red) costainings with offset dorsal limits (D); *ZsGreen⁺* (E) and *Hoxa5⁺* (F) neurons display similar ventral restriction. (G and H) E15.5 whole-mount *Hoxa5::Cre;R26R^{ZsGreen}* (G) or *r5-6::Cre;R26R^{ZsGreen}* (H) sagittal sections costained with *ZsGreen* and *Pax6* (red) or *ZsGreen* and *Hoxa5* (red), respectively, illustrating posterior PN restriction of *Hoxa5⁺* neurons [arrowheads: (G) and (H)], and anterior restriction of r6-derived neurons [arrow (H)]. ML, ventral midline. (I) *Hoxb3/Hoxb4/Hoxb5* nested in situ expression patterns on PN sagittal section (J to M) *Hoxb4* (red) and *Hoxa5* (green) immunostaining of E15.5 *Wnt1::Cre;Ezh2^{fl/fl}* control (J) and (K) and *Wnt1::Cre;Ezh2^{fl/fl}* mutant (L) and (M) AES. In (L) and (M), *Hoxb4* and *Hoxa5* lose their spatial restriction and are ectopically derepressed up to the dorsal edge of the AES.

Is *Ezh2* required to maintain *Hox* nested expression in migrating pontine neurons and PNs? In E14.5 *Wnt1::Cre;Ezh2^{fl/fl}* and *Hoxa2::Cre;Ezh2^{fl/fl}* mutants, *Hoxb4*, *Hoxa5*, and *Hoxb5* were ectopically expressed within the anterior lower rhombic lip and spread ventrodorsally throughout the

pontine migratory stream (Fig. 2, L and M, and figs. S2 and S7). Thus, by preventing *Hox PG4* and *PG5* expression in anterior precerebellar rhombic lip and migrating neuronal progeny, *Ezh2*-mediated repression contributes to the maintenance of molecular heterogeneity in the migratory stream.

This, in turn, may underlie intrinsic differential response of migrating neuron subsets to environmental Ntn1.

Netrin-mediated attraction is counteracted by *Unc5* repulsive receptors (*12*), and *Unc5c* inactivation results in variable ectopic migration of AES stream.

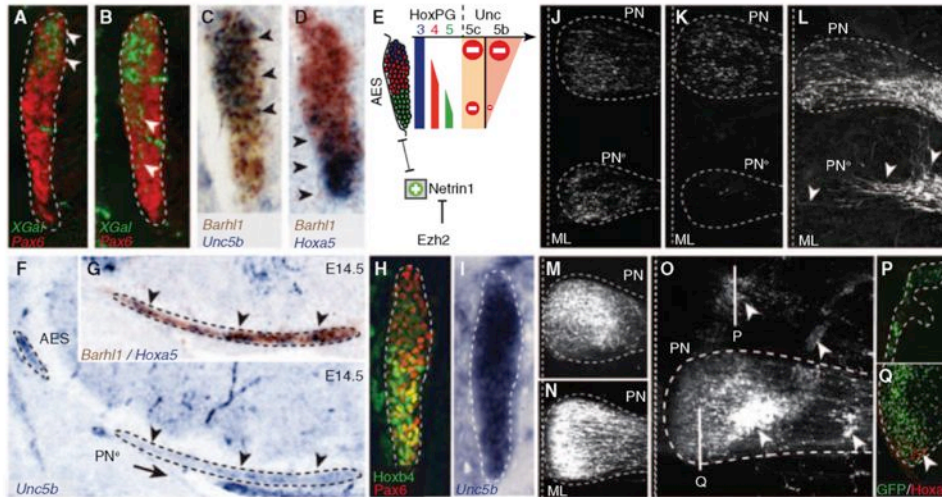
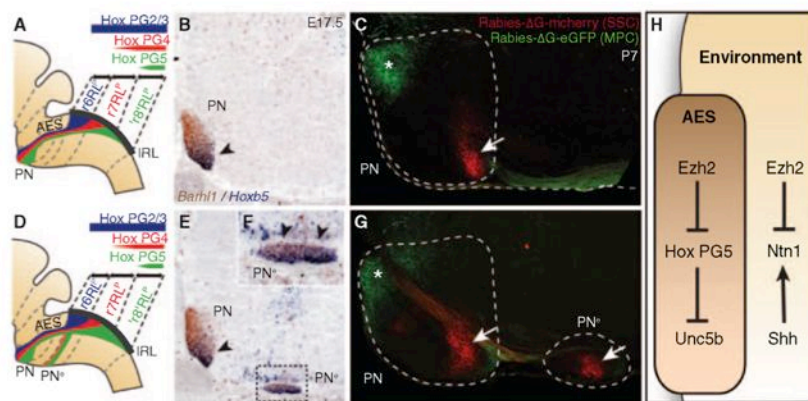


Fig. 3. *Ezh2*- and *Hox*-dependent regulation of *Unc5b* in pontine neuron migration. (A and B) X-gal (green) and Pax6 (red) costainings of E14.5 *Unc5b^{bGal/+}* heterozygotes (A) and *Unc5b^{bGal/bGal}* homozygotes (B) showing X-gal-stained cell distribution in AES (arrowheads). (C to E) *Unc5b/Barhl1* (C) and *Hoxa5/Barhl1* (D) in situ hybridization in E14.5 AES showing complementary dorsoventral expression of *Unc5b* and *Hoxa5* (arrowheads) and summary (E). (F and G) In *r5-6::Cre;Ezh2^{fl/fl}* mutants, PN^o migrating neurons are *Unc5b*-negative (F) and *Hoxa5⁺/Barhl1⁺* (G) (arrowheads). (H and I) In E14.5 *Hoxa5^{-/-}/Hoxb5^{-/-}/Hoxc5^{-/-}* AES, *Unc5b* is up-regulated ventrally (I), whereas *Hoxb4* and *Pax6* are normally expressed (H). (J and K) In utero EP in

E14.5 *r5-6::Cre;Ezh2^{fl/fl}* mutants of *Unc5b/Unc5c/eGFP* strongly reduces at E18.5 ectopically migrating PN^o neurons (K), as compared with EP of eGFP (J), and partially rescues the phenotype. ML, ventral midline. (L to Q) In E13.5 wild type, EP of *Ntn1* results in posterior ectopic pontine neuron migration at E17.5, phenocopying *r5-6::Cre;Ezh2^{fl/fl}* mutants [arrowheads (L)]. Although EP at E13.5 of eGFP (M) or *Unc5c/eGFP* constructs has no apparent effect on migration at E18.5 (N), EP of *Unc5b/eGFP* results in anterior ectopic migration and/or dorsal-lateral arrest [arrowheads (O)]. Immunostaining on sagittal sections shows that anterior ectopic GFP+/Unc5b⁺ electroporated cells are *Hoxa5*-negative (P); *Hoxa5⁺* cells are normally restricted in posterior PN (Q).

Fig. 4. PN regionalization and patterned cortical input. (A, B, D, E, and F), *Hox* expression summary in migrating pontine neurons of control (A) and *r5-6::Cre;Ezh2^{fl/fl}* mutants (D). *Barhl1/Hoxb5* in situ hybridization on E17.5 sagittal sections (B), (E), and (F). In *r5-6::Cre;Ezh2^{fl/fl}* mutants (E) and (F), *Hoxb5⁺* neurons spread throughout the rostrocaudal extent of the ectopic nuclei (PN^os) [arrowheads (F)], whereas, in PNs, they are normally posteriorly restricted as in control [arrowheads: (B) and (E)]. (C and G) Rabies-ΔG viruses injected in control visual/medioposterior cortex (MPC) and SSC anterogradely trace fibers into anterior (green,*) and posterior (red, arrow) PNs (C), respectively. In *r5-6::Cre;Ezh2^{fl/fl}* mutants (G), PN^o lacks innervation by MPC, whereas it is innervated by SSC (arrow). (H) *Ezh2*- and *Hox*-dependent genetic circuitry of intrinsic and extrinsic *Unc5b/Ntn1* regulation.



neurons (13). *Unc5c* is expressed in lower rhombic lip progenitors, down-regulated in migrating neurons, and reactivated upon approaching the midline (fig. S9) (13). Thus, *Unc5c* is unlikely to confer a dorsoventrally biased response of the AES to Ntn1. *Unc5b* has been involved in vascular development (14), though a role in neuronal development was not explored. We found a dorsoventral high-to-low density of cells expressing *Unc5b* (Fig. 3C and fig. S9) and β -galactosidase activity in *Unc5b^{Galv}* fetuses (Fig. 3A). *Unc5b* expression was, in turn, down-regulated when the migratory stream turned toward the midline (fig. S9C). Dorsoventral *Unc5b* transcript distribution in the migratory stream anticorrelated with *Hox PG5* expression (Fig. 3, C and D). In E14.5 *Hoxa5^{-/-};Hoxb5^{-/-};Hoxc5^{-/-}* compound mutants, *Unc5b* was up-regulated in ventral *Hoxb4^{+/+}Pax6^{-/-}* AES neurons (Fig. 3, H and I). Thus, *Hox PG5* normally represses *Unc5b* in ventral AES neurons originating from posterior precerebellar lower rhombic lip.

In E14.5 *Unc5b^{GalvGal}* null mutants, β -galactosidase⁺ cells partially lost their normal dorsal restriction and spread into ventral AES (Fig. 3B). Thus, *Unc5b* contributes to maintaining topographical organization of dorsal AES subsets. In E16.5 *Unc5c^{-/-}* fetuses, dorsal *Unc5b*-expressing AES neurons maintained their normal migratory path, whereas ectopic neurons were *Hox PG5⁺* and mainly *Unc5b*-negative (fig. S9). Therefore, in the absence of *Unc5c*, ventral *Unc5b*-negative AES neurons become more sensitive to Ntn1-mediated attraction than dorsal *Unc5b*-expressing neurons. Similarly, in *r5-6::Cre;Ezh2^{fl/fl}* mutants, *Unc5b*-expressing neurons remain dorsal and pursue their normal migration, whereas *Hox PG5⁺/Unc5b*-negative neurons are preferentially influenced by Ntn1 up-regulation and ectopically attracted to the midline (Fig. 3, F and G, and fig. S2). Moreover, in *Hoxa2::Cre;Ezh2^{fl/fl}* mutants, in which all pontine neurons are *Ezh2^{-/-}/H3K27me3* and migrate through an environment ectopically expressing *Ntn1* (fig. S5), all migrating neurons are prematurely attracted to an ectopic posterior midline position, are *Hox PG5⁺*, and down-regulate *Unc5b* (figs. S2 and S7).

Next, *Unc5b/5c* overexpression by in utero electroporation (EP) of E14.5 lower rhombic lip progenitors was sufficient to cell-autonomously rescue the PN^e phenotype in *r5-6::Cre;Ezh2^{fl/fl}* mutants [enhanced GFP-positive (eGFP⁺) neuron quantification in PN^es compared with PN^s: eGFP ($n = 5$) 33.79% \pm 0.1060; eGFP/*Unc5b/5c* ($n = 5$) 0.64% \pm 0.0044; $P = 0.00011$] (Fig. 3, J and K), which demonstrated that elevating *Unc5* receptor levels counteracts increased Ntn1-mediated attraction. Ntn1 overexpression by EP in E13.5 wild-type fetuses induced ectopic posterior migration of AES neurons (Fig. 3L), partially phenocopying the *r5-6::Cre;Ezh2^{fl/fl}* mutant phenotype and showing that increasing Ntn1 is sufficient to cause ectopic ventral migration of neuronal subsets.

Furthermore, although overexpression of *Unc5c* in E13.5 wild-type fetuses had no apparent effect on AES migration (Fig. 3, M and N), *Unc5b* EP

triggered ectopic anterior migration and/or a block in dorsal position of *Hoxa5*-negative pontine neuron subsets (Fig. 3, O to Q). Therefore, maintaining constitutively high *Unc5b* levels in migrating neurons prevents or delays turning toward the midline; the latter results in ectopic anterior migration. Conditional *Hoxa2* overexpression in rhombic lip derivatives by mating *Wnt1::Cre* with a *ROSA26::(lox-STOP-lox)Hoxa2*-internal ribosome entry site (*IRES*)-eGFP (*Wnt1::Cre;R26K^{Hoxa2}*) allele (10) also resulted in anterior ectopic migration generating rostrally elongated PNs, which maintained high *Unc5b* expression, unlike in control mice (fig. S9). Therefore, although *Hox PG5* are involved in negatively regulating *Unc5b* in the ventral migratory stream, *Unc5b* expression in dorsal AES may be under *Hox PG2*-positive regulation and generates differential responses to environmental Ntn1.

Finally, we investigated whether the PN and PN^e patterning differences in *r5-6::Cre;Ezh2^{fl/fl}* mutants result in distinct cortical inputs. In *P7 Pcp2::Cre;R26R^{tdTomato}* animals (10) expressing *Cre* in medioposterior (including visual) cortex (MPC), *tdTomato⁺* axons projected onto the rostral PN, in agreement with (15), including the *r6RLP* neuron subset (fig. S6). Coinjection of rabies- Δ G-GFP and rabies- Δ G-mCherry into visual and/or MPC and medial somatosensory cortex (SSC) resulted in rostral GFP⁺ and caudal mCherry⁺ axonal inputs onto the PNs, respectively (Fig. 4C). In *r5-6::Cre;Ezh2^{fl/fl}* mutants, PN was targeted both by visual or MPC-derived GFP⁺ (rostrally) and SSC-derived mCherry⁺ (caudally) axons, whereas PN^e was innervated by SSC-derived though not visual/MPC-derived axons (Fig. 4G), correlating with their posterior *Hox PG5⁺* profile (Fig. 4, A, B, and D to F).

During radial migration, correlation to rostrocaudal position of origin is maintained through interaction with glial progenitors (16). How long-range tangentially migrating neurons (17) maintain information about their origin is less well understood. We show that the topographic migratory program of r6- to r8-derived pontine neurons is largely established in progenitor pools according to rostrocaudal origin and maintained in migrating neurons. We found similar organizational principles during lateral reticular nucleus migration (fig. S10). Moreover, the r2 to r5 rhombic lip also gives rise to neurons that migrate tangentially along a short dorsoventral extramural path and populate distinct brainstem cochlear nuclei with a rostrocaudal topography (3). On its caudorostral route, the precerebellar stream migrates ventrally to the cochlear stream (3), although they do not mix despite close cellular proximity, which suggests that rhombomere-specific programs may control appropriate precerebellar neuron position during tangential migration. Indeed, we show that the topography of r6 versus r7 versus r8 origin is preserved throughout migration, mapped along the dorsoventral axis of the pontine stream, and eventually within rostrocaudal subregions of the PNs, correlating with patterned

cortical input. The transcriptional regulation of this tangential migratory program is epigenetically maintained (Fig. 4H). *Ezh2*-mediated repression maintains dorsoventrally restricted environmental distribution of attractive and/or repulsive cues, such as *Ntn1*, and an intrinsically heterogeneous *Hox* transcriptional program in the migratory stream that, in turn, provides neuronal subsets with distinct *Unc5b*-dependent responses to environmental Ntn1, and thus contributes to maintaining the neuronal position during migration.

References and Notes

1. A. Lumsden, R. Krumlauf, *Science* **274**, 1109 (1996).
2. S. Tümpel, L. M. Wiedemann, R. Krumlauf, *Curr. Top. Dev. Biol.* **88**, 103 (2009).
3. A. F. Farago, R. B. Awatramani, S. M. Dymecki, *Neuron* **50**, 205 (2006).
4. J. Altman, S. A. Bayer, *J. Comp. Neurol.* **257**, 529 (1987).
5. C. I. Rodriguez, S. M. Dymecki, *Neuron* **27**, 475 (2000).
6. M. J. Geisen et al., *PLoS Biol.* **6**, e142 (2008).
7. K. T. Yee, H. H. Simon, M. Tessier-Lavigne, D. M. O'Leary, *Neuron* **24**, 607 (1999).
8. S. Nóbrega-Pereira, O. Marín, *Cereb. Cortex* **19** (Suppl. 1), i107 (2009).
9. R. Margueron, D. Reinberg, *Nature* **469**, 343 (2011).
10. Materials and methods are available as supplementary materials on Science Online.
11. E. Bloch-Gallego, F. Ezan, M. Tessier-Lavigne, C. Sotelo, *J. Neurosci.* **19**, 4407 (1999).
12. K. Hong et al., *Cell* **97**, 927 (1999).
13. D. Kim, S. L. Ackerman, *J. Neurosci.* **31**, 2167 (2011).
14. X. Lu et al., *Nature* **432**, 179 (2004).
15. T. B. Leergaard, J. G. Bjaalie, *Front. Neurosci.* **1**, 211 (2007).
16. P. Rakic, *Science* **241**, 170 (1988).
17. M. E. Hatten, *Annu. Rev. Neurosci.* **22**, 511 (1999).

Acknowledgments: We thank K. Balint, F. Boukhtouche, Y.-Y. Lee, C.-Y. Liang, D. Kraus, T. Mathivet, F. Santagati, J. F. Spetz, and A. Yallowitz for technical support and discussion. We are grateful to M. Tessier-Lavigne, S. H. Orkin, E. Callaway, V. Castellani, P. Mehlén, O. Nyabi, and J. Haigh for gifts of mouse lines, probes, or reagents. The mouse transgenic lines *r5-6::Cre;Hoxa2::Cre*, *r5post::Cre*, *r7post::Cre*, *Mafb::CreERT2*, *Hoxa5::Cre*, *ROSA26::(lox-STOPlox)Hoxa2-IRES-EGFP* generated in this research and their respective DNA constructs are available from F.M.R. under a material transfer agreement with the Friedrich Miescher Institute for Biomedical Research, Basel, Switzerland. The SAD G-eGFP and SAD G-mCherry G-deleted rabies viruses used in this research are available from E. M. Callaway under a material transfer agreement with Salk Institute for Biological Studies, La Jolla, CA, USA. T.D. is the recipient of a European Molecular Biology Organization Long-Term Fellowship. Work in F.M.R.'s laboratory is supported by the Swiss National Science Foundation (Sinergia CRSI33_127440), Association pour la Recherche sur la Sclérose en Plaques, and the Novartis Research Foundation.

Supplementary Materials

www.sciencemag.org/cgi/content/full/339/6116/204/DC1
Materials and Methods
Figs. S1 to S10
References (18–37)

27 August 2012; accepted 7 November 2012
10.1126/science.1229326



www.sciencemag.org/cgi/content/full/338/6116/204/DC1

Supplementary Materials for

***Ezh2* Orchestrates Topographic Migration and Connectivity of Mouse Precerebellar Neurons**

Thomas Di Meglio, Claudius F. Kratochwil, Nathalie Vilain, Alberto Loche, Antonio Vitobello, Keisuke Yonehara, Steven M. Hrycaj, Botond Roska, Antoine H. F. M. Peters, Anne Eichmann, Deneen Wellik, Sebastien Ducret, Filippo M. Rijli*

*To whom correspondence should be addressed. E-mail: filippo.rijli@fmi.ch

Published 11 January 2012, *Science* **338**, 204 (2012)
DOI: 10.1126/science.1229326

This PDF file includes

Materials and Methods
Figs. S1 to S10
Full References

Materials and Methods

Generation of *Hoxa5::Cre* BAC line

The BAC clone RP23-20F21 (BACPAC Resources Center at Children's Hospital Oakland Research Institute, Oakland, Calif., USA) containing the entire *Hoxa* cluster was used as a template for bacterial recombination as described previously (18). The plasmid pN21-Cre was used to amplify a Cre-SV40polyA-Frt-Kanamycin-Frt cassette with 70-mer primers containing 50 nucleotides of homology (indicated as caps) surrounding the coding sequence of the *Hoxa5* first exon, such that *Cre* is inserted in-frame with the *Hoxa5* ATG codon. Forward primer: 5'ACGCACAAACGACCGCGAGCCACAAATCAAGCACACATATCAAAAAACAAatgtccaatttactgaccgt3'; reverse primer: 5'CAAGACCCGCGCCCCACGGACGCGTGGATCAGAAAACGGCTGGCTTTACTattccagaagtagtgagga3'. To obtain the *Hoxa5::Cre* BAC construct, EL250 bacteria containing the BAC RP23-20F21 were induced for recombination at 42°C and then electroporated with the Cre-SV40polyA-Frt-Kanamycin-Frt cassette. Bacteria were subsequently arabinose-induced for *Flpe* expression in order to remove the kanamycin cassette. Correct recombination and removal of the resistance gene in the *Hoxa5::Cre* BAC were tested by PCR, restriction enzyme digestion and sequencing. Before microinjection, the modified BAC was linearized by *PI-SceI* digestion. One founder was obtained that displayed the expected *Cre* expression pattern.

Generation of the *MafB::CreERT2* line and tamoxifen treatment

The same approach as above was taken using the BAC clone BAC clone RP23-33A18 (BACPAC Resources Center at Children's Hospital Oakland Research Institute, Oakland, CA). The plasmid pN21-CreERT2 was used to amplify a CreERT2-SV40polyA-Frt-Kanamycin-Frt cassette by using 70-mer primers containing 50 nucleotides of homology (indicated as caps) surrounding the coding sequence of the *MafB* gene, such that the Cre is inserted in-frame with the *MafB* ATG codon.

Forward primer:
 5' GGCCGCAAAGTTTTCCCCGCGGCAGCGGCGGCTGAGCCTCGCTTTTAGCGA
 TGtccaatttactgaccg3';

reverse primer:
 5' GAATAGGGAGTCTGGGCCAGGGCAAGGGCGGGGGCCGGACCCGCCAGGAC
 ctattccagaagtagtgagga3'.

Tamoxifen was dissolved in corn oil and administered by oral gavage at E7.5 (1mg; 100 μ l of 10mg/ml stock solution).

Generation of r5post::Cre, r5-6::Cre and r7post::Cre lines

We generated transgenic mice in which *Cre* is driven by rhombomere-specific enhancers of *Hoxb3* (19) (*r5-post::Cre*), *Hoxa3* (20) (*r5-6::Cre*), or *Hoxb4* (21) (*r7post::Cre*) (figs. S3 and S4), which were mated to Gt(ROSA)26Sor (*R26R*)^{lacZ} (22), *R26R*^{tdTomato} (23), or *R26R*^{ZsGreen} (23) reporter lines.

The mouse lines were created by replacing the LacZ gene of the pKS- β -globin-lacZ vector (BGZ40) (24) with a Cre cassette (Clontech) using homologous recombination. Enhancers for *Hoxb3* (19) (*r5-post::Cre*, 483 bp), *Hoxa3* (20) (*r5-6::Cre*, 629 bp) and

Hoxb4 (21) (*r7-post::Cre*, 400 bp) were amplified by PCR from genomic DNA using the following primers:

	<i>r5-post::Cre:</i>	forward,
5' ATATCCGCGGGATCGGAGAGGAGAGGGCAA;	reverse,	5'
CGCGACTAGTGATCTCCAAGGTCCCCTTTCA.	<i>r5-6::Cre:</i>	forward,
5' ATATCCGCGGCAACTTGAAAGGGAAGAGCC;	reverse,	5'
CGCGACTAGTGATATCAAATAGCAGCGAATCTTC.	<i>r7-post::Cre:</i>	forward,
5' ATATCCGCGGTCCTTGGAAGGTATGAATAG;	reverse,	5'

CGCGACTAGTTGTTACCTCTGAGCCTCTTG. The PCR bands were purified and inserted 5' of the β -globin promoter using restriction sites FslI and XhoI (*r5-6::Cre*) and BglI and PvuII (*r5-post::Cre*, *r7-post::Cre*), thus generating constructs consisting of an enhancer, a β -globin minimal promoter and Cre recombinase encoding sequence. The constructs were linearized, purified and microinjected into the pronuclei of blastocyst embryos. Founders were identified by PCR and screened at P0 after crossing with *R26R^{lacZ}* animals. 72 animals were genotyped (19 for *r5post::Cre*; 38 for *r5-6::Cre*; 15 for *r7post::Cre*). 19 were positive for Cre (8 for *r5post::Cre*; 8 for *r5-6::Cre*; 3 for *r7post::Cre*). 3/8 showed the expected recombination pattern at P0 for *r5post::Cre*; 2/8 for *r5-6::Cre* and 1/3 for *r7post::Cre*, while the other founders showed no, ubiquitous or ectopic patterns of recombination.

Generation of *Hoxa2::Cre* line

For the generation of the *Hoxa2::Cre* transgenic line a 3.5kb EcoRI fragment upstream to the *Hoxa2* promoter (from -3585 to -1) was obtained from the plasmid p314R (25) and subcloned in a native orientation upstream to a β -globin minimal promoter, the Cre gene and a SV40 polyA signal. The transgene fragment was excised by digestion with Sall and

NotI, and purified before microinjection.

Generation of the ROSA::(lox-STOP-lox)Hoxa2-IRES-EGFP mouse line

The conditional Hoxa2 overexpression mouse line was generated by using the Gateway-compatible ROSA26 locus targeting vector as previously described (26). LR reactions were performed between the plasmid pENTR-FLAG-Hoxa2 (containing the Hoxa2 cDNA coding sequence with a 5'FLAG tag) and the destination vector pROSA26-DV1 to obtain the targeting vector pROSA26-FLAG-Hoxa2-IRES-EGFP. This vector was linearized with PvuI and electroporated into the E14 ES cell line. The positive ES cell clones, selected by G418 resistance and screened by PCR, were aggregated with morula-stage embryos obtained from inbred (C57BL/6 x DBA/2) F1 mice. Germline transmission of the ROSA26::(lox-STOP-lox)Hoxa2-IRES-EGFP allele was obtained. Heterozygous and homozygous mice were viable and fertile.

Other mouse lines used in the study

Wnt1::Cre (27), *R26R^{lacZ}* (22), *Ezh2^{fl/fl}* (kind gift from S.H. Orkin) (28), *Hoxa5*, *Hoxb5*, *Hoxc5* knockout mice (29), *Unc5b^{bGal/bGal}* knockout mice (kind gift from M. Tessier-Lavigne) (14) and *Unc5c^{rcm}* (embryos kindly obtained from V. Castellani) (30) were as described. *Pcp2::Cre* (31), *R26R^{dTomato}*, *R26R^{ZsGreen}* (23) and *Shh^{tm2Anc}* (*Shh^{fl}*) mice (32) were obtained from Jackson Laboratory.

Circuit tracing

G-deleted rabies virus vectors encoding mCherry (SADΔG-mCherry) or eGFP (SADΔG-eGFP) were harvested from BHK-B19G cells (kind gift from E. Callaway) and centrifuged as described previously (33). Stereotaxic injections of viruses to different

areas of neocortex or cerebellum were performed via pulled-glass pipettes using a microinjector (Narishige, IM-9B). Pups were anesthetized by hypothermia, injected at P2 and perfused at P7.

In utero electroporation

In utero electroporation was performed on embryos at E13.5 or E14.5 as described previously (34) using different combinations of *eGFP* (pCX-eGFP (35)), *Unc5b* (pcDNA- *ratUnc5b* (36)), *Unc5c* (pcDNA 3.1-*mouseUnc5c*; kind gift from P. Mehlen) and *Netrin1* (pcDNA 3.1-*humanNetrin1*; kind gift from P. Mehlen) expressing vectors diluted to 1 mg/ml in 1x phosphate buffer (PBS1x). Electroporated brains between E16.5 and P0 were fixed for 30 min in paraformaldehyde (PFA, Merck) 4% / PBS1x. For rescue experiments on *r5-6::Cre;Ezh2^{fl/fl}* embryos, the proportions of ectopic neurons were quantified by Imaris (Bitplane). A Student's t-test was used for statistical analysis.

Histological analysis, immunostaining, and *in situ* hybridization

Prenatal or postnatal brains, dissected when necessary, were fixed in 4% PFA diluted in phosphate buffer (PBS 1x) from 30 minutes to overnight. For cryostat sections, tissues were cryoprotected in 10% sucrose (Fluka) / PBS1x and embedded in gelatine 7.5% (Sigma) / 10% sucrose / PBS1x before being frozen at -80°C. Cryostat sections (20 μ m and 30 μ m) were cut (Microm HM560) in coronal and sagittal orientations, respectively. Vibratome sections (80 μ m or 35 μ m for reconstruction) were prepared from postnatal brains after embedding in 4% agarose (Promega)/0.1 M phosphate buffer (pH 7.4). Immunohistochemistry was performed as described in (6, 29) using rabbit anti-mouse

Pax6 (Millipore; AB2237; 1/1000^{em}), anti-Hoxa5 antibody (Sigma; HPA029319; 1/200^{em}), rat anti-mouse Hoxb4 (developed by A. Gould and R. Krumlauf; obtained from the Developmental Studies Hybridoma Bank developed under the auspices of the NICHD and maintained by The University of Iowa, Department of Biology, Iowa City, IA 52242; 1/100^{em}) or rabbit anti-mouse trimethyl-histone H3 Lys27 (07-449; Millipore; 1/250^{em}), followed by species-specific fluorochrome-coupled secondary antibody staining, including donkey anti-rabbit A546 (Invitrogen; 1/1000^{em}) and the donkey anti-rat A488 (Invitrogen; 1/1000^{em}) diluted in solutions containing DAPI (Invitrogen). Simple and double *in situ* hybridizations were performed as described previously(6). The following probes were used: *Barhl1*; *Hoxa2*; *Hoxb3*; *Hoxb4*; *Hoxb5*, *Hoxa5* (6, 29), *Ntn1* (6, 11), *Unc5b* and *Unc5c* (37). X-galactosidase staining on whole embryos, whole brains or cryostat sections was performed as described in (6).

Imaging and Picture Processing

Imaging of fluorescent signals was performed using an Axio imager Z2 upright microscope coupled to a LSM700 Zeiss laser scanning confocal 5x lens (NA 0.25), 10x lens (NA 0.45) or oil/glycerol/water immersion lens 25x (NA 0.8). Stitching of whole-mounts (electroporated brains) was performed using Zen Software at postnatal stages, and using Xuvtools (<http://www.xuvtools.org>) at prenatal stages. Chromogenic staining was examined by classical wide-field or binocular microscopy (Nikon). Fig. 2I is an inverted artificial superposition of chromogenic signals from adjacent sections. In Fig. 3A, B inverted X-Gal signal is artificially projected onto Pax6 immunohistochemistry.

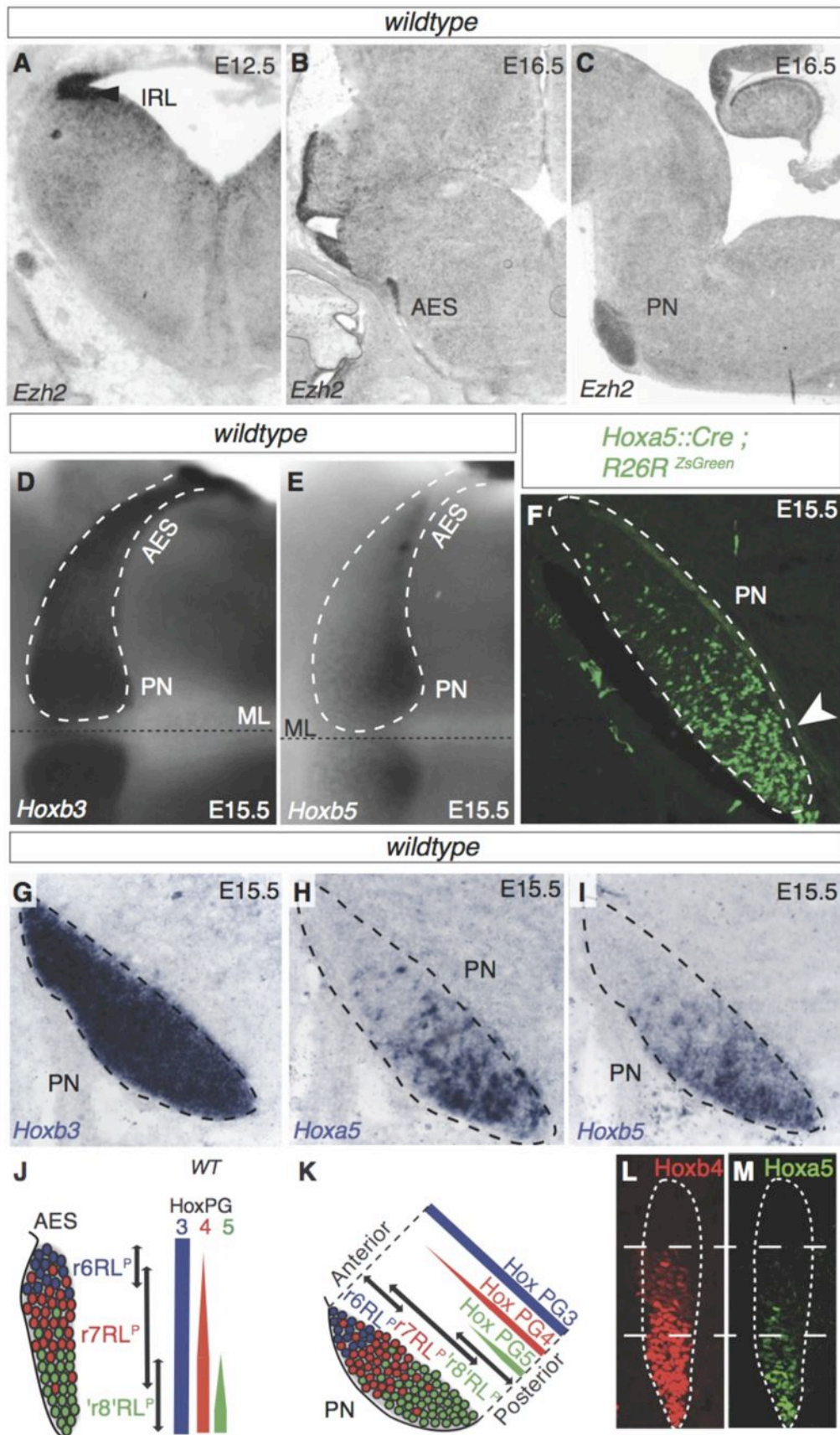


Fig. S1. *Ezh2* and *Hox* gene expression in precerebellar rhombic lip derivatives. (A to C) *Ezh2 in situ* hybridization on coronal (A, B) and sagittal sections (C). At E12.5 *Ezh2* is expressed in lower rhombic lip (IRL, A) and maintained in E16.5 anterior extramural stream (AES, B) and pontine nuclei (PN, C). (D to E) E15.5 whole-mount hindbrains show *Hoxb3* expression in all pontine neurons (D) and *Hoxb5* restriction to the posterior PN (E). (F) Sagittal section of E15.5 *Hoxa5::Cre;R26R^{ZsGreen}* specimen revealing the localization of ZsGreen⁺ neurons to the posterior PN (arrowhead). (G to I) E15.5 PN sagittal sections show *Hoxb3* expression in all pontine neurons (G) and restriction of *Hoxa5*⁺ (H) and *Hoxb5*⁺ (I) cells to the posterior PN. (J to K) Summaries of Fig. 2A-I and fig. S1D-I. (L to M) *Hoxb4* (L) and *Hoxa5* (M) immunostaining on a coronal section of a E14.5 wildtype embryo. ML: ventral midline.

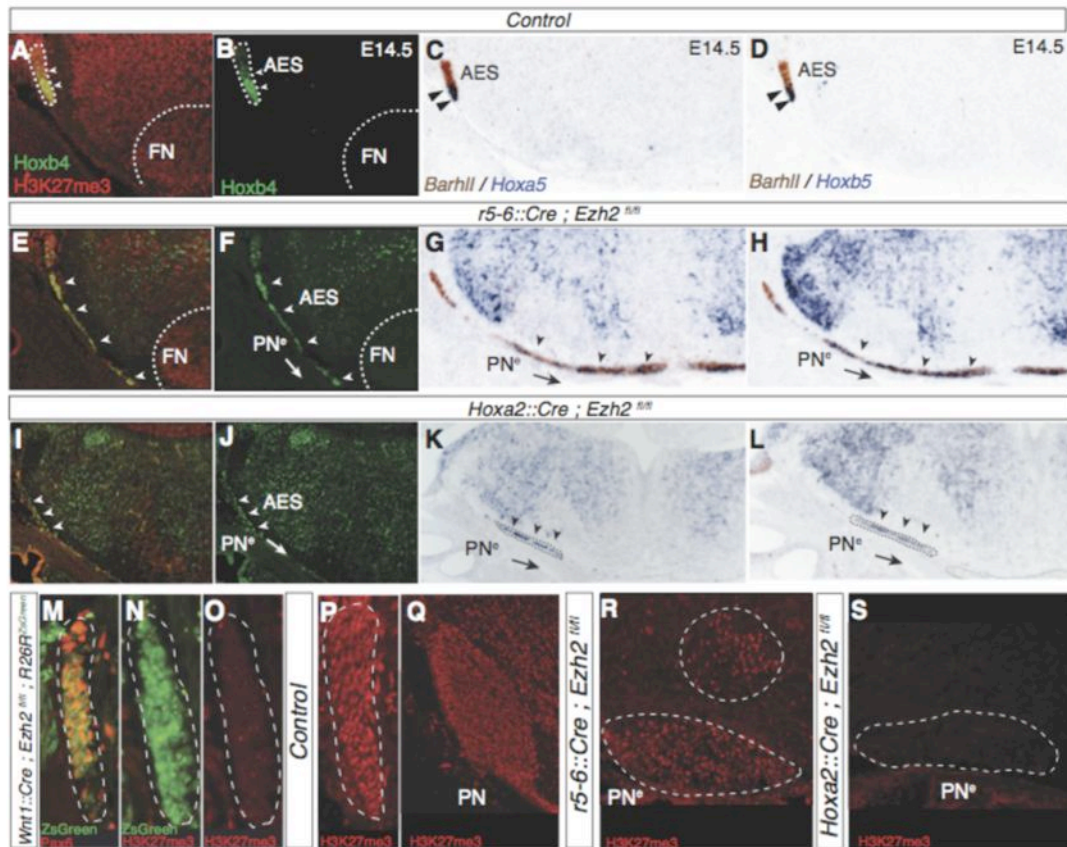


Fig. S2. Hox gene expression in migrating pontine neurons of *Ezh2* conditional mutants. (A to L) H3K27me3/*Hoxb4* immunostaining (A,B,E,F,I,J), *Hoxa5/Barhl1* (C,G,K) and *Hoxb5/Barhl1* (D,H,L) *in situ* hybridization on coronal sections at r5-r6 level in control (A-D), *r5-6::Cre;Ezh2^{fl/fl}* (E-H) and *Hoxa2::Cre;Ezh2^{fl/fl}* (I-L) E14.5 fetuses. Strong reduction of H3K27me3 in the r5-r6 environment of *Ezh2* conditional knockouts (E,F,I,J). In control (A-D), arrowheads show restricted ventral expression of *Hoxb4* (A,B), *Hoxa5* (C) and *Hoxb5* (D) in the anterior extramural stream (AES). In *r5-6::Cre;Ezh2^{fl/fl}* embryos, *Hoxb4*⁺ pontine neurons migrate to ectopic pontine nuclei (PN^e), are *Ezh2*^{+/+} (co-labeled by H3K27me3/*Hoxb4* double immunostaining (arrowheads, E,F)), and express both *Hoxa5* and *Hoxb5* (arrowheads, G,H). In *Hoxa2::Cre;Ezh2^{fl/fl}* embryos, *Hoxb4*⁺ pontine neurons migrate ectopically to PN^e are *Ezh2*^{-/-} as shown by the lack of H3K27me3 (arrowheads, I,J), and express both *Hoxa5* and *Hoxb5* (arrowheads, K,L). The neurons of the facial nucleus (FN), a r4 derivative, still carry the H3K27me3 mark in *r5-6::Cre;Ezh2^{fl/fl}* embryos, showing the specificity of the knockout (E). (M to P) Pax6 (M) and H3K27me3 (N,O,P) immunohistochemistry of *Wnt1::Cre;Ezh2^{fl/fl};R26R^{ZsGreen}* (M-O) and control AES (P) on coronal sections. In the conditional knockout, ZsGreen⁺ pontine neurons express Pax6 (M), but lack the H3K27me3 mark (N,O) in contrast to controls (P). (Q to S) H3K27me3 immunohistochemistry on sagittal sections at E18.5 showing loss of the H3K27me3 mark in environment only (R, *r5-6::Cre;Ezh2^{fl/fl}*) or environment and PN^e (S, *Hoxa2::Cre;Ezh2^{fl/fl}*) unlike in controls (Q).

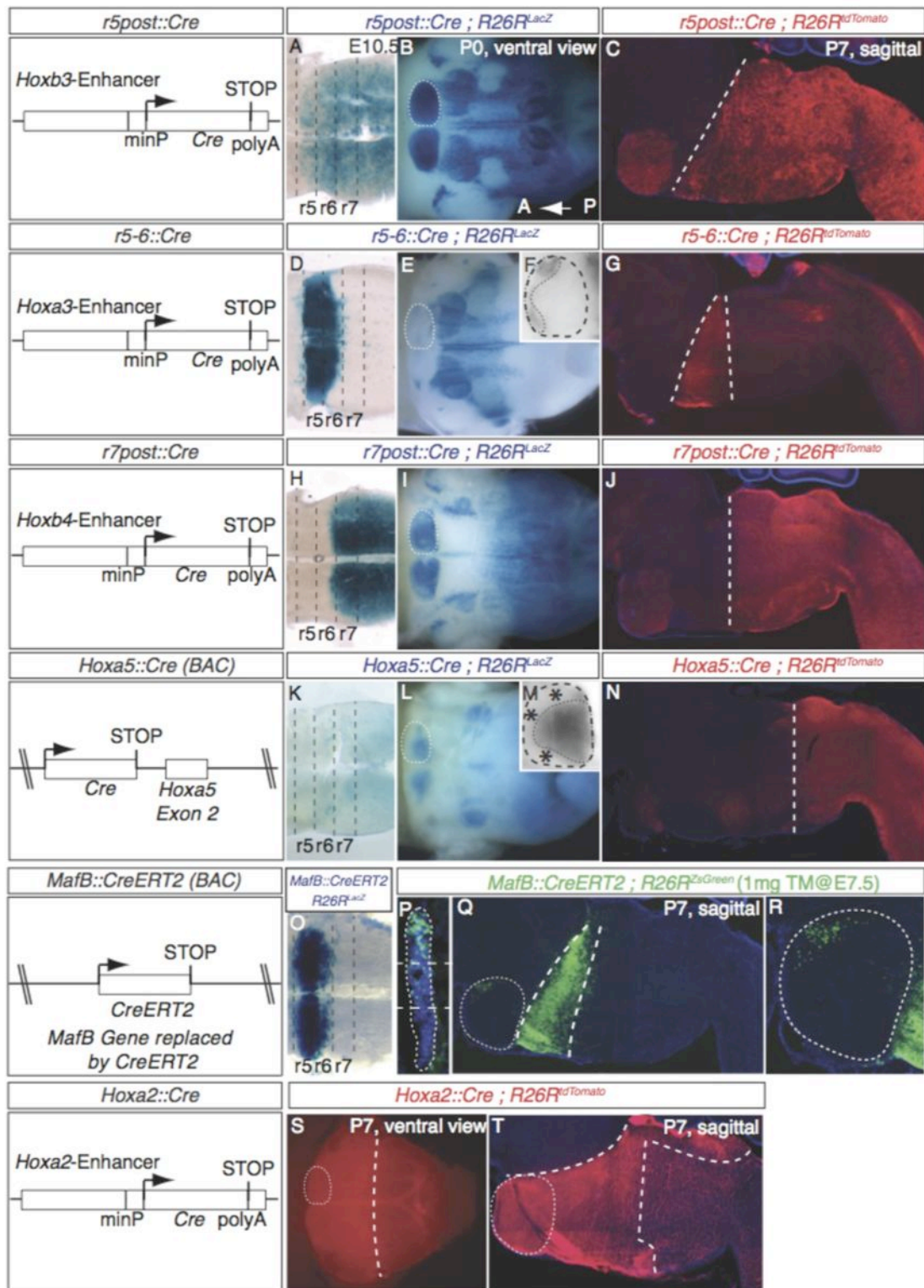


Fig. S3. Generation and characterization of posterior hindbrain Cre-expressing lines. (A,D,H,K,O) Embryos carrying *r5post::Cre* (A), *r5-6::Cre* (D), *r7post::Cre* (H)

and *Mafb::CreERT2* (1mg Tamoxifen@E7.5) (O) transgenes crossed to the *R26R^{LacZ}* floxed reporter and expressing *β-galactosidase (βGal)* at E10.5 in a rhombomere-specific manner, with *r5post::Cre* expression spanning r5 to spinal cord (A), *r5-6::Cre* and *Mafb::CreERT2* spanning r5 and r6 (D, O), and *r7post::Cre* spanning r7 to spinal cord (H). *Hoxa5::Cre* is not expressed in the hindbrain before E10.5 (K). **(B,E,I,L,S)** Detection of the *βGal* on whole-mount hindbrains (ventral views) at P0 show the spatially-restricted progeny of these rhombomeres traced after recombination of the *R26R^{LacZ}* locus in each of these Cre or CreERT2 expressing lines (B,E,I,L) or in (S) using the *R26R^{tdTomato}* reporter line at P7 for *Hoxa2::Cre*. **(F,M)** High magnifications show the segregation of r6 (*r5-6::Cre*, (F)) (rostrally) and *Hoxa5* (i.e. 'r8') (caudally) progenies (M) in the pontine nuclei. **(C,G,J,N,T)** Sagittal sections at P7 show recombined, *tdTomato*⁺ rhombomere progenies of indicated genotypes; segregation of rhombomere-derived territories persists up to postnatal stages. **(P to R)** Coronal (P, E15.5) and sagittal sections (Q,R, P7) of *Mafb::CreERT2; R26R^{ZsGreen}* show the dorsal restriction of r5-6 progeny in the anterior extramural stream (P) and the restriction of ZsGreen⁺ cells to the anterior pontine nuclei (R). r: rhombomere; minP: minimal promoter.

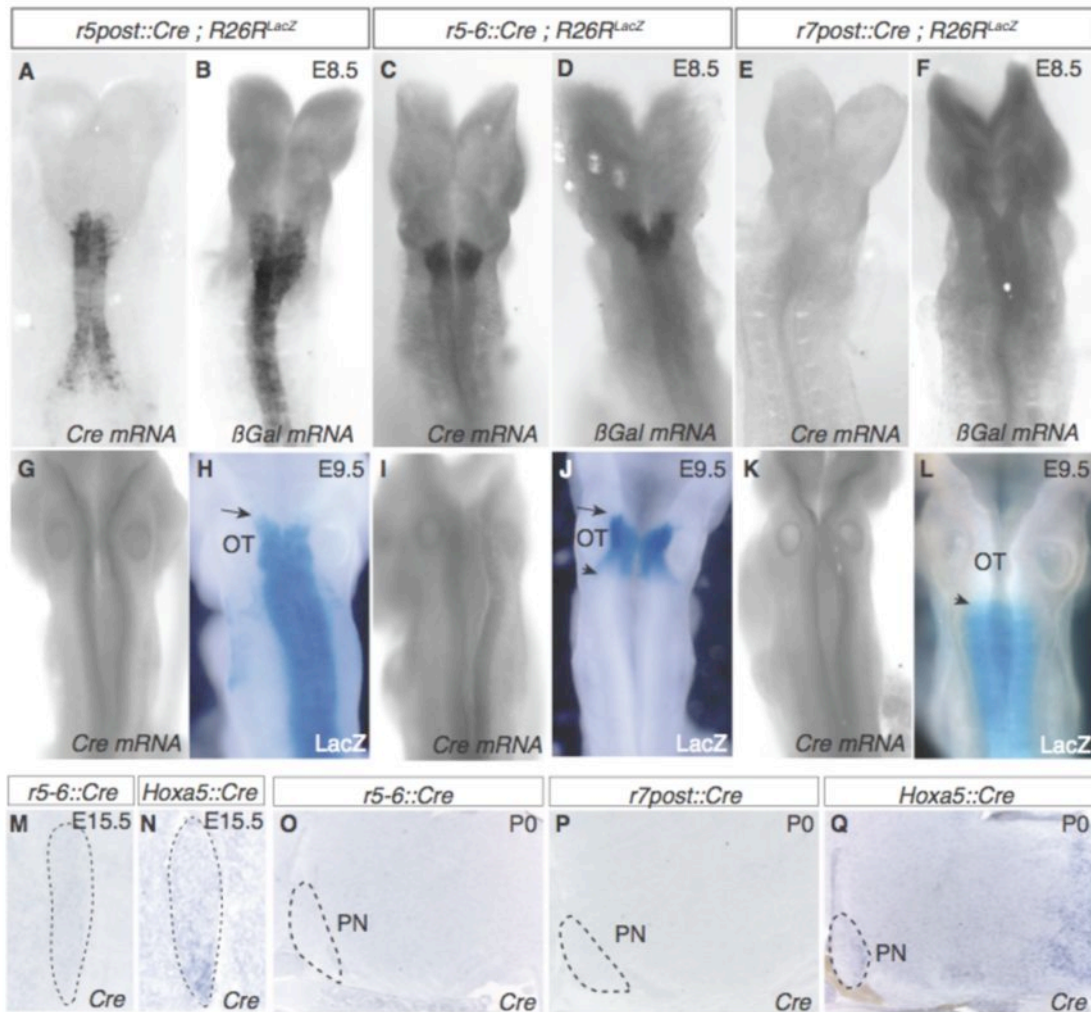


Fig. S4. Cre expression patterns in transgenic lines. (A to D) At E8.5, *Cre* (A,C) and β -galactosidase (β Gal) (B,D) are expressed in *r5post::Cre* (A,B) and *r5-6::Cre* (C,D) whole-mount embryos. (E to F) In *r7post::Cre*, neither *Cre* nor β -Gal are expressed at E8.5. (G, I, K) At E9.5, *Cre* transcripts were not detectable in any of the *Cre* transgenics. (H, J, L) LacZ signals reveal that the *R26R^{LacZ}* locus has recombined in all three *Cre* transgenics at E9.5. *r5post::Cre* (H) and *r5-6::Cre* (J) share the same β Gal anterior boundary (arrow), while *r5-6::Cre* (J) and *r7post::Cre* (L) have their posterior and anterior expression boundaries, respectively, at the r6/r7 border with no overlap (arrowhead). Note that *r7post::Cre;R26R^{LacZ}* show LacZ restricted activity at E9.5 (L), although *Cre* and β Gal transcript levels are below *in situ* hybridization detection at E8.5 and E9.5 (E,F,K). (M to N) *In situ* hybridizations on coronal sections of E15.5 AES show no expression of *Cre* in *r5-6::Cre* (M), while in *Hoxa5::Cre* embryos *Cre* expression faithfully recapitulates endogenous *Hoxa5* expression (N). (O to Q) On P0 sagittal sections, *Cre* transcripts are not present at detectable levels in *r5-6::Cre* (O) and *r7post::Cre* (P), while *Hoxa5::Cre* newborns show *Cre* expression in posterior hindbrain and posterior PN (Q). OT: otic capsule; PN: pontine nuclei.

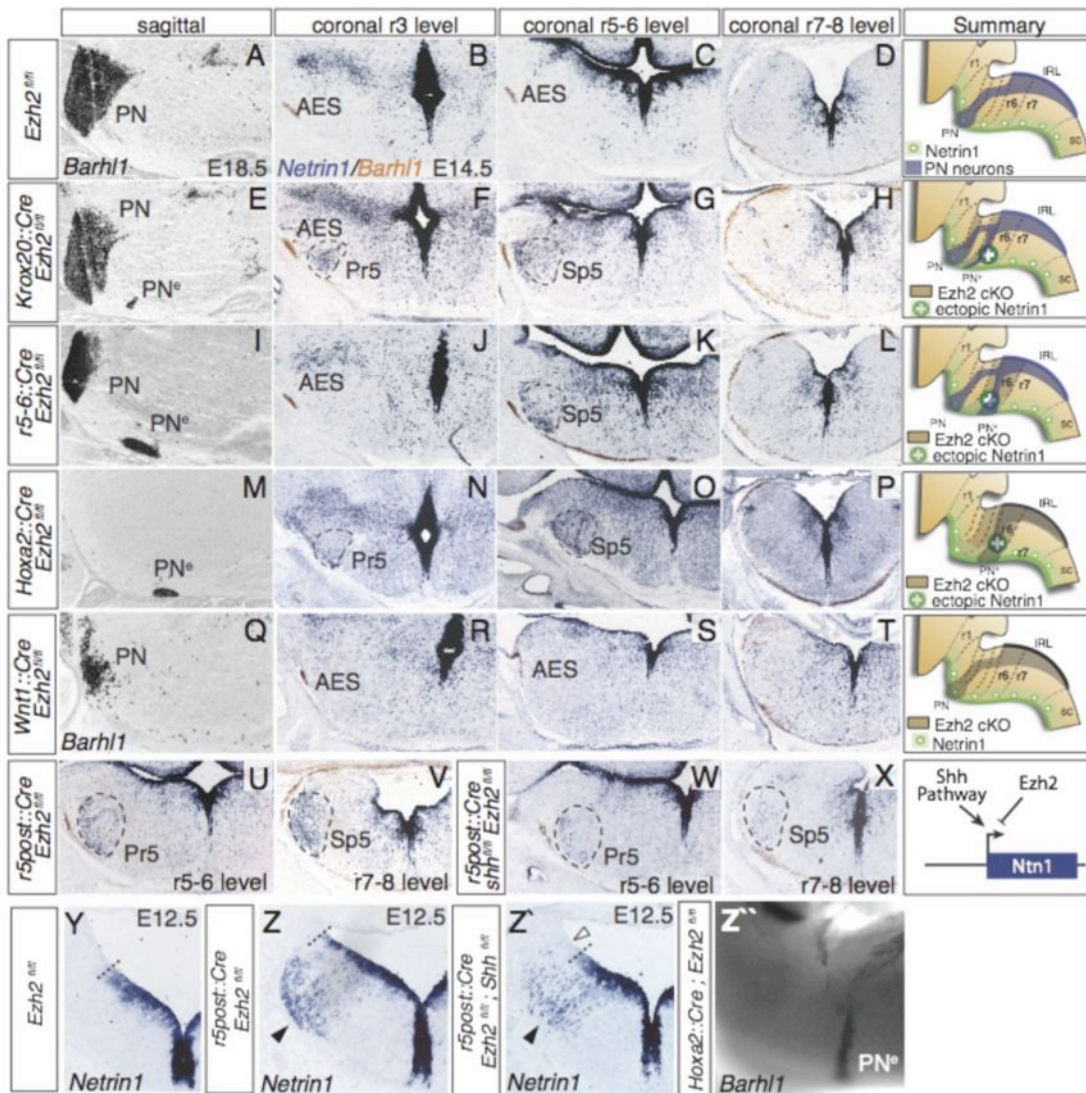
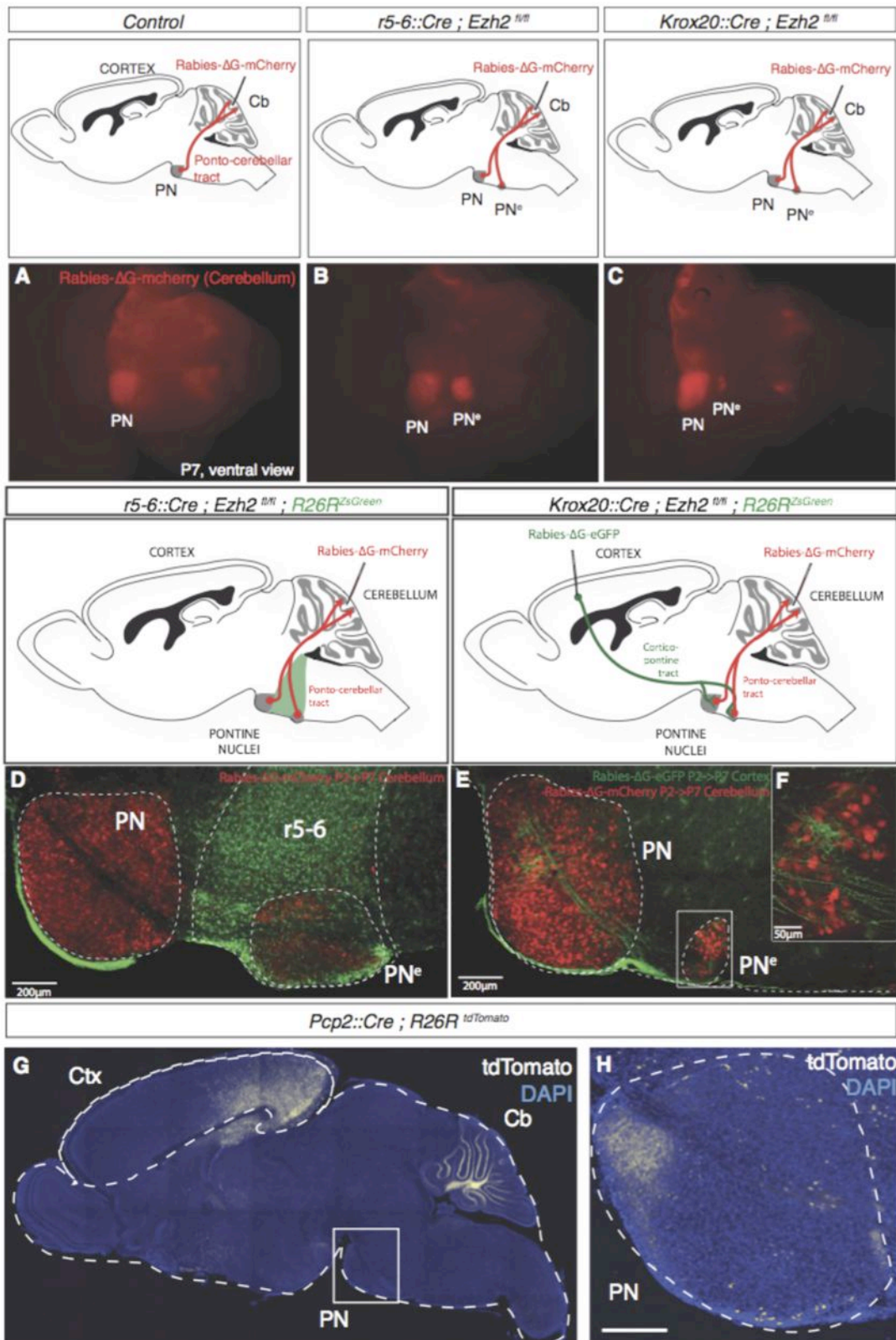


Fig. S5. Analysis of pontine neuron migratory phenotypes in *Ezh2* conditional mutants. (A to T), PN migratory phenotype in control *Ezh2*^{fl/fl} (A-D), *Krox20::Cre;Ezh2*^{fl/fl} (E-H), *r5-6::Cre;Ezh2*^{fl/fl} (I-L), *Hoxa2::Cre;Ezh2*^{fl/fl} (M-P) and *Wnt1::Cre;Ezh2*^{fl/fl} (Q-T) fetuses. *In situ* hybridization on sagittal sections show rostrocaudal distribution of normal (PN) and ectopic (PN^e) *Barhl1*⁺ pontine neurons at E18.5 in the different genotypes (A,E,I,M,Q). Co-detection of *Netrin1* and *Barhl1* transcripts on serial coronal sections taken at the r3, r5/r6 and r7/r8 levels show ectopic expression of *Netrin1* in *Krox20::Cre;Ezh2*^{fl/fl}, *r5-6::Cre;Ezh2*^{fl/fl} and *Hoxa2::Cre;Ezh2*^{fl/fl} (dashed lines, F,G,K,N,O) but not in *Wnt1::Cre;Ezh2*^{fl/fl} and *Ezh2*^{fl/fl} embryos at E14.5. (U to X) Expression of *Netrin1* and *Barhl1* in *r5post::Cre;Ezh2*^{fl/fl} (U, V) and *r5post::Cre;Ezh2*^{fl/fl};*Shh*^{fl/fl} (W,X) at r5/r6 (U, W) and r7/r8 (V, X) levels at E14.5. Ectopic *Netrin1* expression is strongly reduced in *Shh/Ezh2* double cKO (W,X) partially rescuing the *Ezh2* cKO phenotype (U,V). (Y to Z) At E12.5, ectopic *Netrin1* expression (black arrowheads) observed in *r5post::Cre;Ezh2*^{fl/fl} mutants (Z) is absent in controls (Y). (Z') At E12.5, ectopic *Barhl1* expression (black arrowheads) observed in *r5post::Cre;Ezh2*^{fl/fl} mutants (Z) is absent in controls (Z').

Ezh2^{fl/fl} (Y) and partially rescued in *r5post::Cre;Ezh2^{fl/fl};Shh^{fl/fl}* compound mutants (white and black arrowheads, Z). (Z') Migratory phenotypes in *Hoxa2::Cre;Ezh2^{fl/fl}* shown by *Barhl1 in situ* hybridization on E14.5 whole-mount. Summaries show the migratory pathways of wildtype and mutants as well as the proposed genetic interaction between Shh, Ezh2 and Netrin1 in the last column. AES: anterior extramural stream; IRL: lower rhombic lip; r: rhombomere; sc: spinal cord; Pr5: principal trigeminal nucleus; Sp5: spinal trigeminal nucleus; cKO: conditional knockout.



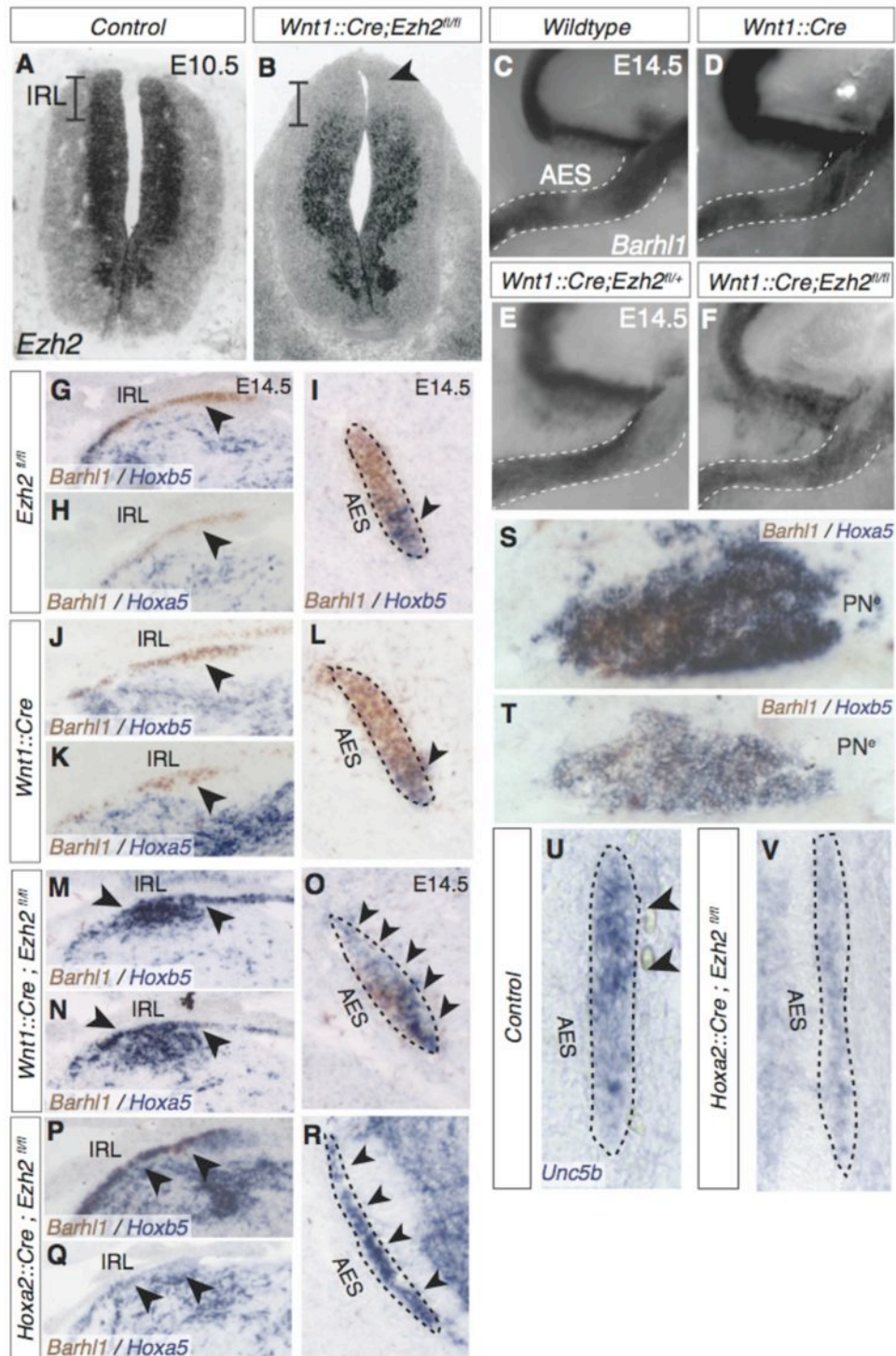


Fig. S7. *Ezh2* cell-autonomous role in rhombic lip and pontine neurons. (A to B) *Ezh2* is downregulated in the lower rhombic lip (IRL) of *Wnt1::Cre; Ezh2^{fl/fl}* embryos at E10.5 (B, arrowhead) compared to controls (A). (C to F) Lateral views of *Barhl1*⁺

Fig. S6. Cortico-ponto-cerebellar connectivity in *Ezh2* conditional mutants. (A to C) Ventral views of P7 whole-mount hindbrains after retrograde tracing with rabies- Δ G-mCherry from cerebellum (Cb) show that Cb is innervated by normal pontine nuclei (PN) in control (A) and both PN and ectopic pontine nuclei (PN^e) in *Krox20::Cre;Ezh2^{fl/fl}* (B) and *r5-6::Cre;Ezh2^{fl/fl}* (C) mutants. (D) Retrograde injections in P7 *r5-6::Cre;Ezh2^{fl/fl};R26R^{ZsGreen}* animals show that PN^e is included within the ZsGreen⁺ domain demonstrating PN^e localization in posterior r5/r6 as well as the duplication of both parts of the PN, i.e. reticulotegmental nucleus (inner nucleus) and pontine gray nucleus (outer nucleus). (E to F) Cortical injections of rabies- Δ G-GFP combined with retrograde cerebellar tracing (rabies- Δ G-mCherry) illustrate that in P7 *Krox20::Cre;Ezh2^{fl/fl}* pups, PN^e (F) is also integrated into cortico-ponto-cerebellar connectivity. Injections were carried out at P2 and analyzed at P7. (G to H) Restricted *tdTomato*⁺ cells in posterior/visual cortex (Ctx) in P7 *Pcp2::Cre;R26R^{tdTomato}* pups (G) and *tdTomato*⁺ axon projection to anterior PN in sagittal sections (H).

anterior extramural stream (AES) in E14.5 wild type (C), *Wnt1::Cre* (D), *Wnt1::Cre;Ezh2^{fl/+}* (E), and *Wnt1::Cre;Ezh2^{fl/fl}* (F) conditional mutant whole-mount hindbrains. (G to R) Co-detection of *Hoxb5* and *Barhl1* (G,I,J,L,M,O,P,R) and *Hoxa5* and *Barhl1* (H,K,N,Q) expression on coronal sections from E14.5 embryos (G-I, *Ezh2^{fl/fl}*; J-L, *Wnt1::Cre*), *Wnt1::Cre;Ezh2^{fl/fl}* (M-O) and *Hoxa2::Cre;Ezh2^{fl/fl}* (P-R) at anterior precerebellar IRL (G,H,J,K,M,N,P,Q) and AES levels (I,L,O,R). In controls *Hoxa5* and *Hoxb5* transcript is absent from the anterior precerebellar IRL (arrowheads, G,H,J,K) and restricted to the ventral AES (I,L). In both *Wnt1::Cre;Ezh2^{fl/fl}* and *Hoxa2::Cre;Ezh2^{fl/fl}* conditional knockouts, *Hoxa5* and *Hoxb5* are expressed ectopically in the anterior precerebellar IRL (arrowheads, M,N,P,Q) and throughout the AES (arrowheads, O,R), while expression is regionalized in controls (arrowheads, H,J). (S to T) Co-detection of *Hoxa5* (S), *Hoxb5* (T) and *Barhl1* (S,T) transcripts in E18.5 *Hoxa2::Cre;Ezh2^{fl/fl}* ectopic pontine nuclei (PN^e) on sagittal sections. (U to V) Dorsal *Unc5b* expression at E14.5 in coronal control AES (U), as compared to *Hoxa2::Cre;Ezh2^{fl/fl}* AES (V) showing *Unc5b* downregulation. PN: pontine nuclei.

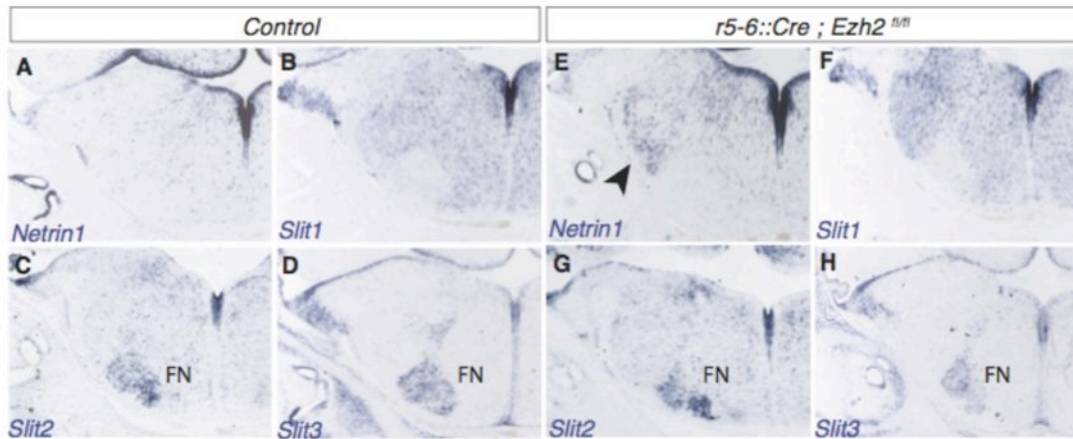


Fig. S8. *Slit1-3* expression patterns in conditional *Ezh2* mutants. (A to H) *In situ* hybridization for *Netrin1* (A,E), *Slit1* (B,F), *Slit2* (C,G) and *Slit3* (D,H) on adjacent coronal sections at r5-r6 level in E14.5 control (A-D) and *r5-6::Cre;Ezh2^{fl/fl}* (E-H). *Netrin1* is ectopically expressed in *r5-6::Cre;Ezh2^{fl/fl}* (arrowhead, E). FN: facial motor nucleus

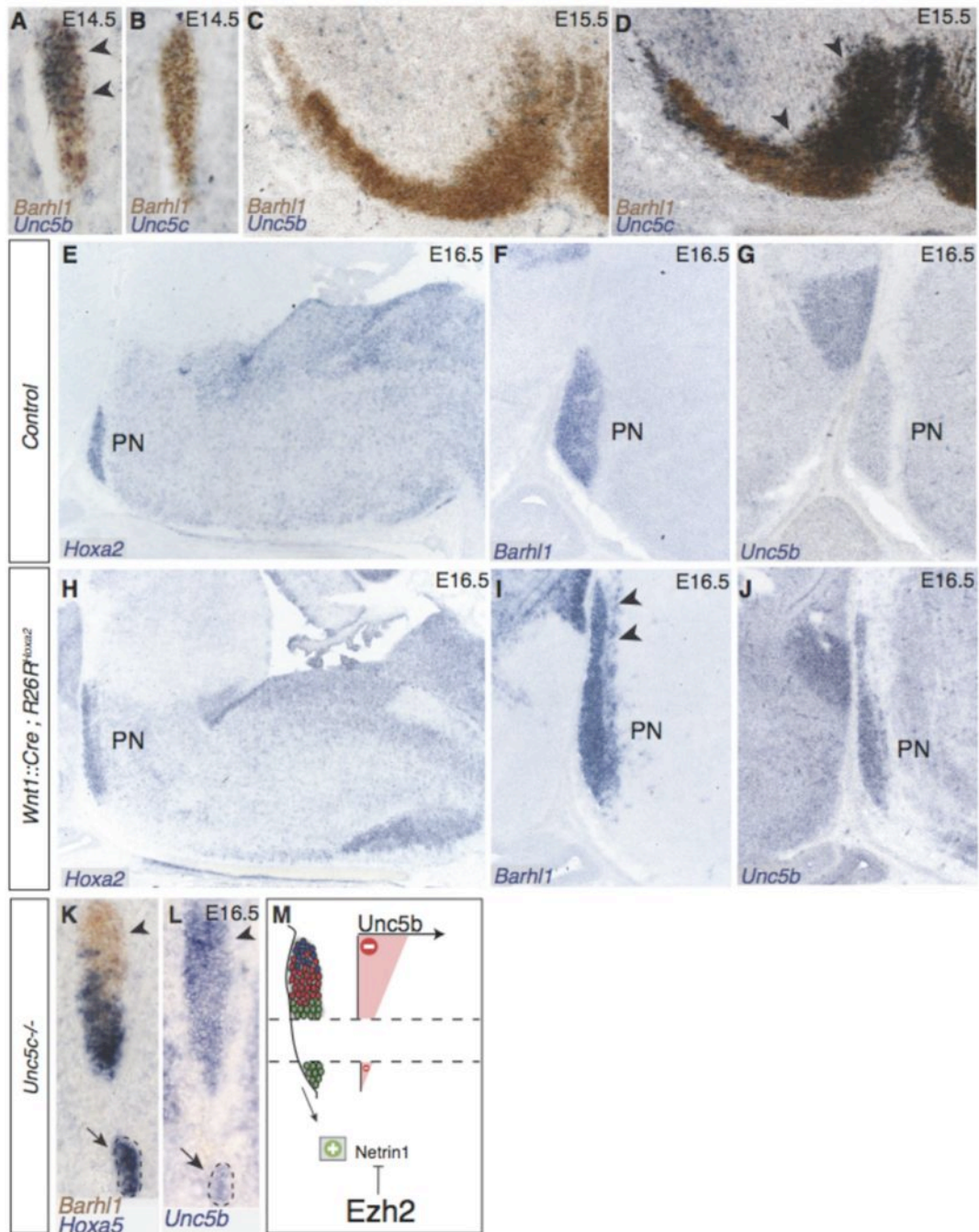


Fig. S9. *Unc5b* and *Unc5c* expression during normal pontine neuron migration and in *Wnt1::Cre;R26R^{Hoxa2}* mutants. (A to D) Double *in situ* hybridizations for *Barhl1/Unc5b* (A,C) and *Barhl1/Unc5c* (B,D) on coronal sections at E14.5 (A,B) and E15.5 (C,D). *Unc5b* transcripts are detected in the dorsal part of the anterior extramural stream (AES) (arrowheads, A) and become undetectable in *Barhl1*⁺ neurons reaching the ventral midline (C). On the contrary, *Unc5c* transcript expression is undetectable in AES neurons (B) while is reactivated during the second phase of ventral migration

(arrowheads, D). (**E to J**) *In situ* hybridization for *Hoxa2* (E,H), *Barhl1* (F,I) and *Unc5b* (G,J) on E16.5 sagittal sections in controls (E-G) and *Wnt1::Cre;R26R^{Hoxa2}* embryos (H-J). In the latter, pontine nuclei (PN) are anteriorly extended (arrow, I) and overexpress *Unc5b* (J), which is undetectable in control E16.5 PN (G). (**K to M**) *Hoxa5/Barhl1* (K) and *Unc5b* (L) expression in E16.5 *Unc5c^{-/-}* AES. Ectopically migrating neurons (arrows) strongly express *Hoxa5* while do not express *Unc5b*, as summarized in (M).

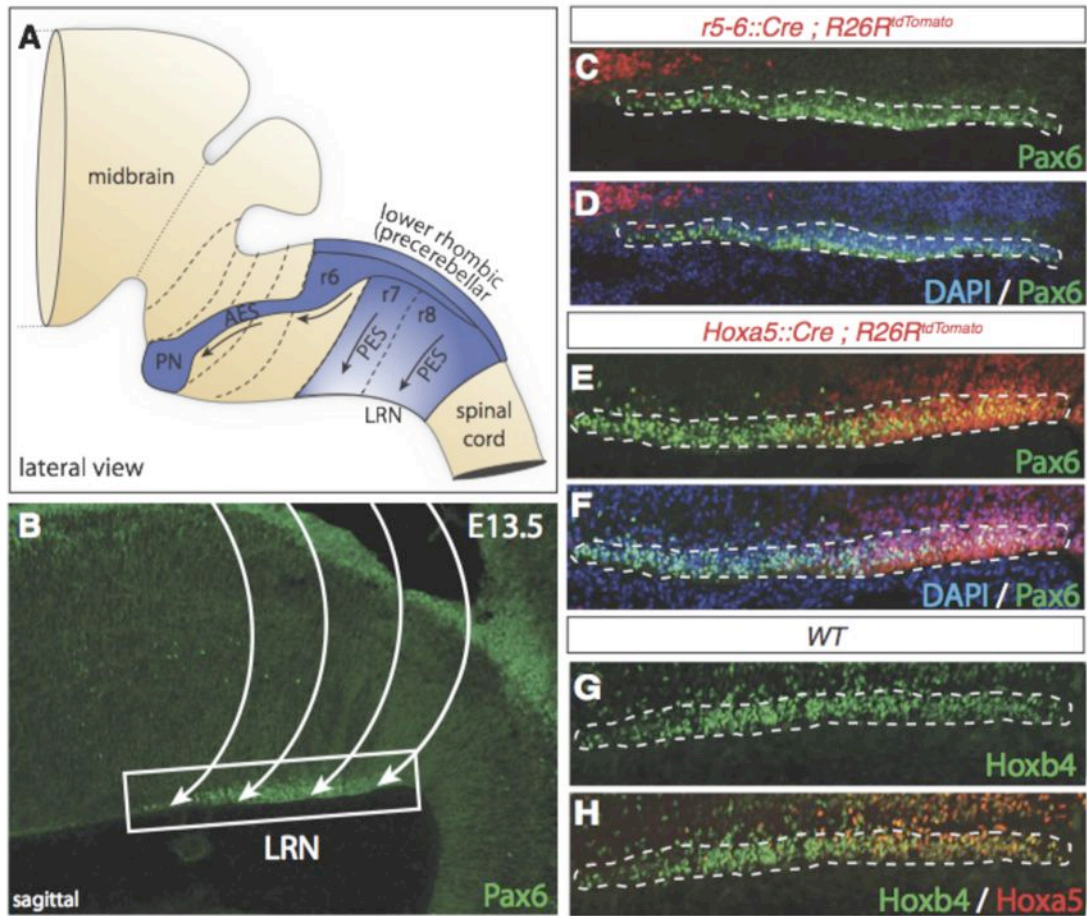


Fig. S10. Topographic organization of migrating lateral reticular nucleus. (A to B) Lateral reticular nucleus (LRN) neurons originate as the pontine nuclei (PN) from the lower rhombic lip (A) and migrate extramurally to the contralateral side. The migratory stream can be visualized by Pax6 immunostaining on E13.5 sagittal sections (B). (C to D) Pax6/DAPI double immunohistochemistry on sagittal sections of *r5-6::Cre;R26R^{tdTomato}* embryos at E13.5 showing that LRN neurons lack r5-6 derived progeny. (E to F) Pax6/DAPI double immunohistochemistry on sagittal sections of *Hoxa5::Cre;R26R^{tdTomato}* embryos at E13.5 showing that posterior LRN neurons are contributed by *Hoxa5::Cre;R26R^{tdTomato}* positive cells. (G to H) Immunohistochemistry for Hoxb4 (G) and Hoxa5 (H) in migrating LRN neurons on sagittal sections show the posterior restriction of Hoxa5 (H) positive cells. PES: posterior extramural stream; AES: anterior extramural stream.

References and Notes:

1. A. Lumsden, R. Krumlauf, Patterning the vertebrate neuraxis, *Science* **274**, 1109–1115 (1996).
2. S. Tümpel, L. M. Wiedemann, R. Krumlauf, Hox genes and segmentation of the vertebrate hindbrain, *Curr. Top. Dev. Biol.* **88**, 103–137 (2009).
3. A. F. Farago, R. B. Awatramani, S. M. Dymecki, Assembly of the brainstem cochlear nuclear complex is revealed by intersectional and subtractive genetic fate maps, *Neuron* **50**, 205–218 (2006).
4. J. Altman, S. A. Bayer, Development of the precerebellar nuclei in the rat: IV. The anterior precerebellar extramural migratory stream and the nucleus reticularis tegmenti pontis and the basal pontine gray, *J Comp Neurol* **257**, 529–552 (1987).
5. C. I. Rodriguez, S. M. Dymecki, Origin of the precerebellar system, *Neuron* **27**, 475–486 (2000).
6. M. J. Geisen *et al.*, Hox paralog group 2 genes control the migration of mouse pontine neurons through slit-robo signaling, *PLoS Biol* **6**, e142 (2008).
7. K. T. Yee, H. H. Simon, M. Tessier-Lavigne, D. M. O'Leary, Extension of long leading processes and neuronal migration in the mammalian brain directed by the chemoattractant netrin-1, *Neuron* **24**, 607–622 (1999).
8. S. Nóbrega-Pereira, O. Marín, Transcriptional control of neuronal migration in the developing mouse brain, *Cerebral Cortex* **19**, i107–13 (2009).
9. R. Margueron, D. Reinberg, The Polycomb complex PRC2 and its mark in life, *Nature* **469**, 343–349 (2011).
10. Materials and methods are available as supplementary material on Science Online.
11. E. Bloch-Gallego, F. Ezan, M. Tessier-Lavigne, C. Sotelo, Floor plate and netrin-1 are involved in the migration and survival of inferior olivary neurons, *J Neurosci* **19**, 4407–4420 (1999).
12. K. Hong *et al.*, A ligand-gated association between cytoplasmic domains of UNC5 and DCC family receptors converts netrin-induced growth cone attraction to repulsion, *Cell* **97**, 927–941 (1999).
13. D. Kim, S. L. Ackerman, The UNC5C netrin receptor regulates dorsal guidance of mouse hindbrain axons, *J Neurosci* **31**, 2167–2179 (2011).
14. X. Lu *et al.*, The netrin receptor UNC5B mediates guidance events controlling morphogenesis of the vascular system, *Nature* **432**, 179–186 (2004).

15. T. B. Leergaard, J. G. Bjaalie, Frontiers: Topography of the complete corticopontine projection: From experiments to principal maps, *Frontiers in neuroscience* **1**, 211–223 (2007).
16. P. Rakic, Specification of cerebral cortical areas, *Science* **241**, 170–176 (1988).
17. M. E. Hatten, Central nervous system neuronal migration, *Annu Rev Neurosci* **22**, 511–539 (1999).
18. E. C. Lee *et al.*, A highly efficient Escherichia coli-based chromosome engineering system adapted for recombinogenic targeting and subcloning of BAC DNA, *Genomics* **73**, 56–65 (2001).
19. T. O. Yau *et al.*, Auto/cross-regulation of Hoxb3 expression in posterior hindbrain and spinal cord, *Dev Biol* **252**, 287–300 (2002).
20. M. Manzanares *et al.*, Conserved and distinct roles of kreisler in regulation of the paralogous Hoxa3 and Hoxb3 genes, *Development* **126**, 759–769 (1999).
21. A. Gould, N. Itasaki, R. Krumlauf, Initiation of rhombomeric Hoxb4 expression requires induction by somites and a retinoid pathway, *Neuron* **21**, 39–51 (1998).
22. P. Soriano, Generalized lacZ expression with the ROSA26 Cre reporter strain, *Nat Genet* **21**, 70–71 (1999).
23. L. Madisen *et al.*, A robust and high-throughput Cre reporting and characterization system for the whole mouse brain, *Nat Neurosci* **13**, 133–140 (2010).
24. M. Studer, A. Lumsden, L. Ariza-McNaughton, A. Bradley, R. Krumlauf, Altered segmental identity and abnormal migration of motor neurons in mice lacking Hoxb-1, *Nature* **384**, 630–634 (1996).
25. F. M. Rijli *et al.*, A homeotic transformation is generated in the rostral branchial region of the head by disruption of Hoxa-2, which acts as a selector gene, *Cell* **75**, 1333–1349 (1993).
26. O. Nyabi *et al.*, Efficient mouse transgenesis using Gateway-compatible ROSA26 locus targeting vectors and F1 hybrid ES cells, *Nucleic Acids Res* **37**, e55–e55 (2009).
27. P. S. Danielian, D. Muccino, D. H. Rowitch, S. K. Michael, A. P. McMahon, Modification of gene activity in mouse embryos in utero by a tamoxifen-inducible form of Cre recombinase, *Curr Biol* **8**, 1323–1326 (1998).
28. M. Puschendorf *et al.*, PRC1 and Suv39h specify parental asymmetry at constitutive heterochromatin in early mouse embryos, *Nat Genet* **40**, 411–420 (2008).
29. D. C. McIntyre *et al.*, Hox patterning of the vertebrate rib cage, *Development* **134**, 2981–2989 (2007).

30. S. L. Ackerman *et al.*, The mouse rostral cerebellar malformation gene encodes an UNC-5-like protein, *Nature* **386**, 838–842 (1997).
31. P. M. Lewis, A. Gritli-Linde, R. Smeyne, A. Kottmann, A. P. McMahon, Sonic hedgehog signaling is required for expansion of granule neuron precursors and patterning of the mouse cerebellum, *Dev Biol* **270**, 393–410 (2004).
32. P. M. Lewis *et al.*, Cholesterol modification of sonic hedgehog is required for long-range signaling activity and effective modulation of signaling by Ptc1, *Cell* **105**, 599–612 (2001).
33. K. Yonehara *et al.*, Spatially asymmetric reorganization of inhibition establishes a motion-sensitive circuit, *Nature* **469**, 407–410 (2011).
34. H. Taniguchi, D. Kawauchi, K. Nishida, F. Murakami, Classic cadherins regulate tangential migration of precerebellar neurons in the caudal hindbrain, *Development* **133**, 1923–1931 (2006).
35. T. Okada, K. Keino-Masu, M. Masu, Migration and nucleogenesis of mouse precerebellar neurons visualized by in utero electroporation of a green fluorescent protein gene, *Neurosci Res* **57**, 40–49 (2007).
36. F. Llambi *et al.*, The dependence receptor UNC5H2 mediates apoptosis through DAP-kinase, *EMBO J* **24**, 1192–1201 (2005).
37. E. D. Leonardo *et al.*, Vertebrate homologues of *C. elegans* UNC-5 are candidate netrin receptors, *Nature* **386**, 833–838 (1997).

3.1.2 “*Ezh2* orchestrates topographic tangential migration and connectivity of precerebellar neurons” (unpublished parts)²

Retinoid signaling and *Ezh2* dependent *Hox* regulation in pontine neurons

To assess all genes regulated by *Ezh2*-mediated silencing at the r5-6 level at pre-migratory stage, we compared the transcriptome profiles of FACS-sorted cells from E11.5 *r5-6::Cre; Ezh2^{fl/+}; R26R^{ZsGreen}* and *r5-6::Cre; Ezh2^{fl/fl}; R26R^{ZsGreen}* embryos (**Figure 19**). Only 18 genes were significantly up-regulated (**Table 5**), whereas 79 genes were down-regulated (**Table 6**), in *Ezh2*-deficient embryos compared with control embryos (fold change >1.5; p<0.05). *Ntn1* was not yet significantly up-regulated at this stage (**Figure 21**, D), indicating progressive ectopic *Ntn1* accumulation in mutants through later stages (Di Meglio et al., 2013 and **Figure 21**, E). Moreover, while no *Hox* genes were significantly down-regulated (**Figure 20**) i) only a handful of *Hox* genes were ectopically de-repressed, namely selected members of ‘trunk’ *Hox PG4, PG5, PG6* and *PG8* (n=8); ii) expression of ‘head’ *Hox PG2* and *PG3* genes was normally maintained in mutants; iii) ‘tail’ *Hox PG10-13* genes were not de-repressed by r5-6-specific *Ezh2* inactivation. Thus, erasure of the H3K27me3 mark following *Ezh2* inactivation in r5-6-derived territory (Di Meglio et al., 2013) is not sufficient to induce generalized *Hox* gene up-regulation (or ectopic de-repression) but has a regional, context-dependent, impact on the transcriptional status of *Hox* clusters. The de-repression of *Hox* genes in *r5-6::Cre; Ezh2^{fl/fl}* can be also confirmed by qPCR (**Figure 21**, C) and in situ hybridization (Di Meglio et al., 2013).

These differential *Hox* transcriptional responses in *Ezh2* mutants may correlate with

² Statement of contribution: Experiments that were included in the first submitted manuscript, but were not included in the published version, will be presented in this subchapter. I contributed to the analysis of microarray and micro-Chip and performed all connectivity experiments. Experiments on retinoic acid injected brains were done by Thomas Di Meglio, qPCRs by Alberto Loche, Microarray by Alberto Loche and Hubertus Kohler, Micro-Chip by Antonio Vitobello and Ching-Yeu Liang.

their local sensitivity to signaling molecule(s). Notably, most of the over-expressed genes, including *Hox*, were retinoic acid (RA) responsive (**Table 7**). RA excess triggers PN migratory defects (Zhang et al., 2003). Higher (60mg/kg) or lower (30mg/kg) RA dosing of pregnant females at E9.5 caused dose-dependent AES ectopic migrations of distinct rostrocaudal extent and severity (**Figure 22**, A-B; **Figure 23**, L), partly mimicking the *Ezh2* knockout migratory phenotype. *Ntn1* and *Hox PG5* genes were ectopically induced in the hindbrain of RA-treated fetuses, similar to *Ezh2* mutants (**Figure 22**, C-F; **Figure 23**, A-D). RA synthesis occurs in the meninges that blanket the AES and PN (Zhang et al., 2003). Analysis of a *RARE::LacZ* retinoid reporter (Rossant et al., 1991) revealed that endogenous RA activity is graded ventrodorsally in the AES and caudo-rostrally in the PN (**Figure 22**, G, **Figure 23**, E), similar to the *Hox PG5* expression patterns. *LacZ* activity was strongly enhanced and ectopically extended into the anterior PN following RA administration as late as E13.5 and E14.5 (**Figure 22**, H).

RA administration at E11.5 (30mg/kg) did not cause migratory defects (**Figure 22**, I-J; **Figure 23**, F-G) but a strong up-regulation of *Hox PG5* in the PN, with *Hoxa5* and to a greater extent *Hoxb5* expression ectopically expanding to the anterior part of the nucleus (**Figure 22**, I-J; **Figure 23**, F-G). The same RA treatment of *r5-6::Cre; Ezh2^{fl/fl}* fetuses exacerbated the PN migratory phenotype. Additional *Hoxa5⁺/Hoxb5⁺* PN neurons were recruited into PN2 at the expense of PN1, compared with untreated mutant fetuses (**Figure 22**, K, M-N; **Figure 23**, H-J). In some mutants, a fraction of PN neurons migrated more rostrally than PN1 (PN0, **Figure 22**, N; **Figure 23**, J), a phenotype never observed in untreated *r5-6::Cre; Ezh2^{fl/fl}*.

Thus, PN neurons maintain the ability to respond to RA signaling and may still potentially change their *Hox* code through post-migratory stages. Maintenance of regionalized *Hox* expression throughout AES migration, and proper spatial restriction of environmental *Ntn1*, result from a balance between *Ezh2*-mediated silencing and RA-induced transcriptional response.

***In vivo* regulation of epigenetic configurations at *Hox* promoters**

How can *Ezh2* widespread distribution contribute to spatially-restricted *Hox* gene expression? We compared the distributions of H3K27me3 and H3K4me3, associated with transcriptionally active chromatin regions (Soshnikova and Duboule, 2009b; Strahl and Allis, 2000), at specific promoters *in vivo* by micro chromatin immunoprecipitation (microChIP) (Dahl and Collas, 2008) on two distinct rostrocaudal subpopulations, namely r5-6 and r7-8 derived cells from E16.5 *r5-6::Cre; R26R^{ZsGreen}* hindbrain (**Figure 24**, A). We compared the epigenetic status of *Hoxa5* and *Hoxb5* (repressed in r5-6, but expressed in r7-8) to that of *Hoxa2* (expressed throughout r5-8) or *Hoxa9* and *Hoxc13* (repressed throughout r5-8) promoters. We found bivalent (Bernstein et al., 2006) H3K27me3:H3K4me3 chromatin domains, whose relative enrichments correlated with the loci expression status. Interestingly, bivalent domains at the *Hoxa5* and *Hoxb5* promoters switched configuration from higher H3K27me3:H3K4me3 levels in r5-6 to opposite higher H3K4me3:H3K27me3 levels in r7-8, correlating with *Hox PG5* transcriptional ‘off-on’ switch, respectively. In contrast, the *Hoxa2* or *Hoxa9* and *Hoxc13* promoters maintained similar ‘on’ or ‘off’ bivalent configurations, respectively, in the two cell populations (**Figure 24**, B). Thus, spatially-restricted *Ezh2*-dependent *Hox* regulation could be partly achieved through local *Hox* promoter-specific modulation of H3K4me3 and H3K27me3 levels along the rostrocaudal axis.

Circuitry in *r5-6::Cre; Ezh2^{fl/fl}* mutants

In *r5-6::Cre; Ezh2^{fl/fl}* mutants, both PN1 and PN2 triggered collateralization of corticospinal axons and innervated the cerebellum (Di Meglio et al., 2013). Stereotactic viral injections further demonstrated that PN2 axons project to the cerebellum and that axonal input to PN2 can be retrogradely traced to cortical layer 5 neurons (**Figure 25**, A-C).

The *r5-6::Cre; Ezh2^{fl/fl}* mutants provide a suitable model to ask whether the establishment of patterned cortical input is related to regional PN pre-patterning (Di Meglio et al., 2013). PN1 and PN2 have distinct cellular and molecular compositions: i) PN2 is only contributed by r7-8RL-derived *Hox PG5⁺* PN neurons; ii) PN2 lacks

the r6RL-derived component; iii) *Hox PG5*-negative r6RL-derived PN neurons contribute only to PN1, where they are rostrally positioned. We examined whether these intrinsic PN1 and PN2 patterning differences result in distinct regional cortical input.

Injection of rabies- Δ G-GFP and - Δ G-mCherry into MPC and medial somatosensory cortex (SSC), respectively, resulted in rostral GFP⁺ and caudal mCherry⁺ axonal input onto the P7 PN (Di Meglio et al., 2013). 3-D reconstructions (**Figure 25**, D-G) confirmed rostrocaudal segregation of cortical GFP⁺ and mCherry⁺ input fibers onto PN from broad visual and somatosensory areas, in agreement with (Leergaard and Bjaalie, 2007).

Fold Change mt/ctrl	adjusted P-value	Gene	Gene Description
9.9760	0.0004	<i>En2</i>	engrailed 2
3.7368	0.0138	<i>Hoxd4</i>	home box D4
3.4299	0.0036	<i>Hoxa5</i>	homeobox A5
2.9932	0.0144	<i>Hoxb8</i>	homeobox B8
2.9123	0.0051	<i>Hoxb4</i>	homeobox B4
2.4885	0.0318	<i>Hoxb5</i>	homeobox B5
2.3446	0.0385	<i>Cnpy1</i>	canopy 1 homolog (zebrafish)
2.2983	0.0131	<i>D130079A08Rik</i>	RIKEN cDNA D130079A08 gene
2.0443	0.0378	NA	NA
2.0413	0.0201	<i>Hoxd8</i>	homeobox D8
1.9709	0.0060	<i>Hoxa4</i>	homeobox A4
1.9489	0.0460	<i>Hoxa6</i>	homeobox A6
1.8350	0.0481	<i>Bmi1</i>	Bmi1 polycomb ring finger oncogene
1.8000	0.0493	NA	NA
1.7801	0.0201	<i>Skap2</i>	src family associated phosphoprotein 2
1.6786	0.0262	<i>Tmem56</i>	transmembrane protein 56
1.6464	0.0485	<i>Nrgn</i>	neurogranin
1.6188	0.0340	<i>Shisa6</i>	shisa homolog 6 (<i>Xenopus laevis</i>)

Table 5 | Upregulated genes in *r5-6::Cre; Ezh2^{fl/fl}; R26R^{ZsGreen}*. Comparison between E11.5 in *r5-6::Cre; Ezh2^{fl/fl}; R26R^{ZsGreen}* specimens to *r5-6::Cre; Ezh2^{fl/+}; R26R^{ZsGreen}* embryos. 18 genes are upregulated in mutants (cutoffs: fold change > 1.5; adjusted *P*-value <0.05).

Fold Change ctrl/mt	adjusted P-value	Gene	Gene Description
68.3400	0.0001	<i>3110007F17Rik</i>	RIKEN cDNA 3110007F17 gene
16.9545	0.0011	<i>3110007F17Rik</i>	RIKEN cDNA 3110007F17 gene
11.1402	0.0011	<i>3110007F17Rik</i>	RIKEN cDNA 3110007F17 gene
8.7098	0.0018	<i>Post</i>	periostin, osteoblast specific factor
7.0817	0.0060	<i>Igf2</i>	insulin-like growth factor 2
6.3381	0.0001	<i>Prrx1</i>	paired related homeobox 1
5.4432	0.0017	<i>Ttr</i>	transthyretin
5.2845	0.0060	<i>H19</i>	H19 fetal liver mRNA
5.1443	0.0051	<i>Penk</i>	preproenkephalin
4.8738	0.0116	<i>Hmcn1</i>	hemicentin 1
4.3737	0.0144	<i>Hmcn1</i>	hemicentin 1
4.0049	0.0131	NA	NA
3.9164	0.0011	<i>Hmcn1</i>	hemicentin 1
3.8902	0.0467	<i>Bgn</i>	biglycan
3.6199	0.0263	<i>Col12a1</i>	collagen, type XII, alpha 1
3.5727	0.0011	<i>Hmcn1</i>	hemicentin 1
3.5416	0.0058	<i>Dct</i>	dopachrome tautomerase
3.4947	0.0087	<i>ErbB3</i>	v-erb-b2 erythrobl. leukemia viral oncogene homolog 3
3.4475	0.0045	<i>Hmcn1</i>	hemicentin 1
3.3814	0.0326	<i>Hmcn1</i>	hemicentin 1
3.3139	0.0439	<i>Foxc2</i>	forkhead box C2
3.3075	0.0211	<i>Hmcn1</i>	hemicentin 1
3.2928	0.0060	<i>Hmcn1</i>	hemicentin 1
3.2036	0.0112	<i>Hmcn1</i>	hemicentin 1
3.1731	0.0186	<i>Gpc3</i>	glypican 3
3.1534	0.0011	<i>Capn6</i>	calpain 6
3.1423	0.0467	<i>Lgals1</i>	lectin, galactose binding, soluble 1
3.1367	0.0017	<i>Six1</i>	sine oculis-related homeobox 1 homolog (Drosophila)
3.1022	0.0387	<i>Dab2</i>	disabled homolog 2 (Drosophila)
3.0761	0.0144	<i>Tgfb1</i>	transforming growth factor, beta induced
3.0566	0.0260	<i>Cnn2</i>	calponin 2
3.0391	0.0144	<i>Hmcn1</i>	hemicentin 1
2.9862	0.0011	<i>Ednra</i>	endothelin receptor type A
2.9696	0.0266	<i>Fbn2</i>	fibrillin 2

2.9377	0.0060	<i>Ddr2</i>	discoidin domain receptor family, member 2
2.9326	0.0305	<i>Hmcn1</i>	hemicentin 1
2.9060	0.0184	<i>Hmcn1</i>	hemicentin 1
2.8964	0.0110	<i>Ogn</i>	osteoglycin
2.8913	0.0060	<i>Hmcn1</i>	hemicentin 1
2.8326	0.0051	<i>H19</i>	H19 fetal liver mRNA
2.8239	0.0032	<i>Itm2a</i>	integral membrane protein 2A
2.7913	0.0131	<i>Hmcn1</i>	hemicentin 1
2.7911	0.0330	<i>Hmcn1</i>	hemicentin 1
2.7743	0.0215	<i>Islr</i>	immunoglobulin superfam containing leucine-rich repeat
2.6926	0.0134	<i>A430107O13Rik</i>	RIKEN cDNA A430107O13 gene
2.6923	0.0046	<i>Cdh19</i>	cadherin 19, type 2
2.6757	0.0290	<i>Hmcn1</i>	hemicentin 1
2.6479	0.0144	<i>Hmcn1</i>	hemicentin 1
2.6466	0.0051	<i>S100a11</i>	S100 calcium binding protein A11 (calgizzarin)
2.5346	0.0376	<i>Hmcn1</i>	hemicentin 1
2.5236	0.0305	<i>Hmcn1</i>	hemicentin 1
2.5183	0.0494	<i>Hmcn1</i>	hemicentin 1
2.4971	0.0116	<i>Colec12</i>	collectin sub-family member 12
2.4926	0.0243	<i>Hmcn1</i>	hemicentin 1
2.4631	0.0144	<i>Pdgfra</i>	platelet derived growth factor receptor, alpha polypeptide
2.4123	0.0338	<i>Hmcn1</i>	hemicentin 1
2.4000	0.0136	<i>Hmcn1</i>	hemicentin 1
2.3950	0.0494	<i>Hmcn1</i>	hemicentin 1
2.3845	0.0436	<i>Slc38a4</i>	solute carrier family 38, member 4
2.3613	0.0298	<i>Hmcn1</i>	hemicentin 1
2.3161	0.0436	NA	NA
2.3088	0.0245	<i>Colla2</i>	collagen, type I, alpha 2
2.2903	0.0138	<i>Sostdc1</i>	sclerostin domain containing 1
2.2833	0.0144	<i>Anxa5</i>	annexin A5
2.2457	0.0402	<i>Hmcn1</i>	hemicentin 1
2.2343	0.0093	<i>Twist2</i>	twist homolog 2 (Drosophila)
2.2284	0.0144	<i>Plp1</i>	proteolipid protein (myelin) 1
2.2266	0.0144	<i>Hmcn1</i>	hemicentin 1
2.2244	0.0100	<i>Foxfla</i>	forkhead box F1a
2.1888	0.0116	<i>Hmcn1</i>	hemicentin 1
2.1564	0.0290	<i>Mmp2</i>	matrix metalloproteinase 2

2.1509	0.0131	<i>Foxf2</i>	forkhead box F2
2.1488	0.0131	<i>Lama4</i>	laminin, alpha 4
2.1379	0.0144	<i>Creb3l2</i>	cAMP responsive element binding protein 3-like 2
2.1253	0.0227	<i>Foxd1</i>	forkhead box D1
2.1158	0.0144	<i>Hmcn1</i>	hemicentin 1
2.1063	0.0186	<i>Itga4</i>	integrin alpha 4
2.0992	0.0417	<i>Hmcn1</i>	hemicentin 1
2.0807	0.0060	<i>Hmcn1</i>	hemicentin 1
2.0630	0.0236	<i>Gm7120</i>	predicted gene 7120
2.0510	0.0144	<i>S100a11</i>	S100 calcium binding protein A11 (calgizzarin)
2.0467	0.0112	<i>Meox2</i>	mesenchyme homeobox 2
2.0242	0.0093	<i>Ceacam1</i>	carcinoembryonic antigen-related cell adh. molecule 1
2.0088	0.0481	<i>Pcolce</i>	procollagen C-endopeptidase enhancer protein
2.0075	0.0378	<i>Hmcn1</i>	hemicentin 1
2.0054	0.0276	<i>Tnc</i>	tenascin C
1.9993	0.0378	<i>Hmcn1</i>	hemicentin 1
1.9988	0.0290	<i>Serpinf1</i>	serine (or cysteine) peptidase inhib., clade F, member 1
1.9939	0.0308	<i>Gpr124</i>	G protein-coupled receptor 124
1.9904	0.0200	<i>Hmcn1</i>	hemicentin 1
1.9778	0.0131	<i>Cxcl12</i>	chemokine (C-X-C motif) ligand 12
1.9768	0.0340	<i>Myl9</i>	myosin, light polypeptide 9, regulatory
1.9758	0.0290	<i>Hmcn1</i>	hemicentin 1
1.9427	0.0240	<i>Sema3c</i>	Semaphorin 3C
1.9274	0.0493	<i>Flrt2</i>	fibronectin leucine rich transmembrane protein 2
1.9125	0.0439	<i>Fkbp10</i>	FK506 binding protein 10
1.8864	0.0186	<i>Foxfla</i>	forkhead box F1a
1.8840	0.0184	<i>Duxbl</i>	double homeobox B-like
1.8721	0.0242	<i>Hmcn1</i>	hemicentin 1
1.8658	0.0467	<i>D14Ert449e</i>	DNA segment, Chr 14, ERATO Doi 449, expressed
1.8579	0.0494	<i>Hmcn1</i>	hemicentin 1
1.8488	0.0268	<i>Duxbl</i>	double homeobox B-like
1.7652	0.0450	<i>Hmcn1</i>	hemicentin 1
1.7290	0.0494	<i>Sepp1</i>	selenoprotein P, plasma, 1
1.7154	0.0402	<i>Slitrk6</i>	SLIT and NTRK-like family, member 6
1.7140	0.0211	<i>Hmcn1</i>	hemicentin 1
1.7130	0.0454	<i>Hmcn1</i>	hemicentin 1
1.7095	0.0242	<i>Hmcn1</i>	hemicentin 1

1.6911	0.0303	<i>Rxrg</i>	retinoid X receptor gamma
1.6884	0.0482	<i>Stard13</i>	StAR-related lipid transfer (START) domain containing 13
1.6872	0.0295	<i>Tns3</i>	tensin 3
1.6843	0.0482	<i>Sox10</i>	SRY-box containing gene 10
1.6773	0.0162	<i>Fbn1</i>	fibrillin 1
1.6701	0.0400	<i>Sec24d</i>	Sec24 related gene family, member D (<i>S. cerevisiae</i>)
1.6578	0.0223	<i>Snai2</i>	snail homolog 2 (<i>Drosophila</i>)
1.6574	0.0194	<i>Dse</i>	dermatan sulfate epimerase
1.6417	0.0454	<i>Lix1</i>	limb expression 1 homolog (chicken)
1.6405	0.0493	<i>Plod2</i>	procollagen lysine, 2-oxoglutarate 5-dioxygenase 2
1.6330	0.0295	<i>Synpo</i>	synaptopodin
1.6295	0.0402	<i>Lrig3</i>	leucine-rich repeats and immunoglobulin-like domains 3
1.6275	0.0450	<i>Ghr</i>	growth hormone receptor
1.6146	0.0378	<i>Hmcn1</i>	hemicentin 1
1.5975	0.0467	<i>Hmcn1</i>	hemicentin 1
1.5872	0.0467	<i>Mreg</i>	melanoregulin
1.5673	0.0340	<i>En1</i>	engrailed 1
1.5433	0.0467	<i>Hmcn1</i>	hemicentin 1
1.5341	0.0340	<i>Copz2</i>	coatamer protein complex, subunit zeta 2

Table 6 | Downregulated genes in *r5-6::Cre; Ezh2^{fl/fl}; R26R^{ZsGreen}*. Comparison between E11.5 in *r5-6::Cre; Ezh2^{fl/+}; R26R^{ZsGreen}* specimens to *r5-6::Cre; Ezh2^{fl/fl}; R26R^{ZsGreen}* embryos. 79 genes are upregulated in controls compared to mutants (cutoffs: fold change > 1.5; adjusted *P*-value <0.05).

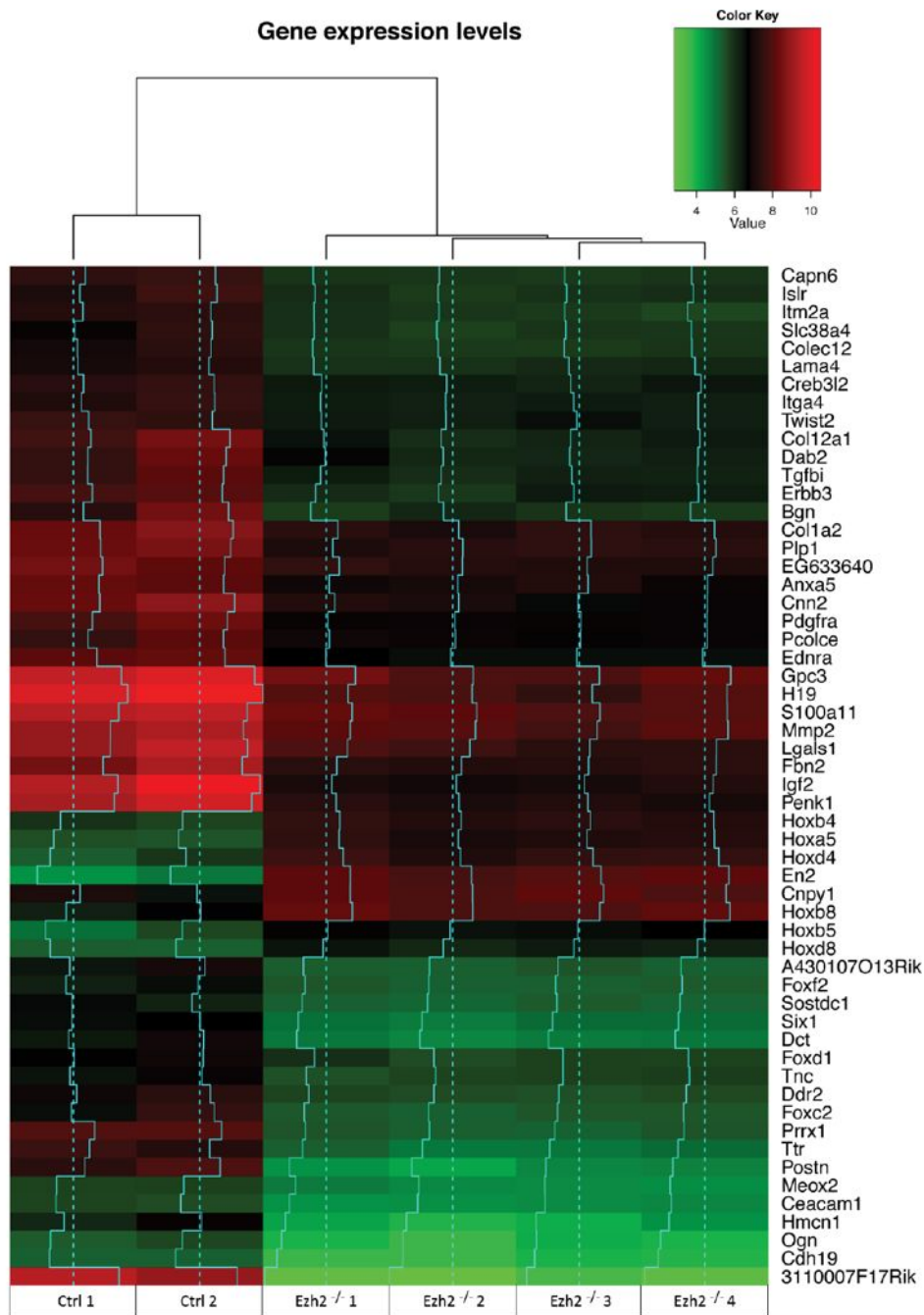


Figure 19 | Transcriptome analysis of $r5-6::Cre;Ezh2^{fl/fl}; ZsGreen$ mutants I. Heat map representation of gene expression levels for two controls ($r5-6::Cre; Ezh2^{fl/+}; ZsGreen$) and four mutants ($r5-6::Cre; Ezh2^{fl/fl}; ZsGreen$) (cutoffs: fold change > 2.0; adjusted P -value < 0.05)

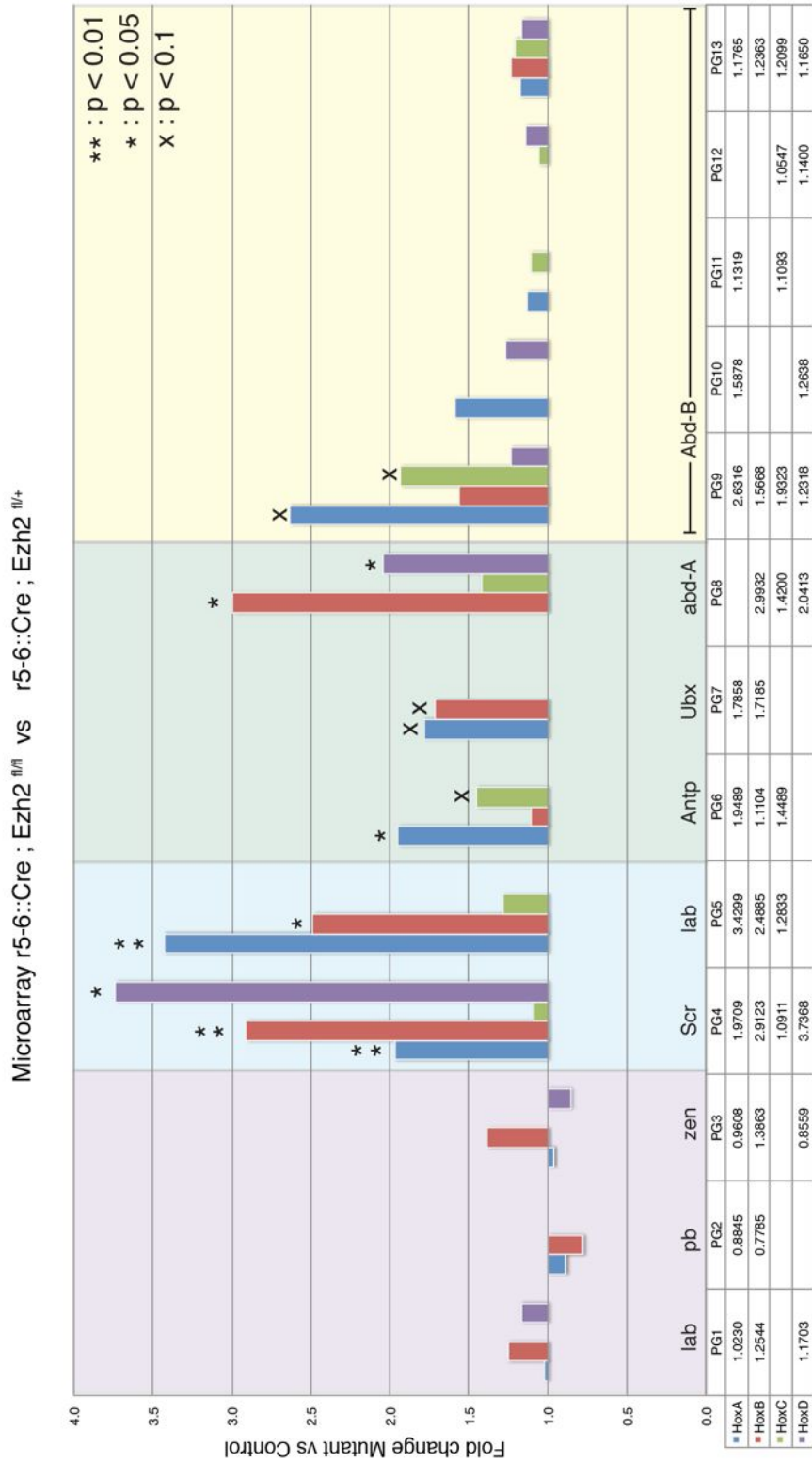


Figure 20 | Transcriptome analysis of *r5-6::Cre; Ezh2^{fl/fl}*; *ZsGreen* mutants II. Fold change representation (*r5-6::Cre; Ezh2^{fl/fl}*; *ZsGreen* vs. *r5-6::Cre; Ezh2^{fl/+}*; *ZsGreen*) of the *Hox* clusters.

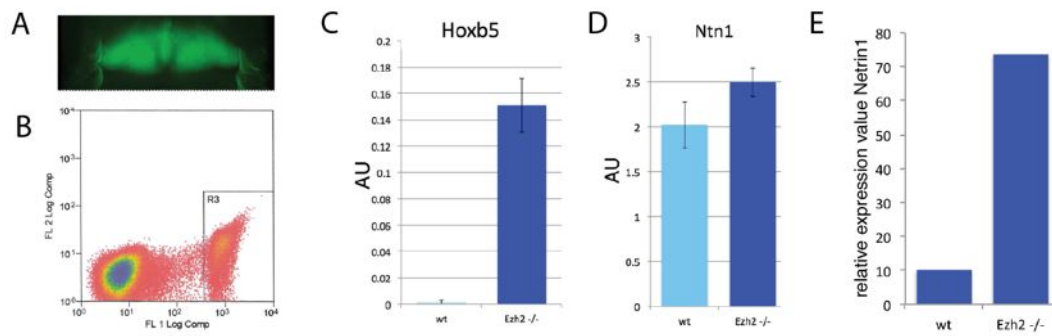


Figure 21 | FACS for Microarray and qPCRs for *Hoxb5* and *Ntn1*. (A) Dissected *ZsGreen*⁺ r5-6 territory from an E10.5 *r5-6::Cre; Ezh2^{fl/fl}; R26R^{ZsGreen}* embryo, prior to fluorescence-activated cell sorting; (B) Example of a sorted population of r5-6 cells (R3 inset), processed and analyzed by gene array. (C, D) Validation of gene array selected genes (*Hoxb5* and *Ntn1*) by qPCR; (E) *Ntn1* expression levels detected by qPCR in E15.5 wild-type (n=4) and *r5post::Cre; Ezh2^{fl/fl}; R26R^{ZsGreen}* (n=2) posterior hindbrain. Measurements are normalized to GAPDH expression.

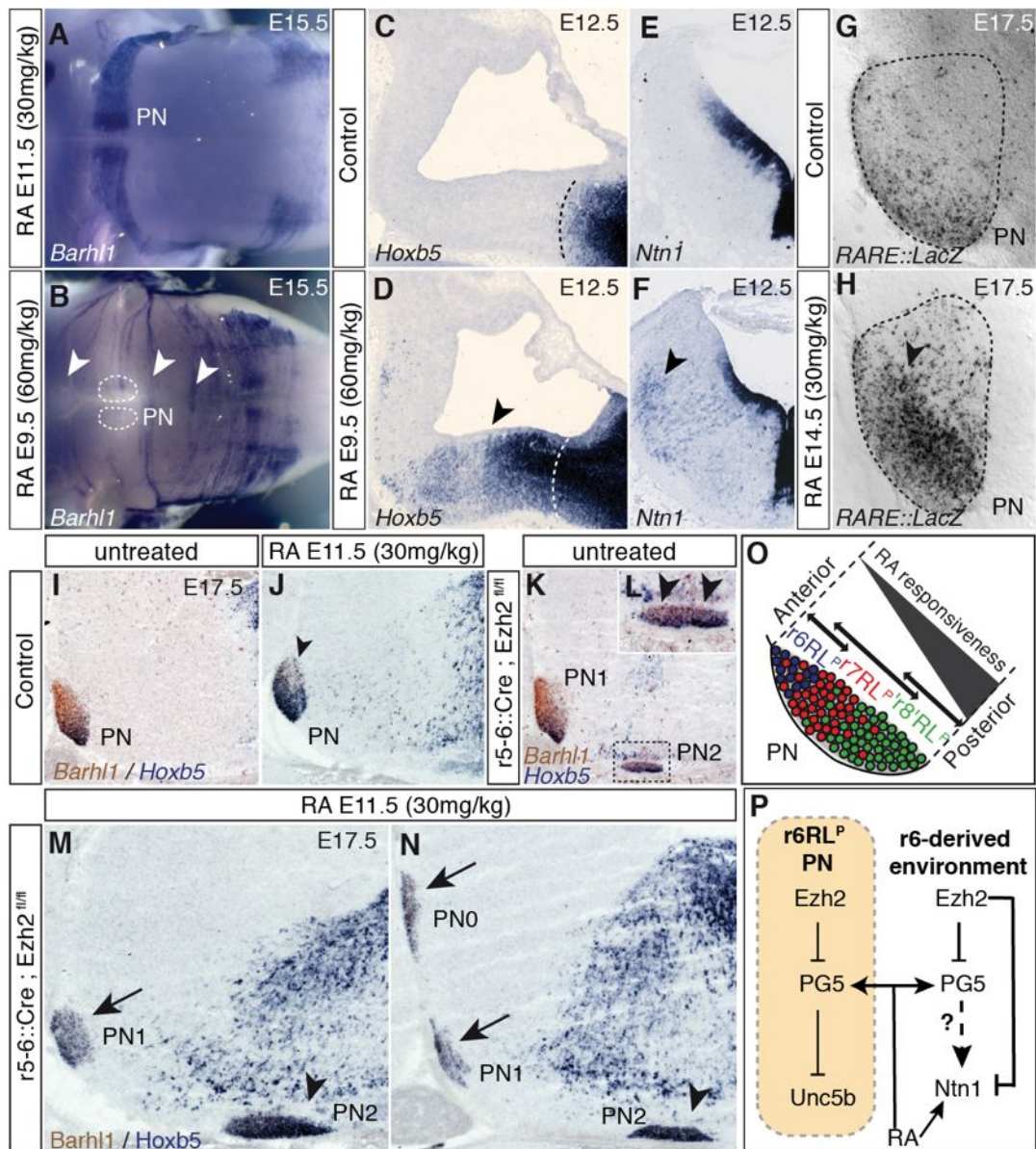
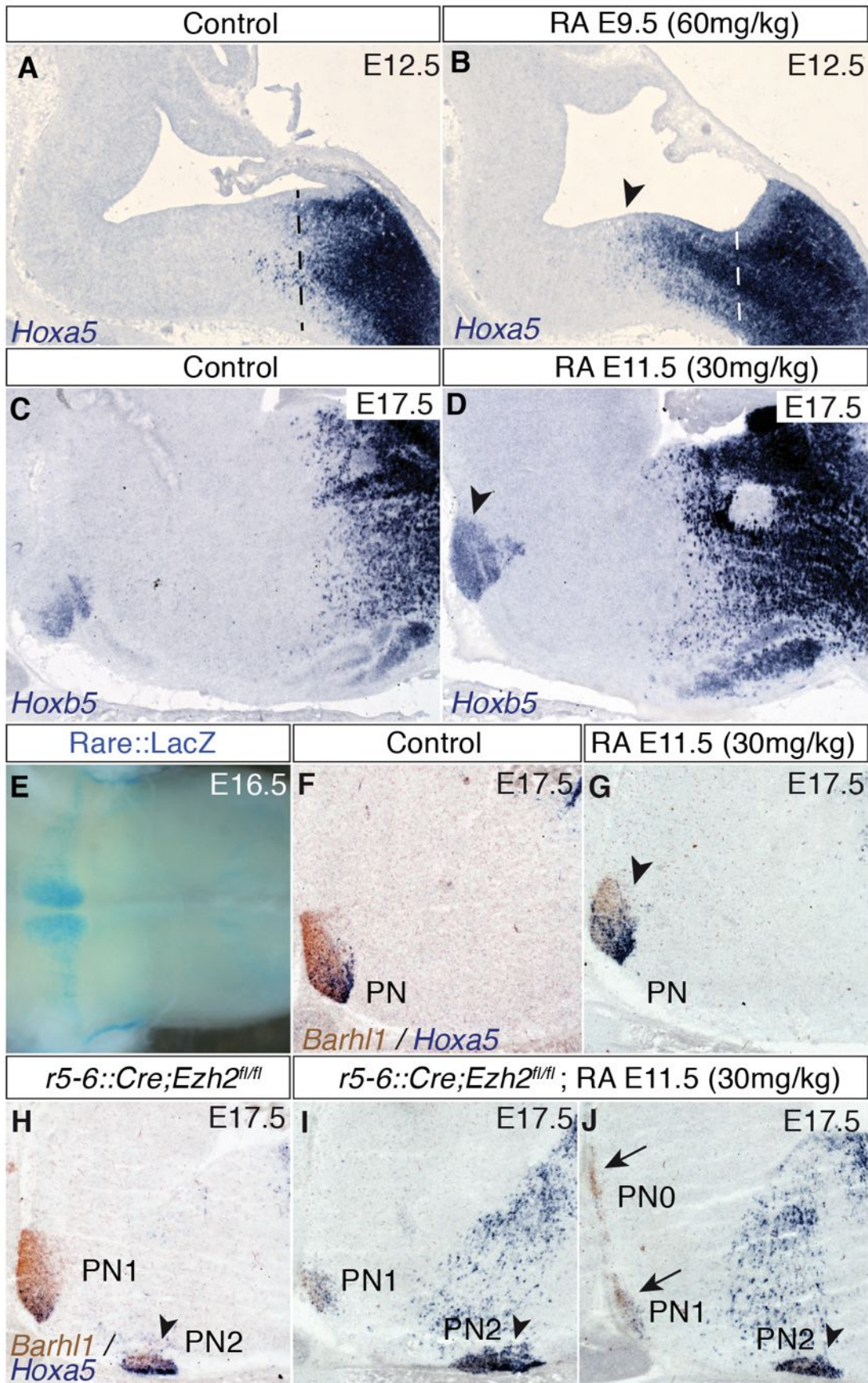


Figure 22 | Retinoid signaling and *Ezh2* dependent *Hox* regulation in pontine neurons. (A, B), *Barhl1*+ PN neuron migratory patterns in E15.5 wholemount hindbrain treated with retinoic acid (RA) at E11.5 (30 mg/kg) (A) or E9.5 (60 mg/kg) (B). No migratory defects in (A), whereas ectopic migrations are in (B). (C- F), *Hoxb5* (C, D) and *Ntn1* (E, F) expression in E12.5 control (C, E) and RA-treated (E9.5) (D, F) embryos. Ectopic *Hoxb5* and *Ntn1* (arrowheads) in (D, F). G-H, X-Gal staining on E17.5 PN sagittal sections of untreated (G) and RA-treated (E13.5 and E14.5) (H) *RARE::LacZ* fetuses. Ectopic b-gal activity (arrowhead) in (H). (I-K), *Hoxb5* and *Barhl1* expression in control (I, J) and *r5-6::Cre; Ezh2^{fl/fl}* (K, L) E17.5 sagittal sections, either in untreated (I, K) or RA-treated (E11.5) (J, M, N) fetuses. Ectopic *Hoxb5* in RA-treated control PN (arrowhead) (J) and mutant PN0, PN1 (arrows), PN2 (arrowhead) (M, N); *Hoxb5* expression throughout untreated mutant PN2 (arrowheads) (K, L). (O, P) Summary *in vivo* interactions between extrinsic and intrinsic *Ezh2*-mediated repression and RA signaling during PN neuron migration, through the regulation of *Hox* PG5 and *Unc5b*.



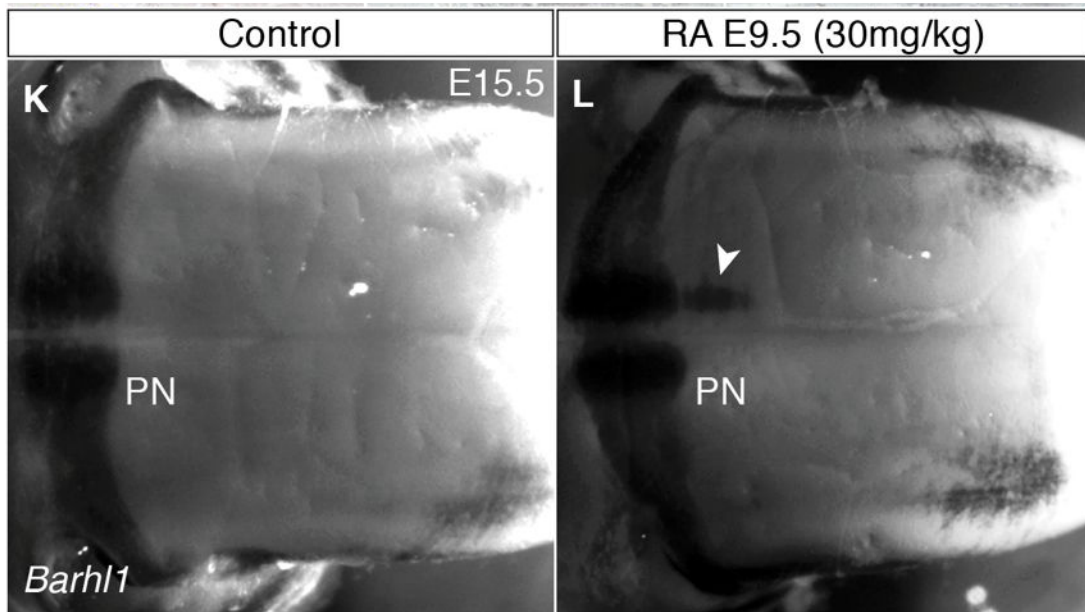


Figure 23 | Retinoid signaling and *Hox* regulation in pontine neurons. (A, B) *Hoxa5* expression in sagittal sections from E12.5 control (A) and RA-treated (60 mg/kg at E9.5) (B) embryos. *Hoxa5* expression spreads more rostrally (arrowhead) in the RA-treated case (B). (C, D) *Hoxb5* expression on sagittal sections from E17.5 control (A) and RA-treated (30 mg/kg at E11.5) (B) fetuses. *Hoxb5* expression is enhanced and ectopically induced in anterior pontine nuclei (arrowhead) in (D). (E), Ventral view of X-Gal stained whole-mount hindbrain from E16.5 *RARE::LacZ* fetuses showing graded caudo-rostral staining in pontine nuclei. (F-J), *Hoxa5* and *Barhl1* expression in control (F,G) and *r5-6::Cre; Ezh2^{fl/fl}* (H-J) E17.5 sagittal sections, either in untreated (F,H) or RA-treated (30 mg/kg at E11.5) (G, I, J) fetuses. Enhanced *Hoxa5* expression (arrowhead) in RA-treated control PN (G) and mutant PN2 (arrowhead), in contrast to PN0 and PN1 (arrow) in (I, J). *Hoxa5* is expressed throughout untreated mutant PN2 (arrowheads) (H). (K, L), *Barhl1*⁺ PN neuron migratory patterns in E15.5 whole-mount hindbrain from untreated (K) or RA-treated (30 mg/kg at E9.5) (L) embryos. PN neuron ectopic migration after RA treatment (arrowhead) in (L).

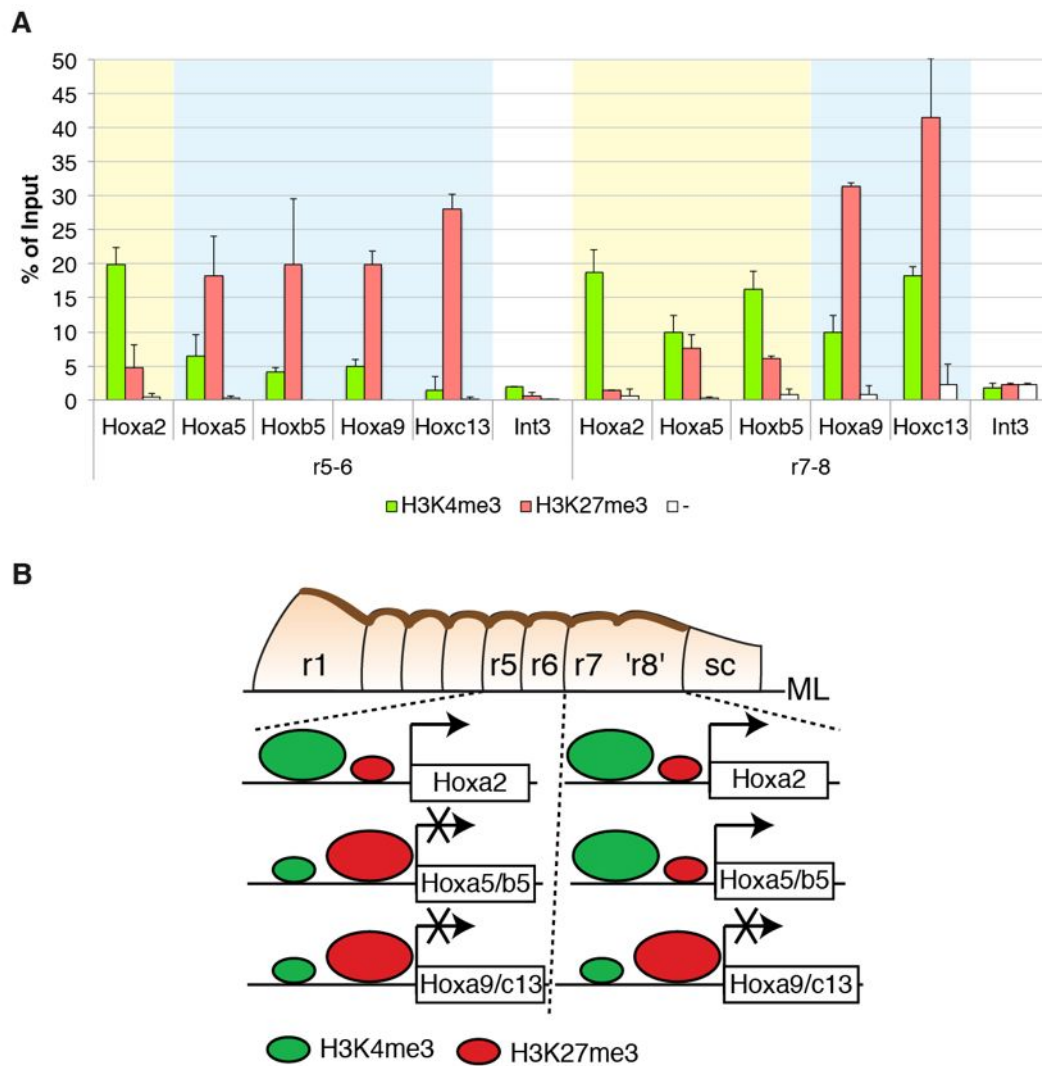


Figure 24 | MicroChIP assay of E16.5 rhombomere 5/6 and rhombomere 7/8. (A) H3K27me3 and H3K4me3 microChIP assays on *Hoxa2*, *Hoxa5*, *Hoxb5*, *Hoxa9*, *Hoxc13* promoters and an intergenic region (negative control, Int-3) from E16.5 *r5-6::Cre; R26R^{ZsGreen}* r5-6 vs. r7-8 derived territories. (-) are controls using Rabbit IgG antibody. **(B)**, Summary of *Hox* distinct epigenetic configurations at r5-6 or r7-8 levels. PN, pontine nuclei; AES, anterior extramural stream.

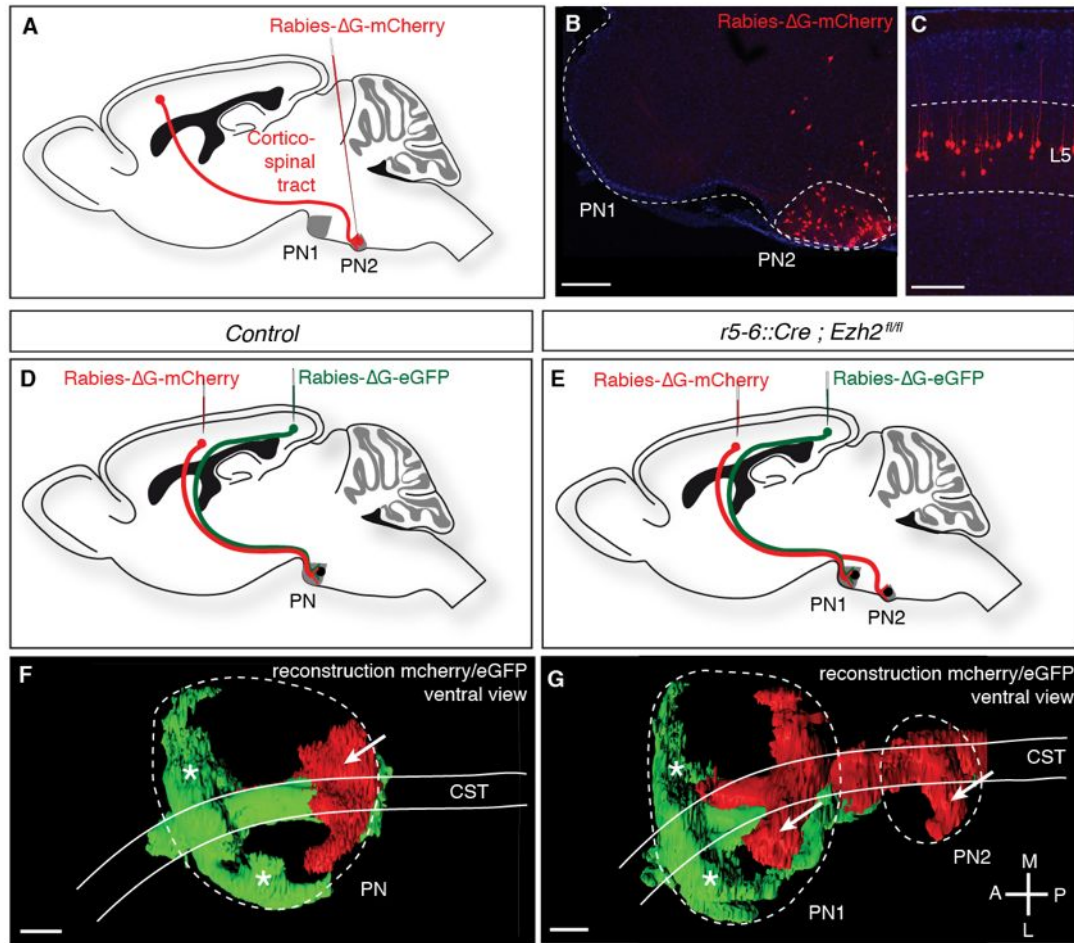


Figure 25 | Pontine nuclei regionalization and patterned cortical input. (A-C), Stereotaxic injection into PN2 and innervation by cortical layer 5 (L5) neurons. (D-I), Input topography 3-D reconstruction of Rabies-ΔG injections in control mice medioposterior/visual (MPC) somatosensory (SSC) cortex (injections illustrated in D, E) trace fibers into anterior (green, *) and posterior (red, arrow) PN, respectively, seen in a ventral (F, G) and lateral (H, I) view. *r5-6::Cre; Ezh2^{fl/fl}* mutants show normal cortical input distribution in PN1; PN2 lacks innervation by MPC (green, *), while is innervated by SSC (red, arrow). Scale: 200 μm, CST, corticospinal tract; M, medial; L, lateral; A: anterior; P, posterior.

gene	gene description	Publication showing interaction with retinoic acid pathway
<i>Bmi1</i>	Bmi1 polycomb ring finger oncogene	Boukarabila, H. et al. The PRC1 Polycomb group complex interacts with PLZF/RARA to mediate leukemic transformation. <i>Genes Dev</i> 23, 1195–1206 (2009).
<i>Cnpy1</i>	canopy 1 homolog (zebrafish)	-
<i>En2</i>	engrailed 2	Cunningham, M. L., Mac Auley, A. & Mirkes, P. E. From gastrulation to neurulation: transition in retinoic acid sensitivity identifies distinct stages of neural patterning in the rat. <i>Dev Dyn</i> 200, 227–241 (1994).
<i>Hoxa4</i>	homeobox A4	Packer, A. I., Mailutha, K. G., Ambrozewicz, L. A. & Wolgemuth, D. J. Regulation of the Hoxa4 and Hoxa5 genes in the embryonic mouse lung by retinoic acid and TGFbeta1: implications for lung development and patterning. <i>Dev Dyn</i> 217, 62–74 (2000).
<i>Hoxa5</i>	homeobox A5	Packer, A. I., Mailutha, K. G., Ambrozewicz, L. A. & Wolgemuth, D. J. Regulation of the Hoxa4 and Hoxa5 genes in the embryonic mouse lung by retinoic acid and TGFbeta1: implications for lung development and patterning. <i>Dev Dyn</i> 217, 62–74 (2000).
<i>Hoxa6</i>	homeobox A6	Bertani, S., Sauer, S., Bolotin, E. & Sauer, F. The noncoding RNA Mistral activates Hoxa6 and Hoxa7 expression and stem cell differentiation by recruiting MLL1 to chromatin. <i>Mol Cell</i> 43, 1040–1046 (2011).
<i>Hoxb4</i>	homeobox B4	Gould, A., Itasaki, N. & Krumlauf, R. Initiation of rhombomeric Hoxb4 expression requires induction by somites and a retinoid pathway. <i>Neuron</i> 21, 39–51 (1998).
<i>Hoxb5</i>	homeobox B5	Oosterveen, T. et al. Retinoids regulate the anterior expression boundaries of 5' Hoxb genes in posterior hindbrain. <i>EMBO J</i> 22, 262–269 (2003).
<i>Hoxb8</i>	homeobox B8	Oosterveen, T. et al. Retinoids regulate the anterior expression boundaries of 5' Hoxb genes in posterior hindbrain. <i>EMBO J</i> 22, 262–269 (2003).
<i>Hoxd4</i>	homeobox D4	Folberg, A., Kovács, E. N. & Featherstone, M. S. Characterization and retinoic acid responsiveness of the murine Hoxd4 transcription unit. <i>J Biol Chem</i> 272, 29151–29157 (1997).
<i>Hoxd8</i>	homeobox D8	Manohar, C. F., Salwen, H. R., Furtado, M. R. & Cohn, S. L. Up-regulation of HOXC6, HOXD1, and HOXD8 homeobox gene expression in human neuroblastoma cells following chemical induction of differentiation. <i>Tumour Biol.</i> 17, 34–47 (1996).
<i>Nrgn</i>	neurogranin	Féart, C. et al. Differential effect of retinoic acid and triiodothyronine on the age-related hypo-expression of neurogranin in rat. <i>Neurobiology of Aging</i> 26, 729–738 (2005).
<i>Shisa6</i>	shisa homolog 6 (Xenopus laevis)	-
<i>Skap2</i>	src family associated phosphoprotein 2	-
<i>Tmem56</i>	transmembrane protein 56	-

Table 7 | References showing interaction between retinoic acid and genes upregulated in *r5-6::Cre; Ezh2^{fl/fl}* embryos

3.1.3 “Partial ipsilateral wiring of subcortical sensory inputs duplicates the facial map” (manuscript, in preparation)³

Similar as in the precerebellar system also the trigeminal system, which relays information about sensory experience from the face, is patterned in a rostro-caudal manner. As it has been described by Oury et al., (2006) different rhombomeric contributions of the trigeminal column as dorsal and ventral PrV or the different portions of the SpV do not only get different input from the trigeminal ganglion, but also their projections have specific target zones in the thalamus.

It is an important determinant for proper neural connectivity to specify if neurons project to the contralateral or ipsilateral side of the brain. Somatosensory processes are largely lateralized with a strong preference for contralateral projections. Exceptions are the visual system in mammals, where projections innervating the thalamus are partially contralateral and ipsilateral. In the following study an artificial scenario was generated in which projections from the trigeminal nuclei are projecting partially ipsilateral and partially contralateral. This was realized by conditional knockout of the *Robo3* gene, a regulator of contralateral crossing, in rhombomere 3 and 5 (using the *Krox20::Cre* driver) that includes the progenitors of the ventral PrV. Hereby most r3 neurons are transformed into ipsilateral projecting neurons, while all neurons from the dorsal PrV (derived from rhombomere 2) stay unrecombined and thereby projected normally to the contralateral side.

Interestingly, conditional knockout of *robo3* in r3/r5 and the resulting mixture of ipsilateral and contralateral sensory inputs lead to a decrease of the size of the thalamic area occupied by r3/5 projections and to a duplication of the sensory map in the cortex. Hereby one map processes purely ipsilateral information while the other solely gets information of the contralateral side.

³ Statement of contribution: My contribution to this manuscript were all experiments using *r2::mcherry*; *Krox20::Cre* ; *Robo3^{fl/fl}* animals as well as their controls, respectively.

Partial ipsilateral wiring of subcortical sensory inputs duplicates the facial map

Nicolas Renier^{1, 2, 3}, Reha S. Erzurumlu⁴, Claudius F. Kratochwil⁵, Christophe Laumonnerie⁵, Filippo M. Rijli⁵, Patricia Gaspar^{2,6} and Alain Chédotal^{1, 2, 3, †}

1 INSERM, U968, Paris, Institut de la Vision, F-75012, France

2 Université Pierre et Marie Curie, Paris 06, Paris, F-75012, France

3 CNRS, UMR_7210, Paris, F-75012, France

4 Department of Anatomy and Neurobiology, University of Maryland School of Medicine, Baltimore, MD 21201-1075, USA

5 Friedrich Miescher Institute for Biomedical Research, CH-4058 Basel, Switzerland

6 INSERM, U839, Institut du Fer à Moulin, Paris, F-75005, France

†Correspondence and request for materials should be addressed to Alain Chédotal.

E-mail: alain.chedotal@inserm.fr

Summary

In mammals, tactile information is mapped topographically onto the contralateral primary somatosensory cortex forming one to one periphery related patterns that are particularly striking in the mouse barrel cortex. Here we describe a mouse mutant where, after an invalidation of the *Robo3* gene in rhombomere 3, a sizeable fraction of the trigeminothalamic inputs project ipsilaterally rather than contralaterally. The mixture of ipsilateral and contralateral sensory inputs creates bilateral whisker maps in the thalamus and cortex. This suggests that ipsi/contralateral competition among the sensory afferents prevails over topographic guidance cues for positioning these afferents in the target. Unilateral sensory deprivation supports an activity-dependent competition between the ipsi/contralateral sensory inputs for cortical space. This study reveals that the somatosensory system can reorganize the topographic map to integrate bilateral sensory information, and shows the importance of competitive interactions between afferents carrying dissimilar sensory inputs as a predominant mapping rule in the somatosensory system.

Introduction

The contribution of genetic and activity-dependent mechanisms to the wiring of sensory maps has been the subject of intense study and debate. Current view is that the general position and orientation of the sensory maps in the cerebral cortex is determined by gradients of morphogens [1], the specific organization of the maps varies across species [2], and according to the sensory modality that it receives [3]. One point of continued controversy however, is the degree to which bilateral representations of a single sensory modality (e.g. vision) are genetically encoded or whether they are shaped by activity-dependent competitive mechanisms [4]. Recent studies in the visual system, suggest that a small change in the crossing of the midline could be the main driver for bilateral sensory representations [5]. Here we examined the result of partial crossing of presynaptic afferents to the somatosensory thalamus in the whisker to barrel pathway of mice, which is normally entirely crossed.

The sensory afferents from the whisker follicles first synapse in the brainstem trigeminal complex. Second order neurons in the principal sensory nucleus of the trigeminal nerve (PrV) carry the whisker-specific inputs entirely to the contralateral ventroposteromedial nucleus (VPM) of the thalamus (Figure 1A; reviewed in [6]. Whisker-specific PrV neurons mostly originate from rhombomere 3 [7]. Ablation experiments and genetic models, where changes in whisker number are faithfully reproduced in the brain map [8,9] showed the influence of sensory neurons in the layout of the facial map.

In vertebrates, midline crossing by developing axons involves many attractive and repulsive axon guidance molecules such as slits and netrin [10]. In the spinal cord and brainstem, one of the key molecules required for crossing is the Roundabout 3 (Robo3) receptor. Several studies in various systems have shown that mice deficient

for Robo3 lack commissures in the hindbrain [11,12,13]. Interestingly, human patients suffering from a rare congenital disease named HGPPS (horizontal gaze palsy with progressive scoliosis) carry mutations in the *ROBO3* gene and have uncrossed sensory pathways [14]. In this study we focused on a conditional mutant mouse in which the *Robo3* gene was inactivated in rhombomere 3 [13]. We anticipated that selective interference with Robo3 signaling in rhombomere 3 would result in purely ipsilateral trigeminothalamic projections and subsequently ipsilateral face and whisker representations in the somatosensory cortex. Unexpectedly, this only caused a partial crossing of the trigeminothalamic axons, resulting in a unique model to analyze the consequence of having both ipsilateral and contralateral sensory afferents in the whisker to barrel pathway. We found that this resulted in the appearance of two functional whisker maps in both the thalamic relay and the barrel cortex. Most interestingly, these maps were entirely segregated as early as postnatal day 4 (P4), indicating a competitive interaction between the ipsi/contralateral afferents that prevailed over a strict topographic organization. This was supported by deprivation experiments showing that the crossed and uncrossed sensory afferents compete for space in both the thalamic relay and the cerebral cortex.

Results

Genetic perturbation of midline crossing signals and emergence of bilateral somatosensory maps.

The whisker to barrel cortex pathway is comprised of three neuronal relays with strict topographic organization and patterning. Each whisker input is represented by a small group of neurons in the ventral part of the PrV (barrelettes), in the VPM (barreloids), and in layer IV of the primary somatosensory cortex (S1, barrels). As

schematized in Fig. 1A, the pathway is ipsilateral in the brainstem and entirely crossed en route to the thalamus and thalamic VPM neurons project ipsilaterally to layers IV and VI of the S1 cortex [9].

We analyzed the whisker to barrel projection in the *Krox20::Cre;Robo3^{lox/lox}* conditional mice that lack most commissural axons in rhombomeres 3 (r3) and r5 [13]. During development, *Robo3* is transiently expressed in r3 neurons, with an expression that stops shortly after axon crossing, suggesting that it does not play a role in later stages of development such as axon targeting [13] and data not shown. Trigeminal ganglion neurons, which project to PrV do not express *Robo3* (Fig. 1B and not shown). As expected, *in situ* hybridization confirmed that *Robo3* expression is deleted from r3 in *Krox20::Cre;Robo3^{lox/lox}* 12 days old (E12) embryos (Fig. 1B, C; n= 3/3).

To visualize the trigeminothalamic pathway, *Krox20::Cre;Robo3^{lox/lox}* mice were crossed to *Tau-lox-Stop-lox-mGFP-IRES-nls-lacZ* mice (*Tau^{GFP}*) [15]. In E12 *Krox20::Cre;Robo3^{lox/+};Tau^{GFP}* controls many GFP+ axons cross the midline at the r3 and r5 level. By contrast, in *Krox20::Cre;Robo3^{lox/lox};Tau^{GFP}* mutants, most of the GFP+ axons failed to cross although they still projected rostrally towards the midbrain (Fig. 1D, E; n=3/3). At E13, coronal sections at the level of r3 confirmed that the density of GFP+ commissural axons at the ventral midline was strongly reduced in *Krox20::Cre;Robo3^{lox/lox};Tau^{GFP}* but also confirmed that a subset of axons still cross (Fig. 1F-I). The r3-specific deletion of *Robo3* did not appear to affect the barrellette patterns in the PrV, as these were quite similar in control and *Krox20::Cre;Robo3^{lox/lox}* P4 mice (n=4/4; Fig. 2A-D) suggesting that the development of the PrV nucleus was not perturbed. To determine whether all neurons in the ventral part of the PrV

expressed Cre recombinase in *Krox20::cre;Robo3^{lox/+};tau^{GFP}* mice, we performed double staining for NeuN and β -gal in adult sections (Fig. 2E, F; n=5). This showed that 88% NeuN⁺ neurons in the ventral part of PrV express β gal but that a small subset of the NeuN⁺ PrV neurons ($10.7 \pm 1.5\%$) was not β gal⁺ and therefore probably did not express Cre recombinase. This suggested that the mutant VPM could receive ipsilateral and contralateral trigeminothalamic inputs. To test this possibility, we performed retrograde tracing experiments. We injected Dil in one VPM and DiA in the contralateral VPM in P4 mice. In the *Krox20::Cre;Robo3^{lox/+}* controls, Dil and DiA labeled neurons were found only in the contralateral PrV nucleus, as expected for commissural neurons (Fig. 3A-D; n=4/4). By contrast, in the *Krox20::Cre;Robo3^{lox/lox}* mutants, DiA and Dil labeled neurons were found in the PrV on both sides of the hindbrain (Fig. 3E-H; n=4/4). While the dorsal part of the PrV almost only contained neurons projecting to the contralateral VPM (as expected from their r2 origin [7]), the ventral domain (whisker-specific) contained a mixture of Dil and DiA labeled neurons, with 3.3 times more neurons traced ipsilaterally than contralaterally. This indicates that in the *Krox20::Cre;Robo3^{lox/lox}* mutants, the ventral part of the PrV, which relays whisker inputs to the VPM, projects bilaterally.

Overall these data suggest that a large fraction of the r3-derived trigeminothalamic axons project ipsilaterally in *Krox20::Cre;Robo3^{lox/lox}* mutants but that some still project contralaterally and might have escaped Cre recombination or started expressing Cre after crossing (see discussion).

To determine whether the bilateral innervation of the VPM by the r3-derived PrV axons modified the topographic organization of the trigeminothalamic projections we used two approaches genetic tracing of r3-derived axons (Fig. 4) and anterograde

tracing (Fig. 5). With the first approach we examined the r3-derived axons using *Krox20::Cre;Robo3^{lox/lox};Tau^{GFP}* and *Krox20::Cre;Robo3^{lox/+};Tau^{GFP}* mice. The sections were stained for cytochrome oxidase to visualize simultaneously the barreloid patterns. In all mutants and controls (n=14 for each genotype), the r3-derived GFP⁺ (r3-GFP⁺) axons projected to the dorsolateral VPM containing the barreloids (Fig. 4). However, the size of the VPM domain targeted by r3-GFP⁺ axons was significantly reduced ($0.20 \pm 0.03 \text{ mm}^2$ in mutant vs $0.40 \pm 0.02 \text{ mm}^2$ in controls; $P = 0.002$). In addition, an abnormal organization of the whisker barreloids was noted in the VPM. In controls, all the barreloid rows coincided with the r3-GFP⁺ axon territory (Fig. 4B-D; n=4/4), whereas in mutants two distinct zones were observed (n=4/4): a lateral VPM domain containing a high density of GFP⁺ axons and a medial VPM domain with only sparse GFP⁺ axons (Fig. 4F-H). These two VPM domains, contained barreloids as noted with cytochrome oxidase staining and were of comparable surface ($0.19 \pm 0.006 \text{ mm}^2$ for the lateral-high GFP⁺ domain and $0.18 \pm 0.003 \text{ mm}^2$ for the medial-low GFP⁺ domain, $P=0.46$). Moreover, they were separated by a cytochrome oxidase-free septum (Fig. 4F-H). These observations suggested that in the *Krox20::Cre;Robo3^{lox/lox}* mice, the VPM became split into two functionally separate domains, each with barreloid patterns (although only one of them contains the bulk of the r3-derived projections).

To confirm this result we anterogradely traced the PrV to VPM projections in P4 mice using carbocyanine dyes. In control mice the PrV-VPM projection was completely crossed (Fig. 5A-D), whereas in mutants, the VPM received a bilateral innervation from the PrV (Fig. 5E-H). This shows that two ascending sensory pathways co-exist in the mutants, a normally crossed PrV-VPM pathway and a new ipsilateral PrV-VPM

pathway. Interestingly, the comparison of the carbocyanine tracings and of the GFP staining (Fig. 4) further revealed that: i) although the ipsilaterally and contralaterally projecting neurons in ventral PrV are intermingled, their projections in the VPM are segregated; and, ii) while the ipsilateral projection corresponded to the lateral VPM domain targeted by GFP⁺ r3-derived axons, the contralateral PrV-VPM projections targeted the medial VPM and corresponded to, at least, two subpopulations: the few GFP⁺ fibers originating from r3 that likely escaped the deletion of Robo3 (Fig. 1F-I) and, notably, GFP⁻ projections. The origin of these GFP⁻ axons is not entirely clear, but could comprise both axons originating in r3 but not expressing Cre (Fig. 2E, F), and/or axons of cells generated outside r3 (Fig. 4).

To explore this second possibility, we examined whether other axonal populations (non r3-derived) may also target the medial VPM area. We examined the r2-derived axons, because previous studies have shown that PrV neurons originating from r2 (i.e. not expressing *Krox20*) target the dorsomedial VPM in a complementary pattern to r3 projecting axons ⁷ (Fig. 6). To simultaneously visualize the r2- and r3-derived trigeminal inputs in the mutant VPM, we generated a transgenic line selectively expressing the red fluorescent protein mCherry in r2-derived neurons and axons and crossed it to the *Krox20::Cre;Robo3^{lox/lox};Tau^{GFP}* line. In the VPM of P6 control mice, the distribution of *mCherry*⁺ r2 and GFP⁺ r3-derived PrV axon terminals was highly complementary, with *mCherry*⁺ axons from r2-projecting neurons confined to the most medial VPM domain that lacks clear barreloids (Fig. 6; n=5), confirming previous observations ⁷. In contrast, in P6 mutants, the *mCherry*⁺ r2-derived axons were detected in the medial VPM area that contains barreloids and overlapped with the GFP⁺ contralateral PrV-VPM inputs (Fig. 6; n=3). The mCherry⁺ area in the medial barreloid domain was larger in mutants than in controls ($0.12 \pm 0.01 \text{ mm}^2$ in

controls vs. $0.26 \pm 0.04 \text{mm}^2$ in mutants, $P=0.028$). The contralateral GFP^+ and $mCherry^+$ domains in the mutant VPM barreloid area were of similar size ($0.26 \pm 0.04 \text{mm}^2$ for the $mCherry^+$ area vs. $0.28 \pm 0.02 \text{mm}^2$ for the GFP^+ area, $P=0.6$). Altogether, these results strongly support the idea that in the mutant the VPM containing the contralateral barreloid map is a composite area targeted by at least three axonal populations: namely, two small subsets of GFP^+ and GFP^- r3-derived axons that remain crossed and a subset of contralateral r2-derived projections that expand their normal innervation area in the mutant dorsomedial VPM.

Formation of bifacial cortical maps

Next, we determined how these segregated ipsi- and contralateral whisker representations in the VPM would influence the formation of the somatosensory map in the cerebral cortex. Tangential sections through layer IV were stained for cytochrome oxidase and Vglut2 immunoreactivity to label thalamocortical afferents¹⁶ (Fig. 7A-D). A striking abnormality in the layout of thalamic afferents was noted in the posteromedial barrel subfield (PMBSF, which corresponds to the representation of the large whiskers) of the *Krox20::Cre;Robo3^{lox/lox}* mice ($n=5/5$; Fig. 7C, D). Barrels were more numerous (52 ± 2 barrels in mutant PMBSF vs. 33 ± 0 in controls), and were reduced in size ($0.04 \text{mm}^2 \pm 0.01$ per barrel in mutants, compared to $0.09 \text{mm}^2 \pm 0.02$ in controls, $P < 0.0001$). Moreover they were arranged into 8 rather than the usual 5 whisker rows, with a clear delineation of two separate cortical zones, a central zone, and a peripheral zone, each containing distinct barrel rows (Fig. 7C, D and Fig. S1). These defects were comparable in both hemispheres and at all ages analyzed (with only slight individual variations; $n=25/25$; Fig. S1). To map the functional whisker representation in this unusual map, we monitored the activation of the immediate early gene *c-fos* following a 1-hour exposure to an enriched sensory environment

[16]. In mice with unilateral trimming of the whiskers (Fig. 7E-G) strong c-fos labeling is normally observed only in the S1 contralateral to the intact whiskers. In *Krox20::Cre;Robo3^{lox/lox}* mice with unilateral whisker trimming, c-fos was activated in the PMBSF of both hemispheres (Fig. 7H-J). Contralateral to the intact whiskers, c-fos activation was visible in the peripheral barrel rows (Contra domain; Fig. 7J). Ipsilateral to the intact whiskers, a mirror image was noted with c-fos activation in the central barrel rows (Ipsi domain; Fig. 7I). These results showed that in *Krox20::Cre;Robo3^{lox/lox}* mice, the crossed and non-crossed trigeminothalamic domains are mapped as two segregated nested domains: a central one processing ipsilateral inputs surrounded by an outer domain processing contralateral inputs (Fig. 7H).

Orientation and polarity of the maps.

The segregation of the two maps led to the crucial question of its topographic organization. Indeed there are two possibilities: i) the thalamic afferents follow topographic guidance cues that are determined by molecular guidance cues expressed in the cortex, with complementary receptor expression in the thalamus; in this case one would expect that neighboring whiskers of the ipsi and contralateral map lie in register with one another; and, ii) the thalamic afferents are clustered following activity-based rules leading functionally coordinated afferents to cluster together, in this case the topographical rule of near neighbors would prevail over the notion of molecular gradients. To analyze the topographic alignment of the ipsilateral and contralateral somatosensory maps, we monitored c-fos expression in S1 after clipping all whiskers except one row or one arc of whiskers on one side (Fig. 8 and data not shown). When the 5 posterior most whiskers of the whisker pad (A1-E1; Fig. 8A) were left intact in control mice, this resulted in the activation of c-fos in a caudal

arc of 5 barrels exclusively in the contralateral S1 (Fig. 8B). Likewise, when the second whisker row (B1-B4; Fig. 8E) was left intact, the corresponding row of barrels was activated in the contralateral S1 (Fig. 8F). In mutants, c-fos activation was bilateral, with a labeling that was in register in both the central (ipsi) and peripheral (contra) PMBSF domains (Fig. 8C, D, G, H). The orientation of the two nested maps was similar to control mice probably due to the patterning activity of morphogens that determine the polarity of the map [17,18]. However, unlike the visual or auditory bilateral maps, we observed that there were discontinuities in the organization of the bilateral somatotopic map, such as a lack of topographic proximity of the ipsi/contralateral representation of a given barrel or barrel row. Rather, there appeared to be a clear separation and independence of the ipsi- and contralateral inputs.

Competition between ipsi- and contralateral inputs for cortical space

To evaluate whether the bilateral thalamocortical maps recruited new cortical space or were included within the normal boundaries of S1, we measured the overall size of the PMBSF. This space was not increased ($2.32 \pm 0.05 \text{ mm}^2$ in controls vs $1.90 \pm 0.12 \text{ mm}^2$ in mutants, $P=0.04$) unlike in other mouse models with duplication of the S1 map where a second S1 map is formed at the expense of other cortical areas^{18, 19} (Fig. 8M, N and Fig. S2). This suggested that the ipsi- and contralateral thalamic inputs compete to occupy a defined cortical space in S1, a feature reminiscent of ocular dominance columns (ODC) in the visual cortex. Accordingly, individual barrels in mutants were roughly half the size ($44 \pm 2\%$) of controls (Fig. 8J-N). To prove the existence of such a competition, we studied the consequence of unilateral deprivation of whisker inputs induced by a neonatal (P1) lesion of the infraorbital nerve [19]. In control mice, barrels were only observed in S1 ipsilateral to the lesion

(Fig. 9A-C; n=3/3). In contrast, in mutants, barrels formed on both sides corresponding to the ipsi- and contralateral representations of the intact whisker pad (Fig. 9D-F; n=5/5). Furthermore, while the infraorbital nerve lesioned side ipsi- and contralateral representations shrunk in size ($50\pm 4\%$ of the unlesioned mutant PMBSF), those corresponding to the intact whiskerpad enlarged in both cortices ($138\pm 10\%$ of the unlesioned mutant PMBSF; Fig. S3). This suggests that there is an activity-dependent competition for cortical space between the ipsilateral and contralateral sensory inputs in the mutant S1.

Discussion

There is a vast literature on the dependence of whisker-specific patterning of facial brain maps on sensory periphery and cortical positioning and size of these maps on intrinsic molecular cues [9]. The present observations demonstrate a novel aspect of whisker-related map formation and show that a genetic defect in the crossing of sensory axon tracts at the midline leads to a completely unexpected anatomical and functional reorganization: duplication of the facial whisker representation with two completely separate maps sharing the same cortical space allotted to somatosensory function. The segregation of these two whisker maps indicates that competitive interactions for space in the S1 cortex are not only based on periphery related signals from the whisker pads, but also on signals that axons acquire while travelling together in the trigeminothalamic pathway.

Trigeminothalamic axons require Robo3 for midline crossing.

Robo3 has been identified as a major player in the crossing of the midline by commissural spinal and brainstem axons [10,11,12]. Here, we found that the

trigeminothalamic axons also depend on Robo3 for midline crossing. PrV neurons transiently express Robo3 at embryonic stages when these neurons cross the midline (E11-E14), and loss of Robo3 prevents the crossing of a large majority of the trigeminothalamic axons. However the axons that remain on the same side have a normal ascending path in the medial lemniscus and target normally the VPM nucleus of the thalamus. Thus, although the axons do not cross the midline, their subsequent axon pathfinding is undisturbed, showing that the complex molecular switch occurring at the midline [10] is not essential. This observation extends previous findings in the visual, precerebellar, oculomotor and auditory systems, which showed that the ipsilateral growth of normally crossed axons does not alter their targeting [11,13,20]. A fraction of the trigeminal axons continued to cross the midline after deletion of Robo3 in r3, which provides the largest number of PrV neurons [7]. There are several reasons that might explain this incomplete effect. On one hand, some PrV neurons may have escaped the recombination and *Robo3* invalidation may be incomplete. In *Krox::Cre* mice, not all PrV neurons express Cre, and others may have expressed Cre too late, after axons have crossed. On the other hand, some PrV neurons may be derived from neighboring rhombomeres and may have migrated to PrV at early embryonic stages as described in other systems [21]. Finally, there may be some functional redundancy in the combination of receptors that guide PrV axons towards the midline and across, but this is very unlikely as *Robo3*-null mice completely lack hindbrain commissures

While we cannot explain definitively the mechanisms underlying partial crossing of PrV trigeminothalamic axons, the fact remains that in *Krox20::Cre;Robo3^{lox/lox}* conditional mice the trigeminothalamic pathway is comprised of a combination of crossed and uncrossed components. Thus, sensory information arising from one

whisker is mapped onto one barrelette in the brainstem, but the same information is mapped bilaterally in the secondary relay in the thalamus and then in the cerebral cortex.

Duplication and segregation of whisker maps.

Because afferents of one barrelette in the PrV carry functional information from one whisker, one could expect that in the following sensory relay stations the information arising from the homologous whiskers on each side of the brain would be mapped side by side, maintaining topographic rules. However, quite unexpectedly, these representations were separate, each being included in a distinct/autonomous map. This indicated a high degree of segregation of afferents arising from the ipsi- and contralateral PrV barrelette. The reason for this is unclear. It is unlikely that segregation of the ipsi- and contralateral projections would be based on a differential rhombomeric origin. Indeed a mixture of r2 and r3 derived trigeminothalamic axons were identified within the contralateral thalamic representation. Another possibility is that the absence of crossing by ipsilateral axons prevents the upregulation or downregulation of cell surface proteins, such as cell-adhesion molecules of the immunoglobulin superfamily, which normally occurs during midline crossing [22,23,24,25]. These may label differentially the surface of ipsilateral and contralateral trigeminothalamic axons and triggers a specific fasciculation or sorting. Interestingly, in *Drosophila*, a Robo code controls the fasciculation of post-crossing axons along the longitudinal axis [26,27]. Another possibility is based on somewhat comparable segregation mechanisms in the visual system: one may surmise that spontaneous neural activity in the trigeminothalamic pathway plays a role in this segregation. Spontaneous activity has been demonstrated in the perinatal PrV [28,29], thus, one

would expect that the nearby cells in the PrV on each side would fire synchronously, whereas the activity would not be synchronous between both sides of the brainstem. However, the fact that within either the ipsi- or contralateral whisker maps, topographic proximity is maintained among whisker barrels, indicated that local “proximity” cues among axons traveling together on each side may overrule the topographic cues in the target areas (as is the case in the olfactory system or in drosophila visual system [30]. Thus the particular organization of the two embedded whisker maps emphasizes an important characteristic of the somatosensory system which combines two different mapping rules, the first being the continuous topographic representation of the body surface, the second being an organization into distinct functional units.

Orientation and competition of the representations.

Contrary to previous observations of experimental map duplication¹⁸ the present orientation of the two whisker maps was similar in the general rostrocaudal and mediolateral axes, indicating that matching gradients of guidance molecules and their receptors was most likely unchanged. This contrasts with the mirror image organization of the sensory maps obtained after experimentally inducing novel source of molecular gradients in the somatosensory cortex [17]. This also contrasts with observations of map duplication in the visual system, caused by a change in the retinal axon crossing at the midline [5], by lack of one eye [31] or by lack of one hemisphere [32]. However in the latter case the mirror image maps are probably due to a conflict between maintaining functionality and mapping labels.

Since the initial description of the whisker “barrels” in the mouse primary somatosensory cortex and their dependence on an intact sensory periphery [33,34] the rodent trigeminal pathway has been used as a model system to investigate mechanisms underlying formation of orderly brain maps and their plasticity. Numerous studies showed that infraorbital nerve lesions or whisker follicle damage during the first few days after birth irreversibly alter or prevent formation of cortical barrels and whisker-specific patterns in the subcortical stations [9]. Furthermore, when a supernumerary whisker follicle develops on the snout a corresponding neural representation or barrel also forms in the brain [8]. Collectively, these findings underscored the role of sensory periphery (the whisker pad) in dictating the patterning of neural elements in the brain. More recent studies focused on the role of intrinsic cortical (or subcortical) molecular gradients that delineate the position and the size of the sensory maps in the cortex and confer specific identities to different populations of cortical neurons [1]. Here we show that a specific mutation that misdirects subpopulations of trigeminothalamic projection neurons can lead to development of bilateral whisker maps in the thalamus and neocortex, independent of the sensory periphery or the cortical positional cues.

While we do not know the functional/behavioral consequences of whisker map duplication in the thalamus and neocortex, our results revealed competitive interactions between the ipsi- and contralateral maps in the cortical territory. Interestingly the polarity of the two maps in the cerebral cortex was similar in both the rostrocaudal and mediolateral orientations, indicating that the thalamocortical maps orient essentially according to molecular gradients expressed in the cerebral cortex.

From a phylogenetic point of view our observations brings new perspectives on how novel sensory representations emerge in evolution, with either parallel or mirror image representations [35] and unilateral or bilateral representations. In this respect our observations are interesting to compare with mechanisms of eye-specific segregation in the visual maps. In the mammalian visual system, ipsi- and contralateral visual inputs from both eyes segregate within distinct domains in the lateral geniculate nucleus and in the cortex [4,36]. Activity-dependent segregation of sensory inputs that do not normally innervate the same target region has been demonstrated previously in the optic tectum of 3-eyed frogs [37]. Our results show for the first time that *de novo* bilateral maps can be created for a sensory representation in which mixing of inputs from the two sides normally does not occur. This suggests that the developmental program, which controls the bilateral segregation of visual and auditory inputs is conserved and can be activated in thalamic nuclei processing the somatosensory modality, with some differences such as continuity in the visual map or discontinuities in the somatosensory maps that may be the reflection of intrinsic functional differences between these modalities. Although brain wiring largely relies on genetically encoded processes our results further illustrate the remarkable plasticity of the mammalian brain and its ability to accommodate changes in afferent wiring in evolution to create new representations, and also its ability, in the context of developmental brain disorders to compensate for major axon guidance defects that otherwise would lead to severe brain dysfunction [14,32,38]. It also suggests that in HGPPS patients, important reorganization of cortical areas may compensate for commissural axon defects occurring in the brainstem.

Experimental Procedures

Mice

All animal procedures were carried out in accordance to institutional guidelines (UPMC and INSERM). Mice were anesthetized with Ketamine (Virbac) and Xylazine (Rompun). The day of vaginal plug is embryonic day 0 (E0) and the day of birth corresponds to postnatal day 0 (P0).

The Robo3 conditional knockout, *Krox20::Cre* knock-in and Tau^{GFP} lines were previously described [13,15,39]. Unless otherwise mentioned, controls were *Robo3^{lox/lox}* or *Krox20::Cre;Robo3^{lox/+}* animals. Double heterozygotes were always similar to wild-type mice. Mice were genotyped by PCR.

The following primers were used for genotyping: the conditional Robo3 allele 5'-CCA AGG AAA AAC TTG AGG TTG CAG CTA G-3' and 5'-GAT TAG GGG AGG TGA GAC ATA GGG-3', the *Krox20::Cre* 5'-AGT CCA TAT ATG GGC AGC GAC-3' and 5'-ATC AGT GCG TTC GAA CGC TA-3', the Tau^{GFP} : 5'-GAG GGC GAT GCC ACC TAC GGC AAG-3' and 5'-CTC AGG GCG GAC TGG GTG CTC AGG-3'. All PCR run have 34 cycles with an annealing temperature of 58°C.

In the Tau^{GFP} line, upon Cre recombination in neurons, the Stop cassette is excised leading to the permanent expression of a myristoylated GFP in axons and of β -galactosidase in nuclei [15].

The *r2::mCherry* line was created by replacing the LacZ gene of the pKS- β -globin-lacZ vector (BGZ40 [40]) with a mCherry cassette (Clontech) using homologous recombination. A r2-specific enhancer from the *Hoxa2* regulatory region [41] was subcloned 5' of the β -globin promoter using the restriction sites SmaI and Aval, thus generating the pR2::mCherry construct. pR2::mCherry was linearized, purified and microinjected into the pronuclei of embryos. Founders were identified by PCR using

5'-GGT GTA CGC GGT TCT CAG AC-3' and 5'- TTA GCG GCC GCA TTA CTT GTA-3' primers and r2-specific expression.

Primers for homologous recombination:

5'-CCT TCC AGA AGC AGA AGC GCG GCG CCA CCA TGG TGA GCA AGG GGC GAG GAT AAC A-3'

5'-TGG CCT GCC CGG TTA TTA TTA TTT TTT ACT TGT ACA GCT CGT CCA TGC CG-3'

Histology and immunocytochemistry

Mice were perfused transcardially with a 4% PFA in 0.12mM phosphate buffer. Cortices were flattened between microscope slides and post-fixed in 4% PFA and vibratome (Leica) sectioned at 50µm. Hindbrains and thalamus were post-fixed in 4% PFA, cryoprotected in 30% sucrose and sectioned at 35µm with a freezing microtome (Microm).

For Cytochrome oxidase staining [42], sections were incubated at room temperature for 24 hours in 10% sucrose, 0,3g/L cytochrome c from equine heart (Sigma), 0,02g/L catalase from bovine liver (Sigma) and 0,25g/L DAB (Sigma). The endogenous fluorescence of the GFP in *Krox20::Cre;Tau^{GFP}* was not affected after the treatment and could be imaged on the same sections, however the GFP signal was further enhanced by immunostaining, as follows:

For immunohistochemistry, neonatal and adults brains were processed as described previously [43]. The following primary antibodies were used: guinea pig anti-Vglut2 (1:1000, Millipore), rabbit anti-βGal (1:1000, Cappel), rabbit anti-c-fos (1:1000, Santa-Cruz), rabbit anti-GFP (1:300, Invitrogen), chicken anti-GFP (1:800, Abcam). The following secondary antibody were used: Donkey Anti-Mouse, Anti-Rabbit and Anti-

Guinea pig coupled to CY3 or CY5 (1:600, Jackson Laboratories), Donkey Anti-Mouse, Anti-Rabbit and Anti-Chicken coupled to Alexa Fluor 488 (1:600, Invitrogen). Sections counterstained with Hoechst 33258 ($10 \mu\text{g ml}^{-1}$, Sigma) Sections were examined with a fluorescent microscope (DM6000, Leica) equipped with a CoolSnapHQ camera (Roper Scientific), a confocal microscope (FV1000, Olympus), or a slide scanner (Nanozoomer, Hamamatsu).

In situ hybridization

Antisense riboprobes were labeled with digoxigenin-11-D-UTP (Roche Diagnostics) as described previously [43] by in vitro transcription of mouse cDNAs encoding *robo3* or an exon specific probe of *robo3* targeting the floxed region [13].

Dil tracing

4% PFA fixed P4 pups were injected with small crystals of 1,1'-dioctadecyl-3,3,3',3'-tetramethylindocarbocyanine perchlorate (Dil, Invitrogen) and 4-(4-(dihexadecylamino)styryl)-*N*-methylpyridinium iodide (DiA, Invitrogen) using glass micropipettes. For anterograde tracing, the dye crystals were injected unilaterally in the PrV. For retrograde tracing of the PrV nuclei, the cortices were removed to expose the thalamus and Dil or DiA crystals were at the level of the VPM.

Brains were kept at 37°C for 4 weeks. Brains were cut in 80 μm sections with a vibratome (Leica) and counterstained with Hoechst.

Infraorbital nerve lesions

P0-P1 pups were cold anesthetized, and an incision was made between the whisker pad and the eye. The nerve was cut with scissors under a dissecting scope. The pups were allowed to recover for 10 days and then perfused.

c-fos expression and whisker activity

P20-P30 mice were anesthetized with ketamine, and all whiskers were trimmed on the left side. In different experiments, either all whiskers were spared on the right side, or only selected whisker rows or arcs were spared. Mice were allowed to recover from anesthesia for 6 to 12 hours, and then left alone in a large (1m x 60cm) “enriched” cage in the dark for 1 hour before being perfused and processed for c-fos immunostaining.

Quantifications and statistical analysis

Areas were calculated with NDPview (Hamamatsu) from cytochrome oxidase staining at P10 or Vglut2 staining done in adults. For quantification of map areas from P10 flattened cortices, the surface in controls was limited to the first 4 barrels in row A, 4 in row B, 6 in row C, 7 in row D and 8 in row E. In *Krox20::Cre;Robo3^{lox/lox}* mutants, the central (ipsi) map area comprises the domain bordered by a thick Vglut2-negative boundary. The peripheral (contra) map area was limited to the barrels located immediately above and below the border of the central ipsilateral map. To determine individual barrel areas in adults, only the largest unambiguous barrels were measured (first 3 barrels for rows E,D,C and first barrels for rows A and B). Areas were assessed on the tangential section showing the most complete map of the PMBSF.

The areas of the VPM nucleus were calculated with NDPview from frontal sections of P4 *Krox20::Cre;Tau^{GFP}* mice stained with cytochrome oxidase and immunostained for GFP, at a mid-level of the VPM, where the barreloids organization was the most obvious.

Results are presented as means \pm SEM. Differences of the means between two sample sets were assessed by two-tailed non-parametric Mann-Whitney test. Statistics were carried out with Prism (Graphpad software).

Acknowledgements

We thank P. Charnay for providing the *Krox20::Cre* line, and S. Arber for the Tau^{GFP} mice. We also thank N. Narboux-Nême for technical help, G. Goodhill, L.J. Richards, M. Feller, J.H. Kaas and C. Sotelo for critical reading of the manuscript.

This work was supported by grants from the Fondation pour la Recherche Médicale (Programme “équipe FRM”) and the Agence Nationale de la Recherche (ANR-08-MNP-030) to A.C, (ANR-08, MNP-032) to PG, and the Ecole des Neurosciences de Paris (ENP) and NIH/NINDS RO1 NS039050 to R.S.E. FMR laboratory is supported by the Swiss National Science Foundation (CRSI33_127440), ARSEP, and the Novartis Research Foundation. N. R. is recipient of a PhD fellowship from the Association Française contre les Myopathies (AFM).

References

1. O'Leary DD, Sahara S (2008) Genetic regulation of arealization of the neocortex. *Curr Opin Neurobiol* 18: 90-100.
2. Kaas JH, Catania KC (2002) How do features of sensory representations develop? *BioEssays : news and reviews in molecular, cellular and developmental biology* 24: 334-343.
3. Leamey CA, Van Wart A, Sur M (2009) Intrinsic patterning and experience-

- dependent mechanisms that generate eye-specific projections and binocular circuits in the visual pathway. *Current opinion in neurobiology* 19: 181-187.
4. Huberman AD, Feller MB, Chapman B (2008) Mechanisms underlying development of visual maps and receptive fields. *Annu Rev Neurosci* 31: 479-509.
 5. Petros TJ, Rebsam A, Mason CA (2008) Retinal axon growth at the optic chiasm: to cross or not to cross. *Annu Rev Neurosci* 31: 295-315.
 6. Erzurumlu RS, Murakami Y, Rijli FM (2010) Mapping the face in the somatosensory brainstem. *Nature reviews Neuroscience* 11: 252-263.
 7. Oury F, Murakami Y, Renaud JS, Pasqualetti M, Charnay P, et al. (2006) Hoxa2- and rhombomere-dependent development of the mouse facial somatosensory map. *Science* 313: 1408-1413.
 8. Welker E, Van der Loos H (1986) Quantitative correlation between barrel-field size and the sensory innervation of the whiskerpad: a comparative study in six strains of mice bred for different patterns of mystacial vibrissae. *The Journal of neuroscience : the official journal of the Society for Neuroscience* 6: 3355-3373.
 9. Erzurumlu RS, Gaspar P (2012) Development and critical period plasticity of the barrel cortex. *Eur J Neurosci* in press.
 10. Chedotal A (2011) Further tales of the midline. *Curr Opin Neurobiol* 21: 68-75.
 11. Marillat V, Sabatier C, Failli V, Matsunaga E, Sotelo C, et al. (2004) The slit receptor Rig-1/Robo3 controls midline crossing by hindbrain precerebellar neurons and axons. *Neuron* 43: 69-79.
 12. Sabatier C, Plump AS, Le M, Brose K, Tamada A, et al. (2004) The divergent Robo family protein rig-1/Robo3 is a negative regulator of slit responsiveness

- required for midline crossing by commissural axons. *Cell* 117: 157-169.
13. Renier N, Schonewille M, Giraudet F, Badura A, Tessier-Lavigne M, et al. (2010) Genetic dissection of the function of hindbrain axonal commissures. *PLoS Biol* 8: e1000325.
 14. Jen JC, Chan WM, Bosley TM, Wan J, Carr JR, et al. (2004) Mutations in a human ROBO gene disrupt hindbrain axon pathway crossing and morphogenesis. *Science* 304: 1509-1513.
 15. Hippenmeyer S, Vrieseling E, Sigrist M, Portmann T, Laengle C, et al. (2005) A developmental switch in the response of DRG neurons to ETS transcription factor signaling. *PLoS Biol* 3: e159.
 16. Nahmani M, Erisir A (2005) VGLUT2 immunocytochemistry identifies thalamocortical terminals in layer 4 of adult and developing visual cortex. *The Journal of comparative neurology* 484: 458-473.
 17. Fukuchi-Shimogori T, Grove EA (2001) Neocortex patterning by the secreted signaling molecule FGF8. *Science* 294: 1071-1074.
 18. Fukuchi-Shimogori T, Grove EA (2003) *Emx2* patterns the neocortex by regulating FGF positional signaling. *Nature Neuroscience* 6: 825-831.
 19. Waite PM, Cragg BG (1982) The peripheral and central changes resulting from cutting or crushing the afferent nerve supply to the whiskers. *Proceedings of the Royal Society of London Series B, Containing papers of a Biological character* Royal Society 214: 191-211.
 20. Rebsam A, Petros TJ, Mason CA (2009) Switching retinogeniculate axon laterality leads to normal targeting but abnormal eye-specific segregation that is activity dependent. *The Journal of neuroscience : the official journal of the Society for Neuroscience* 29: 14855-14863.

21. Cambroner F, Puelles L (2000) Rostrocaudal nuclear relationships in the avian medulla oblongata: a fate map with quail chick chimeras. *J Comp Neurol* 427: 522-545.
22. Dodd J, Morton SB, Karagogeos D, Yamamoto M, Jessell TM (1988) Spatial regulation of axonal glycoprotein expression on subsets of embryonic spinal neurons. *Neuron* 1: 105-116.
23. Stoeckli ET, Sonderegger P, Pollerberg GE, Landmesser LT (1997) Interference with axonin-1 and NrCAM interactions unmasks a floor-plate activity inhibitory for commissural axons. *Neuron* 18: 209-221.
24. Long H, Sabatier C, Ma L, Plump A, Yuan W, et al. (2004) Conserved roles for Slit and Robo proteins in midline commissural axon guidance. *Neuron* 42: 213-223.
25. Nawabi H, Briancon-Marjollet A, Clark C, Sanyas I, Takamatsu H, et al. (2010) A midline switch of receptor processing regulates commissural axon guidance in vertebrates. *Genes Dev* 24: 396-410.
26. Rajagopalan S, Vivancos V, Nicolas E, Dickson BJ (2000) Selecting a longitudinal pathway: Robo receptors specify the lateral position of axons in the *Drosophila* CNS. *Cell* 103: 1033-1045.
27. Simpson JH, Kidd T, Bland KS, Goodman CS (2000) Short-range and long-range guidance by slit and its Robo receptors. Robo and Robo2 play distinct roles in midline guidance. *Neuron* 28: 753-766.
28. Ho SM, Waite PM (1999) Spontaneous activity in the perinatal trigeminal nucleus of the rat. *Neuroreport* 10: 659-664.
29. Waite PM, Ho SM, Henderson TA (2000) Afferent ingrowth and onset of activity in the rat trigeminal nucleus. *The European journal of neuroscience* 12: 2781-

- 2792.
30. Luo L, Flanagan JG (2007) Development of continuous and discrete neural maps. *Neuron* 56: 284-300.
 31. Trevelyan AJ, Upton AL, Cordery PM, Thompson ID (2007) An experimentally induced duplication of retinotopic mapping within the hamster primary visual cortex. *The European journal of neuroscience* 26: 3277-3290.
 32. Muckli L, Naumer MJ, Singer W (2009) Bilateral visual field maps in a patient with only one hemisphere. *Proceedings of the National Academy of Sciences of the United States of America* 106: 13034-13039.
 33. Woolsey TA, Van der Loos H (1970) The structural organization of layer IV in the somatosensory region (SI) of mouse cerebral cortex. The description of a cortical field composed of discrete cytoarchitectonic units. *Brain research* 17: 205-242.
 34. Van der Loos H, Woolsey TA (1973) Somatosensory cortex: structural alterations following early injury to sense organs. *Science* 179: 395-398.
 35. Kaas JH (2004) Evolution of somatosensory and motor cortex in primates. *The anatomical record Part A, Discoveries in molecular, cellular, and evolutionary biology* 281: 1148-1156.
 36. Torborg CL, Hansen KA, Feller MB (2005) High frequency, synchronized bursting drives eye-specific segregation of retinogeniculate projections. *Nature Neuroscience* 8: 72-78.
 37. Constantine-Paton M, Law MI (1978) Eye-specific termination bands in tecta of three-eyed frogs. *Science* 202: 639-641.
 38. Williams RW, Hogan D, Garraghty PE (1994) Target recognition and visual maps in the thalamus of chiasmatic dogs. *Nature* 367: 637-639.

39. Voiculescu O, Charnay P, Schneider-Maunoury S (2000) Expression pattern of a *Krox-20*/Cre knock-in allele in the developing hindbrain, bones, and peripheral nervous system. *Genesis* 26: 123-126.
40. Studer M, Lumsden A, Ariza-McNaughton L, Bradley A, Krumlauf R (1996) Altered segmental identity and abnormal migration of motor neurons in mice lacking *Hoxb-1*. *Nature* 384: 630-634.
41. Ren SY, Pasqualetti M, Dierich A, Le Meur M, Rijli FM (2002) A *Hoxa2* mutant conditional allele generated by Flp- and Cre-mediated recombination. *Genesis* 32: 105-108.
42. Melzer P, Welker E, Dorfl J, Van der Loos H (1994) Maturation of the neuronal metabolic response to vibrissa stimulation in the developing whisker-to-barrel pathway of the mouse. *Brain research Developmental brain research* 77: 227-250.
43. Marillat V, Cases O, Nguyen-Ba-Charvet KT, Tessier-Lavigne M, Sotelo C, et al. (2002) Spatiotemporal expression patterns of *slit* and *robo* genes in the rat brain. *J Comp Neurol* 442: 130-155.

Figure legends

Figure 1

Rewiring of r3 and r5 hindbrain to midbrain/forebrain projections in *Krox20::Cre;Robo3^{lox/lox}* mice.

(A) Schematic representation of the mouse whisker to barrel somatosensory pathway. (B, C) Coronal sections at r3 level in E12 embryos hybridized with a *robo3* probe. No staining is observed in *Krox20::Cre;Robo3^{lox/lox}* mice in r3. Trigeminal ganglion (V) neurons do not express *Robo3*. (D, E) Flat-mount view and scheme (G, I) of the

hindbrain of E12 *Krox20::Cre;Robo3^{lox/+};Tau^{GFP}* (D) or *Krox20::Cre;Robo3^{lox/lox};Tau^{GFP}* embryos (E). Commissures are strongly reduced at r3 and r5 levels in mutants but a subset of axons still cross in r3 (arrowhead in E). GFP⁺ axons still project rostrally towards the midbrain. (F, H) Coronal sections at r3 level in E13 *Krox20::Cre;Robo3^{lox/+};Tau^{GFP}* (F) or *Krox20::Cre;Robo3^{lox/lox};Tau^{GFP}* (H) embryos stained for GFP. GFP⁺ commissures are strongly reduced in mutants, but a few axons are still crossing (H).

Scale bars, 50 μ m (B,C); 300 μ m (D,E) ; 150 μ m (F,H)

Figure 2

Normal organization of the principal trigeminal nucleus (PrV) in *Krox20::Cre;Robo3^{lox/lox}* mice

(A-D) Cytochrome oxidase staining of coronal sections of P4 brains at the level of the PrV, showing the barrellettes. Rows A to E are indicated. The barrellette pattern is similar in Control and *Krox20::Cre;Robo3^{lox/lox}* mutant mice. 5m: Trigeminal motor nucleus, d: dorsal PrV, v: ventral PrV. (E,F) Coronal sections at the level of the PrV in adults *Krox20::Cre;Robo3^{lox/+};Tau^{GFP}*, stained with anti NeuN and anti β Gal. β Gal- and NeuN⁺ cells can be found in the ventral PrV (arrowheads).

Scale bars, 400 μ m (A, C); 100 μ m (B, D); 200 μ m (E); 50 μ m (F)

Figure 3

Incomplete ipsilateral wiring of ventral PrV neurons.

A-H: P4 hindbrain cross sections at the level of the PrV in controls (B-D) and mutants (F-H) after unilateral injections of DiA and Dil in the VPM (depicted in the schematics A and E). D and H are higher magnification views of the insets in B and F

respectively of the ventral PrV contralateral to the Dil injection side. In controls, PrV are labeled by the dye injected in the contralateral VPM. In mutants, the dorsal PrV also has only contralaterally labeled neurons, whereas the ventral PrV contains interspersed ipsilaterally and contralaterally labeled neurons (F-H).

Scale bars, 400 μ m (B,C,F,G); 150 μ m (D-H)

Figure 4

compressed r3-VPM projection in *Krox20::Cre;Robo3^{lox/lox}* mice.

(A-H) Coronal sections of P4 mouse brain through the sensory thalamus (VPM) stained for cytochrome oxidase. In *Krox20::Cre;Robo3^{lox/+};Tau^{GFP}* mice, GFP⁺ axons project to the barreloid area of the VPM (rows A-E are indicated). In *Krox20::Cre;Robo3^{lox/lox};Tau^{GFP}* mice barreloids are found in two regions, a lateral one containing most of the GFP⁺ axons and a medial one (asterisk) containing only a few patches of GFP axons. Arrowheads indicate the boundary between the 2 VPM regions.

Scale bars, 300 μ m (B-D,F-H); 1mm (A, E)

Figure 5

Bilateral innervation of the mutant VPM barreloids

All pictures are coronal sections through the VPM.

(A-H) P4 mice injected bilaterally with Dil and DiA at the level of the PrV nucleus. In controls (A-D), the PrV-VPM projection is entirely crossed. In mutants (E-H), the VPM receives bilateral inputs from the ipsilateral and contralateral PrV.

Scale bars, 200 μ m (B,F); 55 μ m (C, D, G, H)

Figure 6**Invasion of the dorsomedial VPM by r2 inputs**

(A-E) VPM nucleus of P6 *Krox20::Cre;Tau^{GFP};r2::mCherry* control (*Robo3^{lox/+}*; B, C) or mutant (*Robo3^{lox/lox}*; D, E). (A-C) in controls, the r2 (red) and r3-derived axons (green) project to the contralateral VPM. (D-F) in mutants, the r2-derived mCherry⁺ domain is expanded (arrowheads), and the r3-derived GFP⁺ domain is retracted compared to controls. The dashed line in D and E indicate the border between the two domains. (F) Summary diagram in mutants, the PrV-VPM projection is bilateral and contains a mixture of ipsilateral (r3-derived) and contralateral (r2-derived with a small r3 contribution) which segregate into adjacent VPM domains.

Scales bars, 200µm.

Figure 7**Bilateral inputs to the barrel cortex in *Krox20::Cre;Robo3^{lox/lox}* mice.**

(A-D) Tangential sections through the barrel cortex from P10 mice stained for cytochrome oxidase (A,C) or anti-Vglut2 (B,D). Barrels are more numerous and smaller in mutants. Arrowheads indicate a clear boundary delimiting two regions (In and Out) within the large whisker representation. (E) After unilateral whisker trimming in adults : only the contralateral cortex (S1c) receives normal sensory, while the ipsilateral cortex (S1i) is sensory-deprived. (F-J) Flat-mount of S1 in whisker-deprived adult mice immunostained for Vglut2 and c-fos. In *Robo3^{lox/lox}* controls, c-fos staining is high contralateral to the intact whiskers (S1c), whereas in *Krox20::Cre;Robo3^{lox/lox}* mutants, c-fos expression is induced bilaterally in complementary domains processing ipsilateral (Ipsi) and contralateral (Contra) inputs.

Scales bars, 200µm

Figure 8

The somatotopic organization of the mutant inner and outer maps is comparable to controls

(A-I) Flat-mount of S1 in whisker-deprived adult mice immunostained for Vglut2 and c-fos. Drawings in A and E indicate the intact whiskers in pink. (J-L) The size of the C3 barrel is reduced in the mutant ipsilateral (K) and contralateral (L) whisker representations. Barrels are visualized with Vglut2 immunostaining on tangential sections. (M, N) Schematic representation of the whisker map deduced from c-fos activation patterns. Only the whiskers that were tested for c-fos activation are represented: stradlers and the 3 caudalmost arcs of the whisker pad. The size of each disk reflects the surface of the corresponding barrel.

Scales bars, 50 μm (J-L); 200 μm (C-E, G-I)

Figure 9**Activity-dependent competition between ipsilateral and contralateral inputs in mutant barrel cortex**

(A, C, D, F) Cytochrome oxidase staining of P10 cortices after unilateral lesion of the infraorbital nerve at P1. In controls, the barrels do not form in S1 contralateral to the lesion (A), whereas a normal map is seen on the ipsilateral side (B, C). In *Krox20::Cre;Robo3^{lox/lox}* mutants, contralateral to the lesion, barrels form in the domain processing ipsilateral inputs (D, E) and ipsilateral to the lesion a barreless region is noted in the domain processing ipsilateral inputs (area delimited by a dashed line) (F). This area is compressed compared to the contralateral side (D).

Scales bars, 200 μm (A,C,D,F)

Supporting information

Figure S1

Abnormal organization of the barrel cortex in *Krox20::Cre;Robo3^{lox/lox}* mice

(A-L) Barrel cortices of adult mice stained with anti-Vglut2. Left and right cortices of the same animals are presented, showing the similarities in the shape of the map processing ipsilateral inputs (delineated by the dashed line in E, G, L, K) and contralateral inputs in *Krox20::Cre; Robo3^{lox/lox}* mice.

Scale bars, 200µm (A-L)

Figure S2

Surface of individual barrels in *Robo3^{lox/lox}* and *Krox20::Cre;Robo3^{lox/lox}* mice

Individual barrels were matched with c-fos activity and surfaces were quantified in 6 *Krox20::cre;Robo3^{lox/lox}* adult mice and 4 *Robo3^{lox/lox}* mice and compared using ANOVA and Bonferroni Post-test. ns: $p > 0.05$; *: $0.05 < p < 0.01$; **: $0.01 < p < 0.001$; ***: $p < 0.001$.

Figure S3

Surface of the inner S1 map in *Krox20::Cre;Robo3^{lox/lox}* mice after an infraorbital nerve lesion

(A, B, E, F) Cytochrome oxydase staining of barrel cortices from P10 mice, unlesioned (A, B) or after unilateral infraorbital nerve cut at P1 (E, F). The posteromedial barrel field area is shaded. In lesioned *Krox20::Cre;Robo3^{lox/lox}* mutants, the map processing ipsilateral inputs is larger on the side contralateral to the lesion (E) than in unlesioned mutant (B), whereas on the ipsilateral side (F) the map is smaller than in unlesioned mutant (B). C, is a quantification of the surface of

the map processing ipsilateral inputs in lesioned or unlesioned mutants compared to control barrel cortex. Scale bars, 200 μm (A,B,E,F)

Figure 1:

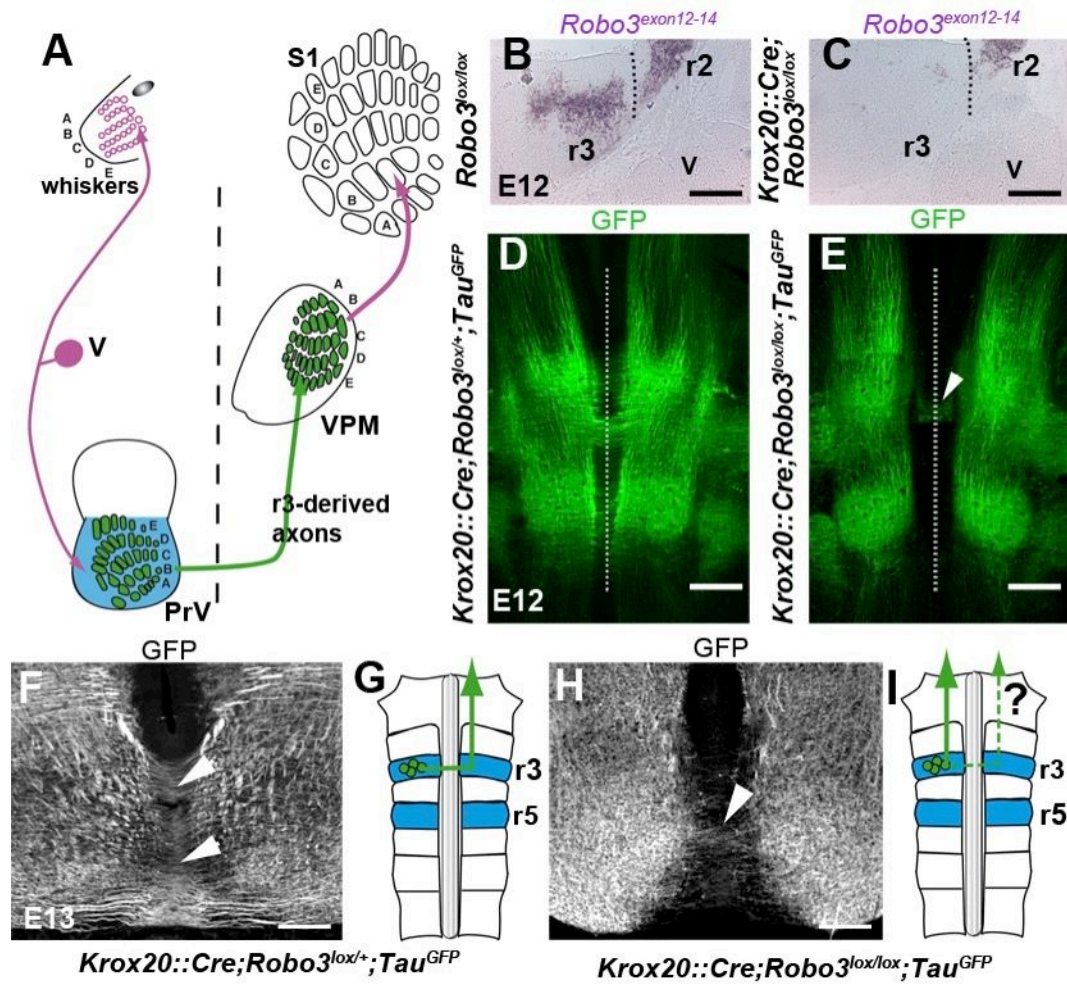


Figure 2:

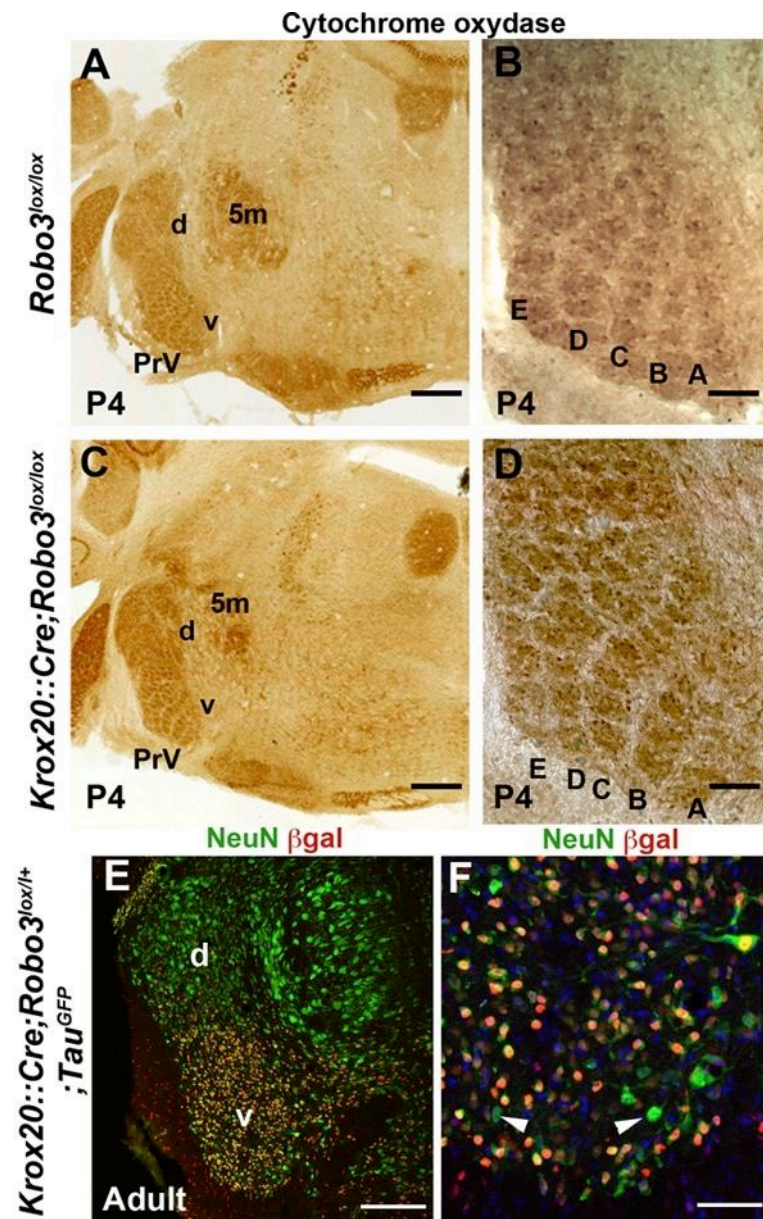


Figure 3:

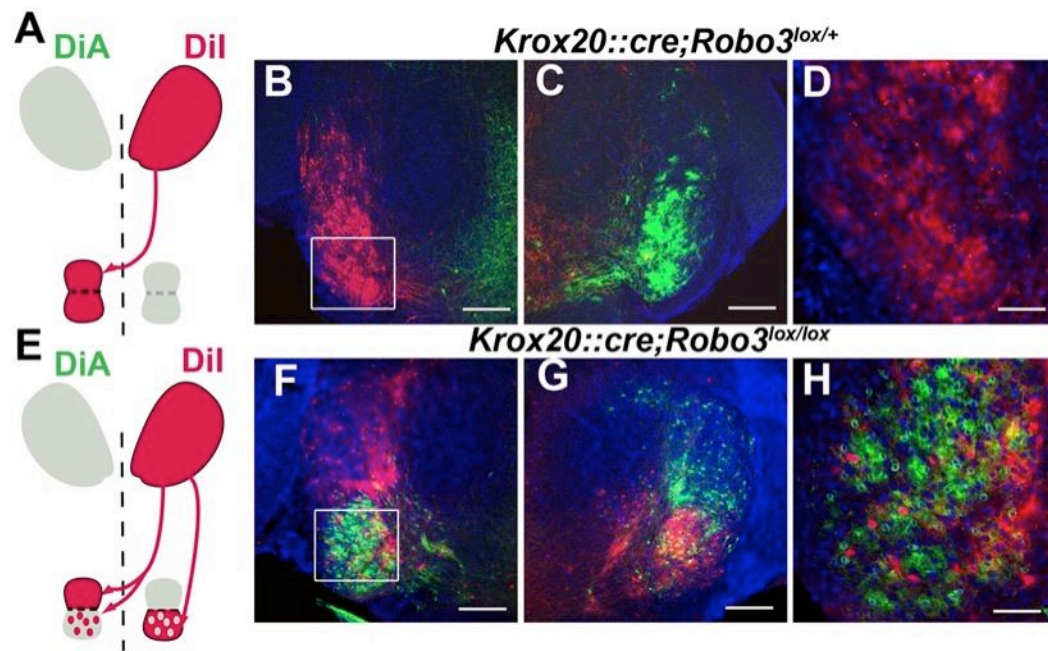


Figure 4:

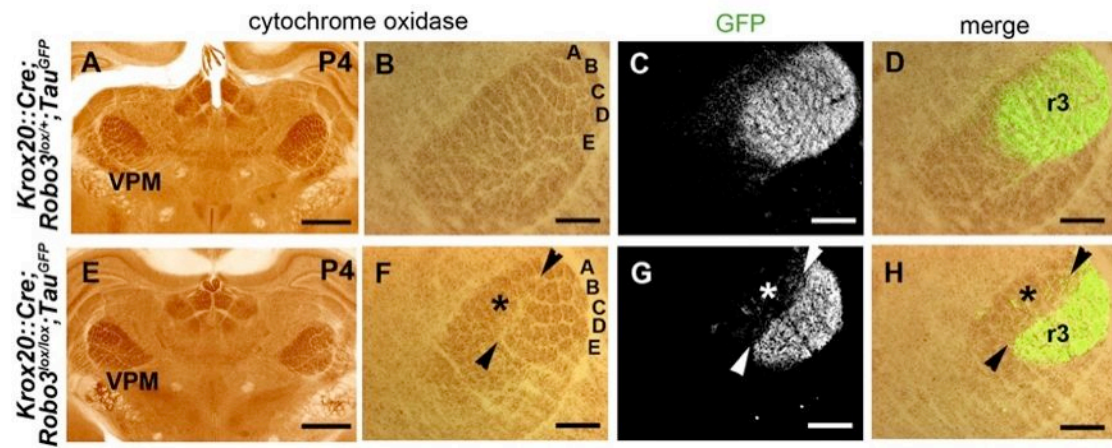


Figure 5:

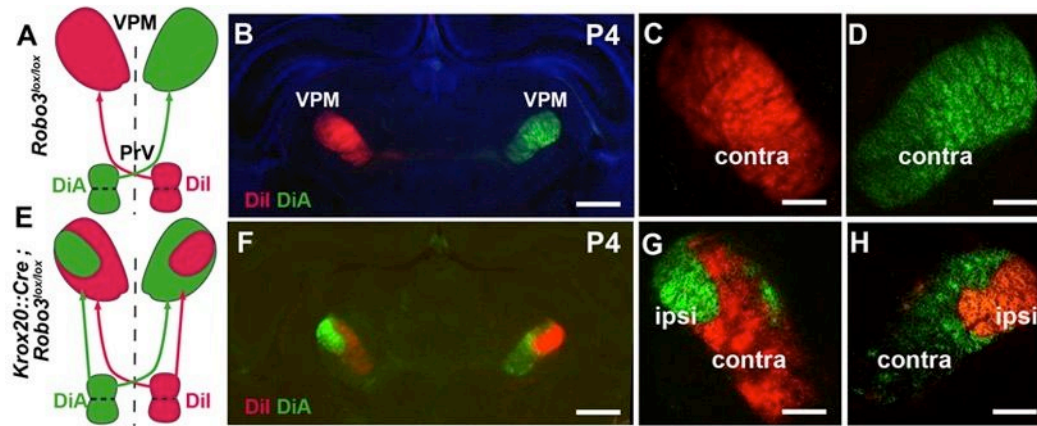


Figure 6:

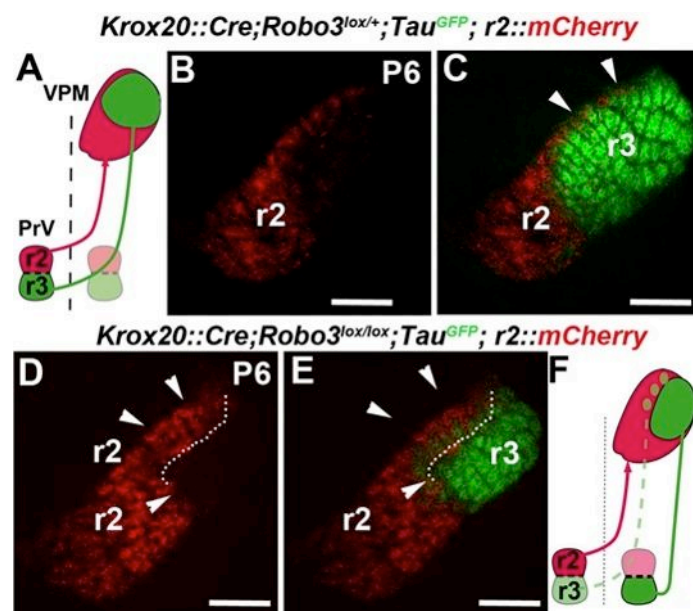


Figure 7:

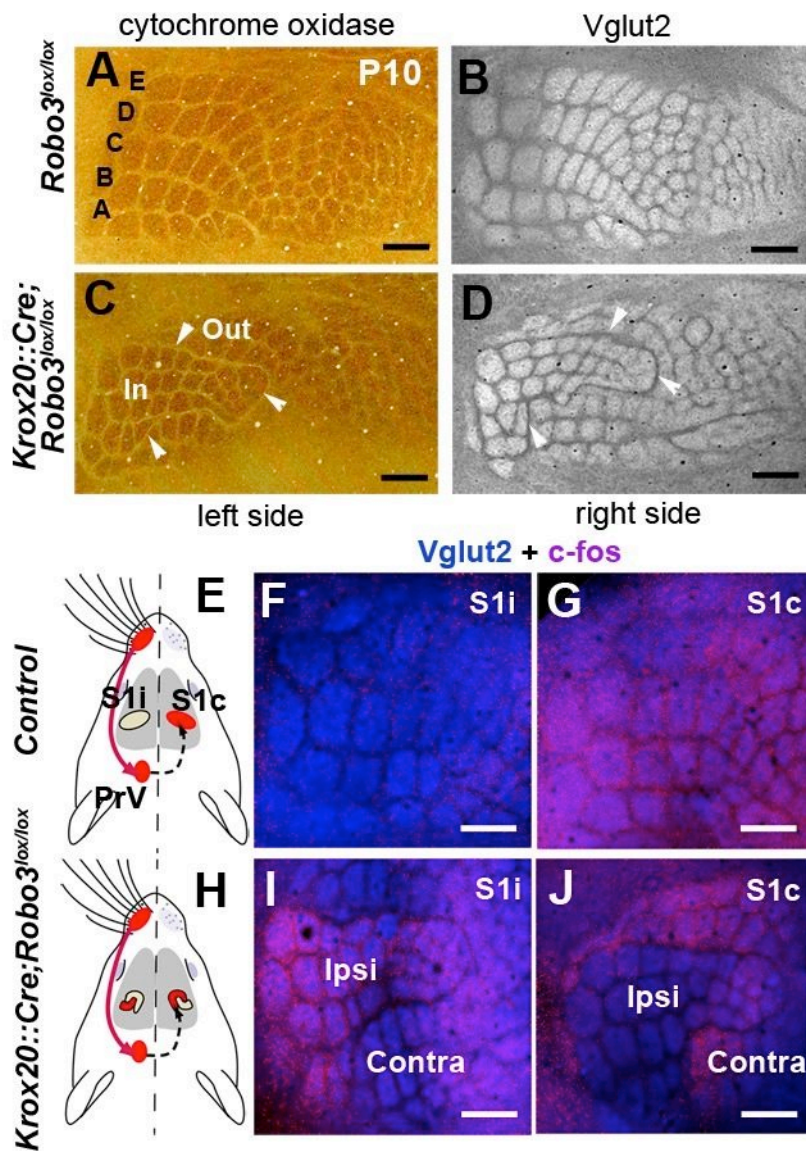


Figure 8:

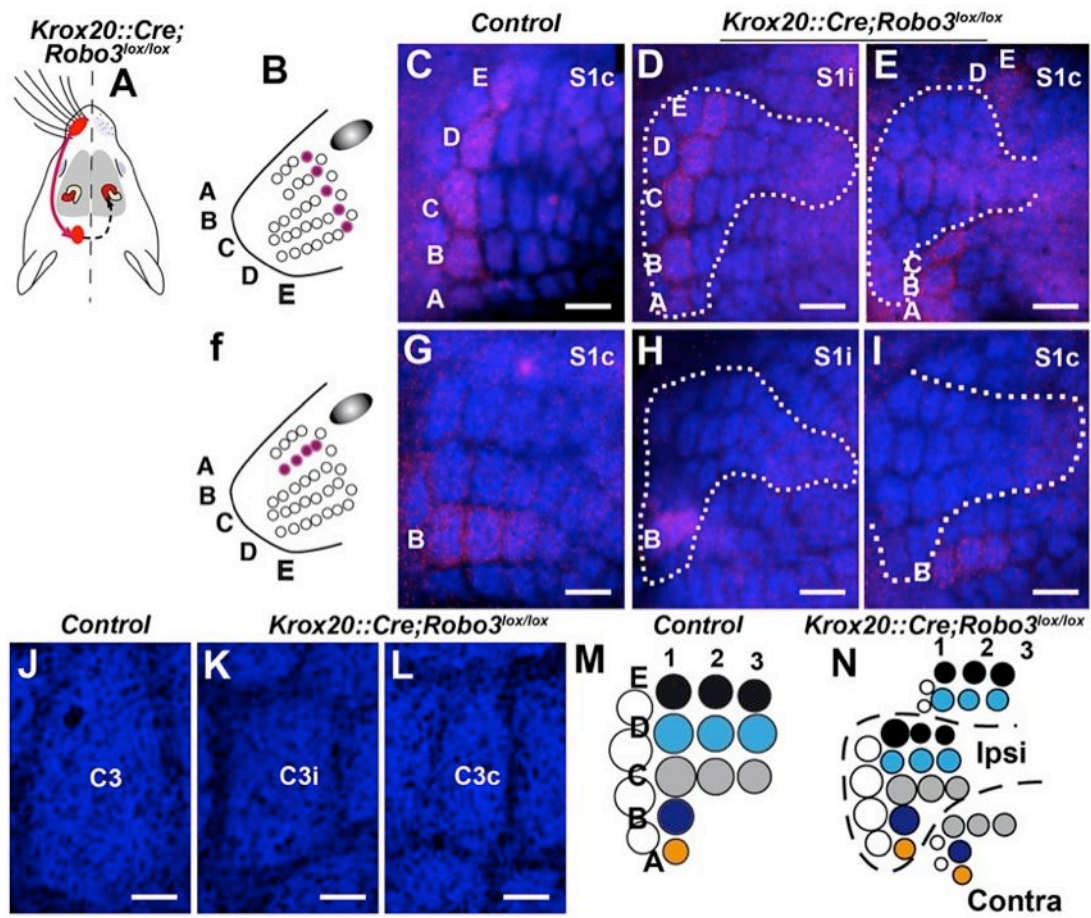


Figure 9:

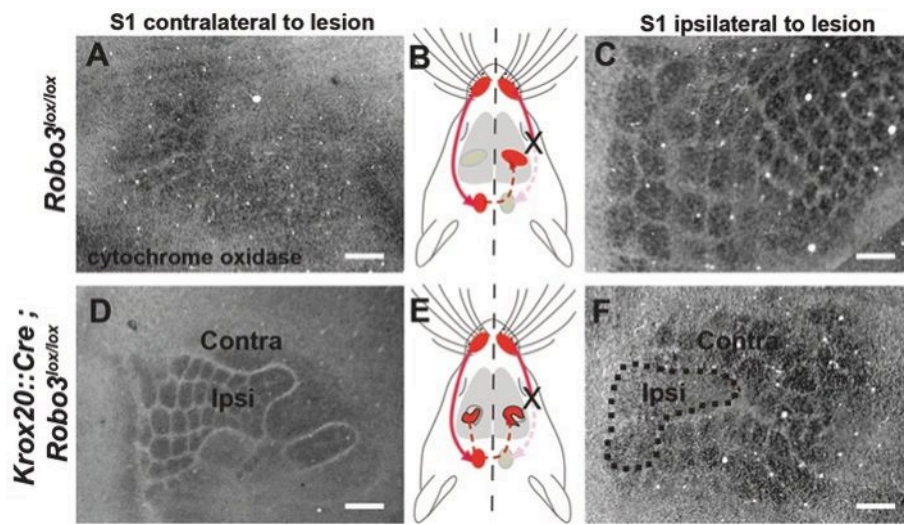


Figure S1:

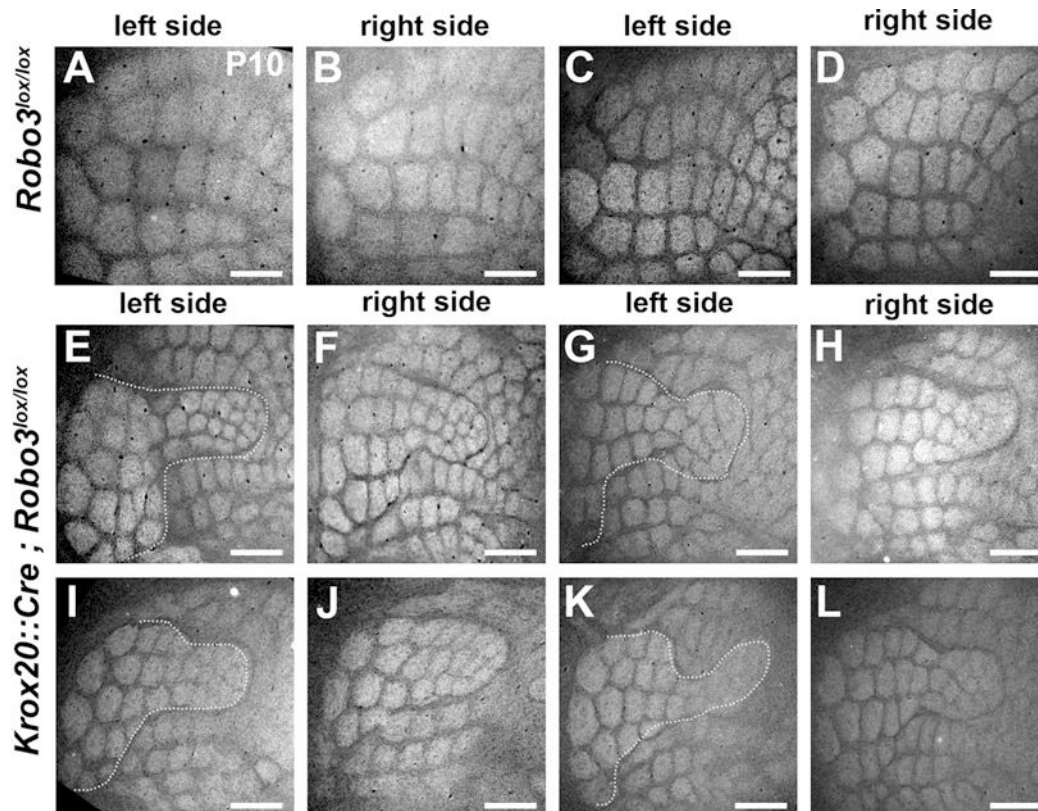


Figure S2:

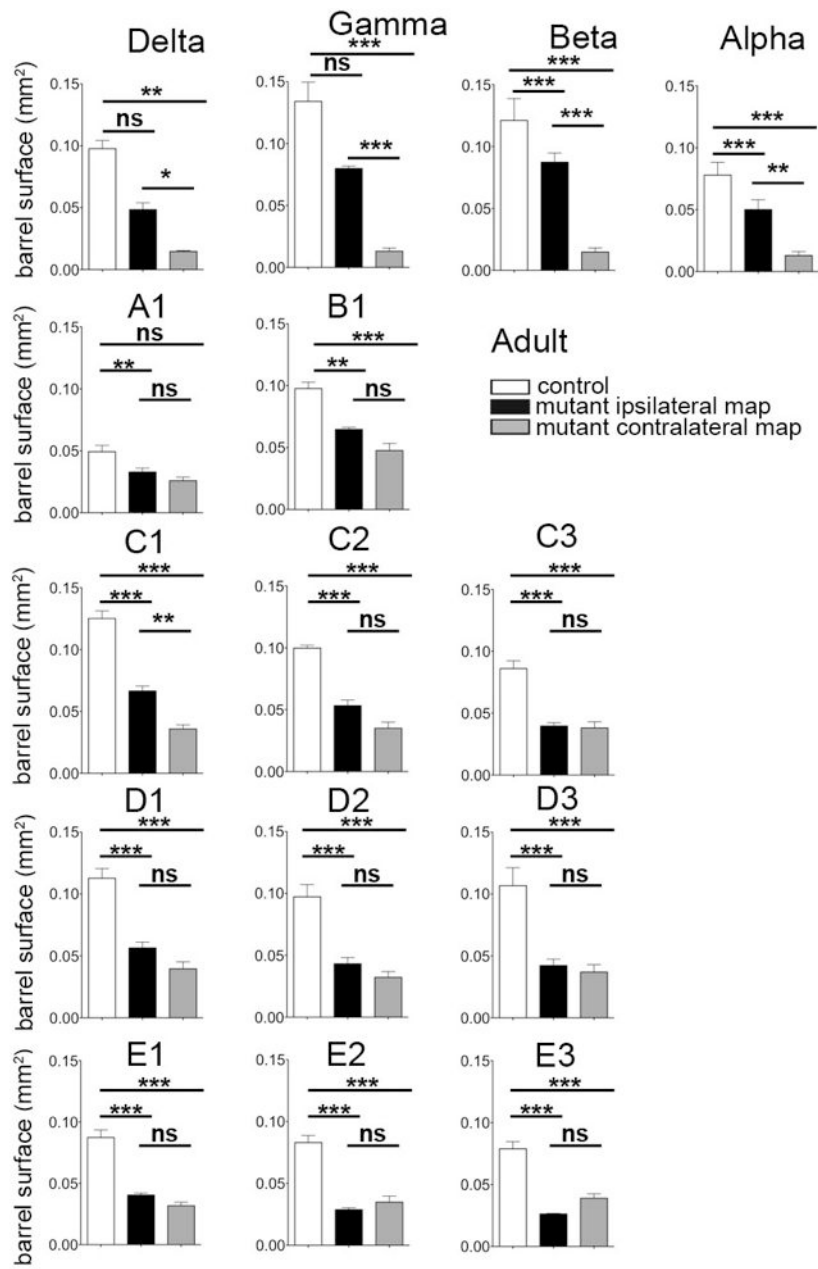
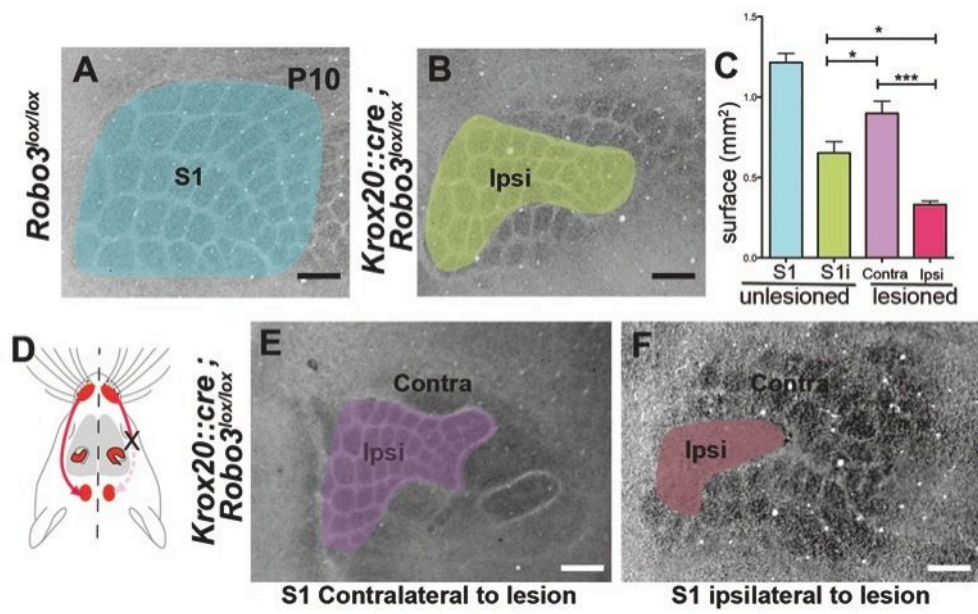


Figure S3:



3.1.4 “Mouse *Hoxa2* genetic analysis provides a model for human microtia and auricle duplication” (submitted manuscript)⁴

Another example for the role of rostro-caudal determinants as *Hox* genes are neural crest cells. In the hindbrain region, neural crest cells migrate from the dorsal margin of the neural tube to the branchial arches, transient segmented structures at the ventral side of the embryo. Branchial arches have a differential contribution from different rhombomeres and generally express similar *Hox* codes as their pre-migratory progenitors.

It is suggested that also in the neural crest system the later development is predetermined already at earlier stages of differentiation putting forward a similar kind of protomap as we demonstrated for the precerebellar system (3.1.1).

The following manuscript describes a role of *Hoxa2*, a determinant for branchial arch 2 derived structures in the generation of the external ear (including the pinna).

Hoxa2 conditional knockouts resulted in absence of the auricle and a duplication of the branchial arch 1 derived ear canal. *Hoxa2*, if overexpressed, was able to induce a duplication of the pinna. It is suggested that *Hoxa2* plays, as *Hox* genes in the precerebellar system, a major role in controlling the terminal fate by controlling in case of the neural crest cells the expression of realizator genes as *Eya1*, *Chd7* and genes of the BMP pathway.

Knowledge acquired during the analysis of the 3-dimensional connectivity patterns in the precerebellar system has been of use for the analysis of the external ear phenotype easing the understanding of the occurring structural changes.

⁴ Statement of contribution: My contribution to this manuscript was the 3D reconstruction of the external ear of *Hoxa2*^{EGFP/+} control and *Hoxa2*^{EGFP/EGFP} mutant mice

***Hoxa2* genetic analysis provides a model for microtia and auricle duplication**

Maryline Minoux^{1,2}, Claudius F. Kratochwil^{1,3}, Sébastien Ducret¹, Shilu Amin⁴, Taro Kitazawa⁵, Hiroki Kurihara⁵, Nicoletta Bobola⁴, Nathalie Vilain¹, and Filippo M. Rijli^{1,3*}

¹ Friedrich Miescher Institute for Biomedical Research, Maulbeerstrasse 66, CH-4058 Basel, Switzerland.

² INSERM UMR 1121, Université de Strasbourg, Faculté de Chirurgie Dentaire, 1, place de l'hôpital, 67 000 Strasbourg, France.

³ University of Basel, CH-4056 Basel, Switzerland.

⁴ School of Dentistry, Faculty of Medical and Human Sciences, University of Manchester, Manchester M13 9PT.

⁵ Department of Physiological Chemistry and Metabolism, Graduate School of Medicine, The University of Tokyo, 7-3-1 Hongo, Bunkyo-ku, Tokyo 113-0033, Japan.

* Corresponding author : Filippo M. Rijli (email: Filippo.Rijli@fmi.ch)

ABSTRACT

External ear abnormalities are frequent in newborns ranging from microtia to partial auricle duplication. Little is known about the molecular mechanisms orchestrating external ear morphogenesis. In humans, *HOXA2* partial loss of function induces microtia. In mice, *Hoxa2* inactivation at early gestational stages results in external auditory canal duplication and auricle absence, whereas its late inactivation results in a hypomorphic auricle, mimicking the human *HOXA2* mutant condition. By genetic fate mapping, we found that the mouse auricle (or pinna) entirely derives from the *Hoxa2*-expressing neural crest-derived mesenchyme of the second pharyngeal arch, and not from a composite of first and second arch mesenchyme, as previously thought. Furthermore, conditional ectopic *Hoxa2* expression in first arch neural crest is sufficient to induce a full pinna duplication, indicating that *Hoxa2* orchestrates the whole external ear morphogenetic program. *Hoxa2* partly controls pinna morphogenesis through the BMP signaling pathway and expression of *Eyes absent-1 (Eya1)* and *Chromodomain helicase DNA-binding protein-7 (Chd7)*, involved in the branchio-oto-renal and CHARGE human syndromes, respectively. Thus, *Hoxa2* loss and gain of function approach in mice provides a suitable model to investigate the molecular etiology of human microtia and auricle duplication.

INTRODUCTION

The external ear is composed of the auricle (or pinna) and the external auditory canal (EAC). A variety of factors can affect its morphogenesis, inducing a wide range of abnormalities such as microtia and partial auricle duplications (1-7). Microtia, which is characterized by a small, abnormally shaped pinna is one of the most common external ear abnormalities; the estimated prevalence ranging from 0.8 to 4.2 per 10 000 births depending on the population (1). External ear abnormalities can occur as the only clinical defect, but in most cases they appear in complex syndromes in which others organs and structures are affected. The most common associated malformations are renal and cardiac abnormalities, vertebral and limb defects (including polydactyly), as well as craniofacial malformations (reviewed in (1)). External ear anomalies are indeed commonly associated with internal and/or middle ear dysplasia, resulting in hearing loss and problems in speech and language development (8). Deciphering the molecular mechanisms involved in external ear morphogenesis is then crucial not only to better understand the defaults affecting the external ear, but also more generally to gain a more comprehensive view of the mechanisms involved in the genetic syndromes in which external ear abnormalities are present.

Genetic diagnostics in humans, as well as loss-of-function experiments in mice have begun to identify signaling factors and transcriptional regulators playing a role during external ear morphogenesis. Among these factors, *Hoxa2*, which is indispensable for the patterning of second pharyngeal arch neural crest cells (NCCs) and their derivatives, plays a crucial role. In humans, a *HOXA2* partial loss of function (missense) mutation has been shown to induce a bilateral microtia associated to an abnormal shape of the auricle (9). Hearing impairment and

partial cleft palate have also been reported (9). A role for *Hoxa2* in external ear morphogenesis is also observed in mice, where its inactivation induces duplication of the EAC and absence of the auricle (10-13). This phenotype is associated with other craniofacial abnormalities, notably a cleft palate and malformations of middle ear structures. Indeed, as a result of *Hoxa2* inactivation, the second arch-derived skeletal elements (including the middle ear stapes) are morphologically transformed into a duplicated set of first arch-like elements (including duplication of the middle ear malleus and incus) (10, 11). By temporally controlled inactivation, we have further shown that the morphogenesis of the auricle requires *Hoxa2* function through advanced developmental stages (14). While early inactivation (i.e. before E11.5) of *Hoxa2* induces the absence of the auricle, reproducing the full knockout phenotype, *Hoxa2* inactivation at later stages, i.e. between E12.5 and E13.5, results in a hypomorphic auricle (14), thus mimicking the human *HOXA2* mutant condition. Altogether, these data emphasize the major role of *Hoxa2* in auricle morphogenesis. However, the molecular determinants regulated by *Hoxa2* during the morphogenesis of the pinna are only beginning to be elucidated (15) and are still largely unknown. Furthermore, it is unclear whether *Hoxa2* is not only necessary but also sufficient to induce and orchestrate the whole developmental program underlying the morphogenesis of the pinna.

By genetic fate mapping, we show here that the mouse pinna derives entirely from the *Hoxa2*-expressing neural crest-derived mesenchyme of the second pharyngeal arch, and not from a combined contribution of first and second arch mesenchyme, as previously thought (1, 4, 16-19). We further show that the EAC develops entirely within the *Hoxa2*-negative first arch-mesenchyme, and not, as previously proposed, from the first pharyngeal cleft at the interface between first and second arches (19, 20). By a conditional gain of function approach, we show that ectopic *Hoxa2* expression in first arch cranial neural crest is alone sufficient to induce the

transformation of the EAC mesenchyme into a mirror image duplication of the pinna. Moreover, functional and molecular analysis revealed that *Hoxa2* controls the formation of the pinna through the BMP signaling pathway, by regulating the expression of *Bone Morphogenetic protein-5 (Bmp5)*, *Bone Morphogenetic protein-4 (Bmp4)* and *Twisted Gastrulation (Tsg)*. Chromatin immunoprecipitation and parallel sequencing (ChIP-Seq) on second arch cells additionally identified *Bmp4* and *Bmp5* as *Hoxa2* direct targets. While *Bmp5* inactivation results in a small pinna (known as the short ear mutation; (21, 22)), we further show that the conditional inactivation of *Bmp4* also partially impairs pinna development. Moreover, *Hoxa2* regulates the expression of *Eyes absent-1 (Eya1)* and *Chromodomain helicase DNA-binding protein-7 (Chd7)*, involved in the branchio-oto-renal and CHARGE human syndromes, respectively (23-25). Thus, *Hoxa2* orchestrates the coordinated morphogenesis of the auricle. This genetic approach in the mouse may represent a suitable model to understand the etiology of human auricle abnormalities.

RESULTS

The pinna is entirely contributed by second arch derived *Hoxa2*⁺ ectomesenchyme

The formation of the external ear occurs early in development (starting at E12.0 in the mouse, sixth week in humans). To map the cellular origin of the pinna, we crossed a rhombomere 4 (*R4*::*Cre* mouse line (26) with the *Z/AP* transgenic reporter line (27). Upon Cre-mediated recombination, the expression of the *Alkaline Phosphatase* (AP) gene is permanently activated in the R4-derived NCC progenitors, thus allowing to assess the contribution of second arch NCCs to the external ear. Notably, we found that the pinna is entirely composed by second arch NCCs (Fig. 1D, E), and not by a combination of first and second arch NCC derived mesenchyme, as previously proposed (1, 4, 16-19). Second arch NCCs also partly contribute to the mesenchyme between the EAC and the otic capsule (Fig. 1B, C).

We next mapped the contribution of *Hoxa2*-expressing (*Hoxa2*⁺) NCCs to the second arch-derived pinna. We used the *Hoxa2*^{*EGFP*(*lox-neo-lox*)} allele in which *EGFP* is knocked-in at the *Hoxa2* locus and conditionally induced in *Hoxa2*⁺ cells by Cre-mediated excision (28). We crossed this line to the *Wnt1*::*Cre* driver that expresses Cre in all NCC progenitors (29). In E14.5 *Wnt1*::*Cre*;*Hoxa2*^{*EGFP*(*lox-neo-lox*)+/-} fetuses, the pinna is composed of *EGFP*-expressing NCCs, thus demonstrating that this structure originates entirely from *Wnt1*⁺/*Hoxa2*⁺ NCC progenitors (Fig. 1F, I, J).

The external auditory canal develops entirely from first arch *Hoxa2* ectomesenchyme

The EAC, an ectodermal structure, is believed to be derived from the first pharyngeal cleft at the interface between first and second arches and to be lined by NCC derived mesenchyme contributed by both arches (19, 20). Unlike this prediction, we found that in E14.5

Wnt1::Cre;Hoxa2^{EGFP(lox-neo-lox)+/-} fetuses, the mouse EAC and its surrounding mesenchyme were entirely composed by *Hoxa2*⁻/*EGFP*⁻ cells, therefore not derived from second arch (Fig. 1G, H, J). Moreover, we observed a sharp spatial segregation between *Hoxa2*⁻/*EGFP*⁻ and *Hoxa2*⁺/*EGFP*⁺ cell populations contributing to the external auditory meatus or the pinna, respectively (Fig. 1J). A similar cell sorting was observed in E14.5 *Hoxa2*^{EGFP} embryos in which *EGFP* is knocked-in at the *Hoxa2* locus and faithfully replaces the *Hoxa2* expression domain (28) (Fig. 1K-N), as well as in E14.5 *R4::Cre;Z/AP* embryos between AP-positive (i.e. second arch derived) and AP-negative (i.e. first arch derived) cellular domains (Fig. 1B-E). Furthermore, analysis at E12.5 confirmed that the EAC (arrow, Fig. 1O) begins to form entirely anterior to the second arch-derived *Hoxa2*⁺/*EGFP*⁺ cells forming the pinna (Pi, Fig. 1O), within the *Hoxa2*⁻/*EGFP*⁻ first arch-derived tissue. Thus, at E12.5 the EAC and the pinna develop opposite and almost equidistant to the vestigial first pharyngeal cleft that maps at the border between *EGFP*⁺/*EGFP*⁻ territories (arrowhead, Fig. 1O); their respective cell contributions from first and second arches never intermingle despite the complex morphogenetic cell movements occurring during their formation.

To investigate the spatial distribution of second arch mesenchymal cells in the absence of *Hoxa2* function, we used *Hoxa2*^{EGFP/EGFP} homozygous mutants embryos in which both alleles of *Hoxa2* drive *EGFP* expression (Fig. 1P). By 3D reconstruction of tissue sections, we confirmed the previously described duplication of the EAC (10-13) (Fig. 2G). Moreover, the duplicated external auditory canal (EAC*) is found within the *Hoxa2*⁺/*EGFP*⁺ domain (Fig. 2H, I, K, L, see also Fig. 1Q-T), while the orthotopic EAC develops entirely into the *Hoxa2*⁻/*EGFP*⁻ territory (Fig. 2H, I, K, L, see also Fig. 1T) as in control E14.5 *Hoxa2*^{EGFP} embryos (Fig. 2A-C, E, F). The border between *EGFP*⁺/*EGFP*⁻ territories is the symmetry axis on either side of which the EAC and its ectopic EAC* counterpart develop (Fig 1T). Furthermore, the 3D reconstruction shows

that in E14.5 *Hoxa2*^{EGFP/EGFP} homozygous mutant embryos, the *EGFP*⁺ cells maintain their normal spatial segregation and do not ectopically intermingle with *EGFP*⁻ cells, despite the fact they have acquired a first arch like identity (compare Fig. 2J with 2D; see also Fig. 1T).

***Hoxa2* organizes spatial patterns of cell proliferation during external ear morphogenesis**

At E14.5, *Hoxa2* expression extensively overlaps with the developing pinna. On horizontal and frontal tissue sections, the *Hoxa2*-expressing domain contains an outer territory including the pinna, and an inner territory sharply segregated from the *Hoxa2*-negative mesenchyme (Fig. 3B, H; the dashed line separates outer and inner *Hoxa2*-expressing territories). The inner domain is strongly *Hoxa2*⁺, whereas the outer domain displays lower expression levels and sparser *Hoxa2* transcript distribution (Fig. 3B, H). The two *Hoxa2* expression territories roughly abut at the base of the bending pinna (arrow Fig. 3B, H). *Hoxa2* is additionally expressed in the mesenchyme at the tip and below the ectoderm on both the dorsal and ventral sides of the pinna (Fig. 3B, H).

The spatial distribution of *Hoxa2* transcripts suggests distinct proliferation/differentiation states of cellular subsets. In E14.5 control fetuses, *Ki67*⁺ NCC-derived proliferating cells are present at the tip and orderly aligned on both the dorsal and ventral sides of the pinna, below the ectoderm, whereas the mesenchymal core of the pinna is only contributed by *Ki67*⁻ post-mitotic differentiating cells (Fig. 3A, C, G). This *Ki67*⁺ cell pattern is quite similar to the *Hoxa2* transcript distribution (compare Fig. 3A with 3B) indicating that, in the pinna, *Hoxa2* is mainly expressed in proliferating NCC-derived cells. In contrast, the inner *Hoxa2* expression domain encompasses both *Ki67*⁺ and *Ki67*⁻ cell subsets (compare Fig. 3A with 3B, and 3G with 3H), with *Ki67*⁺ cells orderly aligned (arrows, Fig. 3A, C, G) and adjacent to *Ki67*⁻ differentiating mesenchymal cells. In addition, at E14.5 a subset of spatially organised *Ki67*⁺ proliferating cells at the base and all along the dorsal aspect of the pinna (arrowhead, Fig. 3A, C, G) does not

express *Hoxa2* (compare Fig. 3A with 3B, and 3G with 3H). This latter population of highly proliferating cells selectively expresses *Eya1* (compare Fig. 3G with 3I), which is involved in the branchio-oto-renal (BOR) syndrome in humans (23, 24) and is essential for pinna development in mice (30). Interestingly, at the beginning of pinna morphogenesis (E12.0-E12.5), *Eya1* and *Hoxa2* appear to be co-expressed in a subset of second arch-derived NCCs at the base of the future pinna (Fig. 4A-C), likely corresponding to the *Eya1*⁺ population devoid of *Hoxa2* expression at later stages (compare Fig. 3I and 3H). In E12.5 *Hoxa2*^{-/-} knockout mutant embryos, this early *Eya1* expression domain was lacking (Fig. 4D, E), suggesting a role of *Hoxa2* in establishing, though not maintaining, the highly proliferative *Eya1*⁺ territory (Fig. 3K, L).

In control *Hoxa2*^{lox/del} trans-heterozygotes, which bear both fully deleted (*Hoxa2*^{del}) and floxed (*Hoxa2*^{lox}) mutant *Hoxa2* alleles (31), the pinna had a normal appearance ((14); Fig. 3A-C), indicating that *Hoxa2* haploinsufficiency in mouse is not sufficient to cause external ear defects. In contrast, in *CMV::CreER^{T2};Hoxa2*^{lox/del} fetuses, Cre-mediated deletion of the *Hoxa2*^{lox} allele by tamoxifen (TM) administration at NCC post-migratory stages (i.e. E12.5, E13.0, and E13.5) ((14); Suppl. Fig. 1), thus bypassing an early *Hoxa2* role and supporting a late requirement for *Hoxa2* in pinna morphogenesis. The smaller and dysmorphic pinna of TM-treated *CMV::CreER^{T2};Hoxa2*^{lox/del} mutant newborns (Suppl. Fig. 1B, D) is reminiscent of the *HOXA2* mutant phenotype in humans (9). Analysis by *in-situ* hybridization confirmed the almost complete loss of *Hoxa2* expression in TM-treated mutants when compared to control embryos (Suppl. Fig. 2).

At E14.5, no apoptotic cells were observed either in control or in TM-induced *CMV::CreER^{T2};Hoxa2*^{lox/del} mutant fetuses (not shown), suggesting that the smaller dysmorphic pinna is not the result of strongly increased cell death. This was also indirectly supported by the persistence of *EGFP*⁺ cells in the outer ear region of full knockout *Hoxa2*^{EGFP/EGFP} fetuses, which

lack a normal pinna (Fig. 1P-T). In contrast, the hypomorphic pinna of E14.5 TM-induced *CMV-CreER^{T2};Hoxa2^{lox/del}* mutant fetuses lacked normal spatial segregation between Ki67⁺ and Ki67⁻ mesenchymal cells (arrows, Fig. 3E, F). Moreover, a mass of proliferating cells abnormally accumulated at the dorsal base of the pinna (asterisks Fig. 3D-F, J). Finally, the inner *Hoxa2* expressing domain appeared disorganised with fewer Ki67⁺ cells and an accumulation of unpatterned Ki67⁻ differentiating cells (arrowheads, Fig. 3D-F, J). These results indicate that after E12.5, *Hoxa2* contributes to the normal size and shape of the external ear by maintaining organised, spatially restricted, local patterns of cell proliferation.

***Hoxa2* regulates *Bmp5* and *Bmp4* expression in developing pinna**

The hypomorphic pinna in TM-treated *CMV::CreER^{T2};Hoxa2^{lox/del}* mutant fetuses is reminiscent of the phenotype of the *short ear* mutation, which inactivates *Bmp5* (21, 22). Thus, *Bmp5* is a suitable candidate to be regulated by *Hoxa2*. In the E14.5 wild type (WT) pinna, *Bmp5* expression is restricted to a subset of the *Hoxa2* expression territory, namely to the mesenchymal cores of the inner and outer *Hoxa2*⁺ domains, though not at the tip or in most of the proliferating mesenchyme of the pinna (Fig. 5A-D). On frontal and horizontal sections of TM-treated *CMV::CreER^{T2};Hoxa2^{lox/del}* mutant fetuses, *Bmp5* expression levels were strongly reduced in the pinna (arrowheads, Fig. 5J, L – compare with Fig. 5F and 5H respectively). We also observed a clear reduction of the spatial extent of *Bmp5* expression in the inner *Hoxa2*-expressing domain (arrows, Fig. 5J, L – compare with Fig. 5F and 5H respectively), with accumulation of *Bmp5* residual expression at the base of the pinna (asterisk, Fig. 5J). The temporal inactivation of *Hoxa2* selectively down-regulates *Bmp5* though not *Paired related homeobox 1 (Prrx1)*, encoding a transcription factor involved in craniofacial development (32) (compare Fig. 5E, G with 5I, K).

We next analysed the expression of *Bmp4*. At E12.0– E12.5, *Bmp4* is expressed in the distal edge (tip) of the forming pinna, as well as in a small number of mesenchymal cells at its base (not shown). This pattern is maintained and extended at E13.5 and E14.5, becoming quite similar to the *Hoxa2* expression pattern. Namely, *Bmp4* is highly expressed in the mesenchymal core of the inner *Hoxa2* expression domain (compare Fig. 6D with 6B, and 6C with 6A). In the pinna, *Bmp4* is expressed at the tip and in the proliferating mesenchyme below the dorsal and ventral ectoderm; it displays lower levels in the differentiating mesenchymal core (Fig. 6C, D). This transcript distribution is complementary to that of *Bmp5* (Suppl Fig. 3A, B); notably, *Bmp4* and *Bmp5* expression patterns together recapitulate the *Hoxa2* expression pattern in the pinna (compare Figs. 5, 6). In E14.5 TM-induced *CMV::CreER^{T2};Hoxa2^{lox/del}* mutant pinna, *Bmp4* expression is absent or strongly reduced (Fig. 6G, H) whereas *Prrx1* (Fig. 6F) and *Teashirt zinc finger family member 2 (Tshz2)* (33) (Fig. 6E) are still expressed at the tip of the pinna and in the inner *Hoxa2*-expressing domain of the TM-treated mutant pinna (Fig. 6I, J).

In summary, the above results strongly indicate that *Hoxa2* is required to maintain normal levels and spatial distribution of *Bmp4* and *Bmp5* transcripts during external ear growth and morphogenesis.

Temporal inactivation of *Hoxa2* results in altered BMP signalling in the developing pinna

The activity of BMPs is modulated in the extracellular space through their interaction with secreted agonists or antagonists. Twisted gastrulation (Tsg) is a secreted BMP modulator involved in mouse head development (34). While no external ear defects are observed in *Tsg^{-/-}* homozygous or *Bmp4^{+/-}* heterozygous mutant mice, compound *Tsg^{-/-};Bmp4^{+/-}* newborn mutants display, in severe cases, low set ears associated to an abnormal shape of the pinna (34), indicating that Tsg is involved in modulating Bmp4 activity during pinna development. In E14.5 WT

embryos, *Tsg* is strongly expressed in a stripe of highly *Ki67*⁺ proliferating cells, in the inner *Hoxa2*⁺ domain (compare Suppl. Fig. 4K (arrow) with Fig. 3G (arrow); and not shown) directly adjacent to the *Bmp4*⁺ mesenchymal core (Suppl. Fig. 4A-O). Interestingly, in E14.5 TM-induced *CMV::CreER*^{T2};*Hoxa2*^{lox/del} mutant pinna, *Tsg* is severely downregulated (Suppl. Fig. 4P-R). These results, together with the down-regulations of *Bmp4* and *Bmp5* expression and the effects on cell proliferation patterns (Figs. 3, 5, 6) further support the notion that *Hoxa2* is involved in the transcriptional regulation of BMP signalling during pinna formation.

To further investigate the downstream effects induced by *Bmp5*, *Bmp4* and *Tsg* down-regulation in *Hoxa2* mutants, we analysed the phosphorylation of Smad1, 5 and 8 nuclear factors, a hallmark of canonical BMP signal transduction (35, 36), by anti-PhosphoSmad1/5/8 immunostaining. In E14.5 control embryos, PhosphoSmad1/5/8 nuclear activation is spatially restricted. PhosphoSmad1/5/8⁺ cells are observed throughout the *Bmp5*⁺/*Bmp4*⁺ territory of the inner *Hoxa2*-expressing domain extending to the base of the pinna (white arrows Suppl. Fig. 3C and Fig. 7A-C), though not in the *Bmp5*⁺/*Bmp4*⁺ mesenchymal core of the developing pinna (Suppl. Fig. 3A-C; Fig. 7A-C). PhosphoSmad1/5/8 activated cells are also detected in the *Ki67*⁺/*Bmp4*⁺ proliferating cells at the tip of the pinna, below the dorsal and ventral ectoderm (Suppl. Fig. 3A, C; Fig. 7A-C), and in the *Eya1*⁺/*Ki67*⁺ highly proliferative domain abutting the pinna mesenchymal core (white arrowheads Suppl. Fig. 3C and Fig. 7A-C).

In E14.5 TM-induced *CMV::CreER*^{T2};*Hoxa2*^{lox/del} mutant pinna, PhosphoSmad1/5/8 activated cells were either strongly reduced or absent both at the base and at the tip of the pinna (white arrows, Fig. 7D-F), showing that the temporal inactivation of *Hoxa2* has strong effects on the regulation of canonical BMP signalling. By contrast, the *Eya1*⁺ stream of PhosphoSmad1/5/8⁺ cells is still present in E14.5 TM-induced mutant embryos (white

arrowheads, Fig. 7D-F), in keeping with the observation that the late inactivation of *Hoxa2* only partially affects this population of *Eya1*⁺ cells (see above; Fig. 3I, L).

Role of *Bmp4* in external ear morphogenesis

Bmp4^{+/-} heterozygous mutant mice survive and do not show external ear defects (not shown). To investigate the possible consequences of further reducing *Bmp4* activity during pinna morphogenesis, we generated *Bmp4*^{lox/del} hypomorph mutants, bearing a fully deleted and a floxed allele of *Bmp4*. Unlike null mutants, *Bmp4*^{lox/del} fetuses survive until E16.5, a stage at which normally the pinna has already folded over the meatus (Fig. 8A, D). In severe cases, *Bmp4*^{lox/del} fetuses display a hypomorphic pinna (Fig. 8B, F), albeit at a low frequency (n = 5/22). When present, the external ear phenotype is always associated with polydactyly (arrows, compare Fig. 8E with Fig. 8C), which also occurs at a low frequency (n = 9/22) in these hypomorphic mutants. Bilateral microphthalmia, smaller body size and subcutaneous edema are other defects also observed in most of the *Bmp4*^{lox/del} hypomorphic mutants (Fig. 8B, compare with Fig. 8A). The weak penetrance of the pinna phenotype is likely due to partial functional redundancy with other members of the BMP family, such as *Bmp5*, and/or the persistence of residual *Bmp4* function in *Bmp4*^{lox/del} hypomorphic mutants. On the other hand, homozygous null mutants for *Bmp4* die around gastrulation (37), thus preventing the analysis of its role in external ear morphogenesis. At any rate, these results highlight an involvement of *Bmp4*, at least to some extent, in the morphogenesis of the pinna.

Bmp4* and *Bmp5* may be direct *in vivo* targets of *Hoxa2

We searched a genome-wide map of *Hoxa2* binding, obtained from second pharyngeal arches (isolated just prior to the formation of the external ear), for *Hoxa2* binding events nearby or

within the *Bmp4* and/or *Bmp5* loci (15). We found binding of *Hoxa2* in proximity of *Bmp4* (72 kb downstream of the *Bmp4* transcription start site (TSS)) and within the third intron of *Bmp5* (52 kb upstream of *Bmp5* TSS). We confirmed *Hoxa2* binding by performing conventional ChIP on second arches dissected from E11.5 wild-type embryos. We found that both *Bmp4* and *Bmp5* regions were enriched in chromatin immunoprecipitated with a *Hoxa2*-specific antibody (Suppl. Fig. 5A). The region bound by *Hoxa2* in the third intron of *Bmp5* is the result of an insertion present only in mice and rat. By contrast, the region located downstream of the *Bmp4* TSS is widely conserved in vertebrates and contains putative Pbx/Hox and Hox binding sites (38) (Suppl. Fig. 5B).

In sum, these data, together with the changes in the expression patterns observed in *Hoxa2* temporal mutants (Figs. 5 and 6), indicate that *Hoxa2* directly regulates the expression of *Bmp4* and *Bmp5* in spatially restricted domains of the developing external ear.

***Hoxa2* is sufficient to induce the complete formation of an ectopic pinna**

To address whether *Hoxa2* is not only necessary but also sufficient for the formation of the pinna we set out a conditional overexpression system in the mouse allowing the ectopic expression of *Hoxa2* in *Hox*-negative NCCs anterior to the second arch. Conditional *Hoxa2* overexpression in NCCs was induced by mating the *Wnt1::Cre* line (29) with a *ROSA^{(lox-stop-lox)Hoxa2-IRES-EGFP}* allele (39) (*Wnt1::Cre;ROSA^{(lox-stop-lox)Hoxa2-IRES-EGFP}*, hereafter designated *Wnt1^{Hoxa2-IRES-EGFP}*) in which *Hoxa2* is conditionally overexpressed in the *Wnt1* lineage upon Cre-mediated recombination, including the cranial NCCs.

Wnt1^{Hoxa2-IRES-EGFP} mutant fetuses die at birth and display craniofacial defects, including malformation of the face, middle ear and skull bones, appearance of ectopic cartilages in the

pharyngeal region, as well as reduction of the size of the lower jaw (Fig. 9; and not shown). Most notably, all of them (n=25/25) display an ectopic, fully formed pinna, which is a mirror-image duplication of its normal orthotopic counterpart (compare Fig. 9A with 9B-E). The ectopic pinna replaces the EAC, and thus likely forms from first pharyngeal arch NCC derived mesenchyme. The orthotopic pinna, derived from the second pharyngeal arch, appears normally shaped, indicating that *Hoxa2* overexpression within its own expression domain from the *ROSA^{(lox-stop-lox)Hoxa2-IRES-EGFP}* allele does not result in overt pinna morphogenetic abnormalities (Fig. 9B-E). It is also noteworthy that *Wnt1^{Hoxa2-IRES-EGFP}* mutant fetuses occasionally display several additional ectopic structures around the eye, whose morphology resemble small ectopic pinnae (black arrows, Fig. 9C, D).

The presence of an internal ribosome entry site (IRES) in the *ROSA^{(lox-stop-lox)Hoxa2-IRES-EGFP}* allele allows to trace the cells ectopically expressing *Hoxa2* by immunohistochemistry with an anti-EGFP antibody. We therefore compared the distribution of EGFP⁺ cells in E14.5 *Wnt1::Cre;Hoxa2^{EGFP(lox-neo-lox)}+/-* fetuses, in which *EGFP* is conditionally expressed in second and more posterior arch NCCs expressing endogenous *Hoxa2* (Fig. 10A), with *Wnt1^{Hoxa2-IRES-EGFP}* fetuses which additionally ectopically express *Hoxa2-IRES-EGFP* in rostral *Hoxa2*-negative territories. In *Wnt1^{Hoxa2-IRES-EGFP}* mutants, the ectopic pinna was entirely contributed by *Hoxa2-IRES-EGFP* expressing cells (Fig. 10B-D). Moreover, the ectopic pinna of *Wnt1^{Hoxa2-IRES-EGFP}* fetuses displays mirror-image duplications of the *Bmp5*, *Bmp4* and *Tsg* expression patterns (Fig. 10E-L and Suppl. Fig.6). Namely, *Bmp4* is expressed at the tip of the duplicated pinna as well as in the mesenchyme at its base (Fig. 10I-L). *Bmp5* and *Tsg* are expressed in the mesenchymal core and at the base of the duplicated pinna (Fig. 10E-H and Suppl. Fig. 6). Interestingly, *Bmp4* is also

expressed in the ectopic structures that form around the eye (Fig. 10L) while *Bmp5* is expressed in the underlying mesenchyme (Fig. 10F-H).

These results not only confirm the molecular identity of the mirror-image duplicated pinna but also that *Hoxa2* is sufficient to induce and maintain the genetic program that underlies the formation of the pinna.

Hoxa2 regulates *Chd7* expression in the pinna

The duplicated pinna induced in *Wnt1^{Hoxa2-IRES-EGFP}* mutants represents a suitable genetic model to identify genes regulated by *Hoxa2* during external ear morphogenesis. Mutation of the chromatin remodeling protein *Chd7* in humans cause a multiple anomaly condition known as the CHARGE syndrome (Coloboma, Heart defects, Atresia of the choanes, Retarded growth and development, Genital hypoplasia and Ear defects including malformation of the auricle and hearing loss) (25). In mouse, *Chd7* is expressed in the E12.5 developing pinna (Suppl. Fig.7). This domain is absent in *Hoxa2^{-/-}* mutant embryos (Suppl. Fig.7), indicating that *Hoxa2* may also regulate the expression of *Chd7*. Indeed, in E14.5 *Wnt1^{Hoxa2-IRES-EGFP}* mutants *Chd7* was ectopically activated in the duplicated pinna, as well in the additional ectopic structures, resembling small ectopic pinnae (Fig. 10M-P). In addition, we detected *Hoxa2* binding in the *Chd7* gene (15) indicating that *Hoxa2* may directly regulate *Chd7* expression (Suppl. Fig.8). These data indicate that *Hoxa2* orchestrates external ear morphogenesis, in part through the regulation of *Chd7* expression.

DISCUSSION

Revisiting human external ear and auditory canal embryological origin

It can be found in classical textbook that the human external ear cartilage is derived from six nodular masses of mesenchyme which appear during the sixth week of development, the hillocks of Hiss, three of which are in the first (mandibular) and three in the second (hyoid) pharyngeal arches respectively, whereas the ear canal is believed to be derived from the first pharyngeal cleft (1, 4, 16-19). The hillocks eventually fuse to form the different parts of the human external ear. The tragus, projecting in front of the ear canal, is derived from the first arch-derived hillocks ((40), and reviewed in (4)). However, it is less clear to which parts of the auricle, mainly composed in human by the crus, the helix (the folded edge of the auricle), the concha, the antihelix, the antitragus and the lobule, the first arch-derived hillocks might contribute to (for review (4)). Indeed, according to some authors the first arch-derived hillocks not only give rise to the tragus, but also to the helix or to the antihelix (reviewed by (4)).

Our fate map in the mouse shows that the part just anterior to the EAC (the mouse homologue of the human tragus) is contributed by *Hoxa2*/*EGFP* cells, indicating that, as in human, this structure derives from the first pharyngeal arch mesenchyme (Fig. 1J, O). In contrast, fate mapping and analysis of *Hoxa2* function reveal for the first time that, in the mouse, the auricle is entirely contributed by the second arch *Hoxa2*-expressing neural crest-derived mesenchyme, and not by both first and second arch derived NCCs (Fig. 1). Secondly, and perhaps most notably, genetic fate mapping further shows that the ectoderm-derived external auditory canal (EAC) invaginates into, and is entirely surrounded by, first arch derived *Hoxa2*-negative mesenchyme (Figs. 1, 2). Thus, in the mouse, the EAC appears to be a first arch derived structure and does not originate at the border between first arch *Hoxa2*-negative and second arch

Hoxa2-positive mesenchyme, i.e. at the first pharyngeal cleft (Fig. 1), as previously assumed (19, 20). The morphology of the human pinna is more complex than in mouse, suggesting that additional components might have been recruited from the developing first arch mesenchyme, as compared to mouse. On the other hand, it is possible that based on our findings in the mouse, the contribution of first arch NCCs to the human pinna is more limited than previously proposed. This conclusion may be further supported by the observation that the auricle is not affected in otocephaly, which is a genetic syndrome resulting from failure of the first arch. Only the tragus, which is known to derive from the first arch, is absent in this syndrome (4). Overall, our results could be of interest from a clinical standpoint since they may facilitate our understanding of human syndromes, notably concerning the correlation between embryological origin of the auricle, gene expression patterns, and the interpretation of the phenotypic outcome of their disruption.

Revisiting the external auditory canal phenotype of *Hoxa2* mutant mouse

By reconsidering the embryological origin of the EAC, our fate map as well as 3D tissue reconstruction allow a better understanding of the previously described mouse *Hoxa2*^{-/-} knockout phenotype (10). The finding that the mouse EAC derives from the first pharyngeal arch, and not from the first pharyngeal cleft, better explains the observed partial duplication of the EAC in *Hoxa2*^{-/-} mutants (10). Our analysis reveals that rather than forming the EAC, the first cleft which maps at the border between *EGFP*⁺ and *EGFP*⁻ NCCs represents the axis of symmetry on either side of which the mirror-image duplication of the EAC occurs in *Hoxa2*^{-/-} mutant mice.

***Hoxa2* is a major determinant of pinna formation**

The inactivation of *Hoxa2* in the mouse results in a mirror image homeotic transformation of second arch-derived middle ear ossicle stapes, styloid process of the temporal bone and lesser horn of the hyoid bone into a duplicated set of first arch-like structures, namely the proximal part of the jaw (Meckel's) cartilage, the incus, malleus, tympanic bone and proximal gonial bone (10, 11). These structures are normally derived from a subset of first arch Hox-negative NCCs essentially derived from the rostral hindbrain, though not from more anterior regions (10, 41-45). Thus, this subset of first arch NCC derived structures and the second arch elements share a common Hox-free ground (default) patterning molecular program upon which *Hoxa2* is able to select second arch identity (10, 41-46).

However, the extension of this model to the NCC-derived external ear was not clear. In *Wnt1^{Hoxa2-IRES-EGFP}* mutant embryos, *Hoxa2* is conditionally overexpressed in Hox-negative cranial NCCs, resulting in abnormalities targeting those structures derived from midbrain and forebrain Hox-negative NCCs, such as the jaw, the face and the skull bones, thus supporting the notion that ectopic Hox gene expression interferes with normal craniofacial development (e.g. (47)). On the other hand, we found that ectopic conditional *Hoxa2* expression is also sufficient to re-pattern first mandibular arch mesenchyme, derived from rostral hindbrain NCCs, and to induce a mirror image transformation into a second arch-like structure, the pinna. The early inactivation of *Hoxa2* in the mouse induces the absence of the pinna, while its inactivation at later stages, i.e. between E12.5 and E13.5, induces a microtia (14), a phenotype mimicking the human *HOXA2* mutant condition (9). In *Hoxa2* deficient mice, the absence of the pinna occurs always in association with a partial duplication of the EAC (10, 12)). In the current study, we show that the pinna and the EAC develop opposite and almost equidistant to the first pharyngeal cleft, which maps at the border between first arch *Hoxa2*-negative and second arch *Hoxa2*-positive NCCs, and which could represent a symmetry axis on either side of which the duplication of the pinna or of the

EAC occurs in *Wnt1^{Hoxa2-IRES-EGFP}* gain of function and *Hoxa2^{-/-}* loss of function mutant embryos, respectively. This further extends the proposal of a Hox-free ground patterning program shared by hindbrain NCCs, and suggests that the first arch derived mesenchyme normally giving rise to the EAC has been homeotically transformed into a duplicated pinna, normally a second arch derived structure.

The ability of *Hoxa2* to re-pattern first mandibular arch NCCs appears to be conserved (48, 49). In this respect, it is surprising that we did not find clear transformations of middle ear first arch skeletal elements (i.e. malleus, incus and tympanic bone) into second arch-like structures (i.e. stapes, styloid process, and lesser horn) in *Wnt1^{Hoxa2-IRES-EGFP}* newborns. However, we did see skeletal malformations in the middle ear region that could be interpreted as partial transformations (not shown). A previous temporal analysis of *Hoxa2* function indicated that middle ear NCCs require *Hoxa2* patterning function at earlier stages than the NCCs contributing to the external ear (14). In the overexpression allele used in this study, *Hoxa2* was inserted in frame at the endogenous ROSA26 locus without the addition of strong promoter sequences (39). Thus, relatively low levels of ectopic *Hoxa2* at early developmental stages may not be sufficient to fully re-pattern middle ear structures. However, delayed accumulation of ectopic *Hoxa2* levels are still sufficient to re-pattern first arch NCC mesenchyme at later stages into an ectopic pinna. Supporting this interpretation, a similar knock-in construct at the ROSA26 locus in which, however, *Hoxa2* is driven by the strong CMV early enhancer/chicken b-actin (CAGS) promoter results in skeletal re-patterning of middle ear structures (H. Kurihara, personal communication).

Several cases in the literature have reported partial or total duplication of the human pinna (2-7). While the genetic basis of such a phenotype has not been investigated, it is tempting to speculate that ectopic HOXA2 expression might underlie the “polyotia” or “mirror ear” observed in humans. As *Hoxa2* alone is able to induce the whole developmental program underlying the

morphogenesis of the pinna, our data moreover suggest that numerous genes involved in human auricle abnormalities are *Hoxa2* target genes.

Towards an understanding of the molecular mechanisms involved in pinna morphogenesis

Our study provides novel insights into the largely unknown molecular program involved in external ear morphogenesis. The identification of such a program could improve our understanding of the HOXA2 mutant phenotype in humans. We have shown that *Hoxa2* regulates the expression of *Eya1* and *Chd7*, both involved in human syndromes associated with external ear abnormalities, namely, the branchio-oto-renal and the CHARGE syndrome, respectively (23-25). Our functional and molecular analysis also reveals that *Hoxa2* controls the formation of the pinna through the regulation of *Bmp5*, *Bmp4* and *Tsg* expression. While the inactivation of *Bmp5* was known to induce a small pinna in mice (21, 22), the role of *Bmp4* in pinna morphogenesis has not been explored. Here, we have generated *Bmp4*^{lox/del} hypomorphic mutant mice and show that they display, albeit at low frequency, a hypomorphic pinna, thus indicating that *Bmp4* is involved in pinna morphogenesis. Functional redundancy between *Bmp4* and other members of the BMP family, such as *Bmp5*, remains to be investigated.

Hoxa2 is also involved in PhosphoSmad1/5/8 nuclear activation. This finding, together with the activation of *Bmp5*, *Bmp4* and *Tsg* expression, indicates *Hoxa2* acts upstream of the BMP canonical signalling pathway during external ear morphogenesis. A recent study has reported a role for *Hoxa2* in activating the Wnt- β -catenin signalling pathway in the second arch, in part through the regulation of *Wnt5a* expression – a gene whose inactivation in mouse affects external ear development (15, 50). Altogether, these data uncover a potential role for BMP and Wnt signalling to instruct external ear morphogenesis downstream of *Hoxa2*; how these pathways interact remains to be determined. More generally, understanding how multiple genes integrate

into functional networks is now necessary for a full comprehension of the molecular processes that underlie normal and defective external ear morphogenesis.

ACKNOWLEDGMENTS

We thank F. Santagati and A. Vitobello for technical assistance and discussion. We are also grateful to B. Hogan for the kind gift of the *Bmp4* conditional allele. M.M. was supported by the Faculté de Chirurgie Dentaire de Strasbourg and Ministère de l'Enseignement Supérieur. S.A. was supported by a grant of the Biotechnology and Biological Sciences Research Council BB/H018123/2 to N.B. Work in FMR laboratory is supported by the Swiss National Science Foundation (Sinergia CRSI33_127440), ARSEP, and the Novartis Research Foundation.

MATERIALS AND METHODS

Mating scheme

For the fate map of the external ear, the Z/AP transgenic mouse line, described in (27), was crossed with the R4::Cre mouse line, described in (26). The $Hoxa2^{EGFP}$, $Hoxa2^{EGFP/EGFP}$ and $Hoxa2^{EGFP(lox-neo-lox)+/-}$ knock-in mouse lines were described in (28). The $Wnt1::Cre;Hoxa2^{EGFP(lox-neo-lox)+/-}$ embryos were obtained by crossing the $Hoxa2^{EGFP(lox-neo-lox)+/-}$ mouse line with the $Wnt1::Cre$ transgenic mouse line, described in (29). The $CMV::CreER^{T2}$ transgenic mouse line was described in (14) and the floxed *Hoxa2* cluster allele was described in (31). For the generation of $CMV::CreER^{T2};Hoxa2^{lox/del}$ mutant embryos, homozygous $Hoxa2^{lox/lox}$ or heterozygous $Hoxa2^{lox/+}$ mice were crossed with $CMV::CreER^{T2};Hoxa2^{del/+}$ mice. The conditional $Bmp4^{lox}$ line was described in (51). For the generation of $Bmp4^{lox/del}$ mutant embryos, homozygous $Bmp4^{lox/lox}$ mice were crossed with $Bmp4^{del}$ mice. In order to induce an ectopic expression of *Hoxa2* in the NCCs anterior to the second pharyngeal arch, the $ROSA^{(lox-stop-lox)Hoxa2-IRES-EGFP}$ transgenic mouse line, described in (39), was crossed with the $Wnt1::Cre$ mouse line.

All animal studies have been approved by the appropriate veterinary authorities.

Tamoxifen treatment

Tamoxifen (Sigma) was dissolved in pre-warmed corn oil (Sigma) to make a 20 mg/ml solution and stored at 4°C. Tamoxifen was administrated orally to pregnant females by means of a gavage syringe. Triple (10 mg at 12.5 dpc, 13.0 dpc and 13.5 dpc) successive administrations (chronic treatment) were provided with 12-hour intervals.

Z/AP staining

E14.5 mouse embryos were fixed overnight in 4% PFA, rinsed in PBS, equilibrated in 20% sucrose and included in Cryomatrix (Thermo Electron Corporation). 20 µm cryostat sections were realized in the frontal and horizontal planes of the embryo. The sections were then fixed 1 hour in 4% PFA, rinsed in PBS at room temperature and then incubated in PBS at 65°C during 1 hour to inactivate the endogenous AP. After the inactivation, sections were rinsed in a solution of NTMT (NaCl 0,1M, Tris HCl 0,1M (pH 9.5), MgCl₂ 0,05M and Tween 20 0,1%). 3,5 µl NBT (Roche 1383213) and 3.5 µl BCIP (Roche 1383221) per ml of NTMT were used for the staining. The sections were rinsed first in water, next in 100% ethanol and mounted onto slides.

Immunohistochemistry

Immunostaining for EGFP on cryosections was performed using a polyclonal rabbit anti-GFP antibody (Molecular Probes Europe BV) and a peroxidase-conjugated goat anti-rabbit IgG or a Alexa 488-conjugated secondary antibody (Beckman Coulter France SA). Detection was performed with DAB chromogen (DAKO SA). Immunostaining for Ki67 was performed on paraffine sections, using a rabbit anti-Ki67 antibody (Novocastra NCL-Ki67p) and a biotinylated anti-rabbit antibody. After an incubation of 30 minutes at room temperature with the Vectastain ABC reagent, the revelation of the peroxylase activity was performed by using DAB chromogen (DAKO SA). For the PhosphoSmad staining, cryostat sections were incubated with PhosphoSmad1/5/8 antibody (Cell Signaling) at 37°C for 3hr, followed by Alexa 488-conjugated secondary antibody (Invitrogen).

3D reconstruction of the external/middle ear

Pictures of consecutive cryostat sections (25 μm) of E14.5 *Hoxa2*^{EGFP} and of E14.5 *Hoxa2*^{EGFP/EGFP} embryos, on which an immunostaining for EGFP was performed, were taken with a Leica fluorescence microscope. Between 49 and 68 sections were aligned using Bitplane AutoAligner 6.0.1 (Manual Alignment). Structures were artificially labeled in separated channels in Adobe Photoshop CS5.1. The artificially labeled structures as well as the GFP channel were transformed into surfaces in Bitplane Imaris 7.5.2 (Surface Area Detail level: 35 μm , Thresholding: Absolute Intensity).

***In-situ* hybridization**

In-situ hybridizations on frontal and horizontal sections were performed as previously described (14). The following RNA probes were used: *Hoxa2* (31), *Eya1* (30), *Bmp5* (52), *Bmp4* (53), *Tsg* (34), *Prrxl1* (54), *Tshz2* (33), *Chd7* (55).

ChIP analysis

ChIP experiments have been performed on second branchial arches isolated from E11.5 CD1 embryos, according to the method described in (15). Immunoprecipitated DNA was subjected to qPCR, using the following primers: *Bmp4* Forwards 5'-TGTGGGATAAAACAGGAGTGC-3' and Reverse 5'-GCTCCCTCAGTTTGGCTAGA-3'; *Bmp5* Forwards 5'-TATGCAGTCTAGGGCCACCT-3' and Reverse 5'-CATTGGGATAAAAGAACCTCAA-3'.

BIBLIOGRAPHY

1. Alasti, F., and Van Camp, G. 2009. Genetics of microtia and associated syndromes. *J Med Genet* 46:361-369.
2. Mishra, S.C., and Misra, M. 1978. Mirror image pinna. *J Laryngol Otol* 92:709-711.
3. Ku, P.K., Tong, M.C., and Yue, V. 1998. Polyotia--a rare external ear anomaly. *Int J Pediatr Otorhinolaryngol* 46:117-120.
4. Hunter, A.G., and Yotsuyanagi, T. 2005. The external ear: more attention to detail may aid syndrome diagnosis and contribute answers to embryological questions. *Am J Med Genet A* 135:237-250.
5. Baschek, V., Steinert, W., and Hildebrandt, L. 2006. [External ear duplication, a rare branchial arch abnormality]. *Laryngorhinootologie* 85:861.
6. Gore, S.M., Myers, S.R., and Gault, D. 2006. Mirror ear: a reconstructive technique for substantial tragal anomalies or polyotia. *J Plast Reconstr Aesthet Surg* 59:499-504.
7. Pan, B., Qie, S., Zhao, Y., Tang, X., Lin, L., Yang, Q., Zhuang, H., and Jiang, H. 2010. Surgical management of polyotia. *J Plast Reconstr Aesthet Surg* 63:1283-1288.
8. Kountakis, S.E., Helidonis, E., and Jahrsdoerfer, R.A. 1995. Microtia grade as an indicator of middle ear development in aural atresia. *Arch Otolaryngol Head Neck Surg* 121:885-886.
9. Alasti, F., Sadeghi, A., Sanati, M.H., Farhadi, M., Stollar, E., Somers, T., and Van Camp, G. 2008. A mutation in HOXA2 is responsible for autosomal-recessive microtia in an Iranian family. *Am J Hum Genet* 82:982-991.
10. Rijli, F.M., Mark, M., Lakkaraju, S., Dierich, A., Dolle, P., and Chambon, P. 1993. A homeotic transformation is generated in the rostral branchial region of the head by disruption of Hoxa-2, which acts as a selector gene. *Cell* 75:1333-1349.
11. Gendron-Maguire, M., Mallo, M., Zhang, M., and Gridley, T. 1993. Hoxa-2 mutant mice exhibit homeotic transformation of skeletal elements derived from cranial neural crest. *Cell* 75:1317-1331.
12. Mark, M., Lohnes, D., Mendelsohn, C., Dupe, V., Vonesch, J.L., Kastner, P., Rijli, F., Bloch-Zupan, A., and Chambon, P. 1995. Roles of retinoic acid receptors and of Hox genes in the patterning of the teeth and of the jaw skeleton. *Int J Dev Biol* 39:111-121.
13. Mallo, M., and Gridley, T. 1996. Development of the mammalian ear: coordinate regulation of formation of the tympanic ring and the external acoustic meatus. *Development* 122:173-179.
14. Santagati, F., Minoux, M., Ren, S.Y., and Rijli, F.M. 2005. Temporal requirement of Hoxa2 in cranial neural crest skeletal morphogenesis. *Development* 132:4927-4936.
15. Donaldson, I.J., Amin, S., Hensman, J.J., Kutejova, E., Rattray, M., Lawrence, N., Hayes, A., Ward, C.M., and Bobola, N. 2012. Genome-wide occupancy links Hoxa2 to Wnt-beta-catenin signaling in mouse embryonic development. *Nucleic Acids Res* 40:3990-4001.
16. Klockars, T., and Rautio, J. 2009. Embryology and epidemiology of microtia. *Facial Plast Surg* 25:145-148.
17. Porter, C.J., and Tan, S.T. 2005. Congenital auricular anomalies: topographic anatomy, embryology, classification, and treatment strategies. *Plast Reconstr Surg* 115:1701-1712.

18. Passos-Bueno, M.R., Ornelas, C.C., and Fanganiello, R.D. 2009. Syndromes of the first and second pharyngeal arches: A review. *Am J Med Genet A* 149A:1853-1859.
19. Schoenwolf, G.C., Larsen, W.J., 2009. Larsen's human embryology 4th ed. Philadelphia, PA: Elsevier/Churchill Livingstone.
20. Jakubikova, J., Stanik, R., and Stanikova, A. 2005. Malformations of the first branchial cleft: duplication of the external auditory canal. *Int J Pediatr Otorhinolaryngol* 69:255-261.
21. Kingsley, D.M., Bland, A.E., Grubber, J.M., Marker, P.C., Russell, L.B., Copeland, N.G., and Jenkins, N.A. 1992. The mouse short ear skeletal morphogenesis locus is associated with defects in a bone morphogenetic member of the TGF beta superfamily. *Cell* 71:399-410.
22. King, J.A., Marker, P.C., Seung, K.J., and Kingsley, D.M. 1994. BMP5 and the molecular, skeletal, and soft-tissue alterations in short ear mice. *Dev Biol* 166:112-122.
23. Abdelhak, S., Kalatzis, V., Heilig, R., Compain, S., Samson, D., Vincent, C., Weil, D., Cruaud, C., Sahly, I., Leibovici, M., et al. 1997. A human homologue of the Drosophila eyes absent gene underlies branchio-oto-renal (BOR) syndrome and identifies a novel gene family. *Nat Genet* 15:157-164.
24. Kochhar, A., Fischer, S.M., Kimberling, W.J., and Smith, R.J. 2007. Branchio-oto-renal syndrome. *Am J Med Genet A* 143A:1671-1678.
25. Vissers, L.E., van Ravenswaaij, C.M., Admiraal, R., Hurst, J.A., de Vries, B.B., Janssen, I.M., van der Vliet, W.A., Huys, E.H., de Jong, P.J., Hamel, B.C., et al. 2004. Mutations in a new member of the chromodomain gene family cause CHARGE syndrome. *Nat Genet* 36:955-957.
26. Oury, F., Murakami, Y., Renaud, J.S., Pasqualetti, M., Charnay, P., Ren, S.Y., and Rijli, F.M. 2006. Hoxa2- and rhombomere-dependent development of the mouse facial somatosensory map. *Science* 313:1408-1413.
27. Lobe, C.G., Koop, K.E., Kreppner, W., Lomeli, H., Gertsenstein, M., and Nagy, A. 1999. Z/AP, a double reporter for cre-mediated recombination. *Dev Biol* 208:281-292.
28. Pasqualetti, M., Ren, S.Y., Poulet, M., LeMeur, M., Dierich, A., and Rijli, F.M. 2002. A Hoxa2 knockin allele that expresses EGFP upon conditional Cre-mediated recombination. *Genesis* 32:109-111.
29. Danielian, P.S., Muccino, D., Rowitch, D.H., Michael, S.K., and McMahon, A.P. 1998. Modification of gene activity in mouse embryos in utero by a tamoxifen-inducible form of Cre recombinase. *Curr Biol* 8:1323-1326.
30. Xu, P.X., Adams, J., Peters, H., Brown, M.C., Heaney, S., and Maas, R. 1999. Eya1-deficient mice lack ears and kidneys and show abnormal apoptosis of organ primordia. *Nat Genet* 23:113-117.
31. Ren, S.Y., Pasqualetti, M., Dierich, A., Le Meur, M., and Rijli, F.M. 2002. A Hoxa2 mutant conditional allele generated by Flp- and Cre-mediated recombination. *Genesis* 32:105-108.
32. Martin, J.F., Bradley, A., and Olson, E.N. 1995. The paired-like homeo box gene MHox is required for early events of skeletogenesis in multiple lineages. *Genes Dev* 9:1237-1249.
33. Caubit, X., Core, N., Boned, A., Kerridge, S., Djabali, M., and Fasano, L. 2000. Vertebrate orthologues of the Drosophila region-specific patterning gene teashirt. *Mech Dev* 91:445-448.

34. Zakin, L., and De Robertis, E.M. 2004. Inactivation of mouse Twisted gastrulation reveals its role in promoting Bmp4 activity during forebrain development. *Development* 131:413-424.
35. Heldin, C.H., and Moustakas, A. 2012. Role of Smads in TGFbeta signaling. *Cell Tissue Res* 347:21-36.
36. Horbelt, D., Denkis, A., and Knaus, P. 2012. A portrait of Transforming Growth Factor beta superfamily signalling: Background matters. *Int J Biochem Cell Biol* 44:469-474.
37. Winnier, G., Blessing, M., Labosky, P.A., and Hogan, B.L. 1995. Bone morphogenetic protein-4 is required for mesoderm formation and patterning in the mouse. *Genes Dev* 9:2105-2116.
38. Meyer, L.R., Zweig, A.S., Hinrichs, A.S., Karolchik, D., Kuhn, R.M., Wong, M., Sloan, C.A., Rosenbloom, K.R., Roe, G., Rhead, B., et al. 2013. The UCSC Genome Browser database: extensions and updates 2013. *Nucleic Acids Res* 41:D64-69.
39. Miguez, A., Ducret, S., Di Meglio, T., Parras, C., Hmidan, H., Haton, C., Sekizar, S., Mannioui, A., Vidal, M., Kerever, A., et al. 2012. Opposing roles for Hoxa2 and Hoxb2 in hindbrain oligodendrocyte patterning. *J Neurosci* 32:17172-17185.
40. Kagurasho, M., Yamada, S., Uwabe, C., Kose, K., and Takakuwa, T. 2012. Movement of the external ear in human embryo. *Head Face Med* 8:2.
41. Kontges, G., and Lumsden, A. 1996. Rhombencephalic neural crest segmentation is preserved throughout craniofacial ontogeny. *Development* 122:3229-3242.
42. Santagati, F., and Rijli, F.M. 2003. Cranial neural crest and the building of the vertebrate head. *Nat Rev Neurosci* 4:806-818.
43. Minoux, M., and Rijli, F.M. 2010. Molecular mechanisms of cranial neural crest cell migration and patterning in craniofacial development. *Development* 137:2605-2621.
44. Takechi, M., and Kuratani, S. 2010. History of studies on mammalian middle ear evolution: a comparative morphological and developmental biology perspective. *J Exp Zool B Mol Dev Evol* 314:417-433.
45. Kuratani, S. 2005. Craniofacial development and the evolution of the vertebrates: the old problems on a new background. *Zoolog Sci* 22:1-19.
46. Minoux, M., Antonarakis, G.S., Kmita, M., Duboule, D., and Rijli, F.M. 2009. Rostral and caudal pharyngeal arches share a common neural crest ground pattern. *Development* 136:637-645.
47. Couly, G., Grapin-Botton, A., Coltey, P., Ruhin, B., and Le Douarin, N.M. 1998. Determination of the identity of the derivatives of the cephalic neural crest: incompatibility between Hox gene expression and lower jaw development. *Development* 125:3445-3459.
48. Pasqualetti, M., Ori, M., Nardi, I., and Rijli, F.M. 2000. Ectopic Hoxa2 induction after neural crest migration results in homeosis of jaw elements in *Xenopus*. *Development* 127:5367-5378.
49. Grammatopoulos, G.A., Bell, E., Toole, L., Lumsden, A., and Tucker, A.S. 2000. Homeotic transformation of branchial arch identity after Hoxa2 overexpression. *Development* 127:5355-5365.
50. Qian, D., Jones, C., Rzadzinska, A., Mark, S., Zhang, X., Steel, K.P., Dai, X., and Chen, P. 2007. Wnt5a functions in planar cell polarity regulation in mice. *Dev Biol* 306:121-133.
51. Kulesa, H., and Hogan, B.L. 2002. Generation of a loxP flanked bmp4loxP-lacZ allele marked by conditional lacZ expression. *Genesis* 32:66-68.

52. Solloway, M.J., and Robertson, E.J. 1999. Early embryonic lethality in Bmp5;Bmp7 double mutant mice suggests functional redundancy within the 60A subgroup. *Development* 126:1753-1768.
53. Hogan, B.L., Blessing, M., Winnier, G.E., Suzuki, N., and Jones, C.M. 1994. Growth factors in development: the role of TGF-beta related polypeptide signalling molecules in embryogenesis. *Dev Suppl*:53-60.
54. ten Berge, D., Brouwer, A., Korving, J., Martin, J.F., and Meijlink, F. 1998. Prx1 and Prx2 in skeletogenesis: roles in the craniofacial region, inner ear and limbs. *Development* 125:3831-3842.
55. Bosman, E.A., Penn, A.C., Ambrose, J.C., Kettleborough, R., Stemple, D.L., and Steel, K.P. 2005. Multiple mutations in mouse Chd7 provide models for CHARGE syndrome. *Hum Mol Genet* 14:3463-3476.

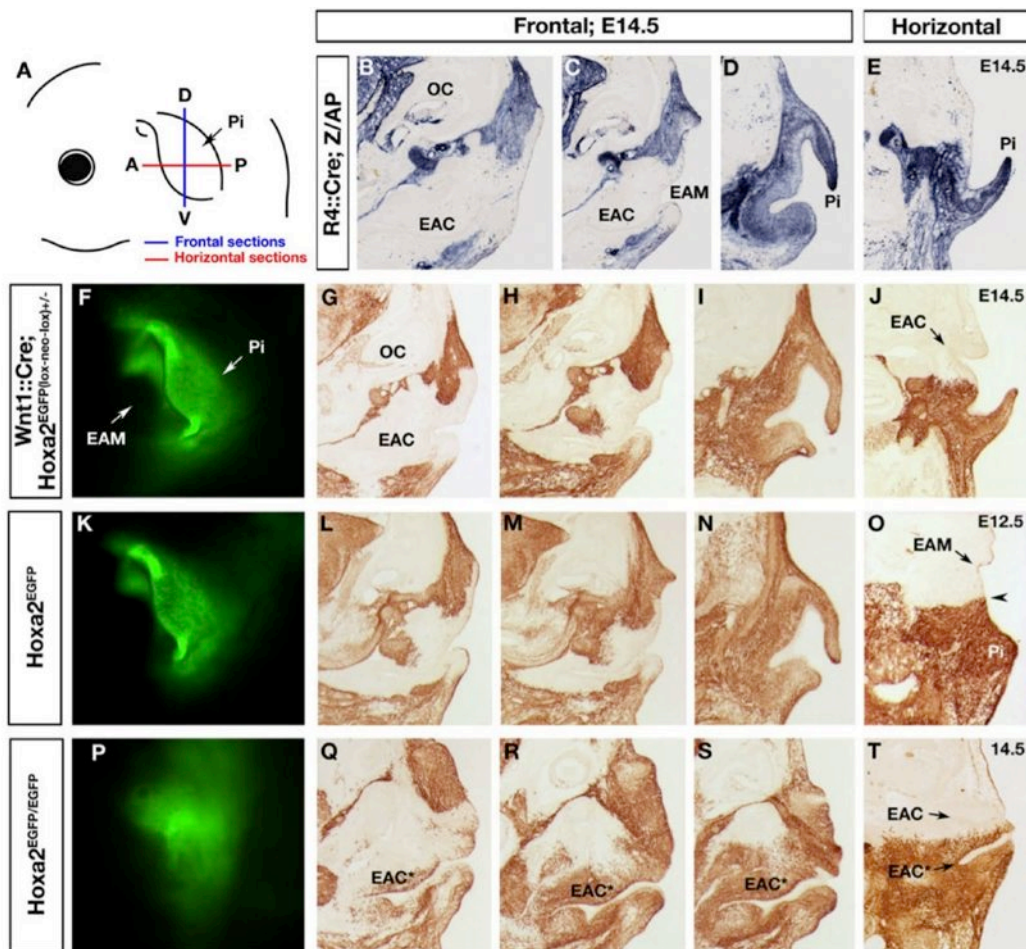


Figure 1: Fate map of the external ear in the presence and absence of *Hoxa2*

(A) Drawing representing the lateral view of the head of a wild type (WT) foetus. The blue and red lines indicate the frontal and horizontal section planes used in this study. (B-E) Z/AP staining performed on frontal (B-D) and horizontal (E) sections realised through the external ear of E14.5 R4::Cre;Z/AP embryos. (F,K,P) Lateral views under fluorescence of the external ear of E14.5 Wnt1::Cre;Hoxa2^{EGFP}/lox-neo-lox^{+/-} (F), Hoxa2^{EGFP} (K) and Hoxa2^{EGFP}/EGFP (P) embryos. (G-J, L-O, Q-T) Anti-EGFP antibody immuno-staining performed on frontal (G-I, L-N, Q-S) and horizontal (J, O, T) sections realised through the external ear of E12.5 Hoxa2^{EGFP} (O), E14.5 Wnt1::Cre;Hoxa2^{EGFP}/lox-neo-lox^{+/-} (G-J), E14.5 Hoxa2^{EGFP} (L-N) and E14.5 Hoxa2^{EGFP}/EGFP (Q-T) embryos. Wnt1::Cre;Hoxa2^{EGFP}/lox-neo-lox^{+/-} and Hoxa2^{EGFP} embryos are heterozygous mutant for *Hoxa2* (*Hoxa2*^{+/-}) whereas Hoxa2^{EGFP}/EGFP embryos are homozygous mutant for *Hoxa2* (*Hoxa2*^{-/-}). No defects are observed in the formation of the external ear of Wnt1::Cre;Hoxa2^{EGFP}/lox-neo-lox^{+/-} and Hoxa2^{EGFP} embryos. Arrowhead in O marks the vestigial first pharyngeal cleft that maps at the border between EGFP⁺/EGFP⁻ territories. In Q-T, note the presence of EGFP⁺ cells around the duplicated EAC (here designed EAC*) present in Hoxa2^{EGFP}/EGFP mutant embryos. On frontal sections: dorsal is up and ventral is down. On horizontal sections: anterior is up and posterior is down. Frontal sections are presented from anterior to posterior (B, G, L, Q sections are more anterior than D, I, N, S sections). Abbreviations : A, anterior; D, dorsal; EAM, external auditory meatus; EAC, external auditory canal; OC, otic capsule; P, posterior; Pi, pinna; V, ventral.

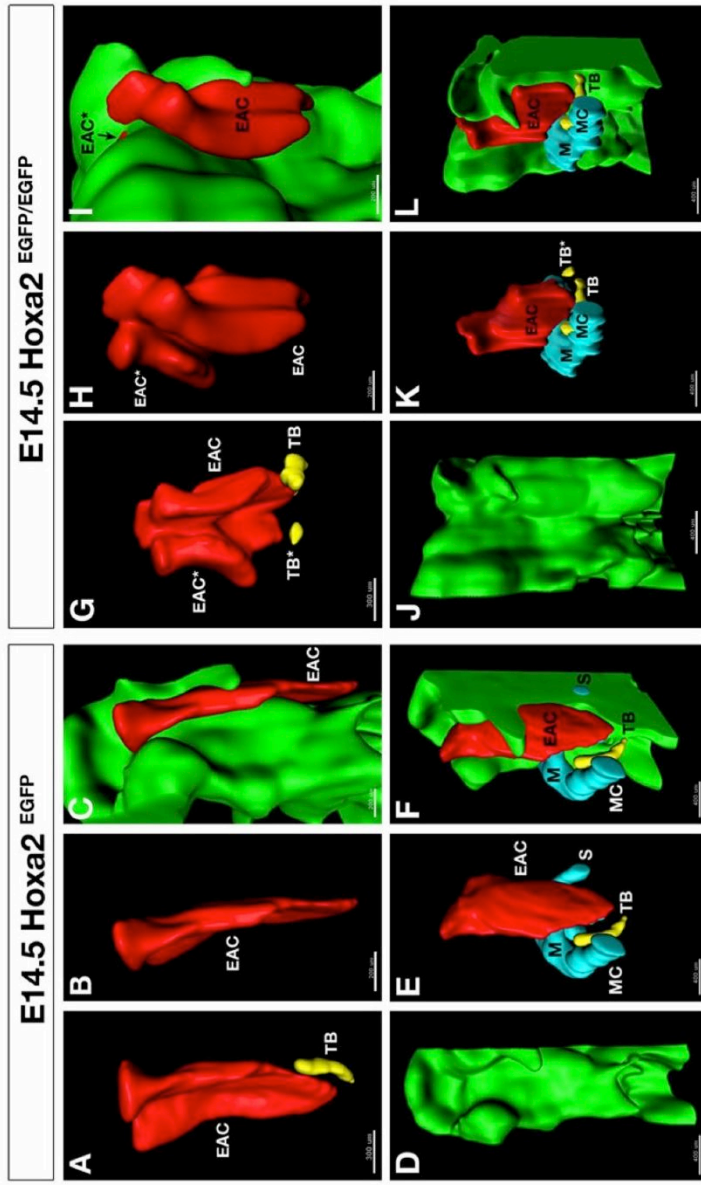


Figure 2: 3D reconstruction of the external ear of E14.5 Hoxa2^{EGFP} control and Hoxa2^{EGFP/EGFP} mutant mouse embryos

(A-F) 3D reconstruction of the external auditory canal (in red), the middle ear ossicles (in blue and yellow) and the EGFP positive domain (in green) performed on E14.5 Hoxa2^{EGFP} control embryo. (G-L) 3D reconstruction of the external auditory canal and its duplicated counterpart (in red), the middle ear ossicles (in blue and yellow) and the EGFP positive domain (in green) performed on E14.5 Hoxa2^{EGFP/EGFP} mutant embryo.

Abbreviations: EAC, external auditory canal; M, Malleus; MC, Meckel's cartilage; TB tympanic bone; S, stapes; EAC* and TB* design the duplicated EAC and TB presents in Hoxa2^{EGFP/EGFP} mutant embryos.

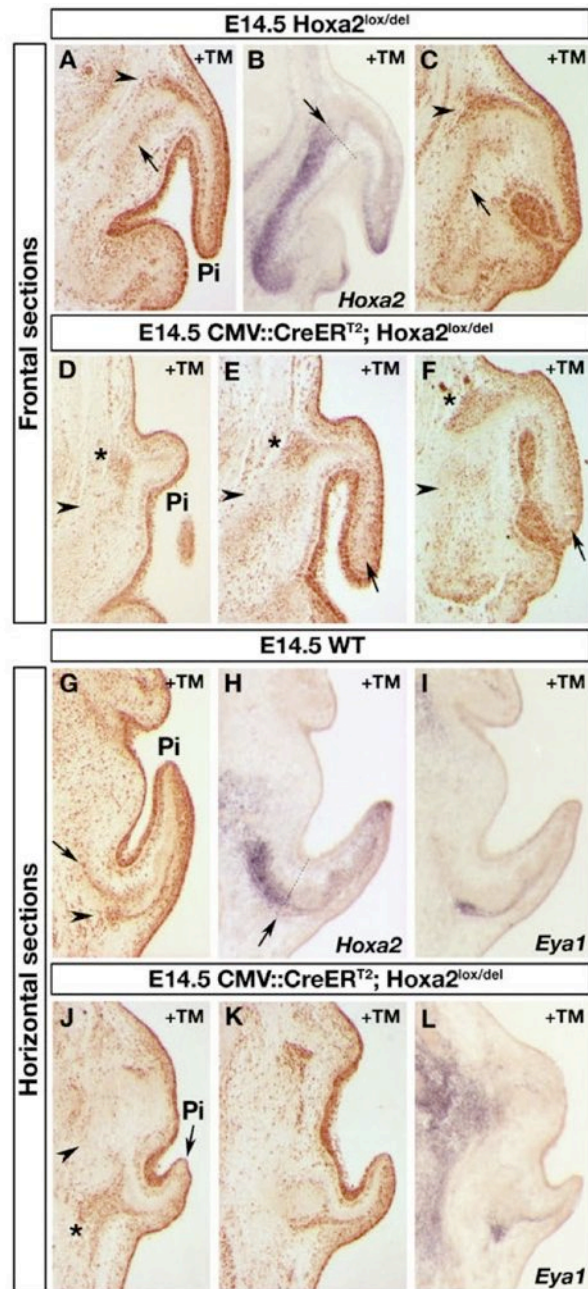


Figure 3: Distribution of proliferative cells in control and TM-induced *Hoxa2* mutant embryos

(A-F) Anti-Ki67 antibody immuno-staining (A, C, D-F) and *Hoxa2* *in-situ* hybridization (B) performed on frontal sections realised through the external ear of E14.5 *Hoxa2^{lox/del}* control (A-C) and *CMV::CreERT2;Hoxa2^{lox/del}* mutant (D-F) embryos treated with tamoxifen (TM) at E12.5, E13, and E13.5. Dorsal is up, ventral is down and sections are presented from anterior to posterior (A and D are more anterior than C and F). (G-L) Anti-Ki67 antibody immuno-staining (G, J, K), as well as *Hoxa2* (H) and *Eya1* (I, L) *in-situ* hybridizations performed on horizontal sections realised through the external ear of E14.5 wild-type (WT) (G-I) and *CMV::CreERT2;Hoxa2^{lox/del}* mutant (J-L) embryos treated with TM at E12.5, E13, and E13.5. Anterior is up, posterior is down and sections are presented from dorsal to ventral (G and J are more dorsal than I and L). In B and H, the dashed line separates outer and inner *Hoxa2*-expressing territories; the black arrow represents the base of the bending pinna where the outer and the inner *Hoxa2* expression territories roughly abut. In A, C, G, the black arrows represent the stream of orderly aligned proliferating cells located in the inner *Hoxa2* expression domain; the black arrowheads represent the stream of orderly aligned proliferating cells starting at the base of the pinna and extending along its dorsal aspect. In D-F and J, the arrows and arrowheads show the disorganisation of the normal spatial segregation between Ki67+ and Ki67- mesenchymal cells in the pinna (arrows in E and F) and in the inner *Hoxa2* expressing domain (arrowheads in D-F and J). The asterisks show the mass of proliferating cells that accumulate at the dorsal base of the pinna. Abbreviation: Pi, pinna.

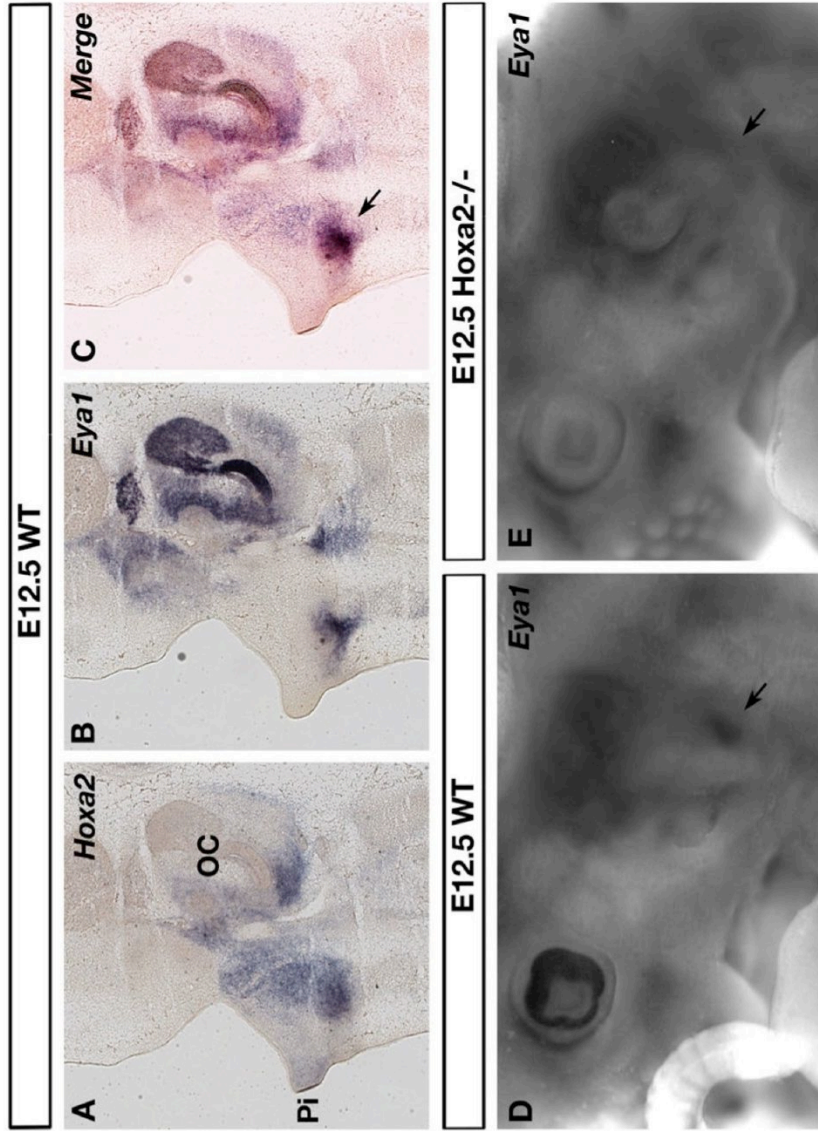


Figure 4: Hoxa2 regulates the expression of *Eya1* at the beginning of external ear morphogenesis

(A, B) *In-situ* hybridizations performed on adjacent horizontal sections realised through the external ear of E12.5 wild-type (WT) embryos using *Hoxa2* (A) and *Eya1* (B) ARN anti-sense probes. In C, a merge of A and B has been realised using Photoshop to highlight the co-expression of *Hoxa2* and *Eya1* in a subset of second arch NCCs (black arrow). Anterior is up, posterior is down. (D, E) *Eya1* whole-mount in-situ hybridizations performed on E12.5 WT (D) and *Hoxa2*^{-/-} mutant (E) embryos. Abbreviations: OC, otic capsule; Pi, pinna.

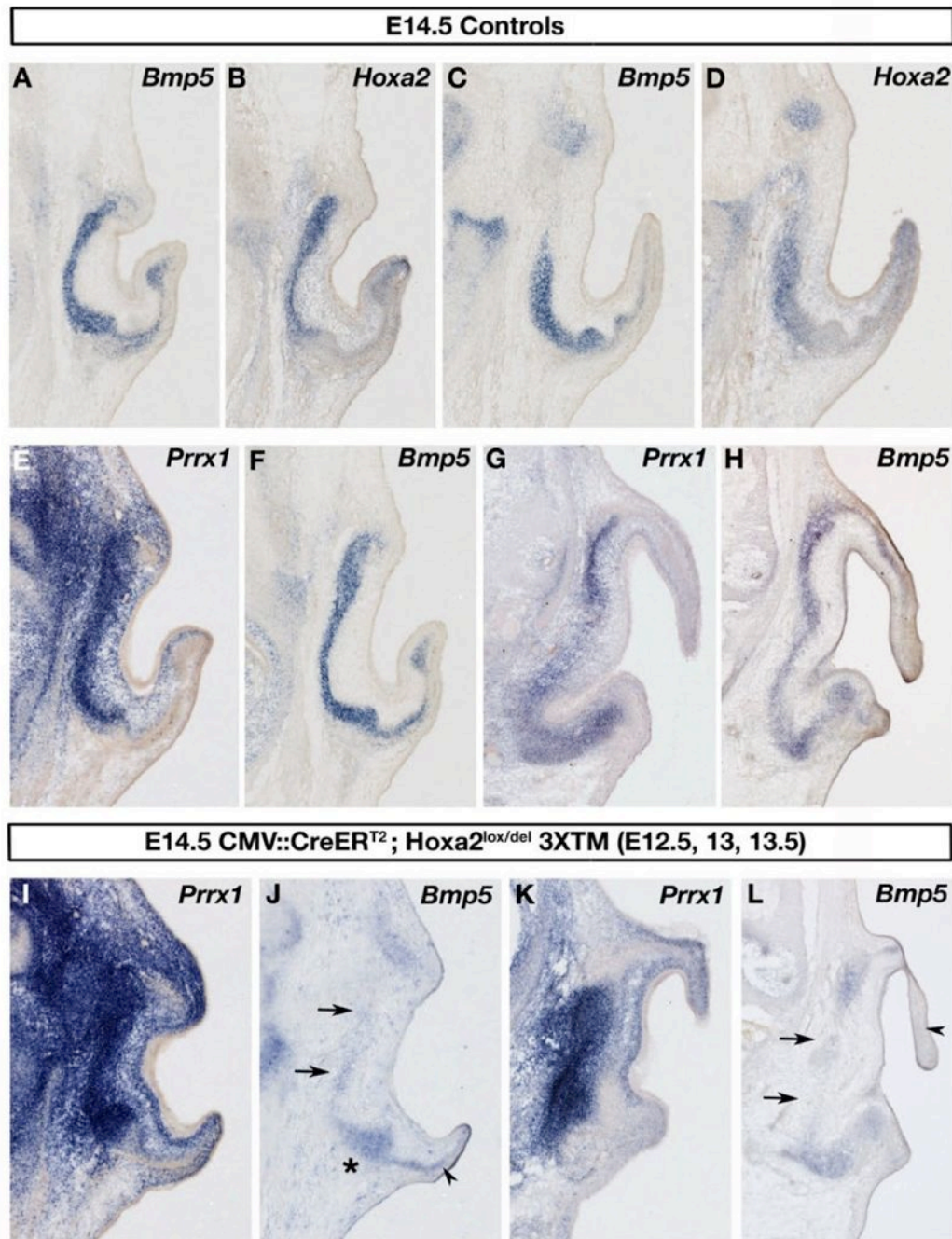


Figure 5: Hoxa2 positively regulates Bmp5

(A-L) *In-situ* hybridizations performed on horizontal (A-D, E, F, I, J) and frontal (G, H, K, L) sections realised through the external ear of E14.5 controls (A-H) and CMV::CreERT²;Hoxa2^{lox/del} mutant embryos treated with tamoxifen (TM) at E12.5, E13, and E13.5 (I-L), using *Bmp5* (A, C, F, H, J, L), *Hoxa2* (B, D) and *Prrx1* (E, G, I, K) ARN anti-sense probes. In J and L, the arrowheads show the reduction of *Bmp5* expression levels in the pinna, the arrows show the reduction of the spatial extent of *Bmp5* expression in the inner *Hoxa2*-expressing domain, and the asterisk shows the accumulation of *Bmp5* residual expression at the base of the pinna of E14.5 CMV::CreERT²;Hoxa2^{lox/del} mutant embryos treated with TM at E12.5, E13, and E13.5. On frontal sections: dorsal is up and ventral is down. On horizontal sections: anterior is up and posterior is down.

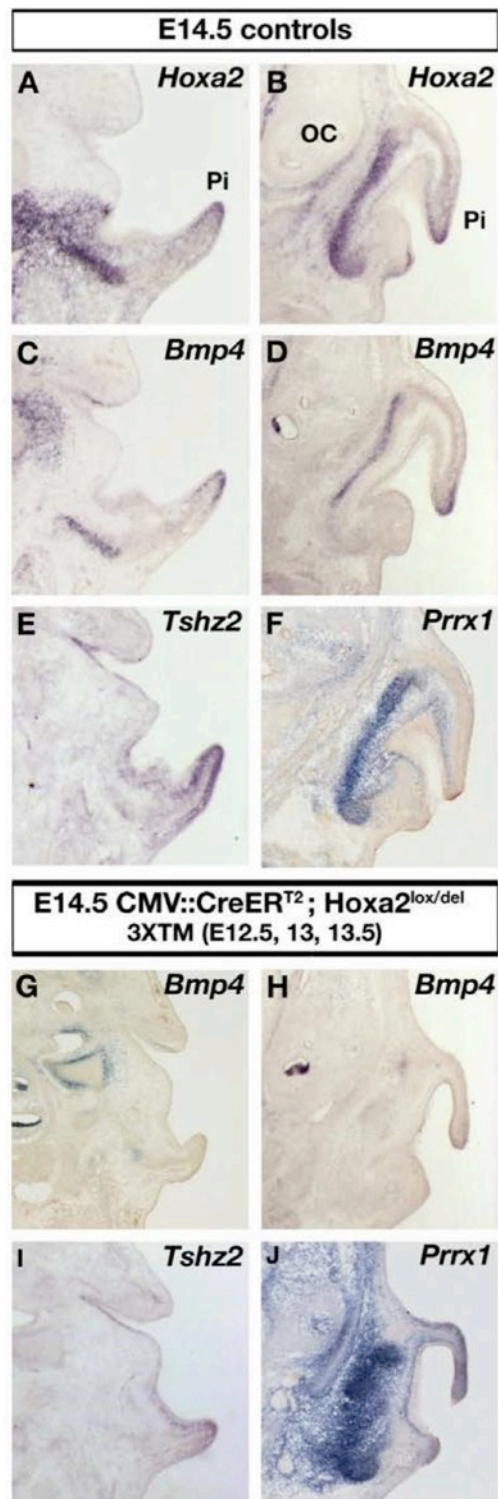


Figure 6: Hoxa2 positively regulates Bmp4

(A-J) *In-situ* hybridizations using *Hoxa2* (A, B), *Bmp4* (C, D, G, H), *Prrx1* (F, J) and *Tshz2* (E, I) ARN anti-sense probes, performed on horizontal (A, C, E, G, I) and frontal (B, D, F, H, J) sections realised through the external ear of E14.5 controls (A-F) and CMV::CreERT²;Hoxa2^{lox/del} mutant embryos treated with tamoxifen (TM) at E12.5, E13, and E13.5 (G-J). On frontal sections: dorsal is up and ventral is down. On horizontal sections: anterior is up and posterior is down. Abbreviations: OC, otic capsule; Pi, pinna.

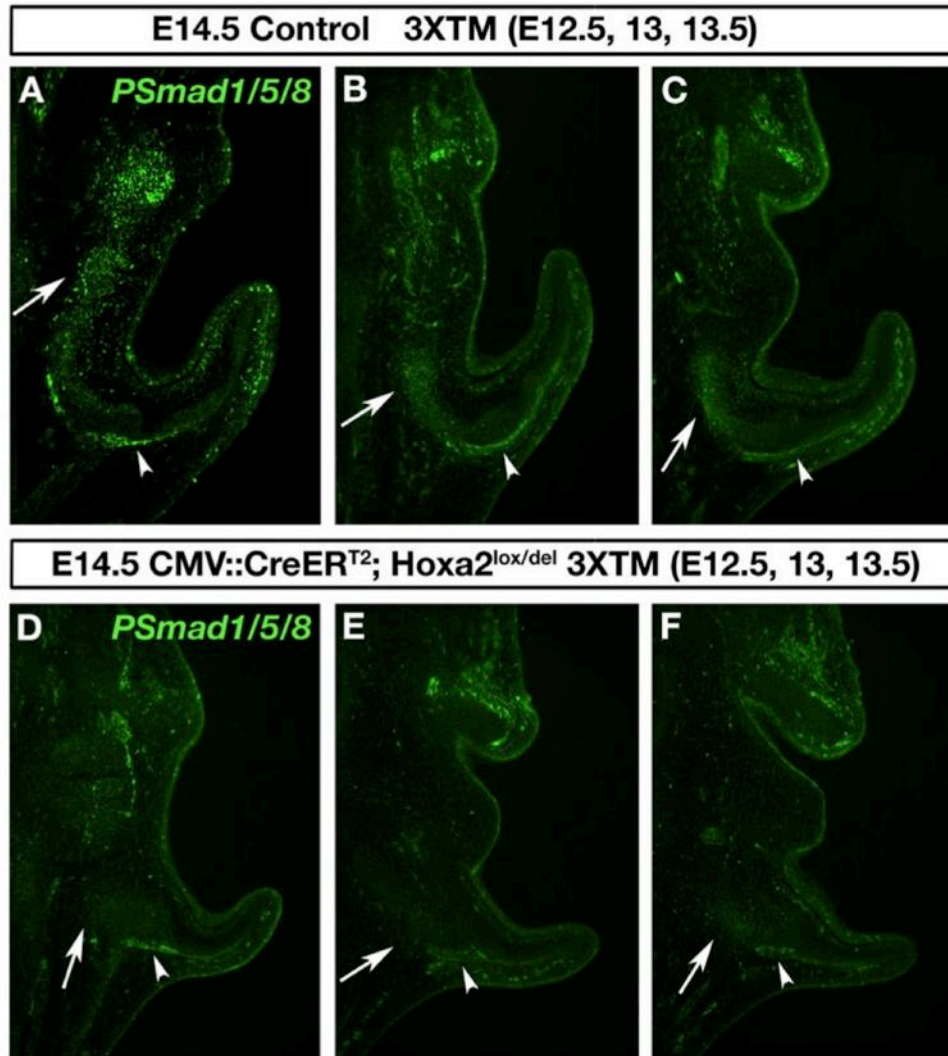


Figure 7: Effect of *Hoxa2* temporal inactivation on the canonical BMP signalling pathway

(A-F) Anti-phosphoSmad 1/5/8 antibody immuno-staining performed on horizontal sections realised through the external ear of E14.5 control (A-C) and CMV::CreER^{T2};Hoxa2^{lox/del} mutant (D-F) embryos treated with tamoxifen (TM) at E12.5, E13 and E13.5. The white arrows show that the phosphoSmad 1/5/8 positive domain located in the inner *Hoxa2*-expressing domain of control embryos (A-C) is absent or strongly reduced in CMV::CreER^{T2};Hoxa2^{lox/del} mutant embryos treated with tamoxifen (TM) (D-F). The white arrowheads show the phosphoSmad 1/5/8 positive domain abutting the pinna mesenchymal core. Anterior is up, posterior is down.

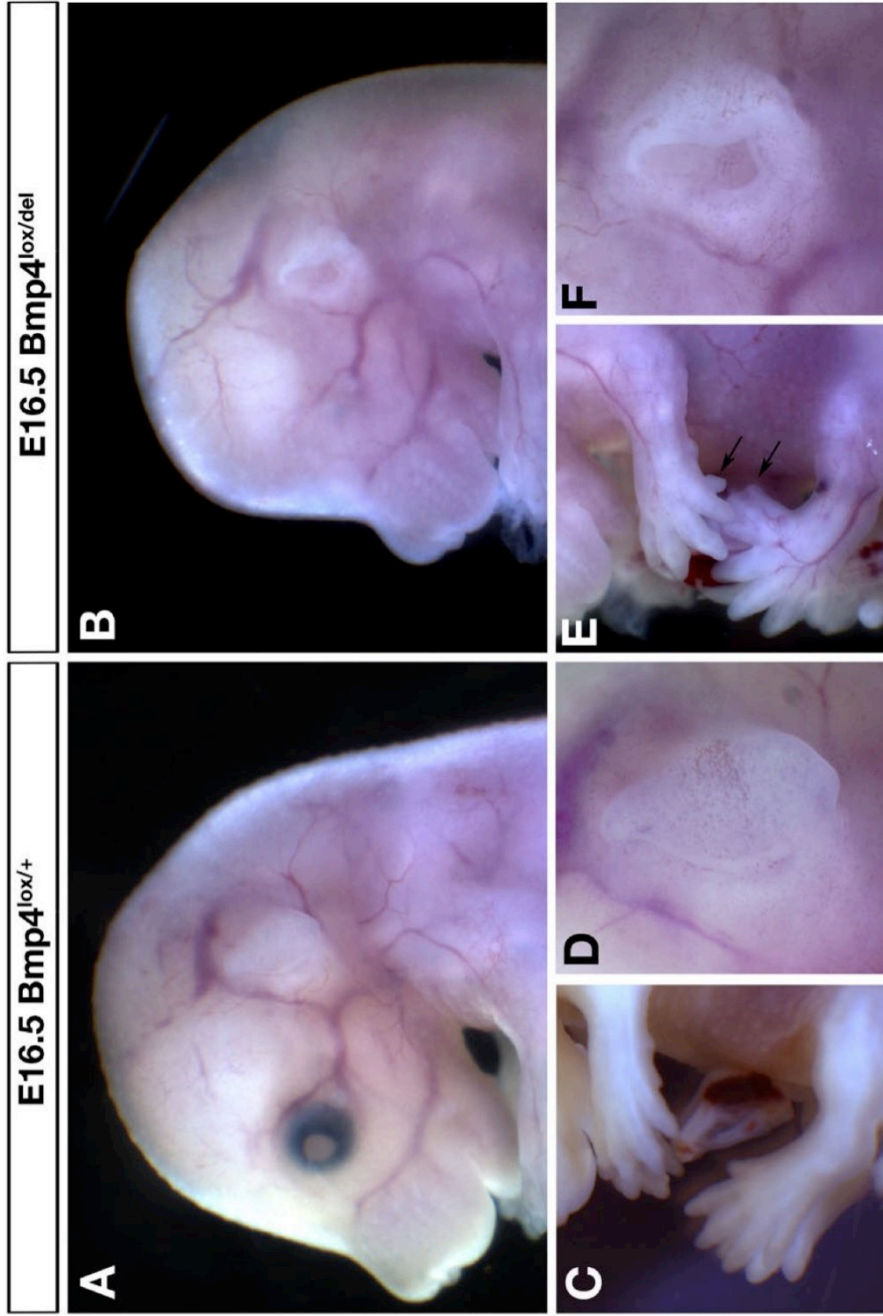


Figure 8: Contribution of Bmp4 in external ear morphogenesis.

(A-F) Lateral views of E16.5 $Bmp4^{lox/+}$ control (A, C, D) and $Bmp4^{lox/del}$ hypomorph (B, E, F) fetuses. C, D and E, F represent a focus on the hindlimb and the pinna of the fetuses shown in A and B respectively. Note the small pinna and the polydactyly presents in $Bmp4^{lox/del}$ mutant fetuses (B, E, F).

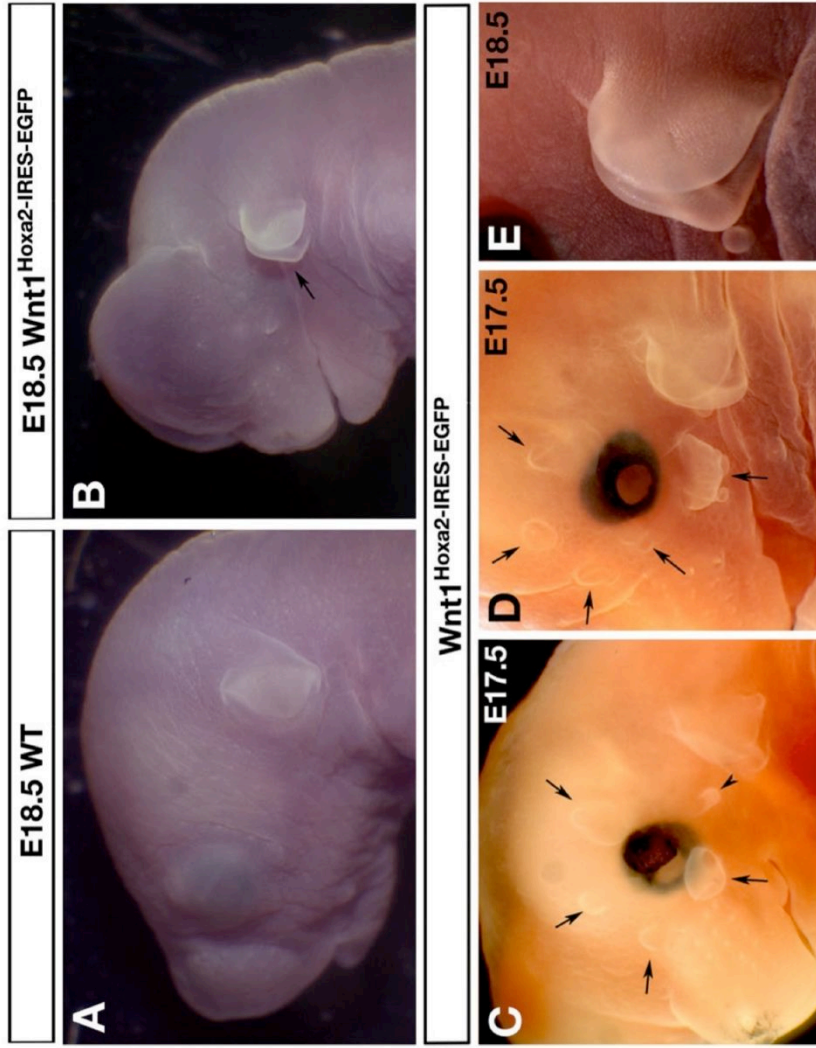


Figure 9: Hoxa2 is sufficient to induce the formation of ectopic pinnae
 (A-E) Lateral views of the head of E18.5 (A, B, E) and E17.5 (C, D) wild-type (WT) (A) and $Wnt1^{Hoxa2-IRES-EGFP}$ mutant (B-E) fetuses. E represents a focus on the duplication of the pinna. The arrow in B shows the duplicated pinna. The arrows in C and D show the ectopic structures, which form all around the eye and which present a morphology resembling small ectopic pinnae.

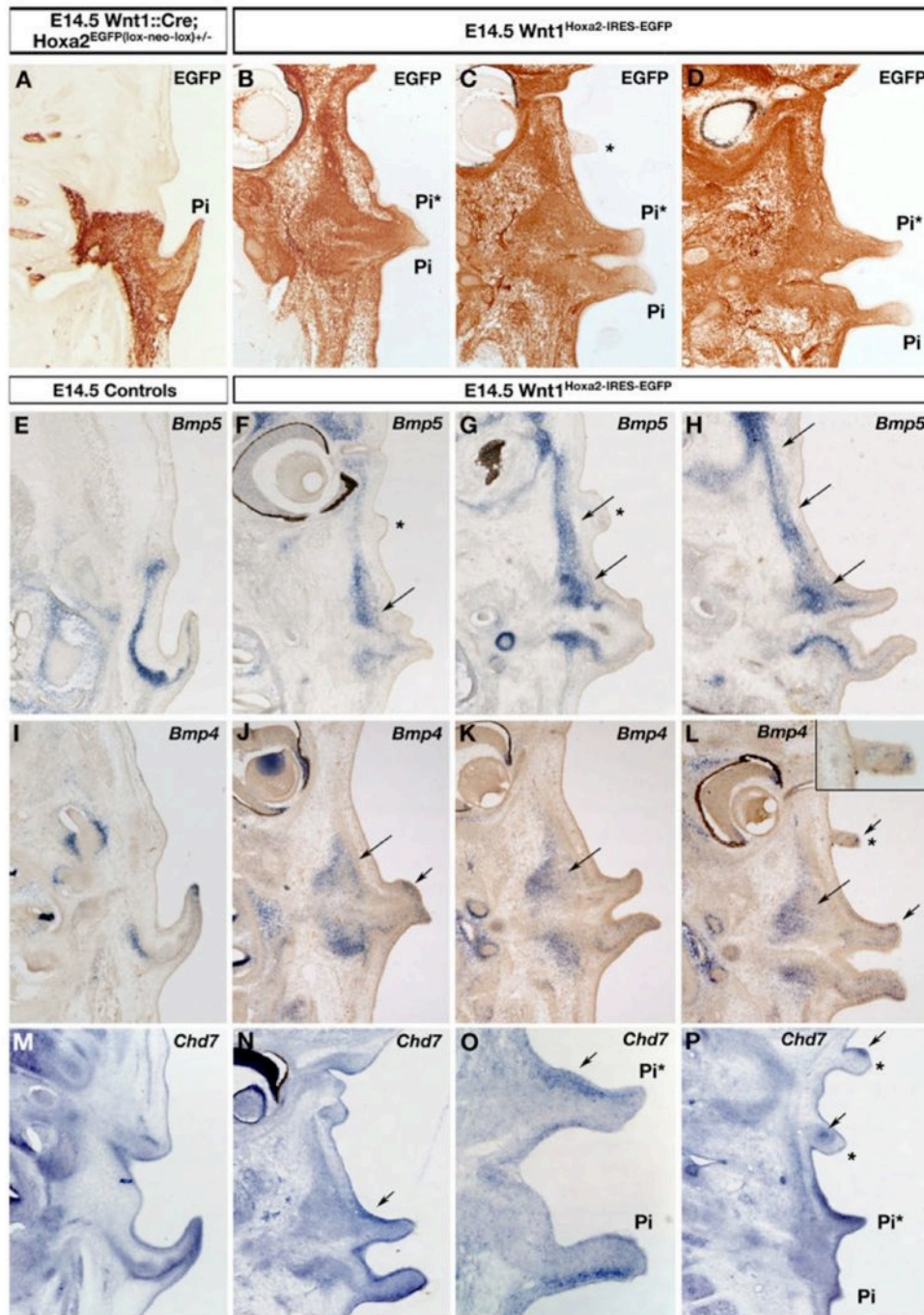
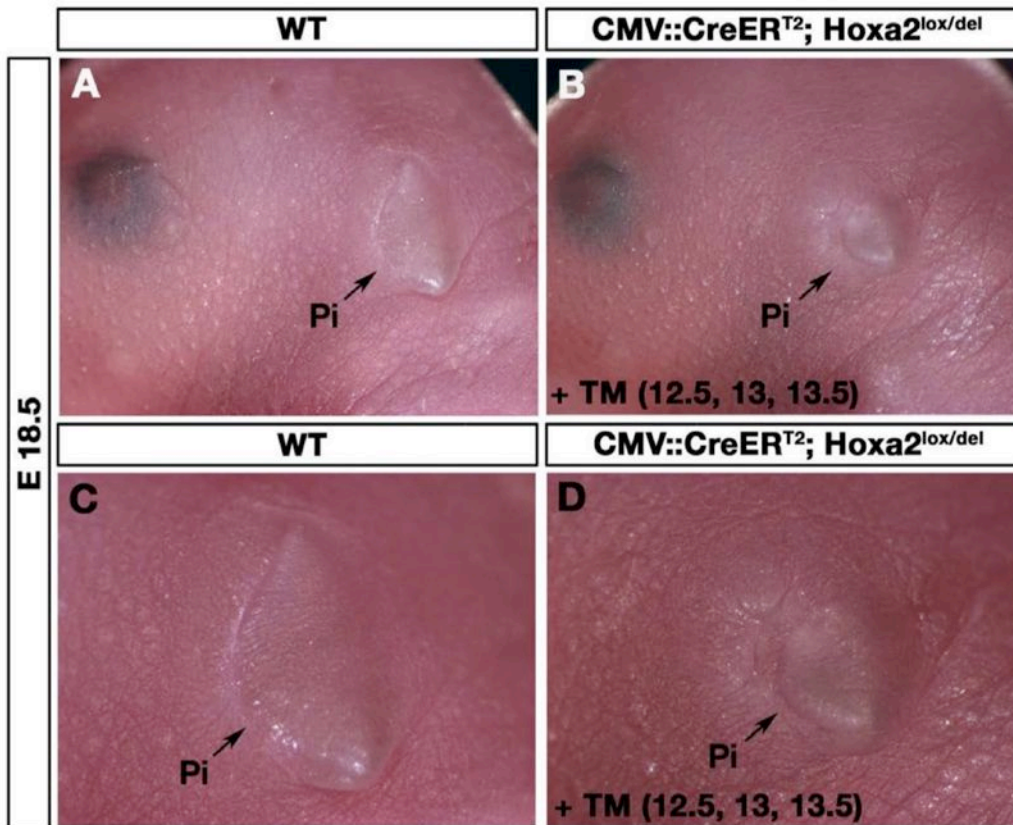


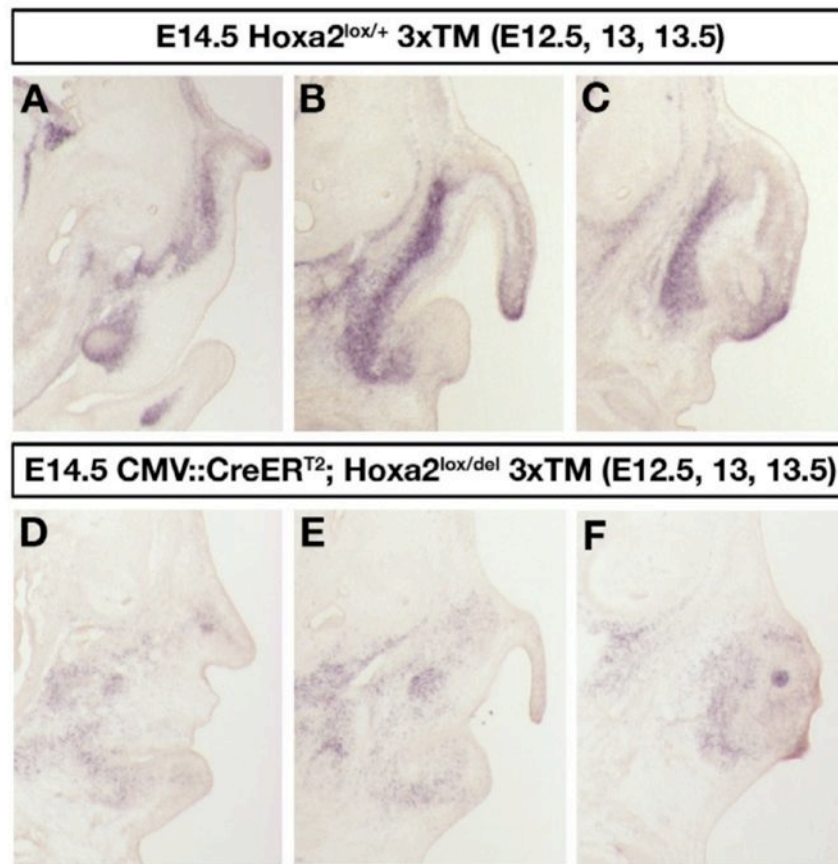
Figure 10: Molecular identity of the duplicated pinna.

(A-D) Anti-EGFP antibody immuno-staining performed on horizontal sections realised through the external ear of E14.5 *Wnt1::Cre;Hoxa2^{EGFP}(lox-neo-lox)^{+/-}* control (A) and *Wnt1^{Hoxa2}-IRES-EGFP* mutant (B-D) embryos. (E-P) *Bmp5* (E-H), *Bmp4* (I-L) and *Chd7* (M-P) *in-situ* hybridizations performed on horizontal sections realised through the external ear of E14.5 control (E, I, M) and *Wnt1^{Hoxa2}-IRES-EGFP* mutant (F-H, J-L, N-P) embryos. Anterior is up, posterior is down. The black arrows display the ectopic expression of *Bmp5*, *Bmp4* and *Chd7* in the duplicated pinna (Pi*) and more anteriorly. The asterisks (*) represent the ectopic structures, which form around the eye. In L, a focus of one of these structures is presented in the right upper corner. *Bmp4* and *Chd7* are expressed in these ectopic structures; *Bmp5* is expressed in the mesenchyme just beneath. Abbreviation: Pi designs the pinna normally present in control embryos, deriving from the second pharyngeal arch.



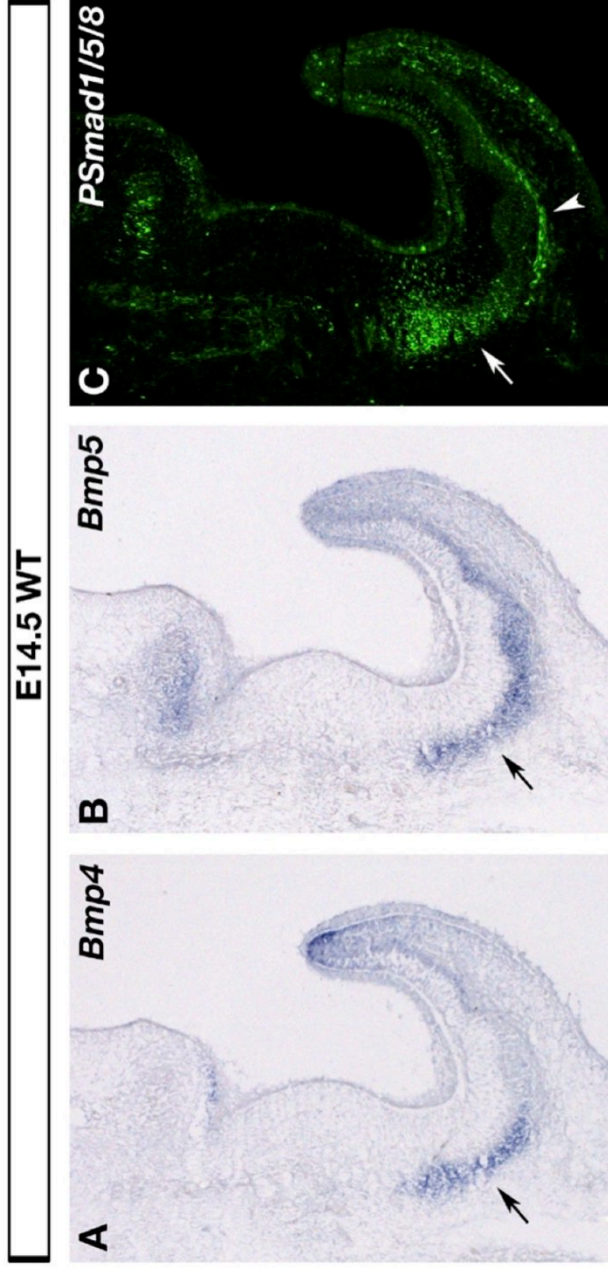
Supplementary figure 1: Temporal contribution of Hoxa2 in external ear morphogenesis.

(A-D) Lateral views of the head of E18.5 wild-type (WT) (A, C) and CMV::CreERT²;Hoxa2^{lox/del} mutant foetus treated with tamoxifen (TM) at E12.5, E13 and E13.5 (B, D). C and D represent a focus on the pinna of the foetus shown in A and B respectively. Note the small pinna induced by late TM treatment (E12.5, E13 and E13.5) on CMV::CreERT²;Hoxa2^{lox/del} mutant foetus (B, D).



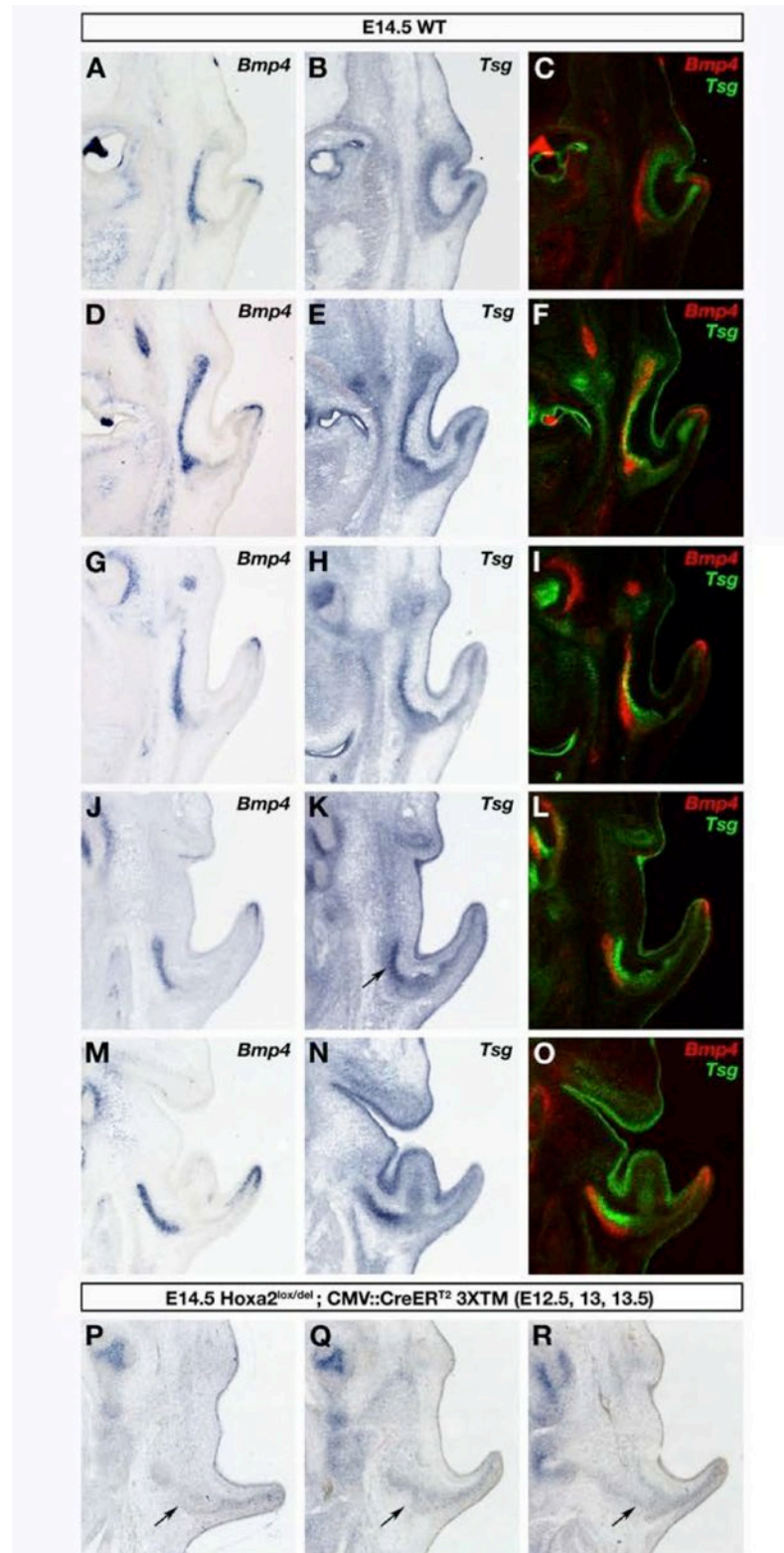
Supplementary figure 2: *Hoxa2* expression after its late temporal inactivation.

(A-F) *Hoxa2* in-situ hybridizations performed on frontal sections realised through the external ear of E14.5 *Hoxa2*^{lox/+} control (A-C) and *CMV::CreERT2*;*Hoxa2*^{lox/del} mutant (D-F) embryos treated with tamoxifen (TM) at E12.5, E13 and E13.5. Dorsal is up, ventral is down and sections are presented from anterior to posterior (A and D are more anterior than C and F). Note the down-regulation of *Hoxa2* expression in *CMV::CreERT2*;*Hoxa2*^{lox/del} mutant embryos treated with TM at E12.5, E13 and E13.5.



Supplementary figure 3: *Bmp4*, *Bmp5* and PhosphoSmad 1/5/8 distribution in external ear

(A-C) *Bmp4* (A) and *Bmp5* (B) *in-situ* hybridizations, as well as anti-phosphoSmad 1/5/8 antibody immuno-staining performed on adjacent horizontal sections realised through the external ear of E14.5 wild-type (WT) embryo. The black arrows in A and B, and the white arrow in C show the *Bmp4*, *Bmp5* and phosphoSmad positive cells at the base of the pinna. The white arrowhead in C shows the restricted stream of phosphoSmad positive cells close to the pinna mesenchymal core of *Bmp5* expression. Anterior is up, posterior is down.



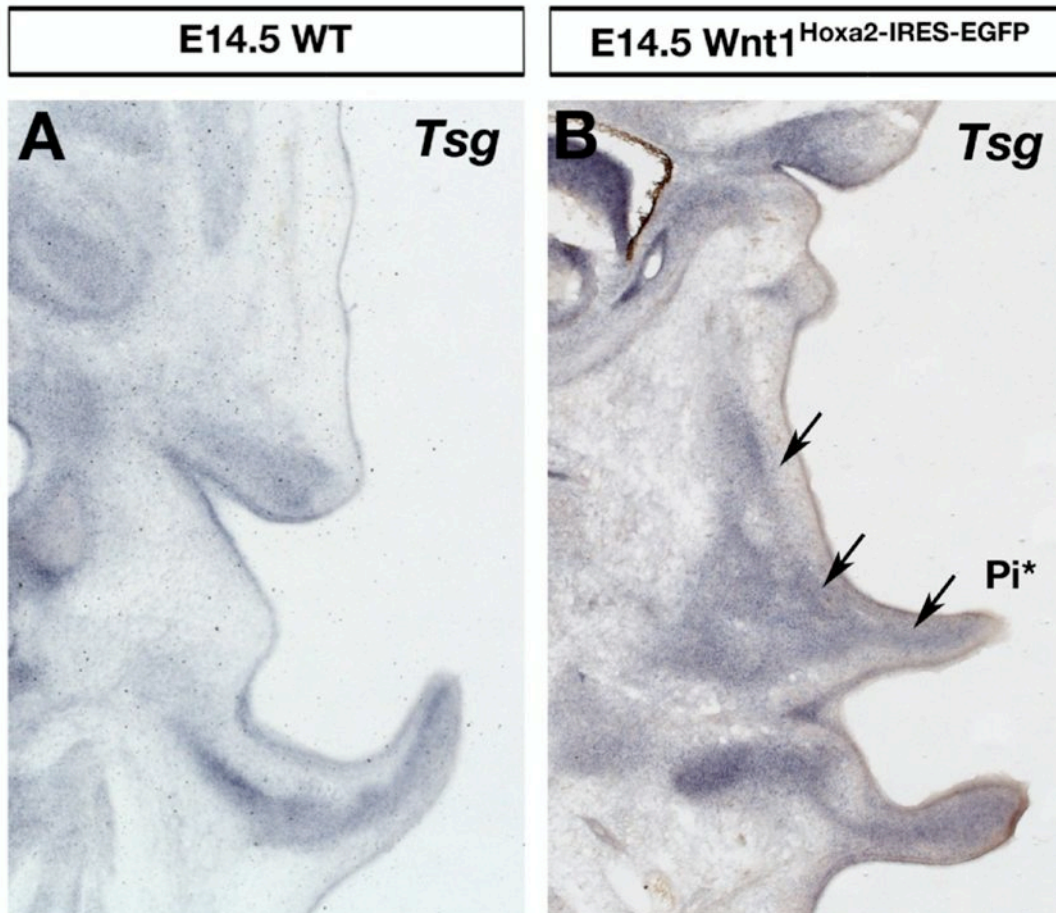
Supplementary figure 4: *Hoxa2* positively regulates *Tsg*

(A-O) *In-situ* hybridizations performed on adjacent horizontal sections realised through the external ear of E14.5 wild-type (WT) embryos and using *Bmp4* (A, D, G, J, M) and *Tsg* (B, E, H, K, N) ARN anti-sense probes. A merge realised with Photoshop, between adjacent sections on which *Bmp4* and *Tsg in-situ* hybridizations has been performed (C, F, I, L, O) show that *Tsg* is highly expressed directly adjacent to the *Bmp4* positive domain. (P-R) *Tsg in-situ* hybridizations performed on horizontal sections realised through the external ear of E14.5 CMV::CreERT²;*Hoxa2*^{lox/del} mutant embryo treated with tamoxifen (TM) at E12.5, E13 and E13.5. Anterior is up, posterior is down.



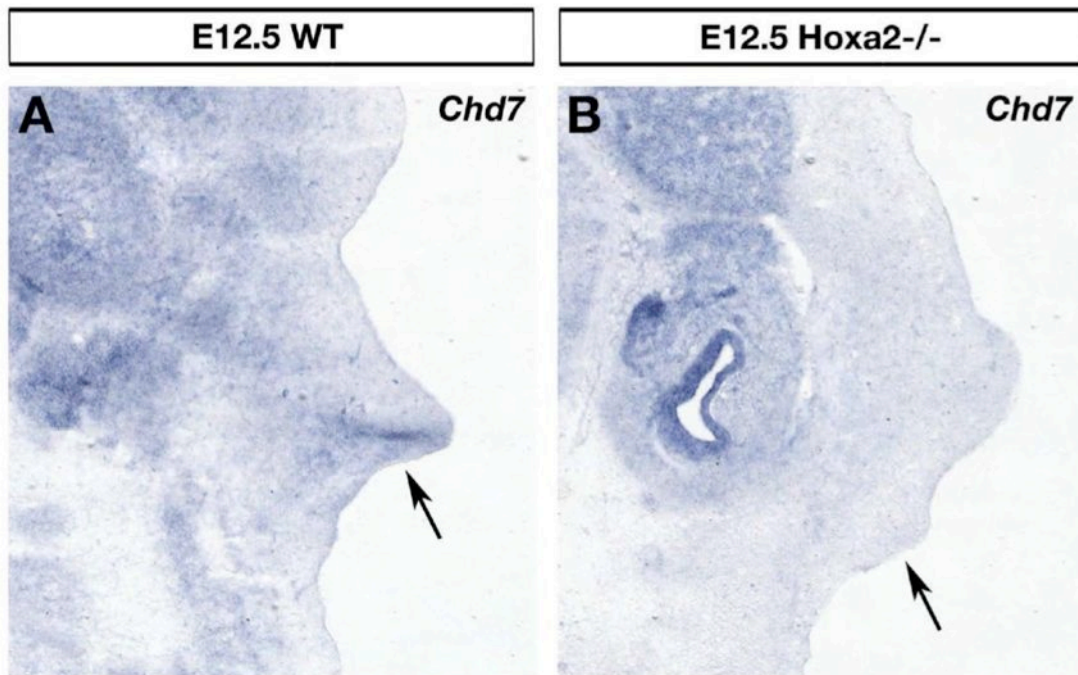
Supplementary figure 5: Validation by qPCR of binding regions linked to *Bmp4* and *Bmp5*

A. Fold enrichment of Hoxa2 over IgG negative control antibody (Neg Ab) is shown for each Hoxa2-bound region. Values correspond to the average of duplicate samples and are representative of two independent experiments. Itih4 is a negative control gene (unbound region). The numbers in brackets correspond to the FDR (False Discovery Rate) of each bound region in Hoxa2 ChIP-seq (15). B. Sequence alignment and conservation of Hoxa2-bound regions across Vertebrates, provided by the UCSC browser (38).



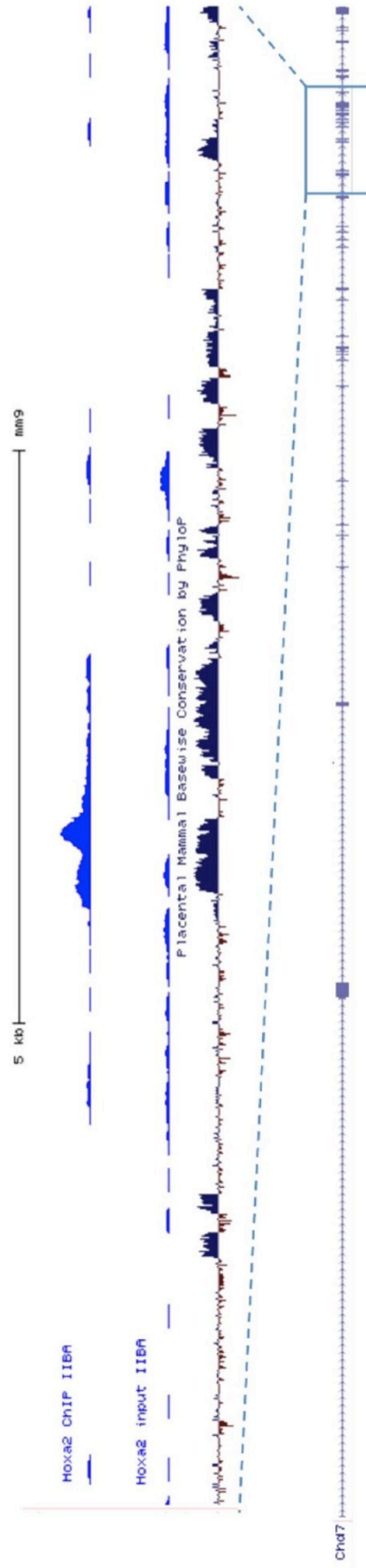
Supplementary figure 6: *Tsg* is ectopically expressed in the duplicated pinna induced by *Hoxa2* gain of function

(A, B) *Tsg* *in-situ* hybridization performed on horizontal sections realised through the external ear of E14.5 Wild type (WT) (A) and $Wnt1^{Hoxa2-IRES-EGFP}$ mutant (B) embryos. Anterior is up, posterior is down. The black arrows display the ectopic expression of *Tsg* in the duplicated pinna (Pi*) and more anteriorly.



Supplementary figure 7: Hoxa2 regulates positively *Chd7*

(A, B) *Chd7* in-situ hybridization performed on horizontal sections realised through the external ear of E12.5 Wild type (WT) (A) and Hoxa2^{-/-} mutant (B) embryos. Anterior is up, posterior is down. The black arrows display the absence of *Chd7* expression in the Hoxa2^{-/-} mutant embryo.



Supplementary figure 8: Hoxa2 binds *Chd7*

Graphic representation of ChIP-seq results (15) showing the *Chd7* locus. Hoxa2 signal is detected 159 kb downstream of *Chd7* TSS, in a region of sequence conservation in placental mammals (38).

3.1.5 “The Cre/Lox system to assess the development of the mouse brain” (Book chapter, submitted manuscript, *Methods in Brain Development*)⁵

The use of the Cre/lox system for the generation of transgenic mouse lines, *in utero* electroporation constructs and the design of new genetic tools is a substantial element of this thesis. Approaches that have been mostly exploited in the course of this PhD thesis or that are considered for further projects are described in detail. This submitted book chapter gives the background and an overview of all techniques using Cre/lox mediated recombination in mice.

⁵ Statement of contribution: The first draft of this book chapter was written by myself. I also generated all figures. Filippo Rijli corrected the manuscript and gave suggestions for improvement of text and figures.

Chapter X

The Cre/Lox system to assess the development of the mouse brain

Claudius F. Kratochwil and Filippo M. Rijli

Friedrich Miescher Institute for Biomedical Research,
Maulbeerstrasse 66, 4058 Basel, Switzerland

Summary

Cre-mediated recombination has become a powerful tool to confine gene deletions (conditional knockouts) or overexpression of genes (conditional knockin/ overexpression). By spatio-temporal restriction of genetic manipulations major problems of classical knockouts such as e.g. embryonic lethality can be circumvented. Furthermore Cre-mediated recombination has broad applicability in the analysis of the cellular behavior of subpopulations and cell types as well as for genetic fate mapping. This chapter will give an overview about applications for the Cre/LoxP system and their execution.

Key words: Cre recombinase, transgenesis, conditional knockout, conditional knockin, CreER^{T2}, Flpe recombinase, MADM, Split-Cre, Brainbow

1. Introduction

After the first gene knockout (KO) in the mouse was obtained by Thomas & Capecchi using site-directed mutagenesis of the HPRT gene in 1987 [1], the *in vivo* function of many genes has been analyzed using this technique. Nevertheless the KO approach has two main restrictions. First of all, genes whose inactivation is embryonically lethal cannot be analyzed for their function in late development and adulthood. Secondly, KOs of genes which have a function in multiple tissues and/or cell types are difficult to analyze, since phenotypes might be combinations of

multiple distinct defects and therefore quite complex to dissect.

In 1994 Gu et. al described for the first time the use of the Cre/Lox recombination system to induce a gene knockout in mice [2]. This technology made it possible to conditionally knockout genes solely in subsets of cells (i.e. in a cell type- or tissue-specific manner), where Cre recombinase is expressed. Two years before, the technique had been already used to conditionally overexpress the SV40 large tumor antigen in mice [3]. The key principle of the Cre mediated recombination is that the recombinase enzyme can catalyze the deletion or inversion of a genomic fragment depending on the orientation of small recognition sequences, called Lox or LoxP sites, flanking such fragment.

Since then, Cre-mediated recombination has been used successfully for many applications, tissues [4-9] and model organisms including e.g. *Drosophila* [10], *Xenopus* [11], zebrafish [12] and plants [13]. Also the recombination mechanism has been elucidated by the analysis of the crystal structure of Cre and the Cre/LoxP interface [14].

In mammalian cells, Cre is the predominantly used recombinase for site-specific recombination and has been shown to be more effective than another (in *Drosophila* widely used) recombination system, the Flp/Frt system from *Saccharomyces cerevisiae* [15]. The Flp recombinase has a similar ability as Cre to delete or invert (and therefore was named **Fl(i)p** recombinase) DNA fragments, though recognizing distinct target sequences. Later on a more efficient version, Flpe, has been created which works reliably in mice [16, 17] and offers a suitable alternative for some applications.

To further restrict the knockout in time, inducible variants of Cre were designed. The most widely used version is CreER^{T2} [18]. Hereby Cre is fused to a mutated ligand-binding domain of the estrogen receptor (ER) [19]. The fusion-protein is normally confined to the cytoplasm, while in the presence of the synthetic ligand tamoxifen or 4-hydroxytamoxifen it translocates to the nucleus, where it can trigger recombination events (see 3.5). A light-activatable Cre recombinase to control activity in time and space has also been generated [20].

Another idea to restrict Cre or CreER^{T2} further in space came from Hirrlinger et al. [21-23]. By splitting Cre into two inactive fragments, which re-gain Cre activity when co-expressed, recombination could be restricted to the intersection of two expression domains (by using different enhancers/promoters for the two fragments). A similar system was established by Farago et al. [24], using a combination of the two

recombination systems Cre/Lox and Flpe/Frt (see 3.6). Both systems have been also tested *in vivo* in transgenic animals.

A powerful tool to fate map cells as well as to analyze gene function on a single-cell resolution was introduced with the MADM (mosaic analysis with double markers) system [25, 26] an adaptation of the MARCM (mosaic analysis with a repressible cell marker) system from *Drosophila* [27]. MADM uses Cre-mediated inter-chromosomal recombination. By employing two markers (e.g. GFP and RFP), not only single cell progenies can be traced, but the combination with mutations makes it possible to distinguish mutant, heterozygous and wild type cells by their distinct fluorescent markers [28] (see in detail in 3.7).

Another attempt to achieve single cell resolution was given by the Brainbow system from Livet et al. [29]. Here, recombination leads to a stochastic choice of expression of a fluorescent protein. Multiple integrations result in a combinatorial color-code, creating approximately 100 distinguishable colors (see 3.8), which is especially helpful for the analysis of the nervous system.

In this chapter, we will focus on the basic principles and applications of the Cre/LoxP and CreER^{T2}/LoxP systems and their variations (Split-Cre, MADM, Brainbow) and will provide strategies and protocols for their use.

2. Materials

2.1 Reporter Mice

1. Rosa 26 LacZ reporter line [30]; available at Jackson Laboratories:
003504 B6.129S4-*Gt(ROSA)26Sortm1Sor/J*
2. Rosa 26 tdTomato reporter line [31]; available at Jackson Laboratories:
007914 B6.Cg-*Gt(ROSA)26Sortm14(CAG-tdTomato)Hze/J*
3. Rosa 26 ZsGreen reporter line [31]; available at Jackson Laboratories:
007906 B6.Cg-*Gt(ROSA)26Sortm6(CAG-ZsGreen1)Hze/J*
4. Brainbow Reporter lines [29]; six transgenic lines available at Jackson Laboratories:
007901 B6.Cg-Tg(Thy1-Brainbow1.0)HLich/J
007910 B6;CBA-Tg(Thy1-Brainbow1.0)LLich/J
007911 B6.Cg-Tg(Thy1-Brainbow1.1)MLich/J

- # 007921 B6.Cg-Tg(Thy1-Brainbow2.1)RLich/J
 # 013731 STOCK Gt(ROSA)26Sor<tm1(CAG-Brainbow2.1)Cle>/J
 # 017492 B6.129P2-Gt(ROSA)26Sor<tm1(CAG-Brainbow2.1)Cle>/J
5. MADM mice [32, 26, 33, 25]; several transgenic lines are available at Jackson Laboratories, the following are the most widely used:
 # 013749 STOCK Tg(ACTB-EGFP,-tdTomato)11Luo/J
 # 013751 STOCK Tg(ACTB-tdTomato,-EGFP)11Luo/J
 # 017932 STOCK Tg(ACTB-EGFP*)10Luo/J
 # 017923 STOCK Tg(ACTB-EGFP*,-tdTomato)10Luo/J
 # 017912 STOCK Gt(ROSA)26Sor<tm6(ACTB-EGFP*,-tdTomato)Luo>/J
 # 017921 STOCK Gt(ROSA)26Sor<tm7(ACTB-EGFP*)Luo>/J

2.2 Generation of genetically modified mice

1. Genomic DNA (for amplifying enhancers)
2. Cloning plasmid(s) (for Cre, CreER^{T2}, Lox-sites, minimal promoter, fluorescent proteins, resistance cassettes (e.g. Addgene))
3. Standard reagents for molecular biology (restriction enzymes (NEB), ligase (NEB), competent E. coli (e.g. DH5alpha, Top10 (Invitrogen)), primers, antibiotics)
4. Modified recombinogenic bacterial strains for recombination [34] (see Note 1)

2.3 Tamoxifen Treatment for CreER^{T2} mediated recombination

1. Gavage/ feeding needle to administer Tamoxifen (Fine Science Tools, 18060-20)
2. Tamoxifen (SIGMA: T-5648)
3. Corn Oil (SIGMA: C-8267) or Sunflower Oil (Supermarket)
4. Syringe (graded in 100µl intervals)

2.4 Genotyping

1. Standard reagents for DNA extraction (1M Tris-HCl pH8.5, 5M NaCl, 0.5M EDTA, 20% SDS, Proteinase K, Isopropanol, Ethanol)
2. Standard reagents and primers for polymerase chain reaction (PCR) or GoTaq® Green Master Mix (Promega, M7112 or M7113)
3. Standard reagents for gel electrophoresis

3. Methods

3.1 Applications of the Cre/LoxP system

To create a conditional knockout, the gene of interest is flanked with recognition sites (LoxP sites; **L**ocus of **c**rossing [**x**-ing]-over of bacteriophage **P1**) for the bacteriophage P1 Cre recombinase [35] (**Fig. 1**). If Cre recombinase is present, the sequence flanked by two LoxP sites (the “floxed” sequence) is excised (if lox sites have the same orientation) or inverted (if lox sites have opposing orientation) (**Fig. 1**). It is also possible to recombine between two different plasmids or chromosomes (inter-chromosomal recombination), which is for example used in the MADM system (see 3.7). The excision of genomic fragments gives the possibility to perturb gene function either (A) completely, by removing the whole gene or the start codon, (B) partly, by removing certain parts/exons of the gene or by truncating it, or to (C) change its expression pattern and levels by excising/replacing/modifying promoter or enhancer elements.

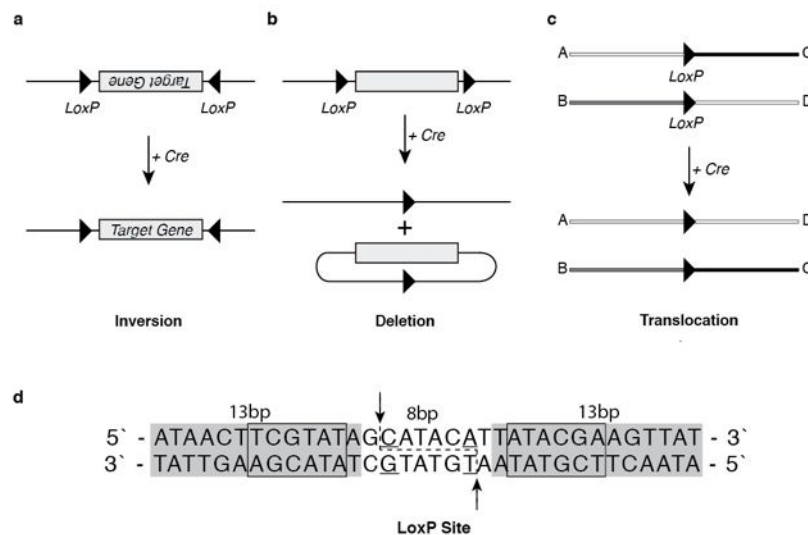


Fig. 1. Distinct genomic outcomes of Cre/LoxP mediated recombination. (a) If two lox sites have opposing directionality, the sequence in between is inverted upon Cre-mediated recombination. The recombination is reversible. (b) If lox sites have the same orientation, the sequence in between is recombined out, resulting in a circular fragment and the sequence lacking this fragment. (c) If LoxP sites are present on two chromosomes, recombination can also occur inter-chromosomally, albeit at a lower frequency than if the LoxP sites are on the same chromosome. (d) The LoxP site is 34 basepair (bp) long. Two palindromic 13bp sequences, containing the Cre binding site (boxed) flank an asymmetric 8bp sequence. Arrows indicate the sites of cleavage during recombination. The underlined basepairs are mutated in the most commonly used variants loxN and lox2722. (modified from [36])

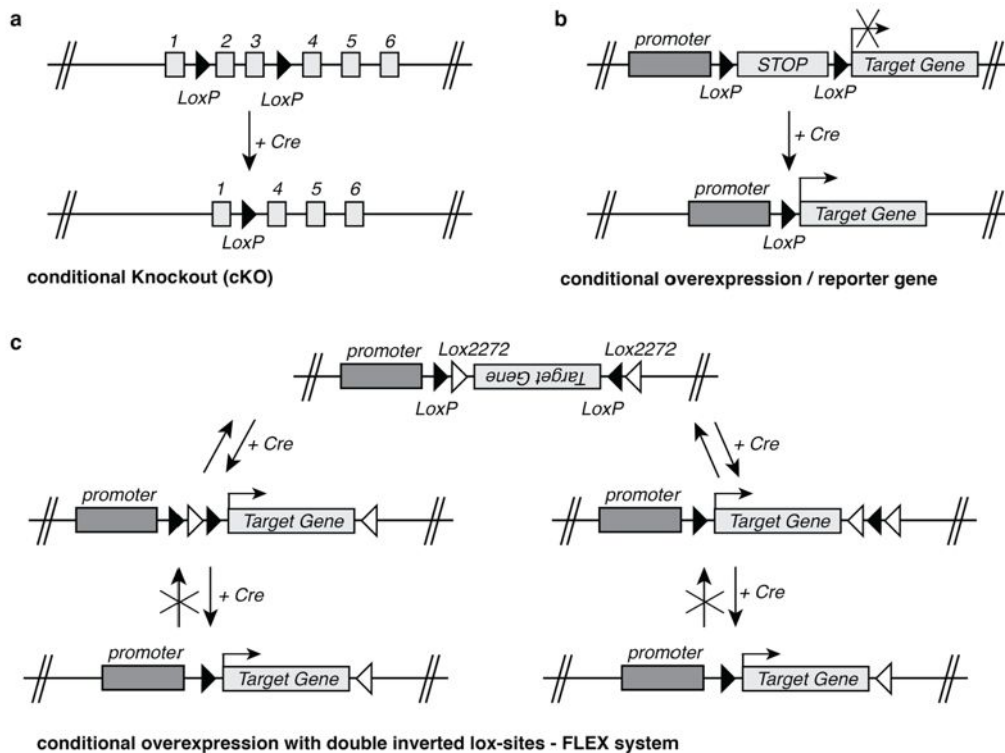


Fig. 2. Three examples for applications using the Cre/LoxP system. (a) The classic approach to generate a conditional knockout is to place LoxP sites in introns either flanking the exon, which contains the ATG or exons that contain functionally important domains. Using this strategy, the probability to interfere with gene expression before Cre recombination is reasonably smaller than if LoxP sites are placed in promoter regions. **(b)** To overexpress genes usually an intervening sequence is placed between promoter and target gene, which blocks transcription. Upon Cre-mediated recombination this sequence is removed, and the gene starts to be expressed under the control of the upstream promoter. **(c)** To reduce the risk of leaking, recently the use of double-inverted lox-sites became an alternative approach (flip-excision switch, or FLEX). Here, the gene of interest is placed in inverted or anti-sense orientation. Cre mediates the inversion of the sequence in the presence of a pair of lox sites in inverted orientation. The use of a second pair of lox sites also in reverse orientation, though incompatible with the first pair, eventually results in an irreversible sense configuration, since both sites lack at the end a partner site, allowing stable transcription.

In a similar way, Cre-mediated recombination can be used to overexpress genes, by excision of an intervening transcriptional termination sequence, flanked by LoxP sites, that prevents the transcription of the target gene [3] (**Fig. 2b**). Since these constructs might result in low levels of leaking readthrough transcription, especially if many copies are present (e.g. when using gene transfer by viruses or electroporation), a different approach (also called flip-excision (FLEX) switch) was created, using LoxP sites, which are put in inverted orientation (**Fig. 2c**), causing an

inversion of the intervening DNA (**Fig. 1**). Thereby the transcription of a gene can be initiated by inverting the open reading frame. Because here none of the LoxP-sites is removed, the inversion would continue forth and back. To interfere with that, a second LoxP-incompatible site pair is introduced (e.g. Lox2272) which results in the termination of the ongoing recombination by cutting out the specific recognition partners of both lox sites (**Fig. 2**) [37].

It should be mentioned that the efficiency of Cre/LoxP-mediated recombination decreases in general with increasing genetic distance, but in principle any desired rearrangement can be made with the Cre/LoxP system [38].

3.2 Designing constructs

The Cre/LoxP is a binary system. On the one hand, the gene of interest has to be flanked by LoxP sites (“floxed”) (**Fig. 1**). On the other hand recombinase expression in the cell or tissue of interest is provided either by (A) a knockin (KI) of *Cre*, (B) a transgene in which *Cre* expression is driven by a specific promoter/enhancer, (C) a Bacterial Artificial Chromosome (BAC) in which *Cre* is inserted in-frame at a specific locus, or (D) transient gene transfer using e.g. viruses or in utero electroporation (**Fig. 3**).

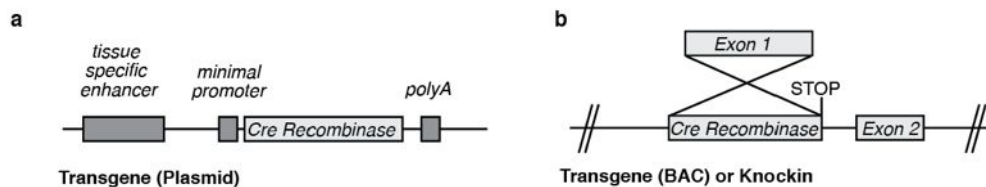


Fig. 3. Two approaches to obtain tissue/cell type specific Cre expression. (a) A tissue specific enhancer is combined with a minimal promoter to drive tissue-specific Cre expression, where the enhancer is active. **(b)** Another approach is site-directed recombination into a Bacterial Artificial Chromosome (BAC) or into the genome of embryonic stem cells.

Many tissue or cell type specific enhancers have been described in the literature. Others can be found in enhancer databases such as e.g. the Vista Enhancer Browser [39], or can be identified by selecting evolutionarily conserved sequences in proximity of genes with expression patterns of interest [40] and by cloning a fragment of a few kilobases of core and proximal promoter in front of the *Cre* recombinase gene. Finally, relevant enhancers can be also identified by genome wide search

e.g. by CHIP-Seq for the p300 protein [41]. If enhancers are used which lack the core promoter element, they are usually combined with the minimal/core promoter (minP) of the human β -globin promoter [42], which is unable to drive efficient transcription if no additional enhancer sequences are present proximally.

3.3 Mouse mating schemes

Once Cre KI (i.e. inserted at specific loci) or Cre-expressing transgenic mice have been created, they need to be crossed to mice carrying LoXP site-bearing conditional alleles, in order to generate double heterozygotes for Cre and the floxed locus. Since most laboratories dispose of multiple Cre drivers, it is more space-efficient to generate a few double heterozygous males for the Cre-expressing line and the conditional allele, and mate them to homozygous conditional mutant females, which can be readily maintained as a pool. However, it should be noted that in this type of crossings double heterozygous Cre/conditional allele and/or homozygous conditional mutant specimen in the absence of Cre-mediated excision usually display a wild type-like phenotype, thus serving as controls. It may be useful to additionally cross a floxed conditional reporter line into the background of Cre/conditional allele double heterozygotes. In many projects this will ease the analysis, as it will allow to: i) have a direct read-out of the cells in which the gene has been knocked out; ii) directly analyze cellular behavior between heterozygotes and homozygotes; and, iii) select tissue or cells using methods such as e.g. fluorescent activated cell sorting (FACS). Conditional Cre-inducible reporter mice in which the reporter genes are inserted in house keeping gene loci are available from the Jackson Laboratories. These lines provide stable and constitutive reporter expression once activated by Cre-mediated excision. In particular, three KIs in the ROSA26 locus are the most frequently used reporter lines since they are highly sensitive to Cre-mediated activation, which either express β -Galactosidase (LacZ) [30], ZsGreen or tdTomato [31], but additional reporter lines expressing other fluorescent proteins are also available (e.g. [43]). The choice depends on the application. β -Galactosidase catalyzes the transformation of X-gal into an insoluble blue enzymatic product and is preferentially used for non-fluorescent histochemistry or whole mount stainings of embryos or organs. The strongly fluorescent proteins ZsGreen (**see Note 2**) or tdTomato are a better choice for fluorescence histochemistry, live imaging or cell sorting.

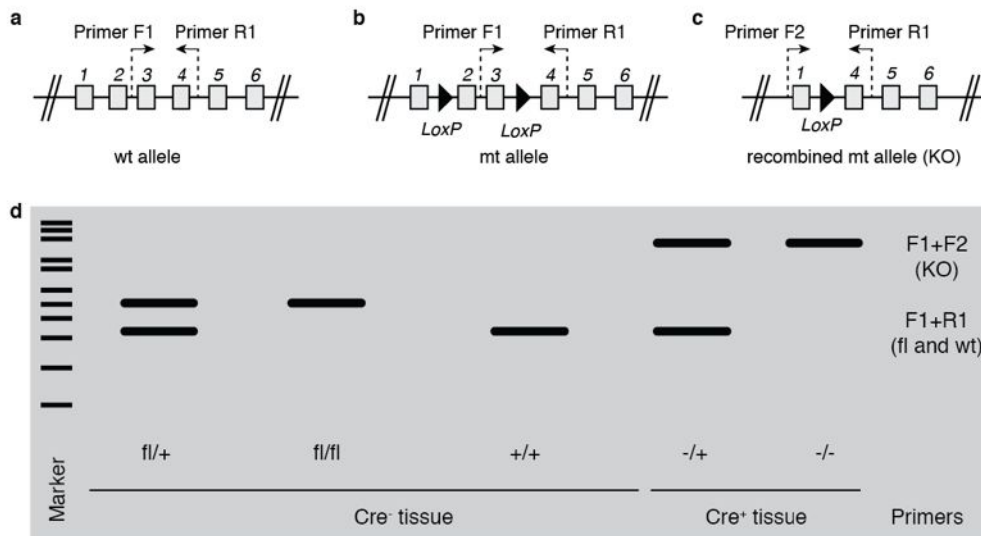


Fig. 5. Genotyping by PCR to detect gene deletion. (a) The targeted allele can be detected by primer Pair 1 (F1 and R1). (b) The floxed allele can be detected by the same primers, yielding a longer amplicon. (c) A distinct primer pair (F2 and R1) detects the Cre-mediated recombination. The non-recombined locus usually cannot be detected, as the amplicon will be too long. (d) Theoretical result of a PCR with different genotypes in Cre-positive (Cre^+) and Cre-negative (Cre^-) tissues.

PCRs for genotyping can be done using standard PCR protocols for genotyping on clipped toes, ears or tails or any other tissue, where recombination has to be tested. We recommend the use of the GoTaq® Green Master Mix (Promega), because it is faster, reduces pipetting mistakes and contaminations and increases reproducibility.

DNA extraction:

1. Prepare Tail Buffer (500ml Stock):

100mM Tris-HCl pH 8.5	50ml of 1M
200mM NaCl	20ml of 5M
5mM EDTA	5ml of 0.5M
0.2% SDS	5ml of 20% SDS
ddH ₂ O	420ml
2. Clip tails or ears and collect them in 1.5ml Eppendorf tubes
3. Add 500 μ l Tail Buffer and 10 μ l Proteinase K (20mg/ml)
4. Digest over night in a water incubator at 55°C or 2h on a shaking dry incubator at 55°C
5. Vortex tubes and centrifuge for 5 minutes at 14000 rpm
6. Collect supernatant in new tube (to remove undigested tissue) with

- 500 μ l Isopropanol (2-Propanol)
7. Shake vigorously and centrifuge for 10-15 minutes at 14000 rpm
 8. Remove supernatant, add 500 μ l 70% Ethanol to wash pellet and remove supernatant again.
 9. Add 500 μ l ddH₂O and vortex vigorously.

Genotyping using GoTaq® Green Master Mix:

1. Aliquot 2x Master Mix into aliquots between 200 μ l and 1ml
2. Prepare Primer Mix for each genotype (100 μ l Stock):

Upstream Primer, 100 μ M	20 μ l
Downstream Primer, 100 μ M	20 μ l
ddH ₂ O	80 μ l

If two Up- or Downstream Primers are needed, use 10 μ l of each.
3. Prepare Master Mix for each primer set:

	1 reaction	20 reactions
GoTaq® Green Master Mix, 2X	3.6 μ l	80 μ l
Primer Mix, 10 μ M for each primer	0.4 μ l	8 μ l
4. Pipet 3.2 μ l genomic DNA template and 4 μ l Master Mix (for many samples a dispenser can be used) per reaction tube. Also half reactions can be done.
5. Annealing conditions should be optimized. It is recommended to design all primers for approximately the same annealing temperature (e.g. 58°C) because PCRs can be pooled in the same block and different primers can be combined. The following program works for many primer sets:

Initial Denaturation	3min	94°C
30-35 cycles:		
Denaturation	40sec	58°C
Annealing	40sec	52°C-62°C
Extension	1min	72°C
Final Extension	5min	72°C
Soak/Refrigeration Cycle	-	4°C
6. Load DNA samples on a 1.5 % Agarose Gel (one band) 2% Agarose Gel (multiple bands with <100bp difference)

3.5 Inducible conditional knockouts

If the gene knockout needs to be induced at a specific developmental stage, a Tamoxifen-inducible form of Cre, CreER^{T2} [18], can be used. In this case, Cre activity is only induced if the synthetic hormone Tamoxifen is administered. For the activation of CreER^{T2} in embryos, pregnant mice are injected with Tamoxifen (dissolved in corn- or sunflower oil) using a gavage needle.

Preparation of Tamoxifen (20mg/ml):

1. Heat 5ml of corn oil in a tube at 37°C for 30 minutes
2. Put tamoxifen at room temperature (RT)
3. Weigh 100mg of Tamoxifen and let the tamoxifen dissolve on a shaker at 37°C; vortex regularly. It will take a few hours till the tamoxifen is completely dissolved
4. Store at 4°C (1 month) or make aliquots (0.5 ml) and store at -20°C

Gavaging:

1. Hold the pregnant female mouse from the back, in a similar fashion as for intraperitoneal injections and secure such that the head cannot move and the oesophagus is straight.
2. Slowly enter the mouth of the animal and proceed along the top of the mouth till the gavage needle enters first oesophagus and than stomach.
3. Slowly inject the oil with 1-10 mg tamoxifen (**see Note 3**) and remove the needle.
4. Minimize the stress of the animal following tamoxifen administration (**see Note 4**).

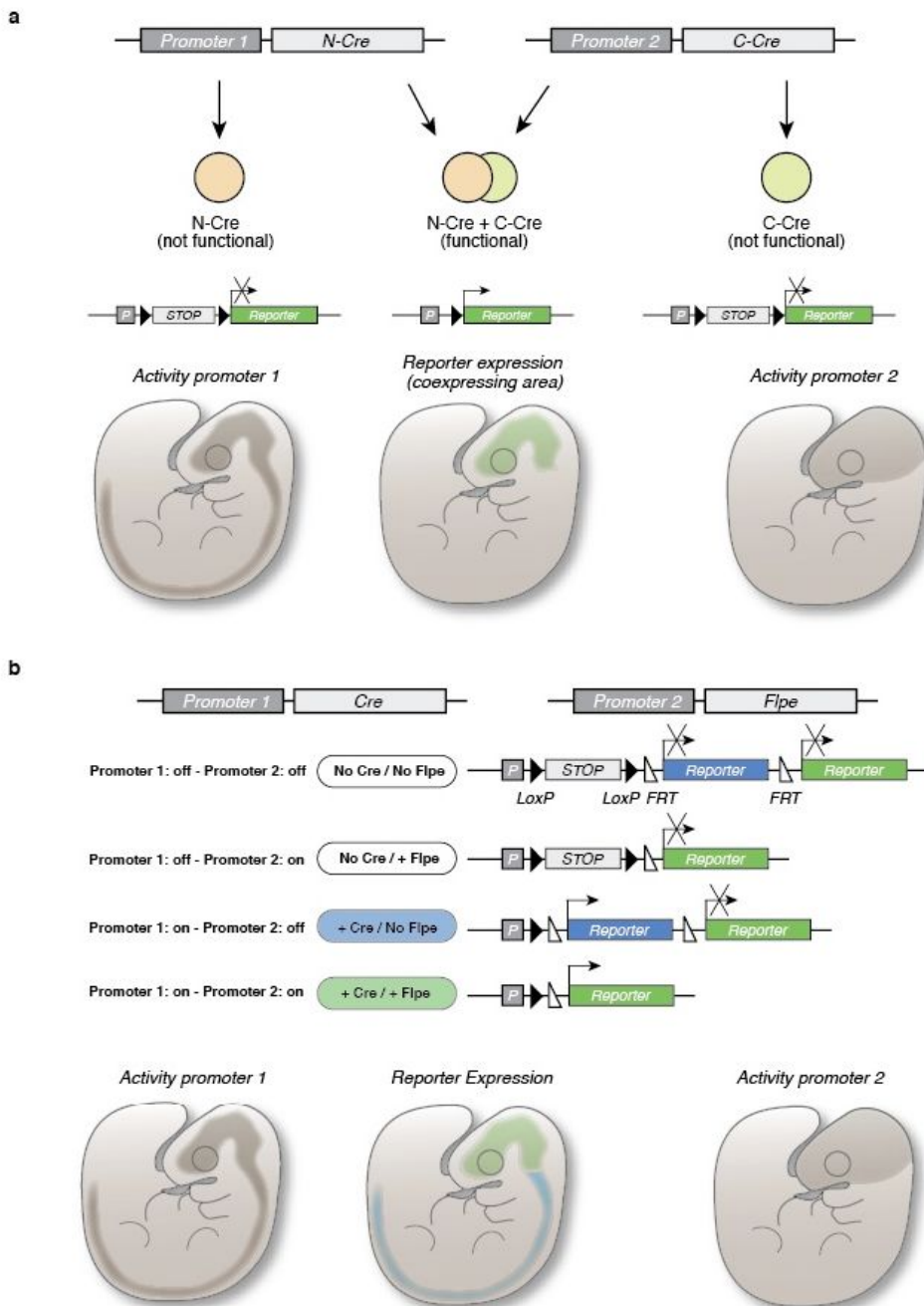


Fig. 6. Tools to generate intersectional recombination (a) In the Split-Cre system, Cre is divided into two inactive fragments expressed under the control of two distinct promoters. In the tissue, or cell type, where both promoters are active, the two fragments are co-expressed resulting in a functional Cre. This triggers a recombination event, e.g. the Cre-mediated activation of a reporter gene. **(b)** The Cre/Flpe system uses two different recombinases recognizing distinct target sites. When both recombinases are active a specific reporter gene is expressed (e.g. GFP) which is not activated by either one of the recombinases alone.

3.6 Intersectional recombination systems

Specificity of Cre recombination in distinct cell subpopulations or cell types may be limited by the lack of specific promoters to drive Cre expression. Two strategies have been designed to achieve higher cellular specificity of gene recombination, which take advantage of the intersectional activities of two promoters in the same cell. The first approach has been elaborated in the Dymecki laboratory [24, 6] to analyze hindbrain development. Hereby the overlapping expression of two different recombinases, Cre recombinase and Flpe recombinase, driven by two different promoters activate the expression of a reporter gene (*GFP*) solely in cells where both recombinases are present (**Fig. 6b**). Additionally the construct contains a reporter (*b-Galactosidase*) which is activated only if *Cre* though not *Flpe* is expressed (**Fig. 6b**).

A second approach was created by Hirrlinger et al. [21, 22], where *Cre* recombinase is split into two inactive parts, N-Cre (the N-terminus) and C-Cre (C-Terminus), which are fused to the constitutive GCN4 protein-protein interaction domain, which has been shown to create stable dimers [44]. When coexpressed in the same cell, N-Cre-GCN4 and C-Cre-GCN4 were able to reconstitute a functional Cre recombinase activity, which can induce recombination (**Fig. 6a**). The system was successfully tested with virus-mediated gene transfer [21, 22] as well as by the use of transgenic mice [23].

3.7 MADM System

The MADM (Mosaic Analysis with Double Markers) is an adaptation in mouse of the conceptually similar MARCM (Mosaic Analysis with a Repressive Cell Marker) used in *Drosophila* [27]. Hereby, rare inter-chromosomal recombination (**Fig. 1c**) during mitosis results in sparse labeling of cells with one of two fluorescent reporter genes (e.g. GFP or RFP). In differentiated cells inter-chromosomal recombination can occur as well, but can only result in the expression of both (GFP and RFP) or no reporter (**Fig. 7**). Because of the low frequency of recombinations during mitosis this allows (A) to follow the behavior of clonally related (i.e., generated from the same progenitor) cells [45] as well as (B) to sparsely generate mutant cells in the background of a heterozygous mouse labeled by a fluorescent marker (e.g. RFP).

Before recombination no fluorescent marker is expressed in MADM mice, because the N-terminus sequence of either one of the two

fluorescent markers (separated by a *LoxP* site) is followed by the C-terminus of the other marker (e.g. N-RFP-LoxP-C-GFP and N-GFP-LoxP-C-RFP), respectively, resulting in non-functional fluorescent proteins. After Cre-induced recombination, N-terminus and C-terminus can be reconstituted to functional fluorescent proteins. (e.g. RFP and GFP in the old versions of MADM, and GFP and tdTomato in the new versions (**Fig. 9**)).

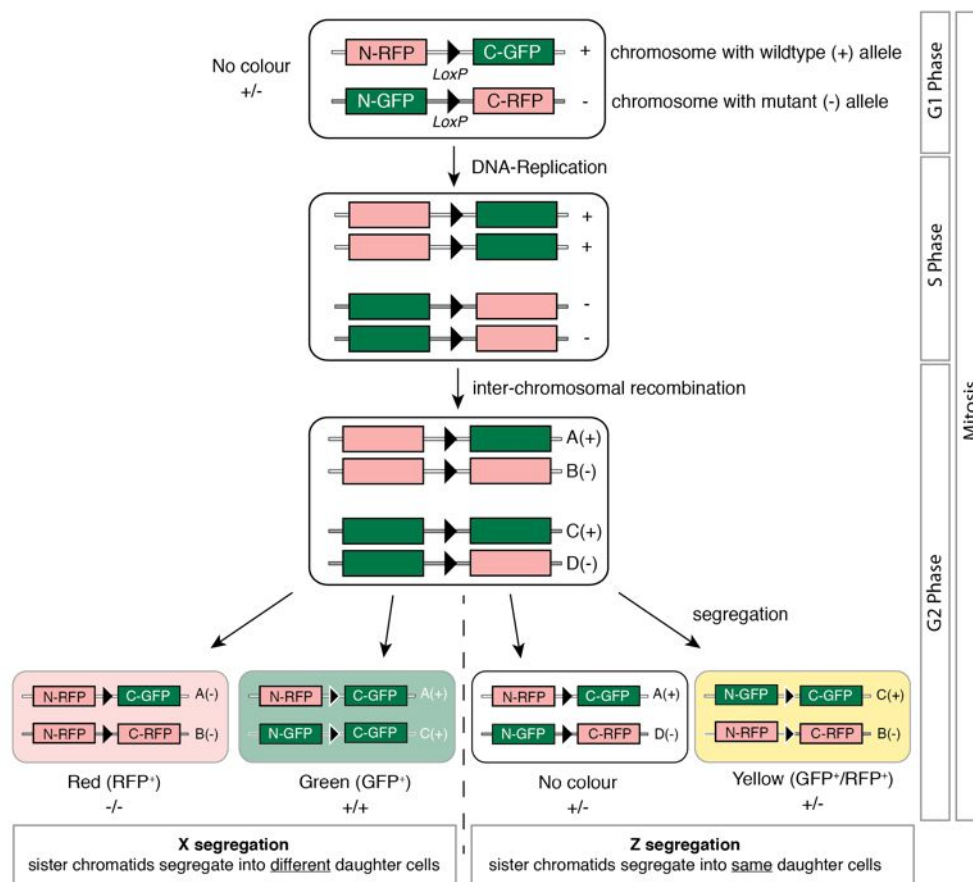


Fig. 7. The MADM system. The MADM system consists of two knock-Ins, which are chimeric genes constituted by the N-Terminus and C-Terminus of two distinct fluorescent proteins (e.g. RFP and GFP). Before Cre-mediated recombination, the chimeric N-RFP/C-GFP or N-GFP/C-RFP alleles result in two non-functional proteins. During the S phase of the mitosis, sister chromatids duplicate and pair. If an inter-chromosomal recombination happens, the correspondingly recombined sister chromatids segregate during the G2 phase into different daughter cells (X-segregation). Two cells of different colours (i.e. expressing either red or green fluorescence) are then generated that also bear distinct genotypes (-/- and +/+). In case each sister chromatids segregate into the same cell a double-labeled and a colourless heterozygote cell (+/-) are produced. A recombination during G1 or G0 (differentiated

cell) phase results in a double-labeled cell. If additionally a mutant allele is recombined onto a MADM-bearing chromosome (while the other MADM containing chromosome has the wild-type allele), X-segregation results in the generation of sibling mutant and wild-type cell, labeled with different fluorescent marker, while Z-segregation or recombination in G1 or G0 phase doesn't change the genotype of the cell.

Since recombination can be tightly controlled by the use of tissue- or cell-specific Cre drivers as well as by Tamoxifen inducible CreER^{T2} drivers for temporal induction, the lineage of single cells can be traced during development and adulthood. Furthermore MADM can be used to selectively knockout genes in labeled cells by introducing (by natural recombination) a mutant allele between the centromere and the MADM transgene, while the second chromosome solely carries the wild-type allele (besides the complementary MADM transgene/knockin). In case of a X-segregation (sister chromatids segregating into different daughter cells) in G2 phase of mitosis two different cells with different colors (red and green) and genotypes (homozygote mutant and homozygote wild-type allele) are generated, while a Z-segregation would result in two heterozygous sister cells (one unlabeled and one labeled with both fluorescent markers) (Fig. 7).

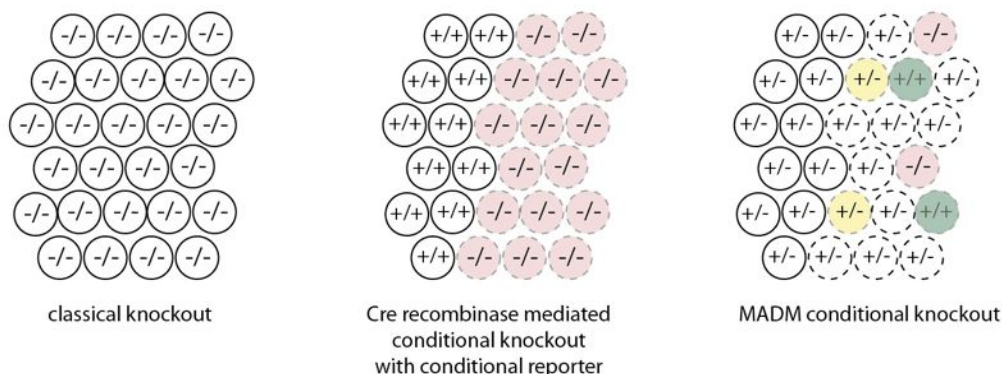


Fig. 8. Advantages of conditional knockouts and MADM conditional knockouts. While classical knockouts give little information about the role of the knocked-out gene in different tissues, the use of conditional knockouts allows the analysis of gene function in selected cell subpopulations or tissues. The MADM system allows furthermore to trace the lineage of single cells with different genotypes (homozygous knockout and wildtype, respectively) in an environment of heterozygous cells.

In contrast to classical (conditional) knockouts, MADM conditional knockouts have several advantages (Fig. 8). First of all, non-cell-autonomous defects can be almost excluded, because just a small proportion of cells carries the homozygous knockout (which can be titrated up or down by the use of a CreER^{T2} driver). Secondly it has clear

advantages, when the cellular character and behavior (cell shape, cell migration, axon guidance) has to be analyzed. Hereby it allows even the direct comparison of cells carrying homozygous mutations and no mutation.

Disadvantages of this technique are that MADM lines are not yet available for all chromosomes, which restricts the use of it at the moment to analyze knockouts of genes located on chr.6, chr.10, and chr.11 and only between the MADM insertion locus and the centromere.

Recently the system has been further optimized by using constructs with tdTomato, a red fluorescent protein brighter than RFP, as well as by making the choice of the second gene to be recombined more flexible (e.g. by substituting a second fluorescent reporter gene with a gene X to be over-expressed) [26].

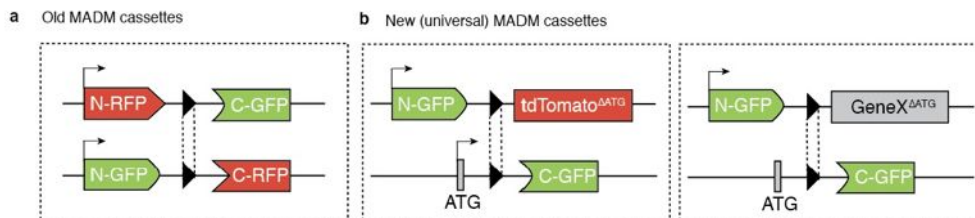


Fig. 9. MADM cassettes. To increase variability in the choice of the second reporter/gene the old cassettes (a) containing GFP and RFP have been replaced by one cassette containing an ATG and the C-terminus of GFP and a second cassette containing N-GFP and an ATG-less tdTomato (b). If another gene except tdTomato should be overexpressed (GeneX) only one transgenic line has to be created making the system more universal.

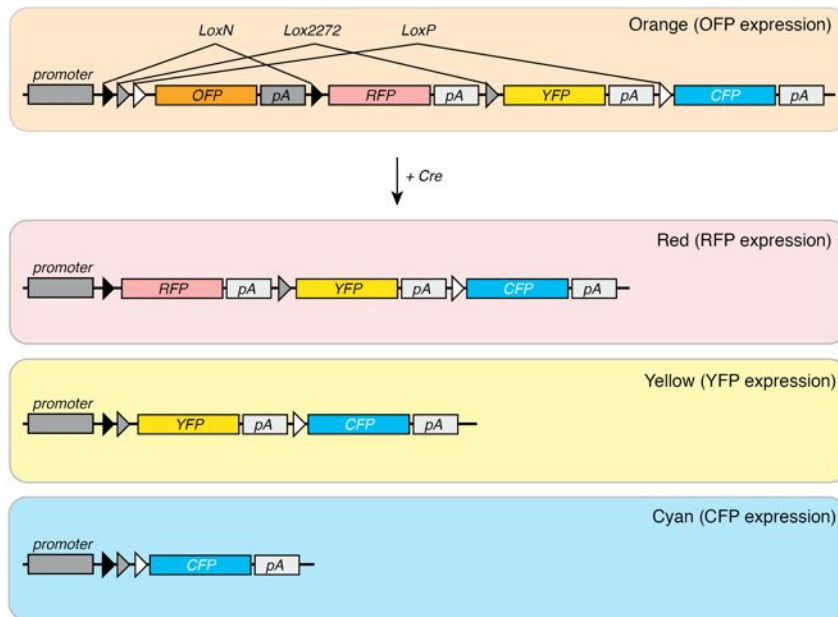


Fig. 10. The Brainbow system. Recombination of the Brainbow 1.1 constructs can result in three possible outcomes. A recombination of the *LoxN* site result in the transcriptional activation of RFP. Because the other two *Lox* sites (*Lox2722* and *LoxP*) lack a second site because they have been placed 3' of the *LoxN* site no further recombination can occur. If the first recombination happens between the *Lox2272* sites the result is expression of YFP, if it happens between the *LoxP* sites it results instead in expression of CFP.

3.8 Brainbow System

An elegant approach to analyze the behavior of single cells in a tissue, especially for the analysis of connectivity patterns in neural circuits, came from the Lichtman group [29]. By the use of different, incompatible *lox* sites (*LoxN*, *Lox2722* and *LoxP*) these authors generated mice, which, in a stochastic manner, are induced to express only one fluorescent protein (YFP, CFP or RFP) as a final recombination event (**Fig. 10,11**).

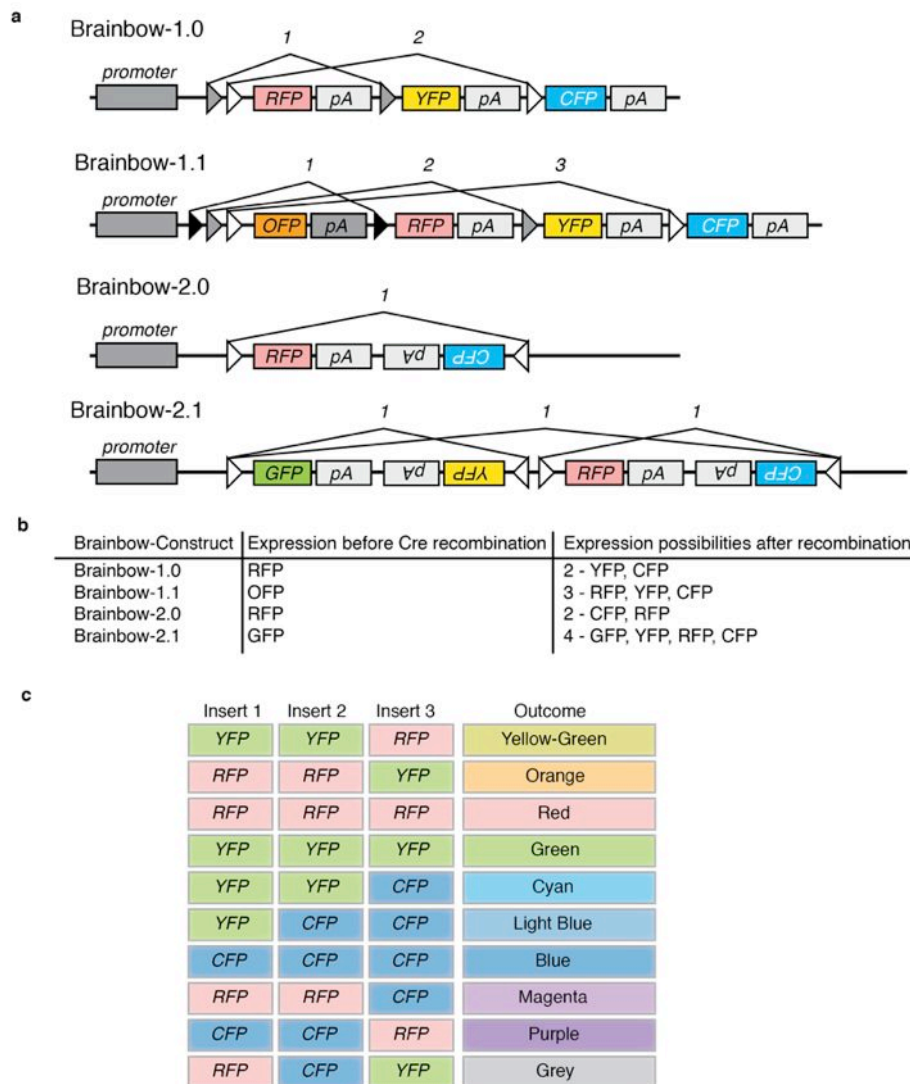


Fig. 11. Overview of Brainbow constructs and principle of “multi-color” brainbow. (a,b) Four brainbow constructs have been generated (a) with different possible outcomes (b). While Brainbow-1.0 and 1.1 recombine only once, Brainbow-2.0 and 2.1 continue to recombine changing the cassette expression pattern after every recombination event. (c) Due to multiple insertions more than 3 different colors are possible. Three insert would give 10 distinguishable colors. Here YFP channel would be set to green and CFP channel to blue, giving a similar principle as the R(ed)G(reen)B(lue) color model of screen displays.

Four different brainbow versions that stochastically express different kinds of fluorescent proteins exist (Fig. 11a,b) and the corresponding transgenic mouse lines are available from Jackson Laboratories. Due to the effect that multiple integrations occur as well as they independently

result in the stochastic choice of one color, combinations of color lead almost 100 distinguishable colors (**Fig. 11c**).

4. Notes

1. Detailed information and trouble-shooting about the use of recombination-mediated genetic engineering can be found here <http://web.ncifcrf.gov/research/brb/recombineeringInformation.aspx> (15/10/12)
2. ZsGreen in contrast to tdTomato is not localizing strongly in cellular extensions like axons or dendrites. For these kind of analyses the tdTomato line (# 007914) would be the recommended choice. For localization of cells ZsGreen (# 007906) is better.
3. For reporter lines and overexpression lines usually 1-2mg of Tamoxifen per pregnant female are sufficient. For the recombination of 2 alleles in mutants 5-10mg (varies between conditional knockout lines) are necessary. The efficiency of the knockout has to be controlled carefully by in situ hybridization and/or immunohistochemistry.
4. In general, stress of the Tamoxifen-treated pregnant female should be kept to a minimum, e.g. by no/reduced change of bedding and limited handling. If the pups are to be analyzed postnatally, there may be problems with delivery, since Tamoxifen interferes with the female hormone system in a dosage-dependent manner. To circumvent this problem, the pups can be recovered by C-section and put in adoption with a foster mother.

Acknowledgements

Work in FMR laboratory in Friedrich Miescher Institute (Basel, Switzerland) is supported by the Swiss National Science Foundation (Sinergia CRSI33_127440), ARSEP, and the Novartis Research Foundation.

References

1. Thomas KR, Capecchi MR (1987) Site-directed mutagenesis by gene targeting in mouse embryo-derived stem cells. *Cell* 51(3):503–512
2. Gu H, Marth JD, Orban PC, Mossmann H, Rajewsky K (1994)

- Deletion of a DNA polymerase beta gene segment in T cells using cell type-specific gene targeting. *Science* 265(5168):103–106
3. Lakso M, Sauer B, Mosinger B, Lee EJ, Manning RW, Yu SH, Mulder KL, Westphal H (1992) Targeted oncogene activation by site-specific recombination in transgenic mice. *Proc Natl Acad Sci USA* 89(14):6232–6236
 4. Sauer B (1998) Inducible gene targeting in mice using the Cre/lox system. *Methods* 14(4):381–392
 5. O'Neal KR, Agah R (2007) Conditional targeting: inducible deletion by Cre recombinase. *Methods Mol Biol* 366:309–320
 6. Kim JC, Dymecki SM (2009) Genetic fate-mapping approaches: new means to explore the embryonic origins of the cochlear nucleus. *Methods Mol Biol* 493:65–85
 7. Wilson TJ, Kola I (2001) The LoxP/CRE system and genome modification. *Methods Mol Biol* 158:83–94
 8. Brault V, Besson V, Magnol L, Duchon A, Héroult Y (2007) Cre/loxP-mediated chromosome engineering of the mouse genome. *Handb Exp Pharmacol* (178):29–48
 9. Feil S, Valcheva N, Feil R (2009) Inducible Cre mice. *Methods Mol Biol* 530:343–363
 10. Siegal ML, Hartl DL (1996) Transgene Coplacement and high efficiency site-specific recombination with the Cre/loxP system in *Drosophila*. *Genetics* 144(2):715–726
 11. Werdien D, Peiler G, Ryffel GU (2001) FLP and Cre recombinase function in *Xenopus* embryos. *Nucleic Acids Res* 29(11):E53–3
 12. Dong J, Stuart GW (2004) Transgene manipulation in zebrafish by using recombinases. *Methods Cell Biol* 77:363–379
 13. Gilbertson L (2003) Cre-lox recombination: Cre-ative tools for plant biotechnology. *Trends Biotechnol* 21(12):550–555
 14. Guo F, Gopaul DN, van Duyne GD (1997) Structure of Cre recombinase complexed with DNA in a site-specific recombination synapse. *Nature* 389(6646):40–46
 15. Nakano M, Odaka K, Ishimura M, Kondo S, Tachikawa N, Chiba J,

- Kanegae Y, Saito I (2001) Efficient gene activation in cultured mammalian cells mediated by FLP recombinase-expressing recombinant adenovirus. *Nucleic Acids Res* 29(7):E40
16. Buchholz F, Angrand P-O, Stewart AF (1998) Improved properties of FLP recombinase evolved by cycling mutagenesis. *Nat Biotechnol* 16(7):657–662
 17. Rodríguez CI, Buchholz F, Galloway J, Sequerra R, Kasper J, Ayala R, Stewart AF, Dymecki SM (2000) High-efficiency deleter mice show that FLPe is an alternative to Cre-loxP. *Nat Genet* 25(2):139–140
 18. Feil R, Wagner J, Metzger D, Chambon P (1997) Regulation of Cre recombinase activity by mutated estrogen receptor ligand-binding domains. *Biochem Biophys Res Commun* 237(3):752–757
 19. Feil R, Brocard J, Mascrez B, LeMeur M, Metzger D, Chambon P (1996) Ligand-activated site-specific recombination in mice. *Proc Natl Acad Sci USA* 93(20):10887–10890
 20. Edwards WF, Young DD, Deiters A (2009) Light-activated Cre recombinase as a tool for the spatial and temporal control of gene function in mammalian cells. *ACS Chem Biol* 4(6):441–445
 21. Hirrlinger J, Scheller A, Hirrlinger PG, et al (2009) Split-cre complementation indicates coincident activity of different genes *in vivo*. *PLoS ONE* 4(1):e4286
 22. Hirrlinger J, Requardt RP, Winkler U, Wilhelm F, Schulze C, Hirrlinger PG (2009) Split-CreERT2: temporal control of DNA recombination mediated by split-Cre protein fragment complementation. *PLoS ONE* 4(12):e8354
 23. Wang P, Chen T, Sakurai K, Han B-X, He Z, Feng G, Wang F (2012) Intersectional Cre Driver Lines Generated Using Split-Intein Mediated Split-Cre Reconstitution. *Scientific Reports* 2:497-
 24. Farago AF, Awatramani RB, Dymecki SM (2006) Assembly of the brainstem cochlear nuclear complex is revealed by intersectional and subtractive genetic fate maps. *Neuron* 50(2):205–218
 25. Zong H, Espinosa JS, Su HH, Muzumdar MD, Luo L (2005) Mosaic analysis with double markers in mice. *Cell* 121(3):479–492
 26. Tasic B, Miyamichi K, Hippenmeyer S, Dani VS, Zeng H, Joo W,

- Zong H, Chen-Tsai Y, Luo L (2012) Extensions of MADM (Mosaic Analysis with Double Markers) in Mice. *PLoS ONE* 7(3):e33332
27. Lee T, Luo L (1999) Mosaic analysis with a repressible cell marker for studies of gene function in neuronal morphogenesis. *Neuron* 22(3):451–461
 28. Hippenmeyer S, Youn YH, Moon HM, Miyamichi K, Zong H, Wynshaw-Boris A, Luo L (2010) Genetic mosaic dissection of *Lis1* and *Ndel1* in neuronal migration. *Neuron* 68(4):695–709
 29. Livet J, Weissman TA, Kang H, Draft RW, Lu J, Bennis RA, Sanes JR, Lichtman JW (2007) Transgenic strategies for combinatorial expression of fluorescent proteins in the nervous system. *Nature* 450(7166):56–62
 30. Soriano P (1999) Generalized *lacZ* expression with the ROSA26 Cre reporter strain. *Nat Genet* 21(1):70–71
 31. Madisen L, Zwingman TA, Sunkin SM, et al (2010) A robust and high-throughput Cre reporting and characterization system for the whole mouse brain. *Nat Neurosci* 13(1):133–140
 32. Luo L (2007) Fly MARCM and mouse MADM: genetic methods of labeling and manipulating single neurons. *Brain research reviews* 55(2):220–227
 33. Potter CJ, Tasic B, Russler EV, Liang L, Luo L (2010) The Q system: a repressible binary system for transgene expression, lineage tracing, and mosaic analysis. *Cell* 141(3):536–548
 34. Zhang Y, Buchholz F, Muyrers JP, Stewart AF (1998) A new logic for DNA engineering using recombination in *Escherichia coli*. *Nat Genet* 20(2):123–128
 35. Sauer B, Henderson N (1988) Site-specific DNA recombination in mammalian cells by the Cre recombinase of bacteriophage P1. *Proc Natl Acad Sci USA* 85(14):5166–5170
 36. Santoro SW, Schultz PG (2002) Directed evolution of the site specificity of Cre recombinase. *Proc Natl Acad Sci USA* 99(7):4185–4190
 37. Schnütgen F, Doerflinger N, Calléja C, Wendling O, Chambon P, Ghyselinck NB (2003) A directional strategy for monitoring Cre-mediated recombination at the cellular level in the mouse. *Nat Rev*

Neurosci 21(5):562–565

38. Zheng B, Sage M, Sheppard EA, Jurecic V, Bradley A (2000) Engineering mouse chromosomes with Cre-loxP: range, efficiency, and somatic applications. *Mol Cell Biol* 20(2):648–655
39. Visel A, Minovitsky S, Dubchak I, Pennacchio LA (2007) VISTA Enhancer Browser--a database of tissue-specific human enhancers. *Nucleic Acids Res* 35:D88–92
40. Engström PG, Fredman D, Lenhard B (2008) Ancora: a web resource for exploring highly conserved noncoding elements and their association with developmental regulatory genes. *Genome Biol* 9(2):R34
41. Visel A, Blow MJ, Li Z, et al (2009) ChIP-seq accurately predicts tissue-specific activity of enhancers. *Nature* 457(7231):854–858
42. Yee SP, Rigby PW (1993) The regulation of myogenin gene expression during the embryonic development of the mouse. *Genes Dev* 7(7A):1277–1289
43. Srinivas S, Watanabe T, Lin CS, Williams CM, Tanabe Y, Jessell TM, Costantini F (2001) Cre reporter strains produced by targeted insertion of EYFP and ECFP into the ROSA26 locus. *BMC Dev Biol* 1:4
44. Hope IA, Struhl K (1987) GCN4, a eukaryotic transcriptional activator protein, binds as a dimer to target DNA. *EMBO J* 6(9):2781–2784
45. Espinosa JS, Luo L (2008) Timing neurogenesis and differentiation: insights from quantitative clonal analyses of cerebellar granule cells. *J Neurosci* 28(10):2301–2312

3.2 Unpublished Results

3.2.1 Further description of generated and analyzed transgenic lines⁶

To address the molecular and cellular aspects of precerebellar system and cortico-ponto-cerebellar circuitry development a major effort was put into the generation and characterization of novel Cre- and reporter-based transgenic mice that constitute instrumental genetic tools. Hereby the aim was to identify subsets of pontine neurons during migration and circuitry formation. These transgenic tools can not only be used to understand the development of the system but also to manipulate the expression of dedicated epigenetic modifiers, transcription factors and guidance molecules. These lines have been partially used in Di Meglio et al. (2013) to fate map the different rhombomeric contributions to the pontine nuclei as well as to conditionally knockout *Ezh2* in pontine nuclei neurons and their migratory environment.

Additionally, some of the generated transgenic mice show expression patterns in other parts of the nervous system that are potentially relevant for later work and will be described in this chapter with a major focus on other hindbrain nuclei. Furthermore, other transgenic lines that were obtained from other laboratories or created in the laboratory of Filippo Rijli will be described for their usability to analyze the development of the precerebellar system.

To screen the different *Cre* lines that have been generated using rhombomere-specific enhancers of *Hoxb3* (Yau et al., 2002) (*r5-post::Cre*), *Hoxa3* (Manzanares et al., 1999) (*r5-6::Cre*) or *Hoxb4* (Gould et al., 1997) (*r7post::Cre*), they were outcrossed to *R26R^{LacZ}* animals, in which upon Cre mediated recombination cells express β -Galactosidase. β -galactosidase is visualized by adding X-Gal, which is hydrolyzed to 5-bromo-4-chloro-3-hydroxyindole generating characteristic blue stain. The expression patterns of the 15 founders that were genotyped positively and developed staining are shown in **Figure 26**. 3/6 had the expected recombination pattern at P0 for *r5post::Cre* (**Figure 26**, E-G) ; 2/8 for *r5-6::Cre* (**Figure 26**, K-L), 1/2 for

⁶ Statement of contribution: Nathalie Vilain performed all *in utero* electroporation in this chapter. The transgenic lines *Hoxa5::Cre* and *Hoxb5::Cre* were generated by Sebastien Ducret.

r7post::Cre (Figure 26, H) and 0/3 for *r6::Cre*, while the other founders showed no (not shown), ubiquitous (Figure 26, C) or ectopic patterns (Figure 26, A-B, D, I-J, M-O) of recombination.

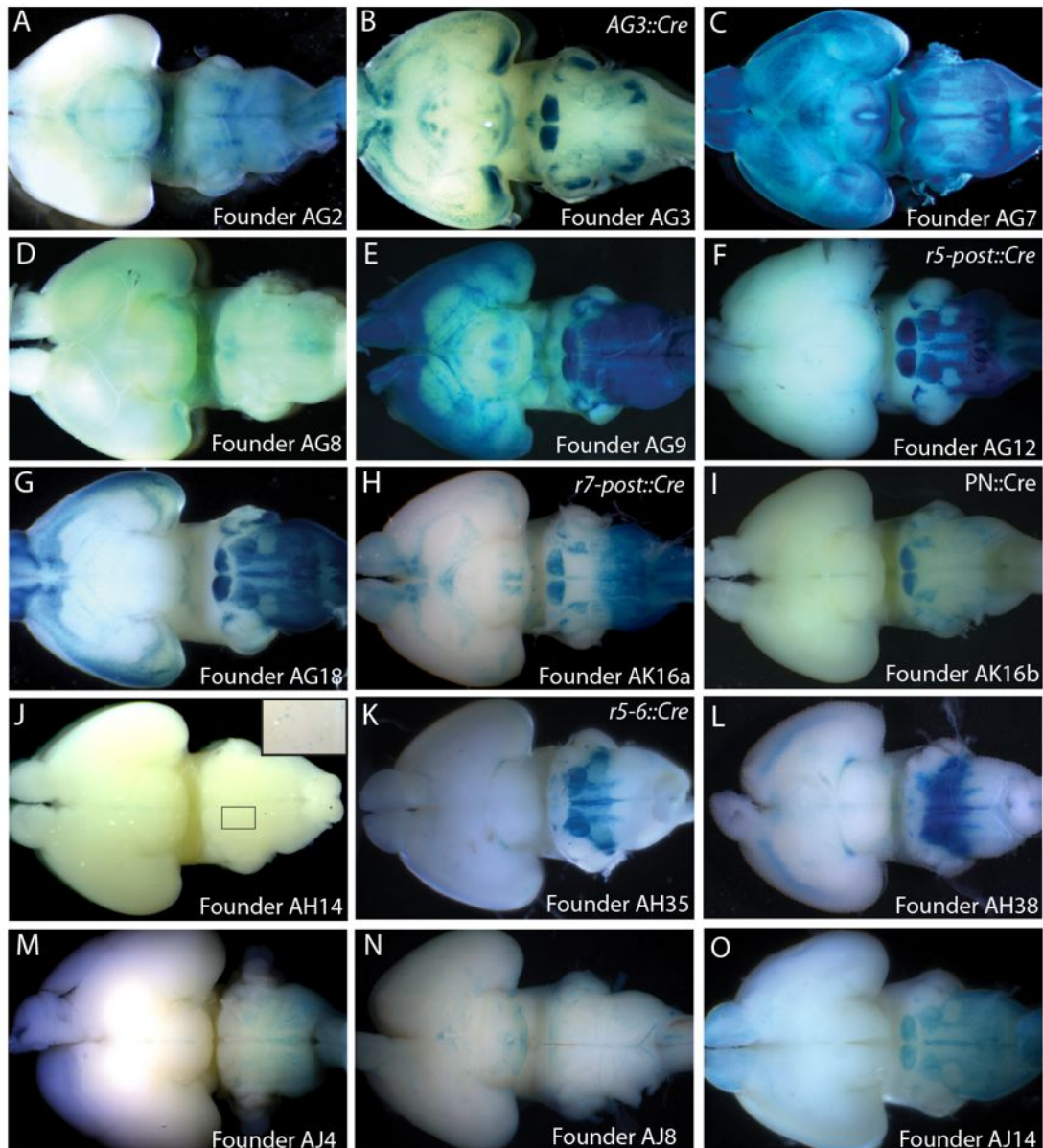


Figure 26 | Screen of outcrosses of transgenic line founders with $R26R^{LacZ}$ mice at P0. (A-M) To screen *Cre* driver line founders for their ability to recombine either the expected rhombomeres or other relevant subpopulations, founders of mice injected with *Hoxb3::Cre* (A-E), *Hoxb4::Cre* (F-G), *Hoxa3::Cre* (H-J) and *Hoxb3_mt::Cre* (K-M) were crossed to $R26R^{LacZ}$ mice, dissected at birth (P0) and revealed by X-Gal staining over night. Founders B, F, H, I and K were maintained.

Two of the founders that showed ectopic expression patterns (**Figure 26, B, I**), were kept, because their expression is specific for nuclei of the precerebellar system. They were named *AG3::Cre* (**Figure 26, B**) and *PN::Cre* (**Figure 26, I**).

Some founders show strong differences in their expression patterns depending on their insertion site. *AG3::Cre* and *r5-post::Cre*, which both have been generated with the same construct do not only show differences in their late expression pattern (**Figure 26, B, D**), but already at early stages at E12.5 (**Figure 27**).

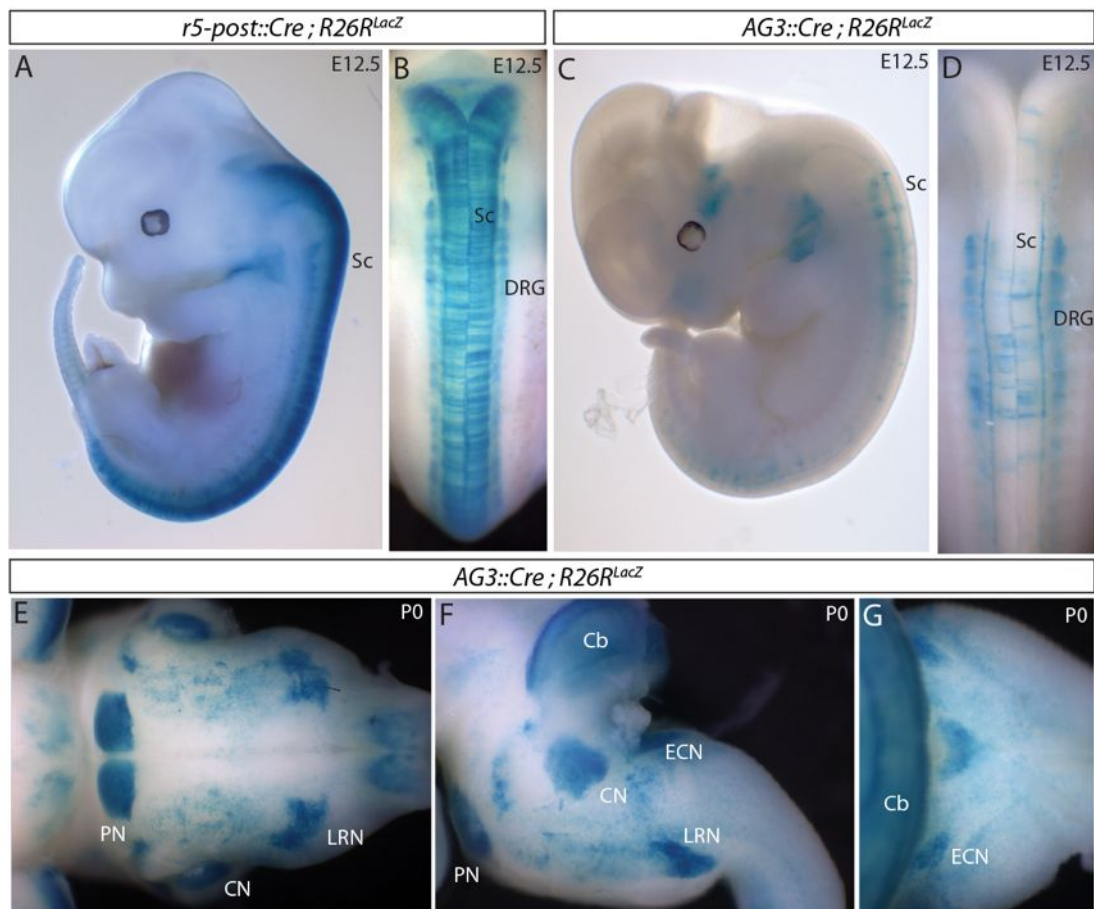


Figure 27 | Characterization of *r5-post::Cre* and *AG3::Cre*. (A-B) *r5-post::Cre ; R26R^{LacZ}* mainly express LacZ in tissues derived from the neural plate including neural crest cells. The whole spinal cord (Sc in A-B) is labeled including the dorsal root ganglia (DRG in B). (C-D) Founder *AG3::Cre* has an untypical expression pattern, differing from other founders injected with the *Hoxb3*-enhancer construct. Also here neural crest cells, as well as parts of the anterior spinal cord are labeled. (E-G) At P0 especially nuclei derived from the *Math1* domain are labeled including cerebellum (cb), pontine nuclei (PN), cochlear nucleus (CN), lateral reticular nucleus (LRN) and external cuneate nucleus (ECN) (E, ventral view; F, lateral view; G, dorsal view).

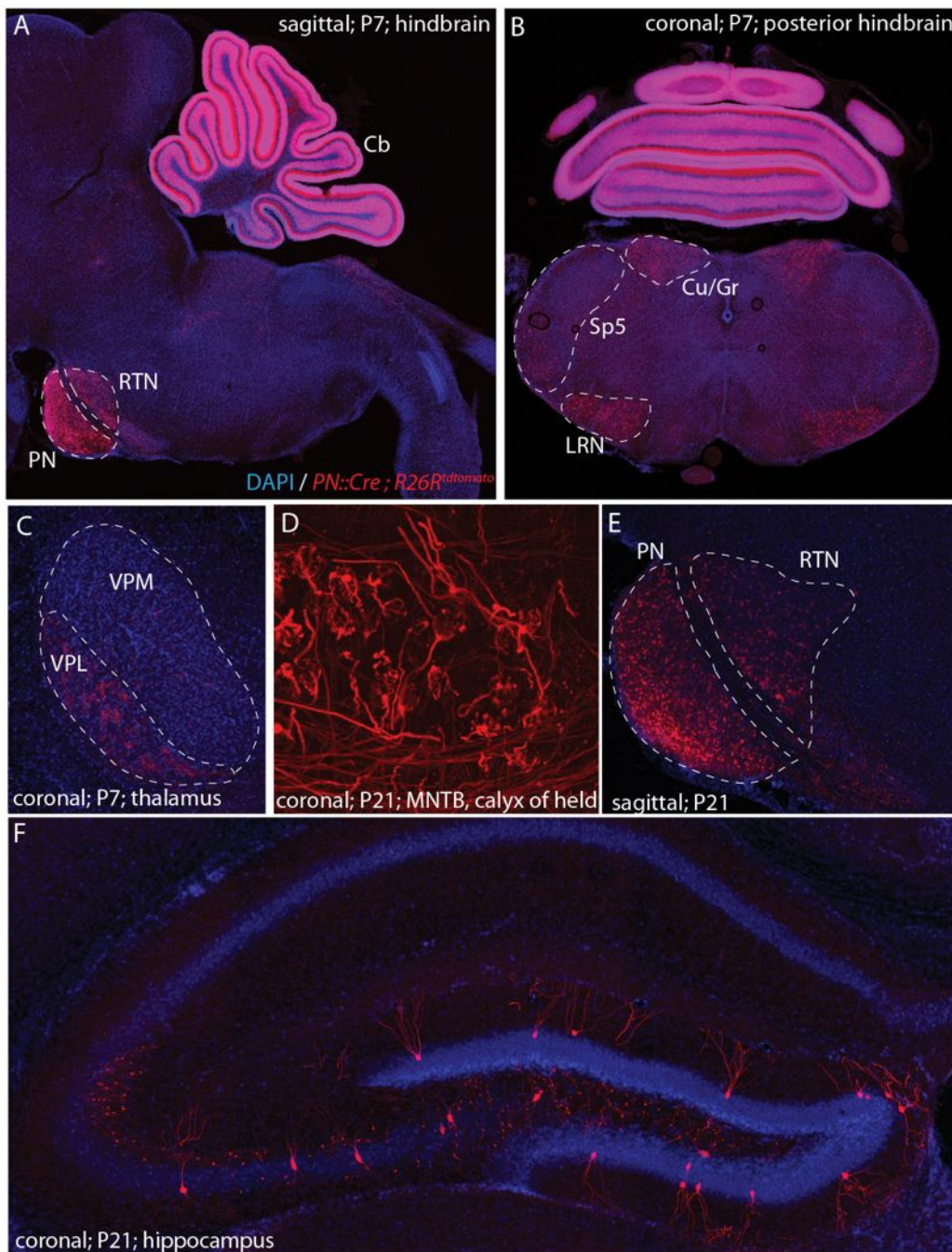


Figure 28 | Description of *PN::Cre* transgene crossed with the *R26R^{tdtomato}* reporter at postnatal stages (P7 and P21). (A, B, E) Sagittal (A, E) and coronal (B) section at P7 (A, B) and P21 (E) show that PN including reticulospinal (RTN) and basal pontine nuclei (PN) and as well as lateral reticular nuclei (LRN), spinal trigeminal nuclei (Sp5) and cuneate (Cu) and gracile (Gr) nuclei are labeled. (C, D, F) *PN::Cre*; *R26R^{tdtomato}* specimen additionally label terminals of the Sp5 in the ventral posterolateral nucleus (VPL) of the thalamus (C), the calyx of held synapses in the medial nucleus of the trapezoid body (MNTB, D) as well as subsets of granule cells in the hippocampal dentate gyrus and CA3 area (F).

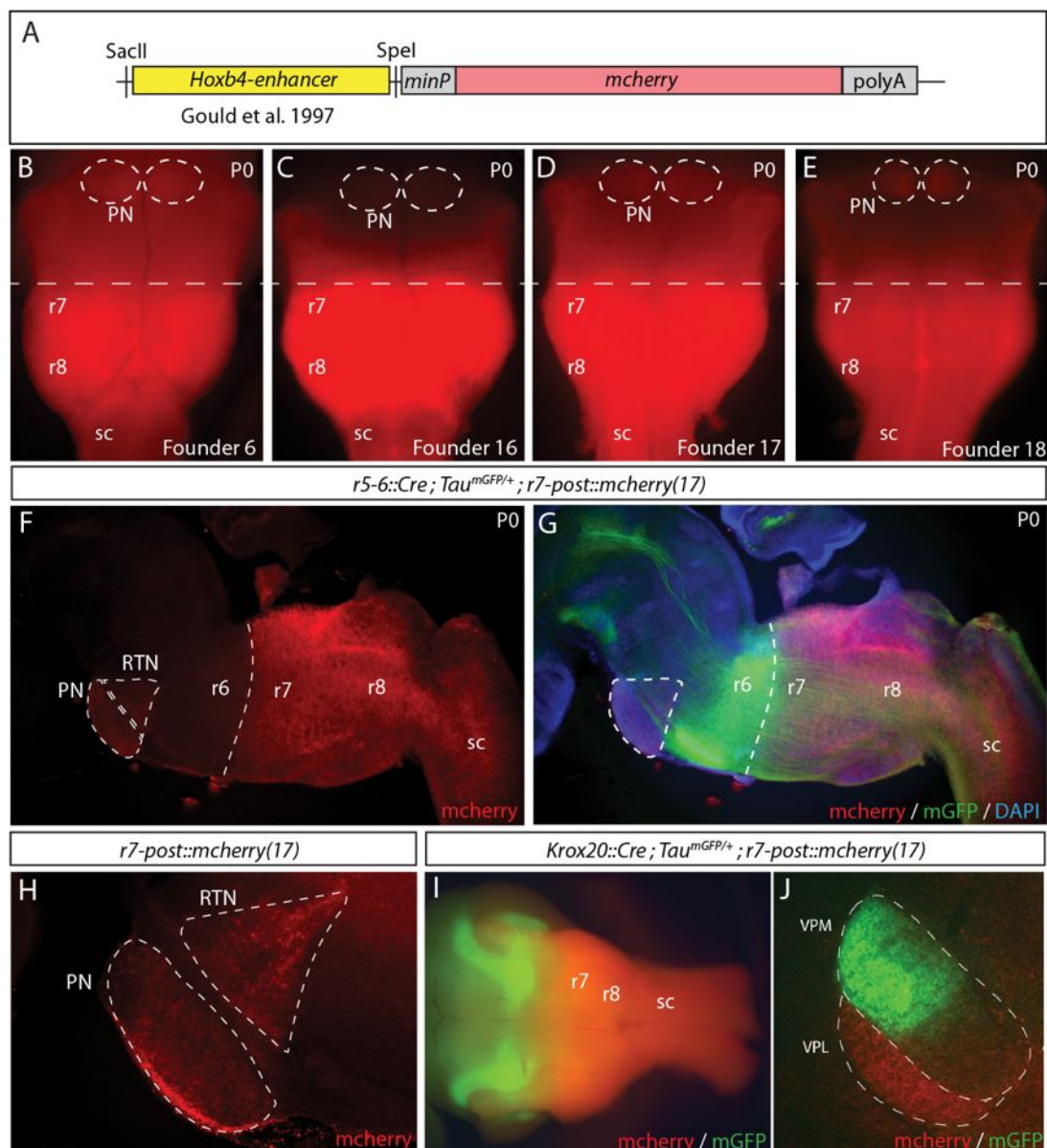


Figure 29 | Characterization of *r7post::mcherry* transgene. (A) The late neuronal enhancer of *Hoxb4* (Gould et al., 1997) was cloned in front of a minimal promoter followed by the mcherry open reading frame and polyA. (B-E) Four out of eight founders showed mcherry fluorescence in the posterior hindbrain as seen here in wholemounts at P0. Pontine Nuclei (PN) and the anterior expression boundary (dashed line) are indicated. (F-G) Sagittal sections show the restrictions to rhombomere 7-8 (r7, r8) and spinal cord (Sc). Crossing with *r5-6::Cre; Tau^{mGFP/+}*, which labels rhombomeres 5 and 6 (Di Meglio et al., 2013) further confirms the rhombomere restriction of *r7post::Cre* (G). (H) The PN are labeled as well (F-H). (I-J) Crossing with *Krox20::Cre; Tau^{mGFP/+}* also shows tiled expression in wholemount specimens (I) as well as specific targeting in the projections of principal (Pr5; green, *Krox20*⁺) and spinal trigeminal nucleus (Sp5; red, *r7post::Cre*⁺) to the VPM (from r3) and VPL (from r7 and r8) of the Thalamus.

While *r5post::Cre* is expressed throughout the whole spinal cord, including the dorsal root ganglia (DRG) and some neural crest derivatives (**Figure 27**, A-B), in *AG3::Cre* Cre expression is restricted to an anterior domain of the spinal cord and its DRGs (**Figure 27**, C-D). At P0, the pattern of *LacZ* expressing cells, resembles the expression of *Math1* (Wang et al., 2005) with labeling in precerebellar nuclei (pontine nuclei, external cuneate nucleus and lateral reticular nucleus) as well as cochlear nuclei and the granule cells of the cerebellum (**Figure 27**, E-G)

Beside *AG3::Cre* another founder, obtained by using the *Hoxb4* enhancer (Gould et al., 1997) also shows an atypical expression pattern using the conditional reporter *R26R^{tdtomato}* at P7 and P21 (**Figure 28**). Due to the pontine nuclei specific expression it was named *PN::Cre*. Beside the pontine nuclei also other precerebellar nuclei are labeled here, including the lateral reticular nuclei (**Figure 28**, B). Additionally, positive cells can be found in cerebellum, spinal trigeminal nucleus (Sp5), cuneate and gracile nucleus, cochlear nucleus and hippocampal granule cells (**Figure 28**, A-B, F). Axonal projections can be seen in thalamus (from gracile and cuneate nucleus) as well as in the superior olive (coming from the cochlear nucleus) (**Figure 28**, C-D).

A further transgenic line, *r7post::mcherry*, was generated by combining the *Hoxb4* enhancer (Gould et al., 1997) with the reporter *mcherry*, replacing in which *Cre recombinase* (**Figure 29**, A). Hereby the aim was to generate a further reporter that can be used in the background of Cre mediated recombinations. Four *mcherry* expressing founders were obtained (**Figure 29**, B-E), all showing comparable expression patterns. Similarly to *r7post::Cre*, *r7post::mcherry* is expressed posteriorly of the rhombomere 6/7 boundary (**Figure 29**, F). Crossings to *r5-6::Cre*; *Tau^{mGFP}* mice further reveal this restriction (**Figure 29**, G). Also the PN are *r7post::mcherry* positive (**Figure 29**, H). Crossing to *Krox20::Cre*; *Tau^{mGFP}*, expressed in rhombomere 3 and 5, reveals the segregated thalamic inputs from the r3/5 and r7/8 trigeminal complex to the thalamus (**Figure 29**, I-J)

Two further transgenic lines have been generated by replacing *Hoxa5* (*Hoxa5::Cre*; Di Meglio et al., 2013) and *Hoxb5* (*Hoxb5::Cre*) by *Cre recombinase* in BACs of the *HoxA* cluster and *HoxB* Cluster, respectively (**Figure 30**, **Figure 31**). Cells recombined by *Hoxa5::Cre* cover rhombomere 8 and spinal cord (**Figure 30**, A-B, Di

Meglio et al., 2013) but also, especially after birth, label cortical cells in layers V and VI (**Figure 30**, C-D). Strong projections to thalamus and cerebellum coming from hindbrain and spinal cord can be visualized as well (**Figure 30**, C, E).

Hoxb5::Cre has a more restricted expression pattern, solely covering the anterior part of the spinal cord and excluding the hindbrain and pontine nuclei (**Figure 31**, A). Thereby, *Hoxb5::Cre; R26R^{tdtomato}* mice allow the analysis of spinal cord projections to hindbrain (**Figure 31**, B), cerebellum (**Figure 31**, B-C) and thalamus (hindbrain (**Figure 31**, D). The discrepancy to the *Hoxb5* expression pattern might be due to different isoforms, which (as shown for other *Hox* genes as *Hoxa5*) have different transcripts controlled by different promoters and therefore different axial expression boundaries (Coulombe et al., 2010).



Figure 30 | Description of *Hoxa5::Cre* transgene. (A-E) Localization of *Hoxa5::Cre ; R26R^{tdtomato}* positive cells in the nervous system. As it can be seen on sagittal sections tdtomato positive cells can be mainly found in the spinal cord (Sc) as well as in the most posterior part of the hindbrain, rhombomere 8 (A-B). Furthermore, the transgene shows expression in a subset of cells in cortical (Ctx) layer V and VI as well as in the Hippocampus (Hc) (C-D). The cerebellum (Cb) is broadly innervated (E).

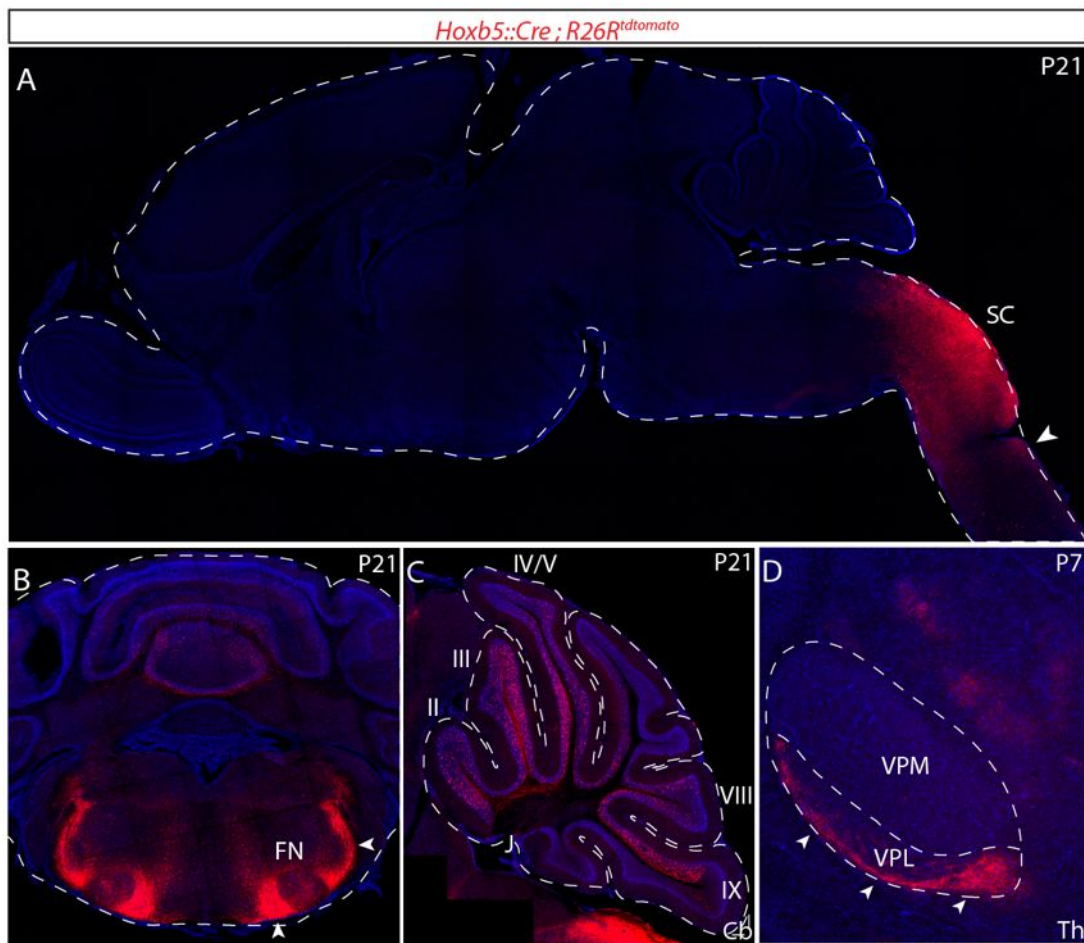


Figure 31 | Description of *Hoxb5::Cre* transgene. (A-D) In *Hoxb5::Cre ; R26R^{tdtomato}* specimen expression is more restricted than in *Hoxa5::Cre ; R26R^{tdtomato}*. Only the most anterior part of the spinal cord is labeled (posterior expression boundary labeled by arrowhead) (A). *Hoxb5::Cre ; R26R^{tdtomato}* positive projections (arrowheads) can be found on coronal sections in the facial nucleus (FN) and around the spinal trigeminal nucleus (B). Mossy fibers terminals in the cerebellum are localized to lobe II, III, IV, V, VIII and IX of the vermis as seen on sagittal sections (C). In coronal sections of the thalamus *Hoxb5::Cre ; R26R^{tdtomato}* positive fibers localize to the external part of the nucleus ventralis posterolateralis, VPL (arrowheads in D).

Many of the analyzed transgenic *Cre* lines result in recombinations of PN neurons as described in Di Meglio et al. (2013) and **Figure 32**. *R5post::Cre*, *PN::Cre*, *Math1::Cre*, *Wnt1::Cre* drivers triggers recombinations throughout the pontine nuclei, *r7post::Cre*, *r5-6::Cre* and *Hoxa5::Cre* solely in subsets of pontine neurons and *r4post::Cre* in all pontine neurons and their environment. To analyze the cortico-ponto-cerebellar circuitry the aim was to find or generate transgenic lines that drive

reporter expression in a) subsets of pontine innervating cells and b) in subsets of pontine nuclei cells. For b) it was especially important to obtain no expression in the cerebellum itself and to label a minimum of other non-pontine cells recombined that also have mossy fiber or parallel fiber projections to the cerebellum.

For the analysis of the cortical input two lines were found to be the most interesting. *Emx1::Cre* (Gorski et al., 2002) labels all cortical neurons and therefore the major input to the pontine nuclei (**Figure 32**, A-D). A second transgene, *Pcp2::Cre* (Lewis et al., 2004) recombines parts of the posterior cortex (including visual cortex) as well as cerebellar Purkinje cells (for which the line was generated in the first place) (**Figure 32**, E-H).

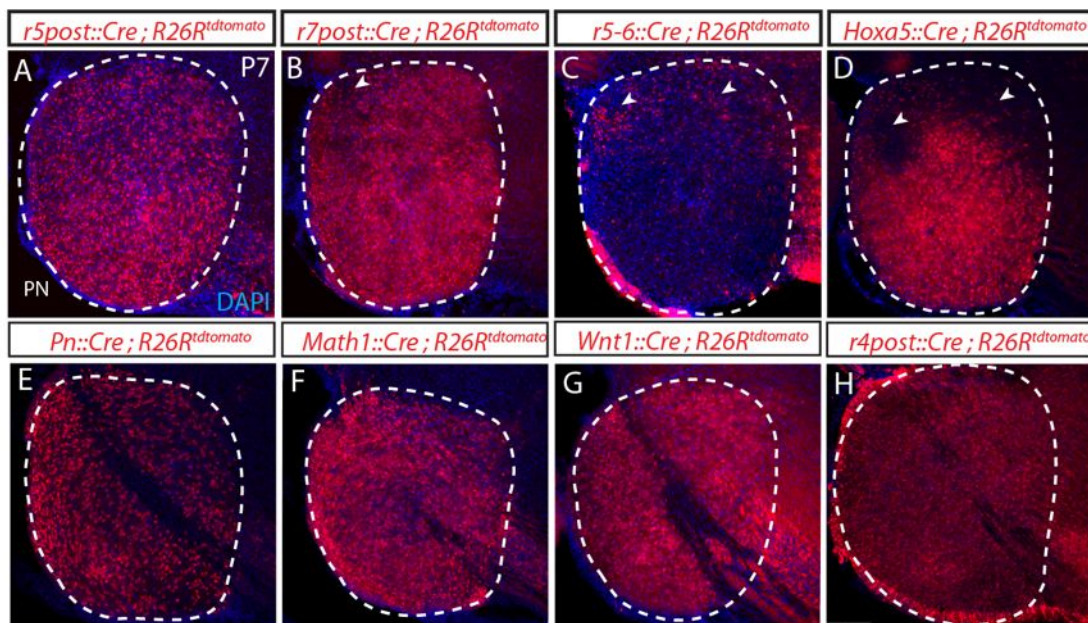


Figure 32 | Genetic tools to label pontine nuclei, their environment and to show their composition. (A-H) To test the ability of the different Cre drivers to recombine PN cells and their surrounding, they were crossed to $R26R^{tdTomato}$ reporter mice. All Cre-drivers are able to recombine PN cells as shown here on sagittal sections, while $r7post::Cre; R26R^{tdTomato}$ (B), $r5-6::Cre; R26R^{tdTomato}$ (C) and $Hoxa5::Cre; R26R^{tdTomato}$ (D) labeled distinct subsets. Anterior cells are not labeled in $Hoxa5::Cre; R26R^{tdTomato}$ and less in $r7post::Cre; R26R^{tdTomato}$ (arrowheads in D and B) but in $r5-6::Cre; R26R^{tdTomato}$ (arrowhead in C). In $Wnt1::Cre; R26R^{tdTomato}$ (G) and $r4post::Cre; R26R^{tdTomato}$ (H) *tdTomato* is also strongly expressed in the environment. $R5post::Cre$ (D), $PN::Cre$ (E) and $Math1::Cre$ (F) recombined PN cells, but not the juxtaposed environment.

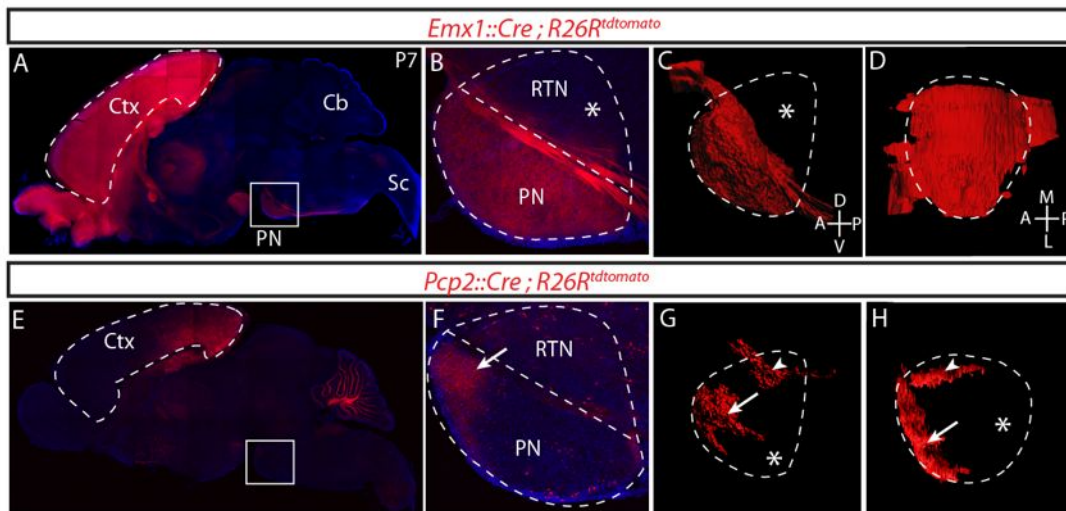


Figure 33 | Innervation of the pontine nuclei by *Emx1::Cre* and *Pcp2::Cre*. (A-D) The pontine nuclei (PN) show broad innervation from the cortex (Ctx), labeled by *Emx1::Cre* as shown on sagittal sections (A). The complete PN is innervated excluding the reticulotegmental nucleus (RTN, asterisk) as it can be seen on sagittal sections as well as reconstructions (lateral view (C) and ventral view (D)). (E-H) *Pcp2::Cre* labels cell of the posterior cortex including visual cortex as it can be seen on sagittal sections (E) and reconstructions from lateral (G) and ventral (H). The innervation is restricted to the anterior part of the nucleus (arrow) and excluded from the posterior (asterisk). A further innervation can be seen in the dorso-medial RTN (arrowhead), which might come from the *Pcp2::Cre* positive purkinje cells, since these projections can't be reproduced by viral tracing from the cortex.

Interestingly, *Emx1::Cre; R26R^{tdtomato}* solely innervates the pontine nuclei and its projections exclude the reticulotegmental nucleus (RTN) (Figure 33, A-D), although it was shown to be innervated by cortical areas in other mammals as e.g. monkeys (Ono and Mustari, 2008). The innervation from the *Pcp2::Cre; R26R^{tdtomato}* positive fibers converges on the anterior pontine gray as reported in Di Meglio et al. (2013). A second zone of innervation lies in the dorsal RTN and due to the fact that these fibers can not be seen in *Emx1::Cre; R26R^{tdtomato}* specimens this projection most likely originates in a non-cortical area. It might be speculated, that it constitutes a feedback-circuit from the cerebellar purkinje fibers that are strongly labeled in *Pcp2::Cre; R26R^{tdtomato}* specimen. Those feedback-circuits (although described as coming from the deep cerebellar nuclei) have been previously described (Schwarz and Schmitz, 1997).

For the pontine neurons, most lines that have been screened show either expression in cerebellar granule cells (*PN::Cre*, *Math1::Cre*, *Wnt1::Cre*) and/or in other mossy fiber/ climbing fiber nuclei (*r5post::Cre*, *r7post::Cre*, *Hoxa5::Cre*; *Wnt1::Cre*, *PN::Cre*, *Math1::Cre*) or have postnatally ectopic expression (*r5-6::Cre*). Therefore these transgenes cannot be used for an in-depth analysis of pontine neuron mossy fiber projections.

Solely two lines, *ChAT::Cre*, a knockin into the *ChAT* locus (Lowell et al., 2006) and *MafB::CreERT2* a BAC transgene in which *MafB* is replaced with *Cre* (Di Meglio et al., 2013) fulfill the requirements of a high specificity to pontine neurons mossy fibers and restriction to a subset of pontine neurons.

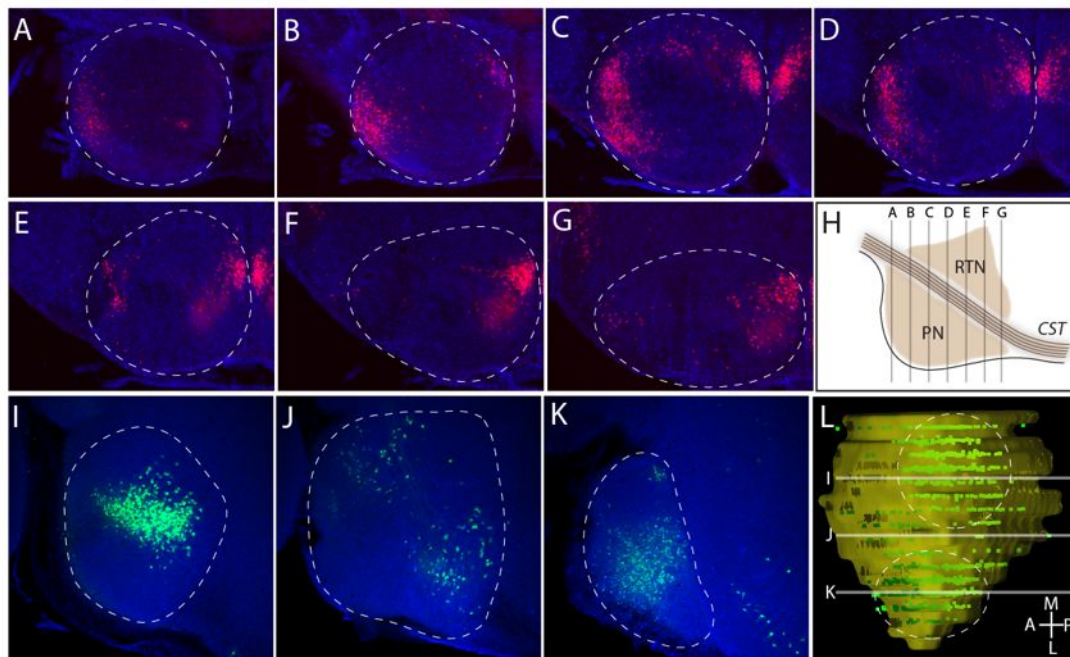


Figure 34 | Characterization of *ChAT::Cre* expressing cells in the pontine nuclei. (A-L) *ChAT::Cre* ; *R26R^{tdtomato}* (A-G)/ *ChAT::Cre* ; *R26R^{ZsGreen}* (I-K) positive cells have a strong restriction in the pontine nuclei (PN). They can be separated into one medio-central domain and one lateral domain. Especially the medio-central domain involves as well part of the reticulotegmental nucleus (RTN) and not just of the basal pontine gray (PGN) as it can be seen on coronal sections (A-G), sagittal sections (I-K) and in 3D-reconstruction from a ventral view (L).

The *ChAT* gene encodes the enzyme Choline acetyltransferase that drives the synthesis of the neurotransmitter acetylcholine by catalyzing the reaction of Acetyl-CoA and choline to acetylcholine and coenzyme A. Choline acetyltransferase and

ChAT::Cre are therefore expressed in cholinergic neurons including motor neurons in hindbrain and spinal cord as e.g. the facial nucleus. Also neurons in the basal forebrain, midbrain and dorsal pons express *ChAT* (Lowell et al., 2006; Madisen et al., 2010; Schäfer et al., 1998). Interestingly, subsets of pontine neurons express Cre in the *ChAT::Cre* background (**Figure 34**), although they lack expression of ChAT itself (Henry and Hohmann, 2012; Schäfer et al., 1998).

ChAT positive pontine cells are distributed into two segregated populations, one medial population in close proximity to the midline and one lateral population (**Figure 34, A-L**). Cells start to express the floxed reporter (in this case $R26R^{tdtomato}$) at P0 (data not shown). Their identity as pontine neurons was confirmed by *in utero* electroporation (Chapter 3.2.2). While the medial population localizes in a medial part of the RTN, the lateral population might be part of the pontine nuclei, more specifically the dorso-lateral pontine nucleus (DLPN).

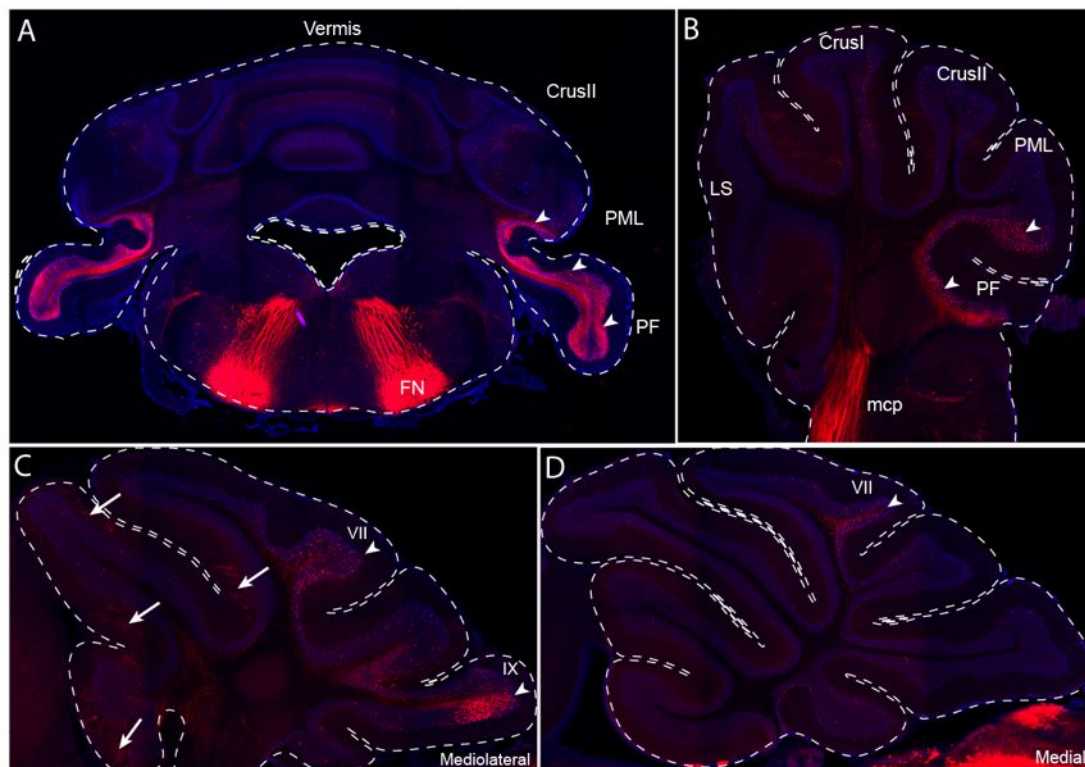


Figure 35 | Characterization of *ChAT::Cre* positive fibers in the cerebellum. (A-D) Distribution of *ChAT::Cre ; R26R^{tdtomato}* positive fibers in the cerebellum. Coronal sections (A) show the strong innervation in paramedian lobe (PML) and paraflocculus (PF). This can be confirmed by sagittal sections at lateral (B), mediolateral (C) and

medial levels (D). At more medial levels also lobe IX and VII have tdtomato positive mossy fibers. In the anterior lobes (arrows) scattered climbing fibers can be seen (C).

Interestingly, also the mossy fiber terminals in the cerebellum are restricted to specific lobes. While the highest density of mossy fiber terminals can be found in the lateral cerebellum, especially in paramedian lobe and paraflocculus, the vermis was poorly innervated with solely some mossy fibers projecting to lobe VII and IX (**Figure 35, A-D**). Although it might be doubted that all of these fibers originate from the pontine nuclei, this segregation was striking. Further experiments in which *ChAT::Cre* animals were electroporated *in utero*, which will be discussed in the next subchapter (Chapter 3.2.2), give further insights into the connectivity of *ChAT::Cre* expressing pontine neurons. Additionally also recombined climbing fibers can be seen in the cerebellum that are mainly located in the anterior part of the vermis (lobe I-VI, **Figure 35, C**).

The second line, *MafB::CreERT2* that has been partially described in (Di Meglio et al., 2013), labels the rhombomere 6 derived pontine neurons in as similar way as the *r5-6::Cre* driver. Indeed *MafB* is the gene that regulates the rhombomere 5 and 6 specific expression of the *Hoxa3* enhancer used for the generation of the *r5-6::Cre* transgene (Manzanares et al., 1999). Due to the fact, that the expression of *Cre* can be tightly regulated by the tamoxifen injection at E7.5, this transgenic line is less receptive to expression in other areas, illustrated by the very confined expression in rhombomere 5 and 6 (**Figure 36**). Solely some glia cells in the flocculus of the cerebellum, which might be even derived from rhombomere 5/6, express the recombined reporter in an unexpected manner (**Figure 37, B**).

Similar to *r5-6::Cre* animals, recombined cells strictly localize in the anterior and anterior-lateral part of the pontine nuclei as it can be seen on sagittal sections (**Figure 36, A-C**) and 3D-reconstructions (**Figure 36, D-E**). Also for the *MafB::CreERT2* transgene two slightly segregated populations exist in the medio-anterior and in the dorso-lateral pontine nuclei. Due to the sparse labeling in *MafB::CreERT2* specimen, also dendritic organizations can be analyzed (**Figure 36, F**). The population in the dorso-lateral pontine nuclei is in a similar location as the lateral population in *ChAT::Cre* specimen.

In contrast to *Chat::Cre* specimens, the connectivity of the *MafB::CreERT2* progeny mossy fibers is slightly more dispersed in the cerebellum (**Figure 37**, A-F). This is characteristic for medial levels of the vermis, where low numbers of terminals can be seen in all lobes (**Figure 37**, A, C, E). Despite the disperse projections to the vermis there is a strong and localized innervation to the paraflocculus (**Figure 37**, B, C-D, F). Thereby, *MafB::CreERT2* and *Chat::Cre* positive cells and fibers seem to share a similar region in the pontine nuclei (dorso-lateral part; DLPN) and a similar target area in the cerebellum (paraflocculus).

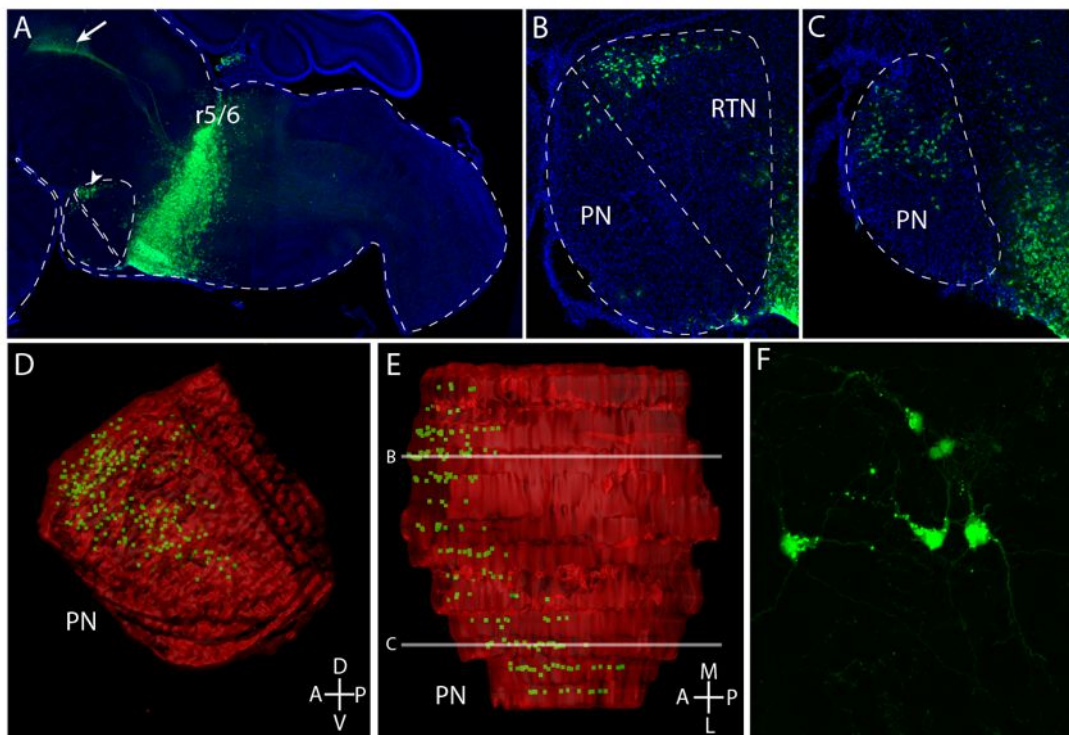


Figure 36 | Characterization of *MafB::CreERT2*. (A) Localization of recombined cells in a sagittal section of a *MafB::CreERT2* ; *R26R^{ZsGreen}* specimen injected with 1mg Tamoxifen at E7.5. Cells localize to rhombomere 5 and 6. Furthermore, cells can be found in the anterior pontine nuclei (PN) and reticulotegmental nucleus (RTN) (arrowhead). A prominent projection to interstitial nucleus of Cajal can be seen as well (arrow). (B-C) Localization inside the PN on a medial (B) and more lateral (C) section. Cells mainly localize to the anterior and lateral part of the PN/RTN. (D-E) Reconstruction of the ZsGreen-positive cells inside the PN from a lateral (D) and ventral (E) view. (F) High resolution picture of ZsGreen positive PN cells.

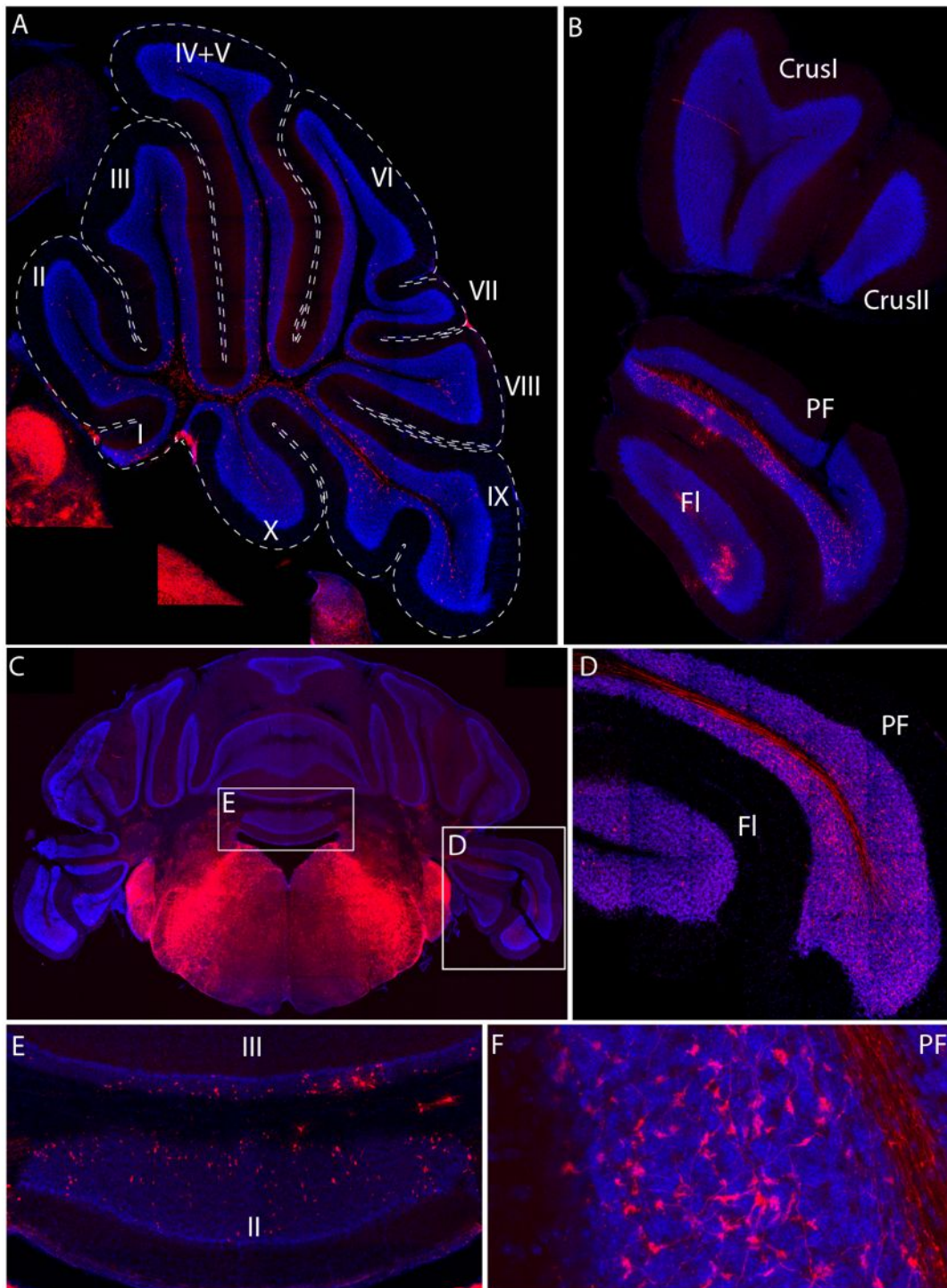


Figure 37 | Cerebellar connectivity of *MafB::CreERT2*; *R26R^{tdTomato}* positive cells. (A) Solely a small number of mossy fiber terminals can be seen on sagittal sections at the level of the vermis. They are mostly scattered in lobes I-V and VIII-X. (B) At lateral levels a higher number can be seen in the paraflocculus (PF), some in the flocculus (FL) and almost none in Crus I-II. (C-F) The high number of synapses in PF can be confirmed by looking at coronal section.

3.2.2 Combination of *in utero* electroporation and genetic tools to assess pontine nuclei connectivity

Chat::Cre and *MafB::CreERT2*, if crossed to reporters, are useful tools to analyze the behavior of subsets of hindbrain mossy fibers. To understand better the targets of pontine fibers, constructs for *in utero* electroporation had to be optimized to be able to analyze projections. If embryos are electroporated at E14.5 mainly neurons at the caudal rhombic lip are transfected. The only part of the precerebellar system, which is labeled at this specific time are the pontine nuclei (Okada et al., 2007). To better visualize the position of nuclei, axons and synapses, three constructs were electroporated: A *tdtomato* with a nuclear localization signal (NLS-tdtomato) to label the cell body / cell nuclei position, a *GFP* with a membrane-localization tag of the MARCKS (myristoylated alanine-rich protein kinase C substrate) protein (MARCKS-GFP/mGFP) (De Paola et al., 2003) and a Synaptophysin-tdtomato fusion protein that localizes to the synapses in the cerebellum (**Figure 38**, **Figure 39**).

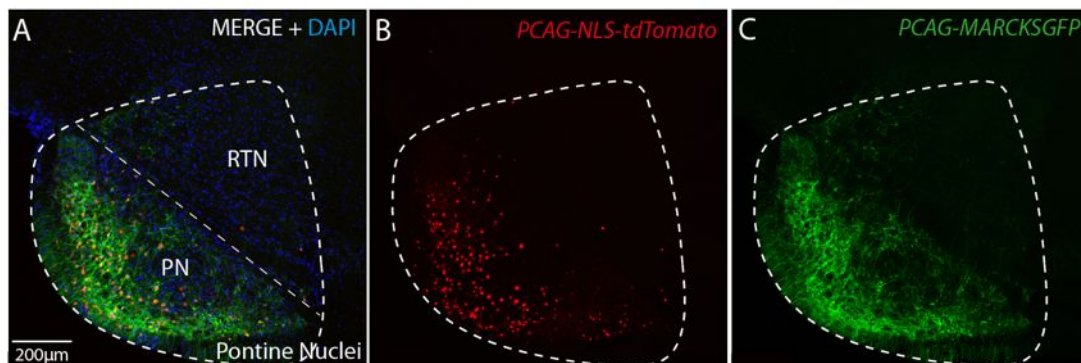


Figure 38 | *In utero* electroporation as a tool to analyze ponto-cerebellar circuitry I. (A-C) Embryos were electroporated with NLS-tdtomato, synaptophysin-tdtomato and mGFP at E14.5 and analyzed at P21. Electroporated cells are mainly located in the outer layers of the pontine nuclei as seen here on sagittal sections. NLS-tdtomato localized to the nucleus of the cells (A-B), while mGFP was also visible in the axonal projections.

Using this approach it is possible to track distribution and structure of cells (**Figure 38**, A-C), axons (**Figure 38**, **Figure 39**) and synapses (**Figure 39**, A-L) on sagittal sections of P21 animals, 25 days after electroporation. As expected NLS-tdtomato localizes to cell nuclei (**Figure 38**, A-C), Synaptophysin-tdtomato to synapses (the mossy fiber rosettes) (**Figure 39**, G-L).

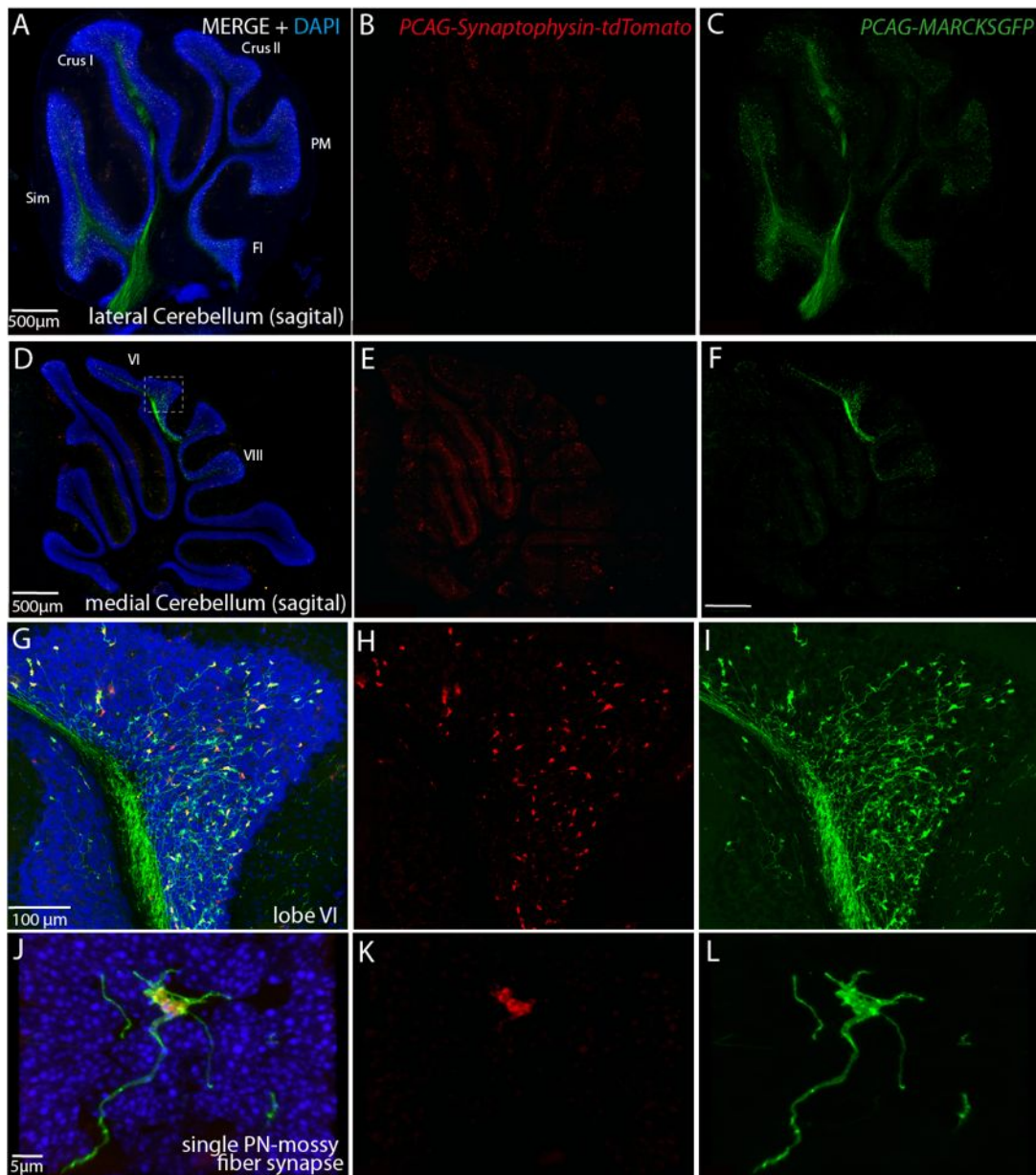


Figure 39 | *In utero* electroporation as a tool to analyze ponto-cerebellar circuitry I. (A-F) Distribution of mossy fiber terminals localization of synaptophysin-tdtomato (A-B, D-E) and mGFP (A, C, D, F) visualized by medial sagittal sections (D-F) and lateral sagittal sections (A-C). (G-L) Higher resolution pictures show the localization in lobe VI (G-I) and the localization of the mGFP construct and the synpophysin-tdtomato construct at the level of one synapse (J-L).

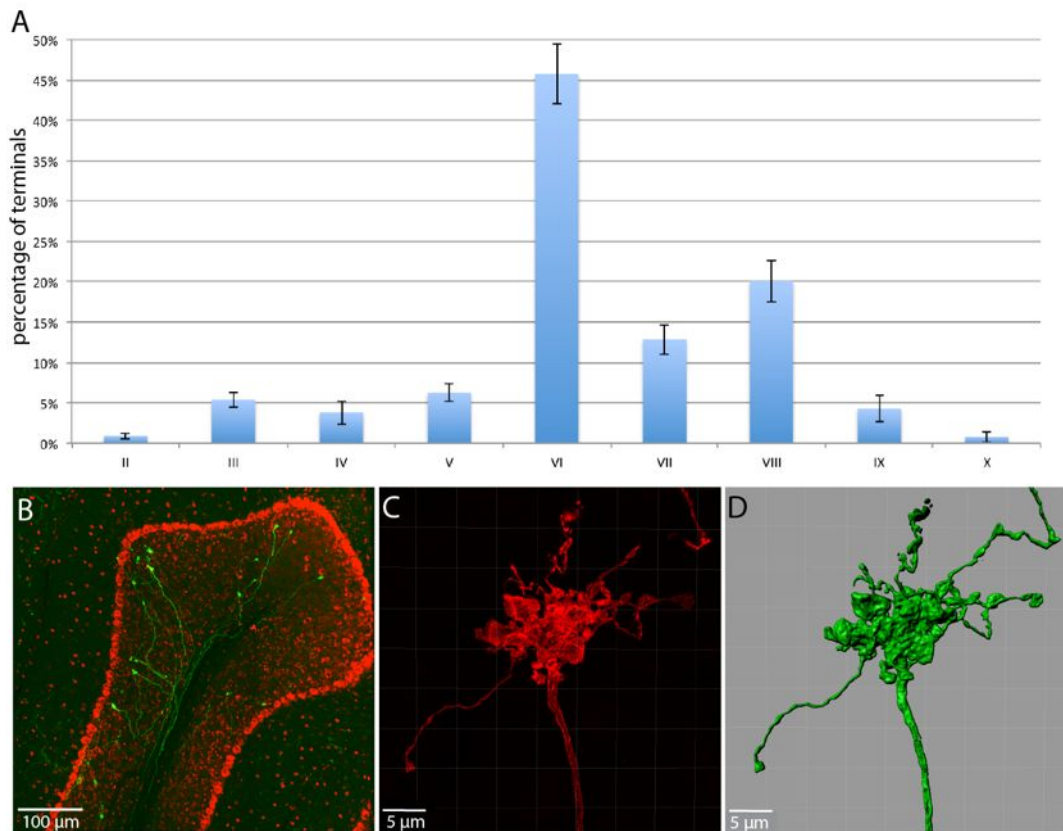


Figure 40 | *In utero* electroporation as a tool to analyze lobe specificity of projections and mossy fiber rosette morphology. (A) *In utero* electroporation allows to analyze the lobe specificity of pontine mossy fibers and gives reproducible results. Here in three cases mossy fiber terminals of embryos electroporated at E14.5 were analyzed at P21 (n=3). Synapses were counted at medial sections and the percentages of terminals per lobe were calculated. Errorbars indicate standard deviation. (B) Example of a more sparsely labeled mossy fibers in lobe V. Red counterstain is a fluorescent nissl staining. (C-D) Furthermore, PN mossy fiber terminals can be analyzed at a very high resolution and reconstructed in 3D. The picture on the left side was taken with a 63x objective, deconvoluted and then reconstructed in Imaris (right picture). PN cells were electroporated at E14.5 with pCAG::Marcks-GFP and analysed at P21.

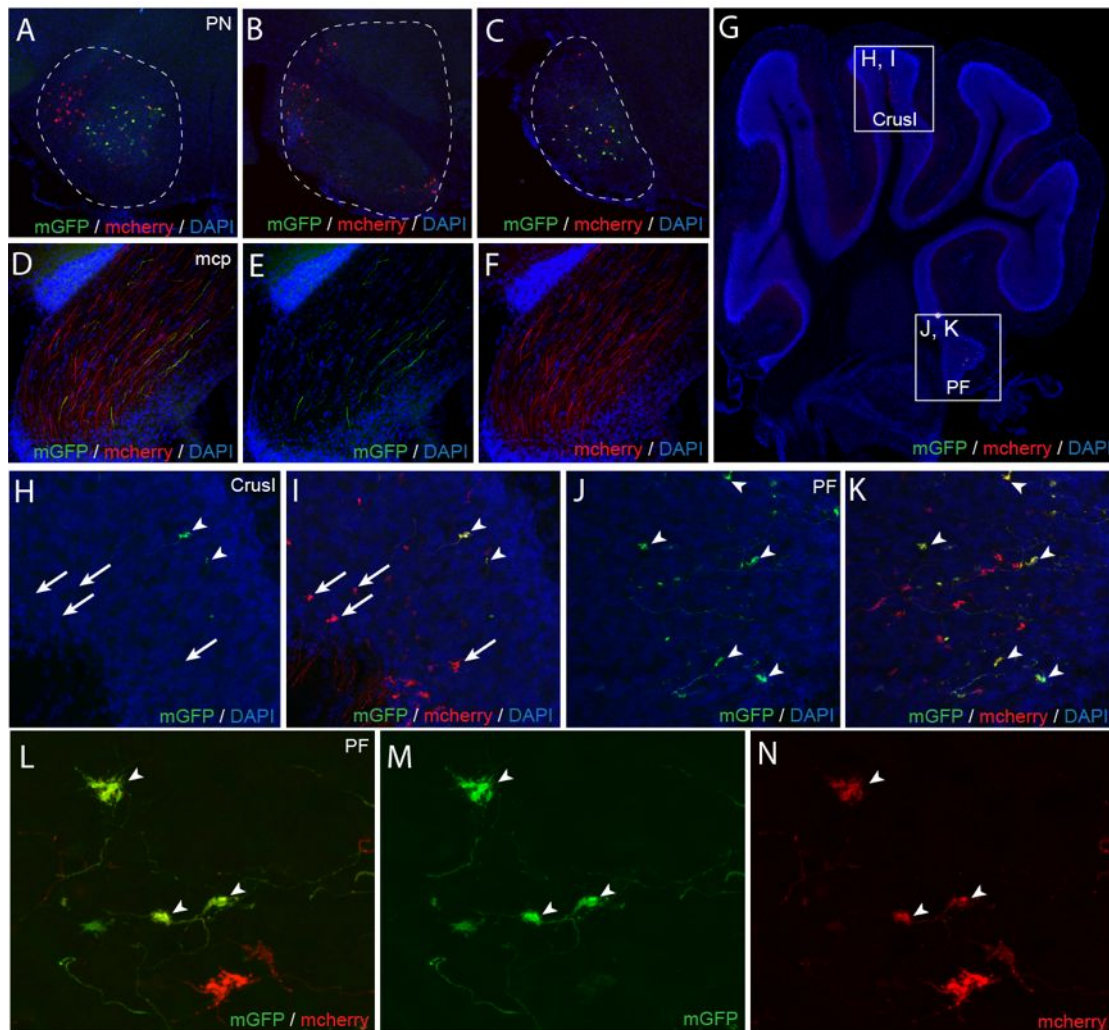


Figure 41 | Characterization of the connectivity of *ChAT::Cre* positive pontine neurons. (A-C) To see the localization of *ChAT::Cre* expressing neurons from the pontine nuclei (PN), Embryos were coelectroporated with Flex-mGFP and mCherry at E14.5 and analyzed at P21. GFP is expected to be only recombined and expressed in *ChAT::Cre* expressing cells in medial and lateral PN (A, C), while mcherry cells are scattered over the nucleus (A-C). (D-F) Projections to the cerebellum are partially segregated with GFP positive fibers more localized to the posterior part of the middle cerebellar peduncle in contrast to mcherry positive fibers. (G-K) GFP positive mossy fiber rosettes (synapses) are absent in the vermis, but can be observed in lateral sections. Most GFP/mcherry positive synapses can be found in the paraflocculus (PF, arrowheads in J-K), while only very few rosettes are GFP/mcherry positive in the Crus I lobe (arrowheads H-I) where most express solely mcherry (arrows H-I). (L-M) High resolution pictures of synapses in the paraflocculus showing colocalization (arrowheads).

These tools do not only allow the high-resolution analysis of mossy fiber and mossy fiber rosette structures (Figure 39, G-L; Figure 40, C-D), but also the analysis of the gross projection pattern of pontine derived mossy fibers. As it can be seen on sagittal

sections, most pontine fibers project to lobus simplex, Crus I and to lobe VI of the vermis (**Figure 39**, A-F). These results are reproducible and can be quantified by counting Synaptophysin-tdtomato positive rosettes and calculating their relative number per lobe (**Figure 40**, A; n=3).

To find out first, if the *ChAT::Cre* cells derive from the rhombic lip and second to estimate, where the *ChAT::Cre* positive pontine nuclei subset projects to, *in utero* electroporation of *mcherry* and *FLEX-GFP* (GFP with double inverted lox sites; see also chapter 3.1.5) was performed in *ChAT::Cre* animals.

Coelectroporation of *mcherry* and *FLEX-mGFP* reveals that both *ChAT::Cre* positive subpopulations can be targeted by *in utero* electroporation. In both lateral and medial *ChAT::Cre* positive areas, cells are found that show *mcherry* expression as well as expression of the recombined *mGFP* (**Figure 41**, A, C). On the other hand, central cells solely express *mcherry* (**Figure 41**, B).

In the cerebellar peduncle (the axon bundle going from pontine nuclei to cerebellum) *mGFP* positive fibers are evidently more localized in the caudal part of the peduncle, while *mcherry* positive fibers spread all over. In the cerebellum all rosettes at the level of the vermis are negative for *mGFP*, but express *mcherry* (data not shown). At lateral levels, *mGFP* positive fibers can be found in paraflocculus and paramedian lobe (**Figure 41**, G-I) and in lower numbers in Crus I (**Figure 41**, G, J-N).

This data suggests that the *ChAT::Cre* pontine fibers project to the lateral cerebellum and therefore to the lobes that are in general strongly innervated by *ChAT::Cre* positive fibers. Since both *ChAT::Cre* positive pontine nuclei populations are labeled by the electroporation, it is unclear, if they each of them project to similar areas or have specific termination zones.

Regarding the progeny of *MafB::CreERT2* positive cells in the pontine nuclei, there is evidence that their fibers project mainly to the paraflocculus of the cerebellar hemispheres. Main arguments are hereby that other lobes of the cerebellum that are strongly innervated by the pontine nuclei have very low numbers of *MafB::CreERT2*; *R26R^{tdtomato}* positive rosettes (**Figure 37**). To confirm this hypothesis, *MafB::CreERT2*; *R26R^{tdtomato}* embryos would have to be electroporated with a GFP vector to screen for GFP/tdTomato terminals (terminals originating from the

MafB::CreERT2 positive progenitors derived pontine neurons). However up to now this experiment did not give any results due to an increased abortion (that can be explained by the combination of tamoxifen treatment and *in utero* electroporation, both increasing the rate of abortion).

To get further insights into the role of transcription factors and guidance factors a system had to be established that is able to address their cell-autonomous role for ponto-cerebellar circuit formation. Although it is possible to obtain coexpression rates of over 80% by coelectroporation of plasmids (Loturco et al., 2009), a system that expresses constructs from the same promoter with the same efficiency would be preferential. Conventional approaches make use of internal ribosomal entry sites (IRES) to express a second gene, i.e. to combine the overexpression of a gene with a reporter. Disadvantage of this system is the low expression of the gene downstream of the IRES site. This can be overcome by the generation of multicistronic constructs using the selfcleaving 2A peptides of the picornavirus that are able to efficiently translate two or more genes (Szymczak et al., 2004).

A vector (*pCAG-MARCKS-GFP-2A-NLS-mcherry*) with an improved version of MARCKS-GFP (improved with mammalian codon usage) followed by the 2A peptide and NLS-mcherry was generated to test this system. When embryos were electroporated with this construct, all cells were coexpressing the two proteins with MARCKS-GFP localized at the membrane and NLS-mcherry localized in the nucleus (**Figure 42 A-I**), illustrating that both proteins are successfully translated and that the peptide chain is cleaved mediated by the 2A sequence.

This system is therefore an appropriate system to analyze ponto-cerebellar connectivity by now replacing the NLS-mcherry sequence of *pCAG-MARCKS-GFP-2A-NLS-mcherry* by a a) Cre-recombinase electroporated in homozygote conditional mutants or b) a gene of interest that will be thereby overexpressed (**Figure 42, J**).

The approach has the advantage that now all MARCKS-GFP positive fibers express *Cre* (and thereby generate a conditional knockout) or overexpress a gene of interest. It is even possible to combine the construct with *pCAG-mcherry* as an internal control allowing a comparison between *mcherry⁺/GFP⁻* fibers (that should behave normally) and *GFP⁺* fibers (that might possess a phenotype).

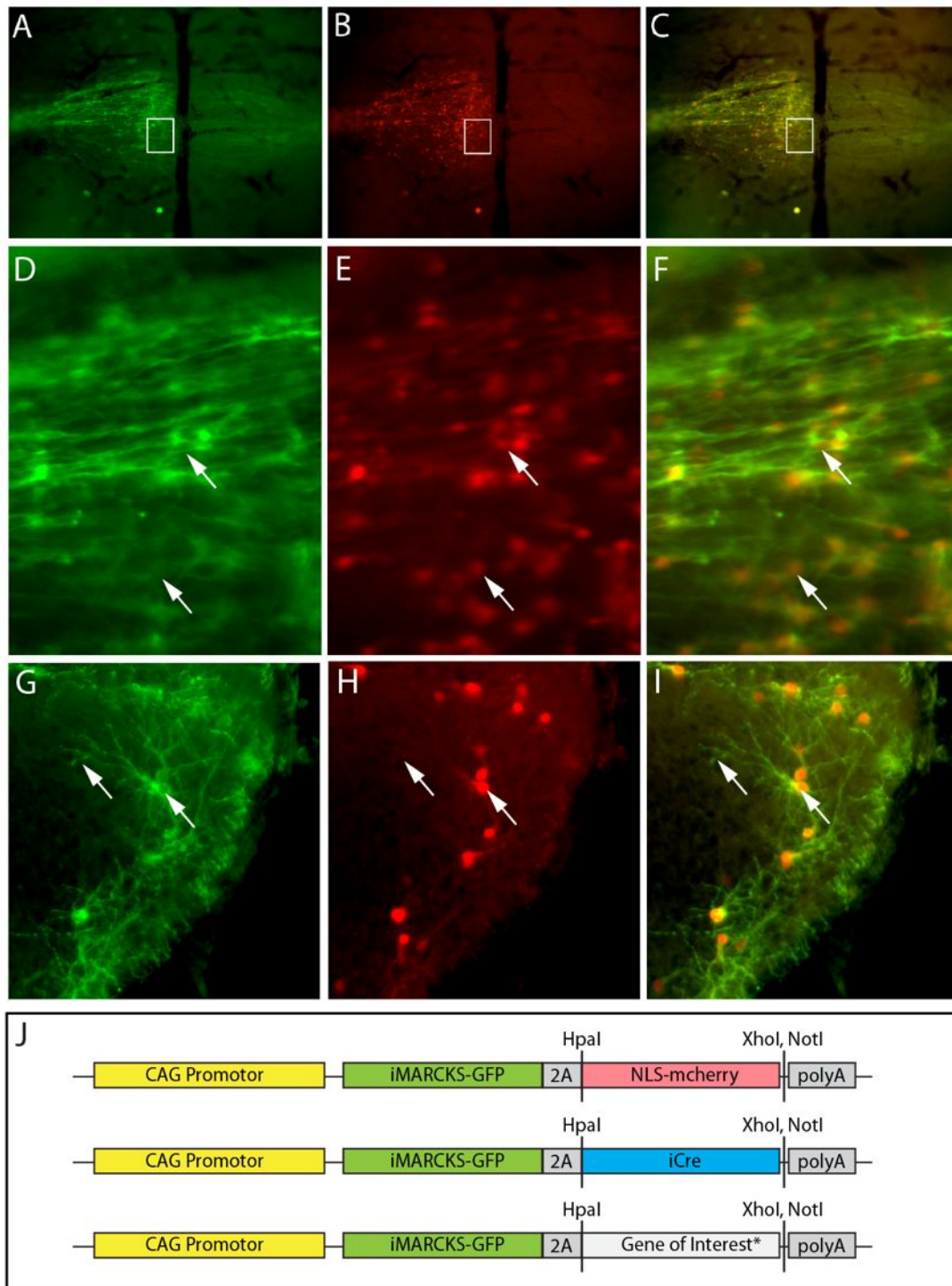


Figure 42 | Coexpression of *in utero* electroporated genes by using 2A-peptide technology. (A-I) To effectively express a reporter and a second gene of interest, constructs with MARCKS-GFP and NLS-mcherry separated by a 2A sequence were designed. All electroporated cells coexpressed GFP and mcherry as it can be seen in ventral views of wholemounts (A-F) and sagittal sections (G-I). (J) This can be now used to robustly overexpress e.g. Cre (to induce the recombination of conditional knockouts) or genes of interest.

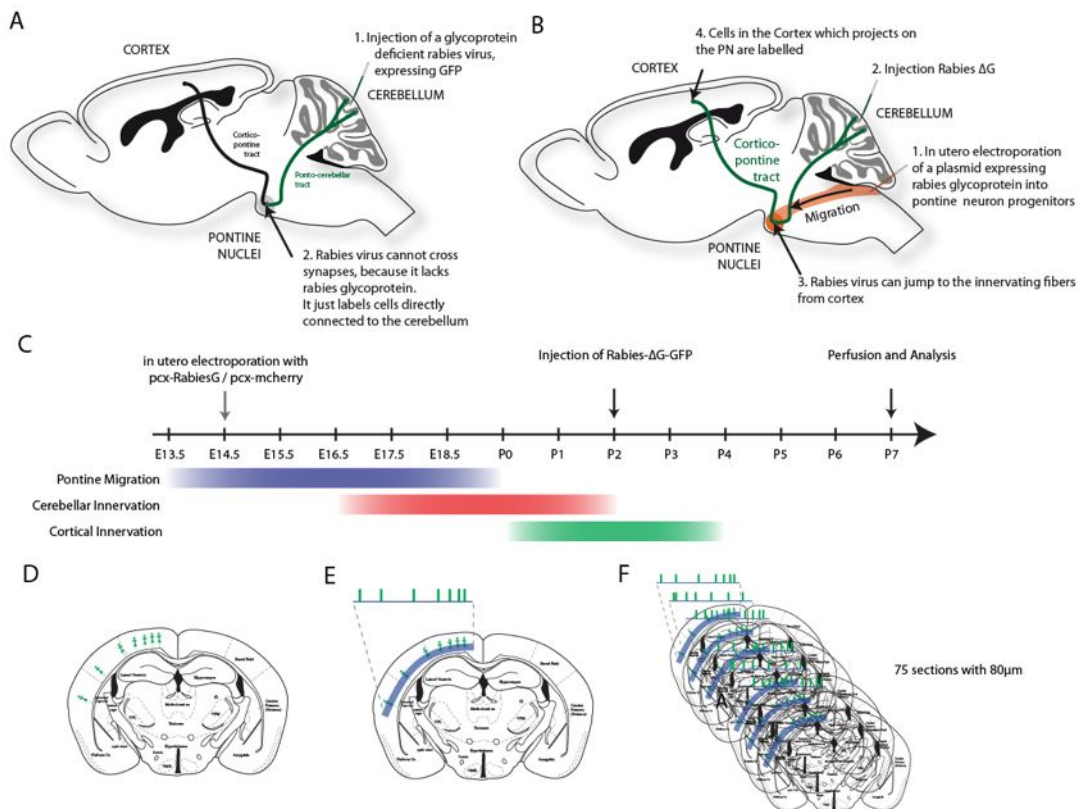


Figure 43 | Concept of the retrograde transsynaptic tracing from cerebellum to cortex via *in utero* electroporation delivery of G-Protein complement I. (A-C) Schematic illustration of the experimental design. If Rabies- Δ G-GFP viruses are injected into the cerebellum, they travel retrogradely to the pontine nuclei (PN), but are not able to cross synapses to infect cortical neurons (A). By supplementing pontine neurons by *in utero* electroporation with the missing G-Protein (glycoprotein), the virus is able to jump to the cortico-pontine fibers and infect cortical cells (B). Embryos are electroporated at E14.5, injected with Rabies- Δ G-GFP at P2 and perfused and analyzed at P7 (C). **(D-F)** To analyze the topography of the cortico-ponto-cerebellar projection, the position of the cells on coronal sections (D) can be transformed into a 2-dimensional space (E) and registered for all sections to generate a 2-dimensional map of cortical cells projecting to the PN (F).

3.2.3 Combination of *in utero* electroporation and rabies virus tracing to assess cortico-ponto-cerebellar connectivity

As shown in Di Meglio et al. (2013) tracing using Rabies- Δ G-GFP/mcherry from cortex (anterograde tracing from Layer 5 neurons) or cerebellum (retrograde tracing from mossy fiber synapses) can be used efficiently to analyze cortico-ponto-cerebellar connectivity.

To achieve a further understanding of the circuitry between cortex and cerebellum, an approach was designed that allows transsynaptic labeling of cortical cells from the cerebellum. Hereby Glycoprotein-deleted rabies viruses carrying GFP (Rabies- Δ G-GFP) were injected into the cerebellar hemisphere at P7. From there the virus transports retrogradely to the pontine mossy fiber neurons. Due to the knockout of the Rabies-Glycoprotein (Rabies-G), the virus is, unlike wildtype rabies viruses, not able to retrogradely jump to presynaptic cells. To allow the restricted retrograde jump, the rabies-glycoprotein is provided to pontine neurons by *in utero* electroporation of a rabies-glycoprotein construct at E14.5. In cells that are positive for Rabies- Δ G-GFP and rabies-glycoprotein, the virus is now able to jump on synapse to infect the cortical layer 5 neurons innervating the pontine nuclei (summarized in **Figure 44**, A-C).

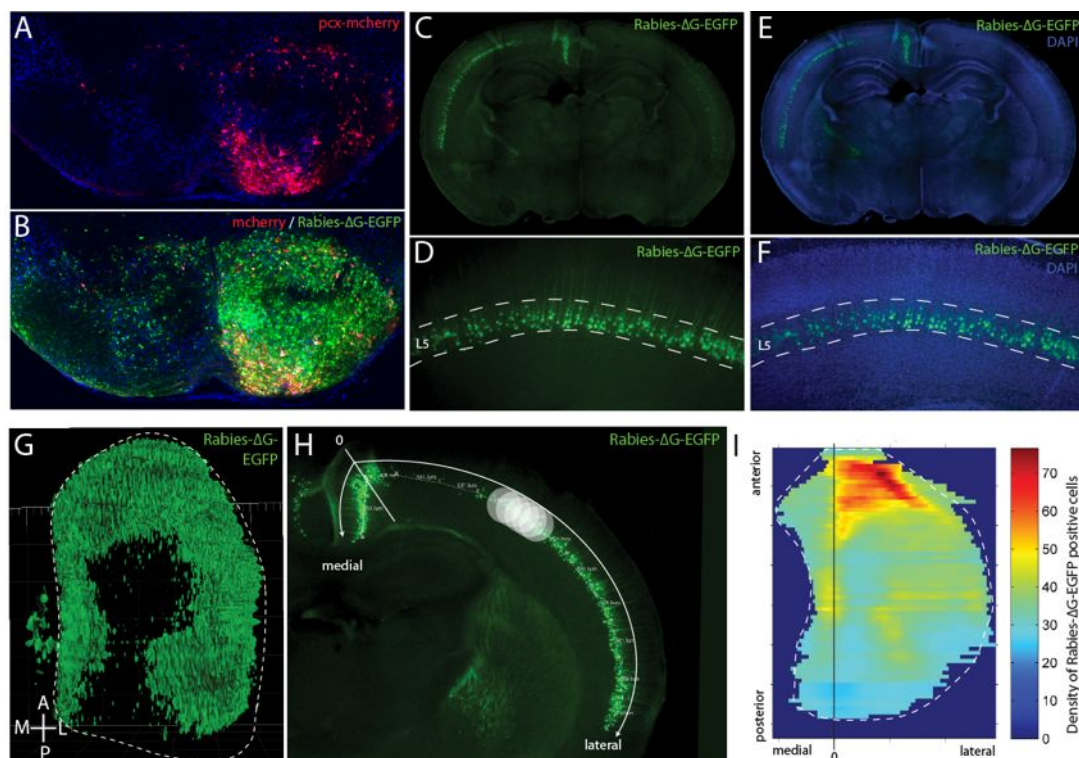


Figure 44 | Concept of the retrograde transsynaptic tracing from cerebellum to cortex via *in utero* electroporation delivery of G-Protein complement II. (A-B) Coronal sections at the PN level show the overlap of cells electroporated with pCAG-mcherry (and pCAG-RabiesG) and cells retrogradely labeled from cerebellum (green). Electroporated cells are mainly ipsilateral, retrogradely traced cells mainly contralateral. **(C-F)** Cells in the cortex are mainly located in layer 5 of the ipsilateral cortex, contralateral cells can be explained by cells which have been traced ipsilaterally and electroporated contralaterally. **(G-I)** There are different ways to visualize the acquired data. Coronal sections can be reconstructed (G) or transformed into a two-dimensional density map (H-I)

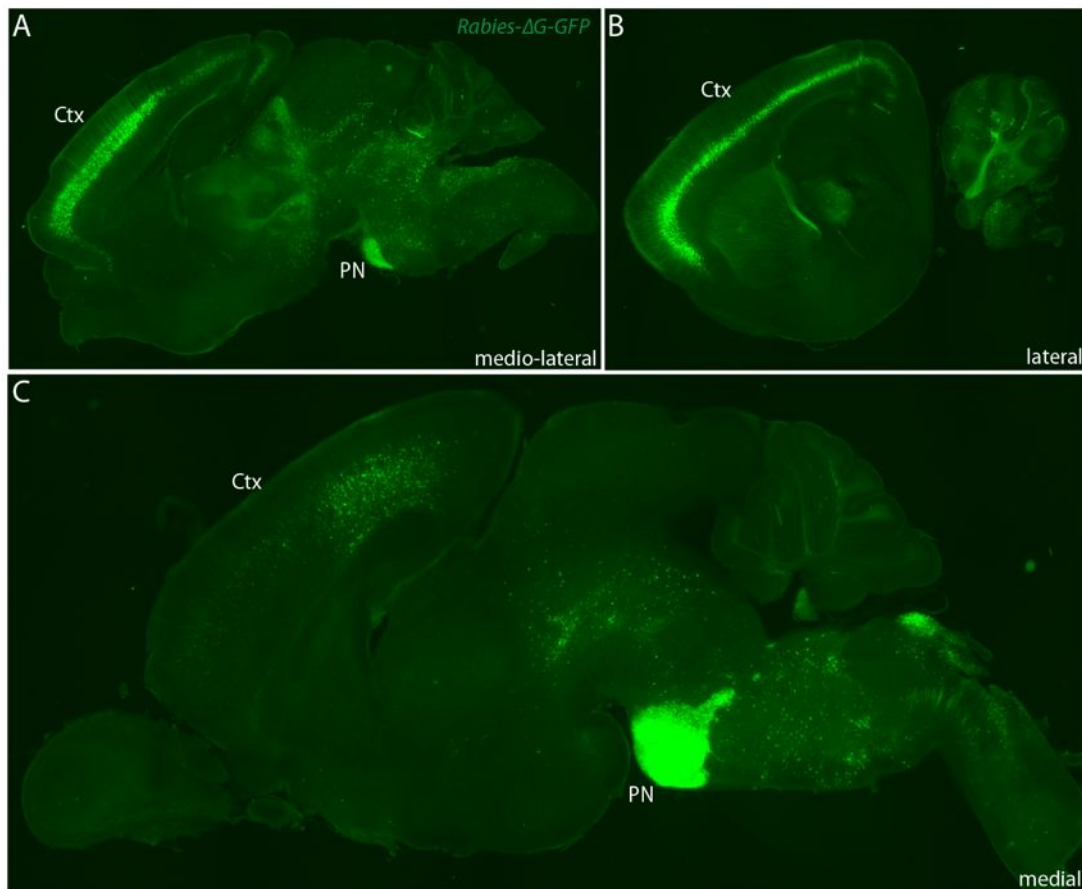


Figure 45 | Retrograde tracing of cortico-ponto-cerebellar connectivity. (A-C) Localization of cells traced back from cerebellum to pontine nuclei (PN) to Cortex (Ctx) using a combination of Rabies- Δ G-GFP injection and *in utero* electroporation of RabiesG (Glycoprotein) on lateral (B), mediolateral (A) and medial sections (C)

Indeed it was possible to obtain cases that were both electroporated with *pCAG-Rabies-G/ pCAG-mcherry* and transfected with Rabies- Δ G-GFP (**Figure 44**, G-H). In these cases the cortical layer 5 was strongly labeled unilaterally, ipsilateral to the electroporated pontine nuclei and contralateral to the injections site in the cerebellum (**Figure 44**, C-F; **Figure 45**, A-C). On the contralateral side, solely a small numbers of cells was labeled, which can be explained by midline-crossing electroporated cells, that projected to the ipsilateral hemisphere.

By the reconstructing of coronal sections of the cortex it is possible to analyze and map cortical neurons innervating pontine nuclei and cerebellum (**Figure 44**, D-F). In this way the labeled cells can be either presented as a whole-cortex-3D-reconstruction

(Figure 44, G) or in a 2-dimensional heatmap by transforming the 3-dimensional cortex into a 2-dimensional map of layer 5 (Figure 44, H-I).

By doing so, it is possible to understand which parts of the cortex are in direct communication with the cerebellum using the pontine nuclei as a relay station.

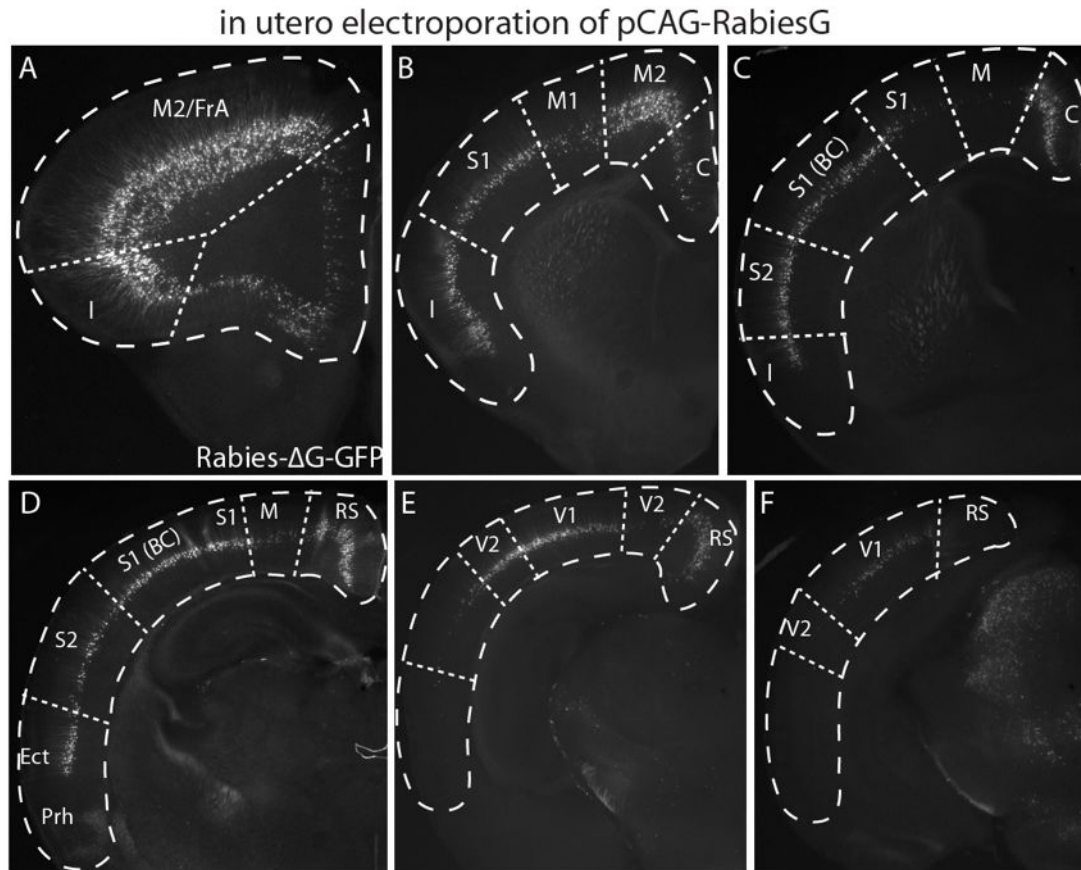


Figure 46 | Retrograde tracing of cortico-ponto-cerebellar connectivity in wildtypes. (A-F) To analyze the cortico-ponto-cerebellar connectivity wildtype embryos were electroporated with Rabies G at E14.5. Coronal sections are taken from anterior (A) to posterior (F). M2: Secondary Motor Cortex; FrA: frontal association cortex; C: Cingulate cortex; M1: Primary motor cortex; S1: Primary Sensory Cortex; I: Insular cortex; S2: Secondary sensory cortex; V1: Primary visual cortex; V2: Secondary visual cortex; RS: Retrosplenial cortex; Ect: Ectorhinal cortex; Prh: Perirhinal cortex

The pontine nuclei receive input from a variety of cortical regions. The highest density of labeled layer 5 cells can be found in the anterior cortex, which includes prefrontal areas as well as the primary and secondary motor cortex (Figure 44, G, I;

Figure 45, A-B; Figure 46; A-C). Furthermore, cells in the somatosensory areas, especially the barrel cortex, visual cortex as well as retrosplenial and perirhinal cortex can be found (**Figure 46; B-F**).

in utero electroporation of pCAG-FLEX-RabiesG in *ChAT::Cre* background

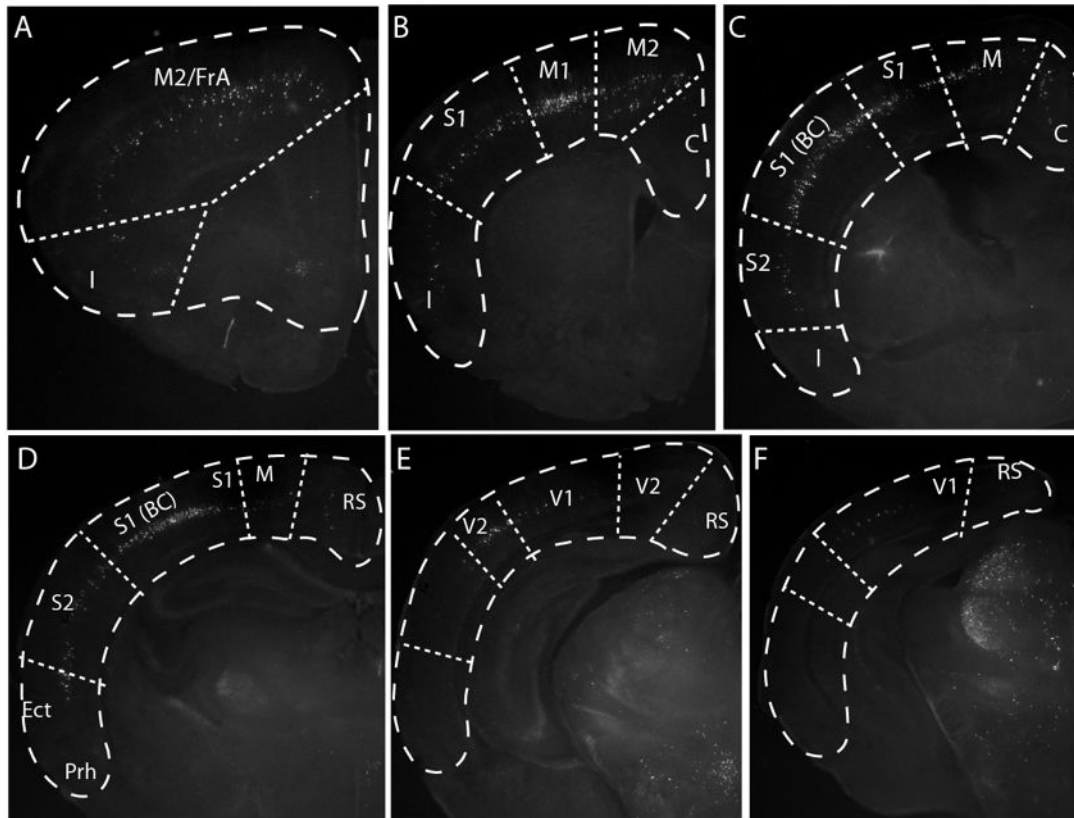


Figure 47 | Retrograde tracing of cortico-ponto-cerebellar connectivity subsets using *ChAT::Cre*. (A-F) To analyze the cortico-ponto-cerebellar connectivity of different pontine nuclei subsets *ChAT::Cre* embryos were electroporated with a loxed RabiesG construct (D-F, J-L). Coronal sections are taken from anterior (A) to posterior (F). In *ChAT::Cre* mice less cortical cells are labeled, obvious reduction of the number of cells can be seen in M2, V1 and RS (retrosplenial cortex) while the number of cells is less reduced in M1, some parts of S1 and V2.

The chosen approach gives further possibilities to select subpopulations of PN cells by a) more specific injections into specific cerebellar regions, b) to modify the amount and identity of electroporated cells by changing the time of electroporation (early electroporation labels more internal, late electroporation more external pontine nuclei layers) or by c) combining the approach with a subpopulation labeling *Cre* line. To restrict the expression of Rabies-Glycoprotein a FLEX-construct was generated and electroporated into *ChAT::Cre* animals. Hereby RabiesG was solely expressed in

ChAT::Cre positive cells, where Cre mediated recombination can occur. The result was a strongly reduced number of GFP labeled cortical neurons (**Figure 47**, A-F). This reduction was especially obvious in some motor areas, somatosensory areas, frontal association, cingulate, insular, ectorhinal and retrosplenial cortex, while higher numbers of cells can be found in primary motor cortex, secondary visual cortex and somatosensory barrel cortex.

4 Discussion

***Ezh2* orchestrates epigenetic regulation of topographic tangential migration**

Polycomb proteins regulate many target genes that control cell fate decisions (Simon and Kingston, 2009). The results of Di Meglio et al. (2013) extend the involvement of *Ezh2* beyond neuronal fate and subtype identity specification (Pereira et al., 2010) to a novel role in orchestrating epigenetic regulation of topographic neuronal guidance in the mammalian brain.

In the radial migratory mode, migrating neurons maintain physical interaction with their glial progenitors throughout migration and their final rostrocaudal location directly correlates to their position of origin (Rakic, 1988). In contrast, the final destination of tangentially migrating neurons is apparently unrelated to starting position (Hatten, 1999). Molecular regional programs and relative original position of progenitors along the AP axis are faithfully ‘transposed’ into the final nucleus, due to a remarkable topographic organization of the migratory AES. Whether this intrinsic molecular and cellular topography is a general feature of tangentially migrating populations in other regions of the brain, or is specific to precerebellar neurons, remains to be determined. The importance of transcription factors to segregate distinct populations of migrating forebrain interneurons begins to emerge (e.g. *Nkx2.1* on-off expression in MGE-derived striatal versus cortical interneurons, respectively (Nóbrega-Pereira et al., 2008)). However, this is the first time that the fine intrinsic organization of a single migratory population (the AES) is revealed, along with the demonstration that its regional transcriptional information is epigenetically maintained.

This system is highly buffered in wild type, as ventral AES neurons maintain their normal migratory pathway despite their low *Unc5c/5b* activity. This is partly due to additional Slit-mediated repulsive activity from the facial motor nucleus maintaining the AES normal migration pathway (Di Meglio et al., 2008; Geisen et al., 2008). However, when the system is challenged by increased environmental *Ntn1* attraction or reduced *Unc5c/5b* repulsion in the AES, this predictably results in stereotypic migratory responses of selected, molecularly defined, subsets of PN neurons. Graded

Unc5c/5b-mediated Ntn1 response within the AES may normally maintain the relative topographic position of PN subsets and/or organize PN topographic projections to cerebellum (Kim and Ackerman, 2011).

PN neurons settle in ‘inside-out’ concentric laminae depending on their birthdate (Altman and Bayer, 1987b). This concentric temporal gradient of neuronal organization in the PN may correlate with patterned axonal input related to temporal maturational gradients of layer 5 cortical neurons (Leergaard and Bjaalie, 2007). Cortical areas are broadly pre-patterned along the rostrocaudal axis by the graded activity of homeobox transcription factors (O’Leary et al., 2007). It is noteworthy that rostrocaudal pre-patterning and regionalization is also observed in the developing PN, thus intersecting a spatial dimension to the temporal gradient model. The pontine nuclei are a fundamental relay station for the transformation of orderly motor and sensory maps in the cerebral cortex into ‘patchy’ representations of input in the granular layer of the cerebellar cortex. Still, little is known about the molecular and cellular mechanisms assembling these complex input-output wiring patterns in PN. Our results strongly suggest that intrinsic pre-mapping of PN from IRL progenitors of distinct rostrocaudal origin may also contribute to organize broad topographic input from distinct cortical areas.

Topography of the corticopontine projection

The projections from pontine to cerebellum have been intensively studied in rats (Azizi et al., 1981; Mihailoff et al., 1981) and monkeys (Brodal, 1982) by performing retrograde tracing. Experiments that have been carried out in rats (that are probably the most comparable to mice) already suggested 30 years ago, that cells of PN and RTN project to multiple locations in both cerebellar vermis and hemispheres (Azizi et al., 1981; Mihailoff et al., 1981). The results give evidence for a high degree of divergence and convergence of single pontine neurons or clusters of pontine cells. Divergence is suggested by the fact that neurons located in similar regions of PN and RTN are labeled by different injection sites, convergence is put forward by the fact that restricted injections result in the labeling of spatially separate pontine neuron populations. The presence of single neurons that project to different lobes could be confirmed later on (Bolstad et al., 2007).

Therefore the complexity of the cerebrocerebellar connectivity seems to arise from properties of the pontine nuclei that do not only relay information from the cortex, but to redistribute permutations of information from cortical sensory and motor input in a con- and divergent manner to different areas of the cerebellum.

As stated before a clear topography has been demonstrated for the cortico-pontine projection (Leergaard and Bjaalie, 2007; Leergaard et al., 1995; Leergaard et al., 2000; Leergaard et al., 2004) and mechanisms have been put forward that could explain the establishment of this topography by birthdate (Leergaard and Bjaalie, 2007; Leergaard et al., 1995) and rostro-caudal axis (Di Meglio et al., 2013) (3.1.1). This is less clear for the ponto-cerebellar connectivity. Tracing data by (Azizi et al., 1981; Broch-Smith and Brodal, 1990; Mihailoff et al., 1981) do not suggest, that either a temporal (that is transformed into a concentric inside-out axis in the PN) or other spatial axes might be strong determinants for the establishment of a potentially topographic ponto-cerebellar connectivity (summarized in **Table 8**). Cells labeled by retrograde tracings of specific lobes do not cluster unambiguously on inside-out, medio-lateral or rostro-caudal axes in the PN (Azizi et al., 1981; Broch-Smith and Brodal, 1990; Mihailoff et al., 1981).

Lobule	Innervated by						Model Organism (References)
	RTN	rostPN	medPN	centPN	latPN	caudPN	
VIa	+++	+	+	+	-	+	Rat (Azizi et al., 1981)
VIb-c	+++	+++	++	+	+	+	Rat (Azizi et al., 1981)
VII	+++	+++	+++	+	+++	+	Rat (Azizi et al., 1981)
VIII	-	-	+	+	++	+++	Rat (Azizi et al., 1981)
IX	+	++	+++	+++	++	+++	Rat (Azizi et al., 1981)
LS	++	+	+	++	-	+	Rat (Mihailoff et al., 1981)
CrusI	+++	+++	++	++	++	-	Rat (Mihailoff et al., 1981)
CrusII	++	++	++	+++	-	++	Rat (Mihailoff et al., 1981)
PML	+++	+++	+++	+++	+++	+++	Rat (Mihailoff et al., 1981)
PFL	?	+++	+++	+	+	+	Cat (Broch-Smith and Brodal, 1990; Nikundiwe et al., 1994b)

Table 8 | Summary of HRP studies on the pontocerebellar system. Summary of the results presented in (Azizi et al., 1981; Broch-Smith and Brodal, 1990; Mihailoff et al., 1981; Nikundiwe et al., 1994b).

In utero electroporations give indirectly further evidence for this hypothesis. By *in utero* electroporations at E14.5 only PN neurons that have not yet migrated out can be labeled, therefore tracing a “temporal subset” that reproducibly localizes in the outer layer of the PN (**Figure 38**), with a slight tendency to be more restricted to outer layers in the caudal part than in the rostral part. Still this subset of pontine neurons that almost completely excludes the RTN strongly labels all cerebellar areas reported to be innervated by the PN (Azizi et al., 1981; Mihailoff et al., 1981; Nikundiwe et al., 1994b) including lobes VI-IX, lobus simplex, CrusI and to lesser extent CrusII, paramedian lobe and paraflocculus. Thereby, it is unlikely that there the temporal neurogenesis gradient of PN neurons has a dominant role for the connectivity to the cerebellum, although it has been suggested as a potential mechanism (Nikundiwe et al., 1994b). Experiments in which *in utero* electroporations is performed at earlier stages (E13.5, E12.5) could further support this hypothesis.

An indeed surprising result, given the degree of divergence and convergence of the ponto-cerebellar projection, were the relatively defined target zones of *Chat::Cre; R26R^{tdtomato}* and *Mafb::CreERT2; R26R^{tdtomato}* positive mossy fibers strongly targeting paraflocculus and paramedian lobe and in *ChAT::Cre* additionally flocculus and lobes VII and IX of the vermis (**Figure 35, Figure 37**). Still the projection patterns of *ChAT::Cre; R26R^{tdtomato}* and *Mafb::CreERT2; R26R^{tdtomato}* specimen are in accordance to retrograde tracing experiments performed in cats (Broch-Smith and Brodal, 1990; Nikundiwe et al., 1994b) in which more than 70% of the neurons labeled after injections in the paraflocculus are located in the rostral half of the pontine nuclei (Nikundiwe et al., 1994b); furthermore they show as well a medial population of cells closely located to the midline (Broch-Smith and Brodal, 1990), similar to the one observed in *ChAT::Cre; R26R^{tdtomato}* mice (**Figure 34**).

It has been already suggested by Broch-Smith and Brodal (1990) and Nikundiwe et al. (1994b) that the paraflocculus projecting areas of the pontine nuclei are also those that mainly get input from visual cortical areas, parietal association cortex and to a lesser extent from primary and secondary sensory and primary motor cortex but on the other hand almost no input from secondary motor areas and prefrontal cortex. This assumption can be confirmed by the retrograde conditional transsynaptic Rabies-ΔG-

GFP tracing (**Figure 47**) in the *ChAT::Cre* background. Here the number of cells labeled in the rostral cortex was strongly decreased compared to controls (**Figure 46**), while cells can still be found in primary sensory and visual cortex. It appears that the *ChAT::Cre* positive pontine nuclei subset constitutes a part of the circuitry, which has a strongly convergent character, conveying information from different sensory areas including visual and somatosensory areas mainly to the cerebellar paraflocculus.

It would be extremely revealing to perform these experiments also in *MafB::CreERT2* specimen, but due to the fact that the expression is solely present at early stages, it cannot be used for this approach. Although the *ChAT::Cre* population in contrast to the *MafB::CreERT2* subpopulation does not necessarily constitute a subset derived from a specific progenitor zone, the *ChAT::Cre* line is a very valuable tool to analyze a specific subset of the cortico-ponto-cerebellar circuitry. Furthermore, the transgenic lines seem to share a common expression in the dorso-lateral pontine nuclei (DLPN) as they share a common target area in the paraflocculus (**Figure 34**, **Figure 35**, **Figure 36**, **Figure 37**). Hence, in contrast to most other parts of the pontine nuclei the *ChAT::Cre* and *MafB::CreERT2* positive subpopulations seem to constitute a neuronal module, that has a relatively restricted projection pattern with a relatively high degree of convergence.

Role of the pontine nuclei for processing visual information.

One part of the pontine nuclei that has been particularly well analyzed is the dorso-lateral pontine nucleus (DLPN). It receives major inputs from the visual cortex (Glickstein et al., 1980; Glickstein et al., 1994) and auditory cortex (Perales et al., 2006) and partially encompasses the subpopulations labeled by *ChAT::Cre* and *MafB::CreERT2*. The DLPN has been involved in optokinetic nystagmus including smooth-pursuit eye movements, ocular following, visually guided motor learning (Tziridis et al., 2011; Tziridis et al., 2009) and visually guided eye movements (May et al., 1988; Ono et al., 2003; Thier and Möck, 2006; Thier et al., 1988; Thier et al., 1989). Together with the RTN (receiving input from non-cortical visual areas) the DLPN constitutes the major relay for visual and visuomotor input into the cerebellum (Glickstein et al., 1994; Thielert and Thier, 1993).

The retrograde tracing of the cerebellum innervating *ChAT::Cre* pontine nuclei cells to the cortex revealed not only cells in the visual cortex, but also in the somatosensory barrel cortex (**Figure 47**), an innervation that has been demonstrated previously by anterograde tracing from the cortex (Broch-Smith and Brodal, 1990).

Although it might be at the first sight not intuitive that an area that is functionally involved in smooth-pursuit eye movements (and thereby stabilizing the image of moving objects) and visually guided movements gets further input from somatosensory areas, spatial information can be extracted as well from sensory systems including receptors in the skin, but especially in case of cats and rodents from the whiskers, relayed by the S1 barrel cortex. Further support for this more general role of the DLPN in sensory guidance comes also from the monkey model, where a role in goal-directed hand-movements was proposed (Tziridis et al., 2009; Tziridis et al., 2011) and from echolocating bats in which the DLPN gets a substantial input from the auditory system, relaying it from there to the cerebellar paraflocculus (Schuller et al., 1991). Both suggest a species-specific integrative role of the DLPN.

Evolution of the precerebellar system and cortico-ponto-cerebellar connectivity

Pontine nuclei have been analyzed in many mammals from rats (Mihailoff et al., 1978) to opossums (Mihailoff and King, 1975), cats (Hoddevik, 1975) and macaques (Glickstein et al., 1980). In other amniotes as reptiles and birds the pontine nuclei have been poorly described and are considered as being specific mammalian structures. Two population of pontine nuclei have been described in chicken, referred to as medial pontine nucleus and lateral pontine nucleus (Brodal et al., 1950; Marín and Puelles, 1995). This two populations are located medially and laterally to the midline at the level of rhombomere 3 / rhombomere 4 and originate at the posterior rhombic lip (Marín and Puelles, 1995). Birds neither have a cortico-spinal tract (Aboitiz et al., 2003) nor pronounced cerebellar hemispheres, their cerebella consist almost entirely of vermis (Butler and Hodos, 2005; Striedter, 2005; Sultan and Glickstein, 2007), thereby PN neurons lack the main input (cortex) as well as their main output areas (cerebellar hemispheres). Still they share some striking similarities

with two nuclei which exist also in mammals, which is the reticulotegmental nucleus (RTN) and the recently described interfascicular trigeminal nucleus (Fu et al., 2013), a nucleus that we also can observe in *in utero* electroporations and in transgenic lines (data not shown). Both nuclei are not innervated by the cortex and have both strong projections to the vermis in rodents (Azizi et al., 1981; Fu et al., 2013; Mihailoff et al., 1981). The mammalian RTN is mainly involved in visually guided eye movements and smooth-pursuit eye movements and innervated almost exclusively from subcortical afferents as e.g. from tectum and thalamus by which it receives visual and oculomotor information (Thielert and Thier, 1993). Considering the importance of the visual and oculomotor system in birds in contrast to somatosensory and tactile information it is likely that a ponto-cerebellar system focused on visual and vestibular information preexisted. Mammals as rodents and monkeys extensively use the somatosensory sense to experience their environment, especially by the use of whiskers (especially in rodents and cats), lips and paws/hands (e.g. in monkeys).

Hence, it can be postulated that the coevolution of cortex, pontine nuclei and cerebellar hemispheres, the three parts of the cortico-ponto-cerebellar circuit, played a pivotal role for the evolution of complex motor behaviors (including the corresponding sensory feedback), since all three areas dramatically increased in size throughout evolution. In humans, almost a third of the hindbrain is taken by the pontine nuclei, and both cortex and cerebellar hemispheres increased dramatically in volume (the hemispheres are therefore also referred to as cerebro- or neo-cerebellum).

A further interesting observation on the evolution of the cortex is, that the cortical topography that is well described in rodents, monkeys and humans (Rakic, 1988; Rakic, 2009) is not as strictly segregated in monotremes and marsupials, the sister groups of mammals (Karlen and Krubitzer, 2007; Lende, 1963; Lende, 1964) and absent in non-mammalian vertebrates (Aboitiz et al., 2003). Marsupials as the opossum and wallaby (Lende, 1963) and monotremes (Lende, 1964) have a strong to almost complete overlap of somatosensory and motor areas in the cortex (Aboitiz et al., 2003).

It is suggested that the spatial segregation of distinct somatic motor and sensory representations developed throughout evolution and comes along with the increasing

occupation of cortical areas with the interpretation of sensory information and the control of motor behavior (Aboitiz et al., 2003; Rakic, 1988; Rakic, 2009). Interestingly this spatial segregation is less obvious in the cerebellum (Apps and Hawkes, 2009); due to the functional role of the cerebellum as a major integrator of motor and sensory information. Therefore the pontine nuclei arose during early mammalian evolution, at a time when the neocortex evolved from the dorsal pallium and the neocerebellum (the hemispheres) evolved in the cerebellum (Butler and Hodos, 2005; Striedter, 2005). Cortex and Cerebellum have a strikingly correlated volumetric evolution (Barton, 2002; Barton and Harvey, 2000) further suggesting a causal relationship between the evolution of these two areas. It is also likely, that the main structure connecting these two areas has an important function during the evolution of these two systems. From an “evo-devo” perspective, it could be even postulated that the highly convergent and divergent circuitry between cortex and cerebellum might even reflect the cortical characteristics of evolutionary early mammals in which somatosensory and motor areas might have been grossly overlapping, as it still is in the pontine nuclei of living mammal species.

Hence, it is possible that the evolution of a stronger connectivity to the cerebellum “outsourced” integrative computations that were performed in the cortex of early mammals to the cerebellum, that due to its structural characteristics is a very powerful part of the brain to compute complex integrations of sensory and motor information (Apps and Garwicz, 2005; Apps and Hawkes, 2009; Ramnani, 2006). This could, from an evolutionary standpoint, explain the gradual decrease of sensory topography, coming along with an increase of divergence and convergence, from the somatotopically continuous sensory maps in the cortex over pontine nuclei to the a fractured somatotopy in the cerebellum. A further evidence for this could be the increase in the precision of the cortico-pontine projection from lower mammals as rodents to monkeys with regard to the somatotopic pattern (Brodal, 1982) that can be interpreted as further specializations of the system.

Outlook

The results of this thesis as well as the established techniques give a conceptual and technical framework to analyze the development, evolution, function and biology of the pontine nuclei and its integration into the cortico-ponto-cerebellar circuitry.

Using the two genetically defined subsets (*ChAT::Cre* and *MafB::CreERT2*) and by the generation of a further transgenic labeling a posterior subset of pontine neurons (*Hoxa5::CreERT2*) it will be possible to extend the knowledge about the molecular mechanisms controlling the circuitry of specific pontine nuclei modules and their role in cortico-ponto-cerebellar connectivity. Furthermore, *in utero* electroporation gives the possibility to analyze the role of genetic determinants as transcription factors or their downstream targets as e.g. guidance factors for the development of the system. Using the 2A system mossy fibers, overexpressing a gene of interest and reporter, can be analyzed at resolutions reaching from gross connectivity to synapse structure.

More precise genetic tools using intersectional Cre recombinase / Flip recombinase techniques (see 3.1.5) could even give the possibility to analyze the role of the *ChAT::Cre* or *MafB::CreERT2* subset in behavior, allowing to look for behavioral correlates and the underlying structural plasticity in the mossy fiber circuitry.

As stated before, also the evolutionary aspects of the pontine nuclei are very interesting. Comparative analysis in mammals (and eventually birds and reptiles) could give new insights into evolutionary principles and the evolution of the cross-talk between higher-order brain areas as pallium and tectum and the cerebellum.

5 References

- Aboitiz, F., Morales, D. and Montiel, J. (2003). The evolutionary origin of the mammalian isocortex: towards an integrated developmental and functional approach. *Behav Brain Sci* 26, 535–52– discussion 552–85.
- Alcántara, S., Ruiz, M., de Castro, F., Soriano, E. and Sotelo, C. (2000). Netrin 1 acts as an attractive or as a repulsive cue for distinct migrating neurons during the development of the cerebellar system. *Development* 127, 1359–1372.
- Alexander, T., Nolte, C. and Krumlauf, R. (2009). HoxGenes and Segmentation of the Hindbrain and Axial Skeleton. *Annu Rev Cell Dev Biol* 25, 431–456.
- Altman, J. and Bayer, S. A. (1987a). Development of the precerebellar nuclei in the rat: III. The posterior precerebellar extramural migratory stream and the lateral reticular and external cuneate nuclei. *J Comp Neurol* 257, 513–528.
- Altman, J. and Bayer, S. A. (1987b). Development of the precerebellar nuclei in the rat: IV. The anterior precerebellar extramural migratory stream and the nucleus reticularis tegmenti pontis and the basal pontine gray. *J Comp Neurol* 257, 529–552.
- Altman, J. and Bayer, S. A. (1997). *Development of the cerebellar system*. CRC.
- Apps, R. and Garwicz, M. (2005). Anatomical and physiological foundations of cerebellar information processing. *Nat Rev Neurosci* 6, 297–311.
- Apps, R. and Hawkes, R. (2009). Cerebellar cortical organization: a one-map hypothesis. *Nat Rev Neurosci* 10, 670–681.
- Azizi, S. A., Mihailoff, G. A., Burne, R. A. and Woodward, D. J. (1981). The pontocerebellar system in the rat: an HRP study. I. Posterior vermis. *J Comp Neurol* 197, 543–548.
- Bantignies, F. and Cavalli, G. (2006). Cellular memory and dynamic regulation of polycomb group proteins. *Curr Opin Cell Biol* 18, 275–283.
- Barton, R. A. (2002). How did brains evolve? *Nature* 415, 134–135.
- Barton, R. A. and Harvey, P. H. (2000). Mosaic evolution of brain structure in mammals. *Nature* 405, 1055–1058.
- Bernstein, B. E., Mikkelsen, T. S., Xie, X., Kamal, M., Huebert, D. J., Cuff, J., Fry, B., Meissner, A., Wernig, M., Plath, K., et al. (2006). A bivalent chromatin structure marks key developmental genes in embryonic stem cells. *Cell* 125, 315–326.
- Bird, A. (2007). Perceptions of epigenetics. *Nature* 447, 396–398.

- Bolstad, I., Leergaard, T. B. and Bjaalie, J. G. (2007). Branching of individual somatosensory cerebropontine axons in rat: evidence of divergence. *Brain structure & function* 212, 85–93.
- Boyer, L. A., Plath, K., Zeitlinger, J., Brambrink, T., Medeiros, L. A., Lee, T. I., Levine, S. S., Wernig, M., Tajonar, A., Ray, M. K., et al. (2006). Polycomb complexes repress developmental regulators in murine embryonic stem cells. *Nature* 441, 349–353.
- Broch-Smith, T. and Brodal, P. (1990). Organization of the cortico-ponto-cerebellar pathway to the dorsal paraflocculus. An experimental study with anterograde and retrograde transport of WGA-HRP in the cat. *Arch Ital Biol* 128, 249–271.
- Brodal, A., Kristiansen, K. and Jansen, J. (1950). Experimental demonstration of a pontine homologue in birds. *J Comp Neurol* 92, 23–69.
- Brodal, P. (1968). The corticopontine projection in the cat. I. Demonstration of a somatotopically organized projection from the primary sensorimotor cortex. *Experimental brain research Experimentelle Hirnforschung Expérimentation cérébrale* 5, 210–234.
- Brodal, P. (1982). Further observations on the cerebellar projections from the pontine nuclei and the nucleus reticularis tegmenti pontis in the rhesus monkey. *J Comp Neurol* 204, 44–55.
- Brose, K., Bland, K. S., Wang, K. H., Arnott, D., Henzel, W., Goodman, C. S., Tessier-Lavigne, M. and Kidd, T. (1999). Slit proteins bind Robo receptors and have an evolutionarily conserved role in repulsive axon guidance. *Cell* 96, 795–806.
- Burne, R. A., Eriksson, M. A., Saint-Cyr, J. A. and Woodward, D. J. (1978). The organization of the pontine projection to lateral cerebellar areas in the rat: dual zones in the pons. *Brain Res* 139, 340–347.
- Butler, A. B. and Hodos, W. (2005). *Comparative vertebrate neuroanatomy*.
- Chamberlain, S. J., Yee, D. and Magnuson, T. (2008). Polycomb repressive complex 2 is dispensable for maintenance of embryonic stem cell pluripotency. *Stem Cells* 26, 1496–1505.
- Chen, S.-Y. and Cheng, H.-J. (2009). Functions of axon guidance molecules in synapse formation. *Curr Opin Neurobiol* 19, 471–478.
- Chédotal, A. (2007). Slits and their receptors. *Adv Exp Med Biol* 621, 65–80.
- Ciani, L. and Salinas, P. C. (2005). WNTs in the vertebrate nervous system: from patterning to neuronal connectivity. *Nat Rev Neurosci* 6, 351–362.
- Coulombe, Y., Lemieux, M., Moreau, J., Aubin, J., Joksimovic, M., Bérubé-Simard, F.-A., Tabariès, S., Boucherat, O., Guillou, F., Larochelle, C., et al. (2010).

- Multiple promoters and alternative splicing: *hoxa5* transcriptional complexity in the mouse embryo. *PLoS ONE* 5, e10600.
- Dahl, J. A. and Collas, P. (2008). A rapid micro chromatin immunoprecipitation assay (microChIP). *Nat Protoc* 3, 1032–1045.
- Danielian, P. S., Muccino, D., Rowitch, D. H., Michael, S. K. and McMahon, A. P. (1998). Modification of gene activity in mouse embryos in utero by a tamoxifen-inducible form of Cre recombinase. *Curr Biol* 8, 1323–1326.
- Dasen, J. S., Liu, J.-P. and Jessell, T. M. (2003). Motor neuron columnar fate imposed by sequential phases of Hox-c activity. *Nature* 425, 926–933.
- Dasen, J. S., Tice, B. C., Brenner-Morton, S. and Jessell, T. M. (2005). A Hox regulatory network establishes motor neuron pool identity and target-muscle connectivity. *Cell* 123, 477–491.
- De Paola, V., Arber, S. and Caroni, P. (2003). AMPA receptors regulate dynamic equilibrium of presynaptic terminals in mature hippocampal networks. *Nat Neurosci* 6, 491–500.
- Di Meglio, T., Kratochwil, C. F., Vilain, N., Loche, A., Vitobello, A., Yonehara, K., Hrycaj, S. M., Roska, B., Peters, A. H. F. M., Eichmann, A., et al. (2013). Ezh2 orchestrates topographic migration and connectivity of mouse precerebellar neurons. *Science (New York, NY)* 339, 204–207.
- Di Meglio, T., Nguyen-Ba-Charvet, K. T., Tessier-Lavigne, M., Sotelo, C. and Chédotal, A. (2008). Molecular mechanisms controlling midline crossing by precerebellar neurons. *J Neurosci* 28, 6285–6294.
- di Sanguinetto, S. A. D. T., Dasen, J. S. and Arber, S. (2008). Transcriptional mechanisms controlling motor neuron diversity and connectivity. *Curr Opin Neurobiol* 18, 36–43.
- Driever, W. and Nüsslein-Volhard, C. (1988a). A gradient of bicoid protein in *Drosophila* embryos. *Cell* 54, 83–93.
- Driever, W. and Nüsslein-Volhard, C. (1988b). The bicoid protein determines position in the *Drosophila* embryo in a concentration-dependent manner. *Cell* 54, 95–104.
- Engelkamp, D., Rashbass, P., Seawright, A. and van Heyningen, V. (1999). Role of Pax6 in development of the cerebellar system. *Development* 126, 3585–3596.
- Erzurumlu, R. S., Murakami, Y. and Rijli, F. M. (2010). Mapping the face in the somatosensory brainstem. *Nat Rev Neurosci* 11, 252–263.
- Ezhkova, E., Pasolli, H. A., Parker, J. S., Stokes, N., Su, I.-H., Hannon, G., Tarakhovskiy, A. and Fuchs, E. (2009). Ezh2 orchestrates gene expression for the stepwise differentiation of tissue-specific stem cells. *Cell* 136, 1122–1135.

- Francis, N. J. and Kingston, R. E. (2001). Mechanisms of transcriptional memory. *Nat Rev Mol Cell Biol* 2, 409–421.
- Fu, Y., Tvrdik, P., Makki, N., Machold, R., Paxinos, G. and Watson, C. (2013). The interfascicular trigeminal nucleus: a precerebellar nucleus in the mouse defined by retrograde neuronal tracing and genetic fate mapping. *J Comp Neurol* 521, 697–708.
- Geisen, M. J., Di Meglio, T., Pasqualetti, M., Ducret, S., Brunet, J.-F., Chédotal, A. and Rijli, F. M. (2008). Hox paralog group 2 genes control the migration of mouse pontine neurons through slit-robo signaling. *PLoS Biol* 6, e142.
- Ghashghaei, H. T., Lai, C. and Anton, E. S. (2007). Neuronal migration in the adult brain: are we there yet? *Nat Rev Neurosci* 8, 141–151.
- Glickstein, M., Cohen, J. L., Dixon, B., Gibson, A., Hollins, M., Labossiere, E. and Robinson, F. (1980). Corticopontine visual projections in macaque monkeys. *J Comp Neurol* 190, 209–229.
- Glickstein, M., Gerrits, N., Kralj-Hans, I., Mercier, B., Stein, J. and Voogd, J. (1994). Visual pontocerebellar projections in the macaque. *J Comp Neurol* 349, 51–72.
- Gorski, J. A., Talley, T., Qiu, M., Puellas, L., Rubenstein, J. L. R. and Jones, K. R. (2002). Cortical excitatory neurons and glia, but not GABAergic neurons, are produced in the Emx1-expressing lineage. *J Neurosci* 22, 6309–6314.
- Gould, A., Morrison, A., Sproat, G., White, R. A. and Krumlauf, R. (1997). Positive cross-regulation and enhancer sharing: two mechanisms for specifying overlapping Hox expression patterns. *Genes Dev* 11, 900–913.
- Gómez-Skarmeta, J. L., Campuzano, S. and Modolell, J. (2003). Half a century of neural pre patterning: the story of a few bristles and many genes. *Nat Rev Neurosci* 4, 587–598.
- Grimaldi, G. and Manto, M. (2011). Topography of Cerebellar Deficits in Humans. *Cerebellum*.
- Guthrie, S. (2007). Patterning and axon guidance of cranial motor neurons. *Nat Rev Neurosci* 8, 859–871.
- Hatten, M. E. (1999). Central nervous system neuronal migration. *Annu Rev Neurosci* 22, 511–539.
- Henry, A. M. and Hohmann, J. G. (2012). High-resolution gene expression atlases for adult and developing mouse brain and spinal cord. *Mamm Genome* 23, 539–549.
- Hirabayashi, Y., Suzki, N., Tsuboi, M., Endo, T. A., Toyoda, T., Shinga, J., Koseki, H., Vidal, M. and Gotoh, Y. (2009). Polycomb limits the neurogenic competence of neural precursor cells to promote astrogenic fate transition. *Neuron* 63, 600–613.

- Hoddevik, G. H. (1975). The pontocerebellar projection onto the paramedian lobule in the cat: an experimental study with the use of horseradish peroxidase as a tracer. *Brain Res* 95, 291–307.
- Huber, A. B., Kolodkin, A. L., Ginty, D. D. and Cloutier, J.-F. (2003). Signaling at the growth cone: ligand-receptor complexes and the control of axon growth and guidance. *Annu Rev Neurosci* 26, 509–563.
- Jessell, T. M. (2000). Neuronal specification in the spinal cord: inductive signals and transcriptional codes. *Nature reviews genetics* 1, 20–29.
- Jürgens, G. (1985). A group of genes controlling the spatial expression of the bithorax complex in *Drosophila*. *Nature* 316, 153–155.
- Karanikolas, B., Figueiredo, M. and Wu, L. (2009). Polycomb Group Protein Enhancer of Zeste 2 Is an Oncogene That Promotes the Neoplastic Transformation of a Benign Prostatic Epithelial Cell Line. *Mol Cancer Res*.
- Karlen, S. J. and Krubitzer, L. (2007). The functional and anatomical organization of marsupial neocortex: evidence for parallel evolution across mammals. *Prog Neurobiol* 82, 122–141.
- Kennedy, T. E., Serafini, T., la Torre, de, J. R. and Tessier-Lavigne, M. (1994). Netrins are diffusible chemotropic factors for commissural axons in the embryonic spinal cord. *Cell* 78, 425–435.
- Kim, D. and Ackerman, S. L. (2011). The UNC5C netrin receptor regulates dorsal guidance of mouse hindbrain axons. *J Neurosci* 31, 2167–2179.
- Krauzlis, R. J. (2004). Recasting the smooth pursuit eye movement system. *J Neurophysiol* 91, 591–603.
- Kumbasar, A., Plachez, C., Gronostajski, R. M., Richards, L. J. and Litwack, E. D. (2009). Absence of the transcription factor Nfib delays the formation of the basilar pontine and other mossy fiber nuclei. *J Comp Neurol* 513, 98–112.
- Leergaard, T. B. and Bjaalie, J. G. (2007). Frontiers: Topography of the complete corticopontine projection: From experiments to principal maps. *Frontiers in neuroscience* 1, 211–223.
- Leergaard, T. B., Alloway, K. D., Mucic, J. J. and Bjaalie, J. G. (2000). Three-dimensional topography of corticopontine projections from rat barrel cortex: correlations with corticostriatal organization. *J Neurosci* 20, 8474–8484.
- Leergaard, T. B., Alloway, K. D., Pham, T. A., Bolstad, I., Hoffer, Z. S., Pettersen, C. and Bjaalie, J. G. (2004). Three-dimensional topography of corticopontine projections from rat sensorimotor cortex: comparisons with corticostriatal projections reveal diverse integrative organization. *J Comp Neurol* 478, 306–322.
- Leergaard, T. B., Lakke, E. A. and Bjaalie, J. G. (1995). Topographical organization

- in the early postnatal corticopontine projection: a carbocyanine dye and 3-D computer reconstruction study in the rat. *J Comp Neurol* 361, 77–94.
- Leergaard, T. B., Lillehaug, S., De Schutter, E., Bower, J. M. and Bjaalie, J. G. (2006). Topographical organization of pathways from somatosensory cortex through the pontine nuclei to tactile regions of the rat cerebellar hemispheres. *Eur J Neurosci* 24, 2801–2812.
- Lemons, D. and McGinnis, W. (2006). Genomic evolution of Hox gene clusters. *Science (New York, NY)* 313, 1918–1922.
- Lende, R. A. (1963). Cerebral cortex: a sensorimotor amalgam in the marsupial. *Science (New York, NY)* 141, 730–732.
- Lende, R. A. (1964). Representation in the cerebellar cortex a primitive mammal. Sensorimotor, visual and auditory fields in the echidna (*Tachyglossus aculeatus*). *J Neurophysiol* 27, 37–48.
- Leung, C., Lingbeek, M., Shakhova, O., Liu, J., Tanger, E., Saremaslani, P., Van Lohuizen, M. and Marino, S. (2004). Bmi1 is essential for cerebellar development and is overexpressed in human medulloblastomas. *Nature* 428, 337–341.
- Lewis, E. B. (1978). A gene complex controlling segmentation in *Drosophila*. *Nature* 276, 565–570.
- Lewis, P. M., Gritli-Linde, A., Smeyne, R., Kottmann, A. and McMahon, A. P. (2004). Sonic hedgehog signaling is required for expansion of granule neuron precursors and patterning of the mouse cerebellum. *Dev Biol* 270, 393–410.
- Liu, A. and Niswander, L. A. (2005). Bone morphogenetic protein signalling and vertebrate nervous system development. *Nat Rev Neurosci* 6, 945–954.
- Loturco, J., Manent, J.-B. and Sidiqi, F. (2009). New and improved tools for in utero electroporation studies of developing cerebral cortex. *Cereb Cortex* 19 Suppl 1, i120–5.
- Lowell, B. B., Olson, D. and Yu, J. (2006). Development and phenotype of ChAT-IRES-Cre mice. *MGI Direct Data Submission*.
- Luo, L. and Flanagan, J. G. (2007). Development of continuous and discrete neural maps. *Neuron* 56, 284–300.
- Lupo, G., Harris, W. A. and Lewis, K. E. (2006). Mechanisms of ventral patterning in the vertebrate nervous system. *Nat Rev Neurosci* 7, 103–114.
- Maden, M. (2002). Retinoid signalling in the development of the central nervous system. *Nat Rev Neurosci* 3, 843–853.
- Madisen, L., Zwingman, T. A., Sunkin, S. M., Oh, S. W., Zariwala, H. A., Gu, H., Ng, L. L., Palmiter, R. D., Hawrylycz, M. J., Jones, A. R., et al. (2010). A robust

- and high-throughput Cre reporting and characterization system for the whole mouse brain. *Nat Neurosci* 13, 133–140.
- Manto, M. (2009). Mechanisms of human cerebellar dysmetria: experimental evidence and current conceptual bases. *J Neuroeng Rehabil* 6, 10.
- Manzanares, M., Cordes, S., Ariza-McNaughton, L., Sadl, V., Maruthainar, K., Barsh, G. and Krumlauf, R. (1999). Conserved and distinct roles of kreisler in regulation of the paralogous Hoxa3 and Hoxb3 genes. *Development* 126, 759–769.
- Marillat, V., Sabatier, C., Failli, V., Matsunaga, E., Sotelo, C., Tessier-Lavigne, M. and Chédotal, A. (2004). The slit receptor Rig-1/Robo3 controls midline crossing by hindbrain precerebellar neurons and axons. *Neuron* 43, 69–79.
- Marín, F. and Puelles, L. (1995). Morphological fate of rhombomeres in quail/chick chimeras: a segmental analysis of hindbrain nuclei. *Eur J Neurosci* 7, 1714–1738.
- Marín, O. and Rubenstein, J. L. (2001). A long, remarkable journey: tangential migration in the telencephalon. *Nat Rev Neurosci* 2, 780–790.
- Mason, I. (2007). Initiation to end point: the multiple roles of fibroblast growth factors in neural development. *Nat Rev Neurosci* 8, 583–596.
- May, J. G., Keller, E. L. and Suzuki, D. A. (1988). Smooth-pursuit eye movement deficits with chemical lesions in the dorsolateral pontine nucleus of the monkey. *J Neurophysiol* 59, 952–977.
- McConnell, S. K. (1995). Strategies for the generation of neuronal diversity in the developing central nervous system. *J Neurosci* 15, 6987–6998.
- Mihailoff, G. A. (1983). Intra- and interhemispheric collateral branching in the rat pontocerebellar system, a fluorescence double-label study. *Neuroscience* 10, 141–160.
- Mihailoff, G. A. and King, J. S. (1975). The basilar pontine gray of the opossum: a correlated light and electron microscopic analysis. *J Comp Neurol* 159, 521–552.
- Mihailoff, G. A., Burne, R. A. and Woodward, D. J. (1978). Projections of the sensorimotor cortex to the basilar pontine nuclei in the rat: an autoradiographic study. *Brain Res* 145, 347–354.
- Mihailoff, G. A., Burne, R. A. and Woodward, D. J. (1982). Projections of the sensorimotor cortex to the basilar pontine nuclei in the rat: an autoradiographic study. *Brain Res* 145, 347–354.
- Mihailoff, G. A., Burne, R. A., Azizi, S. A., Norell, G. and Woodward, D. J. (1981). The pontocerebellar system in the rat: an HRP study. II. Hemispherical components. *J Comp Neurol* 197, 559–577.
- Moazed, D. and O'Farrell, P. H. (1992). Maintenance of the engrailed expression

- pattern by Polycomb group genes in *Drosophila*. *Development* 116, 805–810.
- Murthy, V. N. (2011). Olfactory maps in the brain. *Annu Rev Neurosci* 34, 233–258.
- Narita, Y. and Rijli, F. M. (2009). Hox genes in neural patterning and circuit formation in the mouse hindbrain. *Curr. Top. Dev. Biol.* 88, 139–167.
- Nikundiwe, A. M., Bjaalie, J. G. and Brodal, P. (1994a). Lamellar organization of pontocerebellar neuronal populations. A multi-tracer and 3-D computer reconstruction study in the cat. *Eur J Neurosci* 6, 173–186.
- Nikundiwe, A. M., Bjaalie, J. G. and Brodal, P. (1994b). Lamellar organization of pontocerebellar neuronal populations. A multi-tracer and 3-D computer reconstruction study in the cat. *Eur J Neurosci* 6, 173–186.
- Nolte, C. and Krumlauf, R. (2007). Expression of Hox genes in the nervous system of vertebrates. *HOX gene expression* 14–41.
- Nóbrega-Pereira, S., Kessar, N., Du, T., Kimura, S., Anderson, S. A. and Marin, O. (2008). Postmitotic Nkx2-1 controls the migration of telencephalic interneurons by direct repression of guidance receptors. *Neuron* 59, 733–745.
- O'Leary, D. D. M., Chou, S.-J. and Sahara, S. (2007). Area patterning of the mammalian cortex. *Neuron* 56, 252–269.
- Okada, T., Keino-Masu, K. and Masu, M. (2007). Migration and nucleogenesis of mouse precerebellar neurons visualized by in utero electroporation of a green fluorescent protein gene. *Neurosci Res* 57, 40–49.
- Ono, K., Yasui, Y. and Ikenaka, K. (2004). Lower rhombic lip-derived cells undergo transmedian tangential migration followed by radial migration in the chick embryo brainstem. *Eur J Neurosci* 20, 914–922.
- Ono, S. and Mustari, M. J. (2008). Smooth Pursuit-Related Information Processing in Frontal Eye Field Neurons that Project to the NRTP. *Cerebral Cortex* 19, 1186–1197.
- Ono, S., Das, V. E. and Mustari, M. J. (2003). Role of the dorsolateral pontine nucleus in short-term adaptation of the horizontal vestibuloocular reflex. *J Neurophysiol* 89, 2879–2885.
- Oury, F. and Rijli, F. M. (2007). [Hoxa2: a key gene for the facial somatosensory map]. *Med Sci (Paris)* 23, 247–249.
- Oury, F., Murakami, Y., Renaud, J.-S., Pasqualetti, M., Charnay, P., Ren, S.-Y. and Rijli, F. M. (2006). Hoxa2- and rhombomere-dependent development of the mouse facial somatosensory map. *Science (New York, NY)* 313, 1408–1413.
- Pearson, J. C., Lemons, D. and McGinnis, W. (2005). Modulating Hox gene functions during animal body patterning. *Nature reviews genetics* 6, 893–904.

- Perales, M., Winer, J. A. and Prieto, J. J. (2006). Focal projections of cat auditory cortex to the pontine nuclei. *J Comp Neurol* 497, 959–980.
- Pereira, J. D., Sansom, S. N., Smith, J., Dobenecker, M. W., Tarakhovsky, A. and Livesey, F. J. (2010). Ezh2, the histone methyltransferase of PRC2, regulates the balance between self-renewal and differentiation in the cerebral cortex. *Proceedings of the National Academy of Sciences* 107, 15957–15962.
- Philippidou, P., Walsh, C. M., Aubin, J., Jeannotte, L. and Dasen, J. S. (2012). Sustained Hox5 gene activity is required for respiratory motor neuron development. *Nat Neurosci*.
- Porcher, A. and Dostatni, N. (2010). The bicoid morphogen system. *Curr Biol* 20, R249–54.
- Puschendorf, M., Terranova, R., Boutsma, E., Mao, X., Isono, K.-I., Brykczynska, U., Kolb, C., Otte, A. P., Koseki, H., Orkin, S. H., et al. (2008). PRC1 and Suv39h specify parental asymmetry at constitutive heterochromatin in early mouse embryos. *Nature Genetics* 40, 411–420.
- Qu, Q., Crandall, J. E., Luo, T., McCaffery, P. J. and Smith, F. I. (2006). Defects in tangential neuronal migration of pontine nuclei neurons in the *Largemyd* mouse are associated with stalled migration in the ventrolateral hindbrain. *Eur J Neurosci* 23, 2877–2886.
- Rakic, P. (1974). Neurons in rhesus monkey visual cortex: systematic relation between time of origin and eventual disposition. *Science (New York, NY)* 183, 425–427.
- Rakic, P. (1988). Specification of cerebral cortical areas. *Science (New York, NY)* 241, 170–176.
- Rakic, P. (2009). Evolution of the neocortex: a perspective from developmental biology. *Nat Rev Neurosci* 10, 724–735.
- Ramnani, N. (2006). The primate cortico-cerebellar system: anatomy and function. *Nat Rev Neurosci* 7, 511–522.
- Ray, R. S. and Dymecki, S. M. (2009). Rautenlippe Redux -- toward a unified view of the precerebellar rhombic lip. *Curr Opin Cell Biol* 21, 741–747.
- Ren, S.-Y., Pasqualetti, M., Dierich, A. E., Le Meur, M. and Rijli, F. M. (2002). A Hoxa2 mutant conditional allele generated by Flp- and Cre-mediated recombination. *Genesis* 32, 105–108.
- Renier, N., Schonewille, M., Giraudet, F., Badura, A., Tessier-Lavigne, M., Avan, P., De Zeeuw, C. I. and Chédotal, A. (2010). Genetic dissection of the function of hindbrain axonal commissures. *PLoS Biol* 8, e1000325.
- Rivera-Pomar, R. and Jäckle, H. (1996). From gradients to stripes in *Drosophila*

- embryogenesis: filling in the gaps. *Trends Genet* 12, 478–483.
- Rodriguez, C. I. and Dymecki, S. M. (2000). Origin of the precerebellar system. *Neuron* 27, 475–486.
- Rogers, K. W. and Schier, A. F. (2011). Morphogen gradients: from generation to interpretation. *Annu Rev Cell Dev Biol* 27, 377–407.
- Rossant, J., Zirngibl, R., Cado, D., Shago, M. and Giguère, V. (1991). Expression of a retinoic acid response element-hsplacZ transgene defines specific domains of transcriptional activity during mouse embryogenesis. *Genes Dev* 5, 1333–1344.
- Round, J. and Stein, E. (2007). Netrin signaling leading to directed growth cone steering. *Curr Opin Neurobiol* 17, 15–21.
- Sabatier, C., Plump, A. S., Le Ma, Brose, K., Tamada, A., Murakami, F., Lee, E. Y.-H. P. and Tessier-Lavigne, M. (2004). The divergent Robo family protein rig-1/Robo3 is a negative regulator of slit responsiveness required for midline crossing by commissural axons. *Cell* 117, 157–169.
- Schäfer, M. K., Eiden, L. E. and Weihe, E. (1998). Cholinergic neurons and terminal fields revealed by immunohistochemistry for the vesicular acetylcholine transporter. I. Central nervous system. *Neuroscience* 84, 331–359.
- Schuller, G., Covey, E. and Casseday, J. H. (1991). Auditory Pontine Grey: Connections and Response Properties in the Horseshoe Bat. *Eur J Neurosci* 3, 648–662.
- Schwartz, Y. B. and Pirrotta, V. (2007). Polycomb silencing mechanisms and the management of genomic programmes. *Nature reviews genetics* 8, 9–22.
- Schwarz, C. and Schmitz, Y. (1997). Projection from the cerebellar lateral nucleus to precerebellar nuclei in the mossy fiber pathway is glutamatergic: a study combining anterograde tracing with immunogold labeling in the rat. *J Comp Neurol* 381, 320–334.
- Schwarz, C. and Thier, P. (1999). Binding of signals relevant for action: towards a hypothesis of the functional role of the pontine nuclei. *Trends Neurosci* 22, 443–451.
- Seeger, M., Tear, G., Ferres-Marco, D. and Goodman, C. S. (1993). Mutations affecting growth cone guidance in *Drosophila*: genes necessary for guidance toward or away from the midline. *Neuron* 10, 409–426.
- Shen, K. and Scheiffele, P. (2010). Genetics and cell biology of building specific synaptic connectivity. *Annu Rev Neurosci* 33, 473–507.
- Simon, J. A. and Kingston, R. E. (2009). Mechanisms of polycomb gene silencing: knowns and unknowns. *Nat Rev Mol Cell Biol* 10, 697–708.

- Simon, J. A. and Tamkun, J. W. (2002). Programming off and on states in chromatin: mechanisms of Polycomb and trithorax group complexes. *Curr Opin Genet Dev* 12, 210–218.
- Sing, A., Pannell, D., Karaiskakis, A., Sturgeon, K., Djabali, M., Ellis, J., Lipshitz, H. D. and Cordes, S. P. (2009). A vertebrate Polycomb response element governs segmentation of the posterior hindbrain. *Cell* 138, 885–897.
- Soriano, P. (1999). Generalized lacZ expression with the ROSA26 Cre reporter strain. *Nature Genetics* 21, 70–71.
- Soshnikova, N. and Duboule, D. (2009a). Epigenetic regulation of vertebrate Hox genes: A dynamic equilibrium. *Epigenetics : official journal of the DNA Methylation Society* 4.
- Soshnikova, N. and Duboule, D. (2009b). Epigenetic temporal control of mouse Hox genes in vivo. *Science (New York, NY)* 324, 1320–1323.
- Strahl, B. D. and Allis, C. D. (2000). The language of covalent histone modifications. *Nature* 403, 41–45.
- Strick, P. L., Dum, R. P. and Fiez, J. A. (2009). Cerebellum and nonmotor function. *Annu Rev Neurosci* 32, 413–434.
- Striedter, G. F. (2005). Principles of Brain Evolution. *Sinauer Associates, Sunderland, MA, USA* 436.
- Struhl, G. (1981). A gene product required for correct initiation of segmental determination in *Drosophila*. *Nature* 293, 36–41.
- Studer, M., Lumsden, A., Ariza-McNaughton, L., Bradley, A. and Krumlauf, R. (1996). Altered segmental identity and abnormal migration of motor neurons in mice lacking Hoxb-1. *Nature* 384, 630–634.
- Su, I.-H., Basavaraj, A., Krutchinsky, A. N., Hobert, O., Ullrich, A., Chait, B. T. and Tarakhovskiy, A. (2003). Ezh2 controls B cell development through histone H3 methylation and Igh rearrangement. *Nat Immunol* 4, 124–131.
- Sultan, F. and Glickstein, M. (2007). The cerebellum: Comparative and animal studies. *Cerebellum* 6, 168–176.
- Suvà, M.-L., Riggi, N., Janiszewska, M., Radovanovic, I., Provero, P., Stehle, J.-C., Baumer, K., Le Bitoux, M.-A., Marino, D., Cironi, L., et al. (2009). EZH2 is essential for glioblastoma cancer stem cell maintenance. *Cancer Res* 69, 9211–9218.
- Szymczak, A. L., Workman, C. J., Wang, Y., Vignali, K. M., Dilioglou, S., Vanin, E. F. and Vignali, D. A. A. (2004). Correction of multi-gene deficiency in vivo using a single “self-cleaving” 2A peptide-based retroviral vector. *Nat Biotechnol* 22, 589–594.

- Tabata, T. (2001). Genetics of morphogen gradients. *Nature reviews genetics* 2, 620–630.
- Terranova, R., Yokobayashi, S., Stadler, M. B., Otte, A. P., Van Lohuizen, M., Orkin, S. H. and Peters, A. H. F. M. (2008). Polycomb group proteins Ezh2 and Rnf2 direct genomic contraction and imprinted repression in early mouse embryos. *Dev Cell* 15, 668–679.
- Tessier-Lavigne, M. and Goodman, C. S. (1996). The molecular biology of axon guidance. *Science (New York, NY)* 274, 1123–1133.
- Thielert, C. D. and Thier, P. (1993). Patterns of projections from the pontine nuclei and the nucleus reticularis tegmenti pontis to the posterior vermis in the rhesus monkey: a study using retrograde tracers. *J Comp Neurol* 337, 113–126.
- Thier, P. and Möck, M. (2006). The oculomotor role of the pontine nuclei and the nucleus reticularis tegmenti pontis. In *Progress in Brain Research*, pp. 293–320. Elsevier.
- Thier, P., Koehler, W. and Buettner, U. W. (1988). Neuronal activity in the dorsolateral pontine nucleus of the alert monkey modulated by visual stimuli and eye movements. *Experimental brain research Experimentelle Hirnforschung Expérimentation cérébrale* 70, 496–512.
- Thier, P., Koehler, W. and Buettner, U. W. (1989). Investigation of the dorsolateral basilar pontine grey of the alert monkey. *Brain Behav Evol* 33, 75–79.
- Trainor, P. and Krumlauf, R. (2000). Patterning the cranial neural crest: hindbrain segmentation and Hox gene plasticity. *Nat Rev Neurosci* 1, 116–124.
- Tziridis, K., Dicke, P. W. and Thier, P. (2009). The role of the monkey dorsal pontine nuclei in goal-directed eye and hand movements. *J Neurosci* 29, 6154–6166.
- Tziridis, K., Dicke, P. W. and Thier, P. (2011). Pontine Reference Frames for the Sensory Guidance of Movement. *Cereb Cortex*.
- Voiculescu, O., Taillebourg, E., Pujades, C., Kress, C., Buart, S., Charnay, P. and Schneider-Maunoury, S. (2001). Hindbrain patterning: Krox20 couples segmentation and specification of regional identity. *Development* 128, 4967–4978.
- Vrieseling, E. and Arber, S. (2006). Target-induced transcriptional control of dendritic patterning and connectivity in motor neurons by the ETS gene *Pea3*. *Cell* 127, 1439–1452.
- Wang, C., Zhao, J.-J., Lu, C.-L., Han, X.-D., An, L.-S. and Ma, X. (2010). Polycomb group proteins are essential for spinal cord development. *Front Biosci* 15, 1018–1022.
- Wang, F., Nemes, A., Mendelsohn, M. and Axel, R. (1998). Odorant receptors govern

- the formation of a precise topographic map. *Cell* 93, 47–60.
- Wang, V. Y., Rose, M. F. and Zoghbi, H. Y. (2005). Math1 expression redefines the rhombic lip derivatives and reveals novel lineages within the brainstem and cerebellum. *Neuron* 48, 31–43.
- Wilson, S. W. and Houart, C. (2004). Early steps in the development of the forebrain. *Dev Cell* 6, 167–181.
- Wingate, R. (2005). Math-Map(ic)s. *Neuron* 48, 1–4.
- Wolpert, L. (1969). Positional information and the spatial pattern of cellular differentiation. *J. Theor. Biol.* 25, 1–47.
- Wurst, W. and Bally-Cuif, L. (2001). Neural plate patterning: upstream and downstream of the isthmus organizer. *Nat Rev Neurosci* 2, 99–108.
- Wyngaarden, L. A., Delgado-Olguin, P., Su, I.-H., Bruneau, B. G. and Hopyan, S. (2011). Ezh2 regulates anteroposterior axis specification and proximodistal axis elongation in the developing limb. *Development* 138, 3759–3767.
- Yau, T. O., Kwan, C. T., Jakt, L. M., Stallwood, N., Cordes, S. and Har Sham, M. (2002). Auto/cross-regulation of Hoxb3 expression in posterior hindbrain and spinal cord. *Dev Biol* 252, 287–300.
- Yee, K. T., Simon, H. H., Tessier-Lavigne, M. and O'Leary, D. M. (1999). Extension of long leading processes and neuronal migration in the mammalian brain directed by the chemoattractant netrin-1. *Neuron* 24, 607–622.
- Yonehara, K., Balint, K., Noda, M., Nagel, G., Bamberg, E. and Roska, B. (2011). Spatially asymmetric reorganization of inhibition establishes a motion-sensitive circuit. *Nature* 469, 407–410.
- Ypsilanti, A. R., Zagar, Y. and Chédotal, A. (2010). Moving away from the midline: new developments for Slit and Robo. *Development* 137, 1939–1952.
- Zhang, J., Smith, D., Yamamoto, M., Ma, L. and McCaffery, P. (2003). The meninges is a source of retinoic acid for the late-developing hindbrain. *J Neurosci* 23, 7610–7620.
- Zhu, Y., Matsumoto, T., Mikami, S., Nagasawa, T. and Murakami, F. (2009). SDF1/CXCR4 signalling regulates two distinct processes of precerebellar neuronal migration and its depletion leads to abnormal pontine nuclei formation. *Development* 136, 1919–1928.

Acknowledgements

The experimental work of this thesis was done in the laboratory of Dr. Filippo Rijli in the Friedrich Miescher Institute for Biomedical Research in Basel, Switzerland between July 2008 and March 2013.

I want to thank Filippo Rijli for his intellectual and technical support during this time. I thank him for the inspiring discussions we had as well his support and the possibility to pursue various projects on my own. I also want to thank the members of my thesis committee, Alain Chédotal, Silvia Arber, Peter Scheiffele, Pico Caroni and Botond Roska for their helpful comments and suggestions and Rainer Friedrich who chaired the examination.

Furthermore, I want to thank especially Thomas Di Meglio, who is an extremely passionate and technically skilled postdoc. He had a major contribution to the success of the Science publication. Many thanks also to Nathalie Vilain and Sebastien Ducret for their excellent scientific and technical contributions, Nathalie especially for the help on *in situ* hybridizations and electroporations, Sebastien for his help in generating transgenic lines. I also thank Dominik Kraus, who will continue the project on the precerebellar connectivity and with whom I enjoyed a lot working together. He helped as well for the *in vivo* electroporation and helped with proofreading. Last but not least I want to thank the rest of the lab including the actual members Ahmad Bechara, Kajari Karmakar, Alberto Loche, Maryline Minoux, Antonio Vitobello and the former members Christophe Laumonnerie, Yuichi Narita and Liseth Parra.

Many thanks also to Fatiha Boukhtouche for technical advice for *in utero* electroporation and immunostainings, Keisuke Yonehara for advice for viral injections, Kamill Balint for help with Rabies production, Ching-Yeu Liang and Antonio Vitobello for doing Chip-seq experiments, Alberto Loche for the microarray and the qPCRs and many other FMI members and group leaders for helpful discussions and their scientific input.

I also want to acknowledge the help of the FMI facility members, which are extraordinary helpful including Steve Bourke, Laurent Gelman, Patrick Schwarb, Aaron Ponti (Imaging), Jean-François Spetz (Transgenic Facility), Hubertus Kohler

(FACS), Tim Roloff (Microarray), Alan Naylor, Thomas Nyffenegger, Sjoerd van Eden (IT), Birgit Heller and Tamara Ramadan (Animal Facility).

Many thanks also to Jan Beckmann, Eva-Maria Enneking, Steffen Wolff, Raiko Stephan, Daniel Udvari, Susanne Finger, Irene Kalchhauser, Jun Lee, Katharina Krimm, Thomas Frank, Volker Busskamp, Steve Bourke, Francois Grenier, Jan Gründemann, Elisabeth Meyer and Ingo Jever as well as the members of the SC Novartis II for a great time in- and outside of FMI.

Last but not least I want to thank my parents for supporting me during all these years.

Curriculum Vitae

■ Personal Information

Name:	Claudius Frank Kratochwil
Address:	Schönaustrasse 40, CH-4058 Basel
Email:	Kratochwil.Claudius@gmail.com
Date of birth:	13.12.1983
Place of birth:	Freiburg, Germany
Nationality	German

■ Education

July 2008 – April 2013	PhD Thesis, Friedrich Miescher Institute, Basel, Switzerland Laboratory of Prof. Dr. Filippo Rijli “Transcriptional and epigenetic regulation of neuronal migration and circuitry development in the murine hindbrain”
September 2007 – July 2008	Diploma Thesis, Albert Ludwigs University Freiburg, Germany Laboratory of Prof. Dr. Wolfgang Driever “Characterization of the Catecholaminergic Circuitry in Zebrafish”
October 2004 – July 2008	Diploma studies in biology, Albert Ludwigs University Freiburg, Germany Main subjects: Developmental Biology, Neurobiology, Animal Physiology, Neuropathology - Grade: 1.0 (1=best, 6=worst)

■ Research Projects and Internships

October 2006 – July 2007	Institute for Biology, Albert Ludwigs University Freiburg, Germany Laboratory of Prof. Dr. Wolfgang Driever Two research projects on „In vivo electroporation in zebrafish“ and “Genomic mapping of N-ethyl-N-nitrosourea (ENU) induced mutations affecting the developing dopaminergic system in zebrafish”
August 2006 – October 2006	Neuroscience Center, University of Helsinki, Finland Laboratory of Prof. Dr. Eero Castrén Research project on the „Role of FMRP in human and murine neocortex development“
March 2006 – April 2006	Department of Neuropathology, University Hospital Freiburg, Germany Laboratory of Prof. Dr. Benedikt Volk Internship about “Diagnostics in Neuropathology” and “Stem cell therapies in Huntington Disease”
August 2005 – October 2005	Max Planck Institute for brain research, Frankfurt am Main, Germany Laboratory of Prof. Dr. Ralf Galuske / Prof Dr. Wolf Singer Internship about “Invasive and noninvasive Methods to analyze neuronal activity in primary visual cortex”

■ Scholarships

July 2008 – April 2013	Scholarship “International PhD program” funded by Friedrich Miescher Institute for Biomedical Research, Basel
---------------------------	---

■ Publications

- DI MEGLIO, T.*, KRATOCHWIL, C. F.*, VILAIN, N., LOCHE, A., VITO BELLO A, YONEHARA, K., ROSKA, B., PETERS, A. H. F. M., WELLIK, D., DUCRET, S. and RIJLI, F. M. (2013): *Ezh2* orchestrates topographic tangential migration and connectivity of precerebellar neurons. *Science* **339**, 204-207.
- KASTENHUBER, E.*, KRATOCHWIL, C. F.*, RYU, S.*, SCHWEITZER, J. and DRIEVER, W. (2010). Genetic dissection of dopaminergic and noradrenergic contributions to catecholaminergic tracts in early larval zebrafish. *J Comp Neurol* **518**, 439–458.
- TERVONEN, T. A., LOUHIVUORI, V., SUN, X., HOKKANEN, M.-E., KRATOCHWIL, C. F., ZEBRYK, P., CASTRÉN, E. and CASTRÉN, M. L. (2009). Aberrant differentiation of glutamatergic cells in neocortex of mouse model for fragile X syndrome. *Neurobiol. Dis.* **33**, 250–259.

* equal contribution

■ Presentations on national and international meetings

- CRG Barcelona / FMI Basel - Joint PhD Meeting, Barcelona, May 20-23 2011: KRATOCHWIL, C. F. and RIJLI, F. M.: Transcriptional regulation of hindbrain circuitry development. (invited speaker)
- 40th Annual meeting of the Society for Neuroscience, San Diego, November 15–19 2010: DI MEGLIO, T., KRATOCHWIL, C. F., VILAIN, N., DUCRET, S. and RIJLI, F. M.: Hox paralogue group 2 genes control distinct steps of pontine neuron tangential migration in the mouse brainstem. (poster presentation)
- 39th Annual meeting of the Society for Neuroscience, Chicago, October 17-21 2009: KRATOCHWIL, C. F. and RIJLI, F. M.: Generation of genetic tools to study development of myelencephalic nuclei circuitry in the mouse. (poster presentation)
- LMCB London / FMI Basel - Joint PhD Meeting, Emmetten/Switzerland, June 12-15 2009: KRATOCHWIL, C. F. and RIJLI, F. M.: Transcriptional regulation of topographic circuitry in the precerebellar system. (poster presentation)
- 38th Annual meeting of the Society for Neuroscience, Washington D.C., November 15-19 2008: KASTENHUBER, E., SCHWEITZER, J., KRATOCHWIL, C. F., KERN, U., RYU, S. and DRIEVER, W.: Establishment of catecholaminergic circuitry in the zebrafish. (poster presentation)
- 8th International Meeting on Zebrafish Development & Genetics, Madison, June 25-29 2008: KOCH P., KRATOCHWIL C. F. and DRIEVER W.: Optimization of in vivo electroporation in the zebrafish brain. (poster presentation)
- 37th Annual meeting of the Society for Neuroscience, San Diego, November 3-7 2007: TERVONEN, T. A., SUN, X., HOKKANEN, M.-E., KRATOCHWIL, C. F., ZEBRYK, P., CASTRÉN, E. and CASTRÉN, M. L.: Developmental abnormalities in neocortex formation of Fmr1 knockout mouse. (poster presentation)
- 5th European Zebrafish Genetics and Development Meeting, Amsterdam, July 12-15 2007: KOCH P.*, KRATOCHWIL C. F.*, LEDDEROSE J., FILIPPI A. and DRIEVER W.: Optimization of in vivo electroporation in the zebrafish brain. (poster presentation)

* equal contribution